# Development of stapled peptides targeting the Ral GTPases

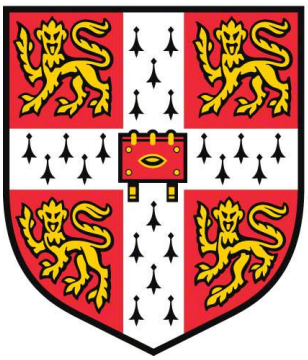


**Catherine Hurd**

Department of Biochemistry

University of Cambridge


September 2020

This dissertation is submitted for the degree of Doctor of Philosophy

## Declaration

This dissertation is the result of my own work and includes nothing which is the outcome of work done in collaboration except as specified in the Acknowledgements. It is not substantially the same as any that I have submitted, or, is being concurrently submitted for a degree or diploma or other qualification at the University of Cambridge or any other University or similar institution.

I further state that no part of my dissertation has already been submitted, or is being concurrently submitted for any such degree, diploma or other qualification at the University of Cambridge or any other University or similar institution.

It does not exceed the prescribed word limit of 60,000 words for the Degree Committee of the Faculty of Biology.

## Acknowledgements

Firstly, I would like to thank my supervisors, Darerca Owen and Helen Mott, for their generous support and guidance over the past four years. They have given a lot of their time to help me to develop as a researcher, and for that I am very grateful.

I would like to thank AstraZeneca for funding this work and for allowing me to spend time on their site on Granta Park, which was a very valuable opportunity to see the inner workings of a pharmaceutical company. With thanks to Sarah Ross and Nicky Whalley, who have contributed to many useful discussions about the project and organized the provision of cell lines. Jefferson Revell was very generous with his time, providing training and advice for peptide synthesis at the AstraZeneca labs and during many useful and enthusiastic discussions about the project, for which I am very grateful. I would also like to thank the rest of the peptide lab who have always been so welcoming and helpful during my visits to Granta Park.

The expertise of Paul Brear has been invaluable for all the work relating to the X-ray crystal structures, providing advice for crystallization conditions, carrying out the data acquisition and for solving the structures. In addition, Paul Brear and Katherine Stott have been very helpful in providing training and advice in the Biophysics facility. Many thanks also to Marc de la Roche and Jonathan Gadsby for assistance with confocal microscopy experiments.

My time is Cambridge would not have been the same without all of the amazing members of the Mott/Owen group, who have made the lab a truly enjoyable place to work. Their friendship and support have been very important to me, and I thank them for the many hilarious coffee chats and pub trips over the past four years.

I would also like to thank William Golding, who has been a rock to me for the past seven years and who is always able to find the positive in any situation.

Finally, I owe so much to my Mum and Stepdad, Ruth and Simon Tobi, for their continued love and support. Writing this thesis during the national lockdown would have been so much more difficult without their wonderful company, and I will always treasure that time spent together.

## Abstract

The *ras* genes are the most commonly mutated oncogenes in human cancers, with mutations occurring in approximately 20% of human tumours. However, more than 30 years of attempts to target Ras proteins therapeutically have yielded no effective therapies in the clinic, leading the proteins to be widely deemed 'undruggable'. In recent years, there has been substantial evidence implicating the Ral GTPases, RalA and RalB, which are activated downstream of Ras, as critical drivers of cell growth and metastasis in numerous Ras-driven cancers. Therefore, targeting this pathway may provide an effective method for inhibition of oncogenic Ras signalling. Prior work identified stapled peptides based on the Ral effector, RLIP76, that can bind to the Ral GTPases and disrupt downstream signalling. To improve the affinity of these peptide sequences, an affinity maturation was performed on the Ral-binding domain of RLIP76 from which potential sequence changes were identified. The work described in this thesis aimed to identify sequences from this selection with improved affinity for Ral proteins to guide the design of second-generation stapled peptides targeting the Ral GTPases. *In vitro* validation of the selection sequences enabled the identification of several sequence substitutions that together improved binding to Ral proteins by more than 20-fold. The effects of individual residue substitutions on the affinity for Ral proteins were determined using biophysical assays and two 1.5 Å co-crystal structures of the tightest-binding mutants in complex with RalB revealed the key interactions formed. The sequences were successfully translated into stapled peptides based on RLIP76, resulting in peptides with improved affinity compared to the wild-type parent sequence. The peptides have been shown to be selective for the active form of Ral, with undetectable binding to a panel of related small GTPases in *in vitro* assays. The binding site of the lead peptide on RalB has been determined by NMR and was found to overlap with multiple Ral-effector interactions. The peptides were able compete with multiple Ral-effector interactions *in vitro* and in cellular lysates. This work demonstrates how manipulation of a native binding partner can assist in the rational design of stapled peptide inhibitors targeting a protein-protein interaction.

## Abbreviations

| | |
|---|---|
| ADP | Adenosine diphosphate |
| AEEP | 9-Amino-4,7-dioxanonanoic acid |
| Arf | ADP ribosylation factor |
| BSA | Bovine serum albumin |
| CD | Circular dichroism |
| Cdc42 | Cell division control protein 42 homolog |
| CPP | Cell-penetrating peptide |
| DCE | 1,2-Dichloroethane |
| DCM | Dichloromethane |
| DHFR | Dihydrofolate reductase |
| DIC | *N,N'*-Diisopropylcarbodiimide |
| DIPEA | *N,N*-Diisopropylethylamine |
| DMF | Dimethylformamide |
| ECL | Enhanced chemiluminescence |
| EDT | 1,2-Ethanedithiol |
| EDTA | Ethylenediaminetetraacetic acid |
| FAM | 5-Carboxyfluorescein |
| FKBP | FK502-binding protein 12 |
| FP | Fluorescence polarization |
| Fpa | L-4-fluorophenylalanine |
| FTase | Farnesyltransferase |
| FTI | Farnesyltransferase inhibitor |
| GAP | GTPase activating protein |
| GDI | Guanine nucleotide dissociation inhibitor |
| GDP | Guanosine diphosphate |
| Gdn-HCl | Guanidine hydrochloride |
| GEF | Guanine nucleotide exchange factor |
| GFP | Green fluorescent protein |
| GGTase | Geranylgeranyltransferase |
| GGTI | Geranylgeranyltransferase inhibitor |
| GMPPCP | β,γ-Methyleneguanosine 5'-triphosphate |
| GMPPNP | Guanosine 5'-[β,γ-imido]triphosphate |
| GST | Glutathione S-transferase |
| GTP | Guanosine triphosphate |
| HATU | 1-[Bis(dimethylamino)methylene]-1H-1,2,3-triazolo[4,5-b]pyridinium 3-oxide hexafluorophosphate |
| HCTU | O-(1H-6-Chlorobenzotriazole-1-yl)-1,1,3,3-tetramethyluronium hexafluorophosphate |

| | |
|---|---|
| HOBt | Hydroxybenzotriazole |
| HPLC | High performance liquid chromatography |
| HRV-3C | Human Rhinovirus 3C |
| IPTG | Isopropyl β-d-1-thiogalactopyranoside |
| ITC | Isothermal titration calorimetry |
| LC-MS | Liquid chromatography-mass spectrometry |
| MALDI-ToF MS | Matrix-assisted laser desorption/ionization time of flight mass spectrometry |
| MBP | Maltose-binding protein |
| MQ | Milli Q (water) |
| Nal | D-β-naphthylalanine |
| NMP | N-Methyl-2-pyrrolidone |
| NMR | Nuclear magnetic resonance |
| PBS | Phosphate buffered saline |
| PCR | Polymerase chain reaction |
| PDB | Protein data bank |
| PEG | Polyethylene glycol |
| PEI | Polyethylenimine |
| PMSF | Phenylmethylsulfonyl fluoride |
| POI | Protein of interest |
| PPI | Protein-protein interaction |
| PROTAC | Proteolysis-targeting chimera |
| Rab | Ras-like in brain |
| Ral | Ras-like |
| Ran | Ras-like nuclear |
| Ras | Rat sarcoma |
| RBD | Ral binding domain |
| Rho | Ras homology |
| RLIP76 | Ral interacting protein 76 kDa |
| RMSD | Root-mean-square deviation |
| SAW | Sterile analytical water |
| SDS | Sodium dodecyl sulfate |
| SDS-PAGE | Sodium dodecyl sulfate–polyacrylamide gel electrophoresis |
| SPA | Scintillation proximity assay |
| TEMED | Tetramethylethylenediamine |
| TFA | Trifluoroacetic acid |
| TIPS | Triisopropylsilane |

## Contents

# 1 Introduction

## 1.1 Ras superfamily of small GTPases

The Ras superfamily of small GTPases are master regulators of a vast range of cellular processes. There are more than 150 small GTPases in the human superfamily, which is divided into Ras, Rho, Rab, Ran and Arf families based on sequence homology and physiological function. While these proteins contain a very similar core structure, they perform dramatically different functions in the cell. The Ras (Rat sarcoma) family regulates cell proliferation and survival, Rho (Ras homologous) family members are regulators of actin cytoskeletal rearrangement and cell motility, Rab (Ras-like in brain) proteins regulate membrane trafficking, Ran (Ras-like nuclear) is involved with nucleocytoplasmic transport and Arf (ADP ribosylation factor) proteins regulate vesicle trafficking (1).

## 1.2 Common features of small GTPases

All small GTPases share a conserved G domain of approximately 20 kDa, containing several 'G box' sequences that allow these proteins to bind the guanine nucleotides, guanosine diphosphate (GDP) and guanosine triphosphate (GTP), with high affinity. Nucleotide binding also involves coordination of a magnesium cation ($Mg^{2+}$). The GTPases exist in two conformationally distinct states; they are inactive when bound to GDP and active in the GTP-bound state where they are competent to bind downstream effectors. They are therefore able to act as molecular switches, with their activation status being controlled by regulatory proteins.

### 1.2.1 Regulation of small GTPases

Small GTPases can hydrolyse GTP to GDP rendering them inactive but intrinsic rates of hydrolysis are very slow, as is the exchange of GDP for GTP for their activation. Their signalling is therefore modulated by regulatory proteins known as Guanine nucleotide Exchange Factors (GEFs) and GTPase Activating Proteins (GAPs), with each GTPase family having a distinct set

of regulators associated with them (for reviews see (2, 3)). GEFs turn on signalling by assisting in the exchange of GDP for GTP; binding of a GEF results in a conformational change that reduces the affinity of the GTPase for the bound nucleotide. As intracellular GTP is far more abundant than GDP (approximately 20-fold higher) this leads to the replacement of the bound nucleotide with GTP, delivering the proteins to their active conformation. The GTPase cycle is summarised in Figure 1.1.

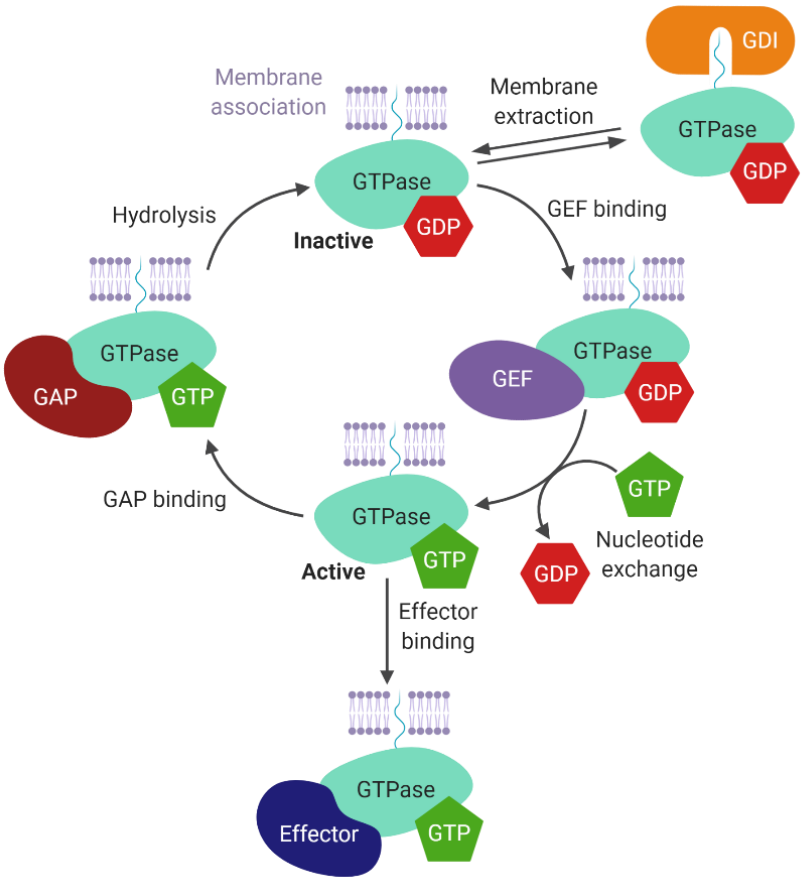


**Figure 1.1. The GTPase cycle.** GTPases are inactive when bound to GDP. Ras, Rho and Rab proteins have associated guanine nucleotide dissociation inhibitors (GDIs) and GDI-like partners that can extract them from the membrane in the inactive form, sequestering them in the cytosol. Binding of a GEF catalyses exchange of GDP for GTP by promoting the loss of GDP followed by GTP binding, which occurs as a result of far higher intracellular concentrations of GTP. In the GTP-bound form the small GTPases are activated and are competent in effector binding. They are deactivated by binding to GAPs, which stimulate hydrolysis of GTP to GDP. The vast majority of small GTPases are lipid modified and are membrane bound. Figure created with BioRender.com.

Signalling is switched off by GAPs, which aid hydrolysis of GTP to GDP. This occurs through stabilization of a conserved glutamine (residue 61 in Ras) in an orientation where it can

position a water molecule to attack the terminal phosphate bond in GTP. Additionally, GAPs contain an arginine finger that extends into the phosphate binding site and stabilizes the transition state during hydrolysis.

In addition to GEFs and GAPs, the Ras, Rho and Rab proteins are negatively regulated by Guanine nucleotide Dissociation Inhibitors (GDIs) and GDI-like proteins, which maintain the inactive form of the proteins. They do this by two mechanisms: they bind the lipid group of GDP-bound small GTPases to prevent membrane localization, hence sequestering them in the cytosol, and also prevent exchange for GTP by binding at the switch regions to stabilize the GDP-bound form.

### 1.2.2 The G domain

The G domain is a compact domain of around 20 kDa that is conserved across all GTP-binding proteins including the Ras superfamily of small GTPases and heterotrimeric G proteins (reviewed in (4, 5)). The archetypal domain is comprised of a hydrophobic core of six β-strands surrounded by five α-helices that are connected by a series of loops. Five of these loops comprise key motifs for GTP-binding proteins; these regions are termed G1-G5 and are highly conserved across the Ras superfamily, although the G5 motif is less well conserved among other GTP-binding proteins. Figure 1.2 depicts the location and sequences of these key GTP-binding motifs.

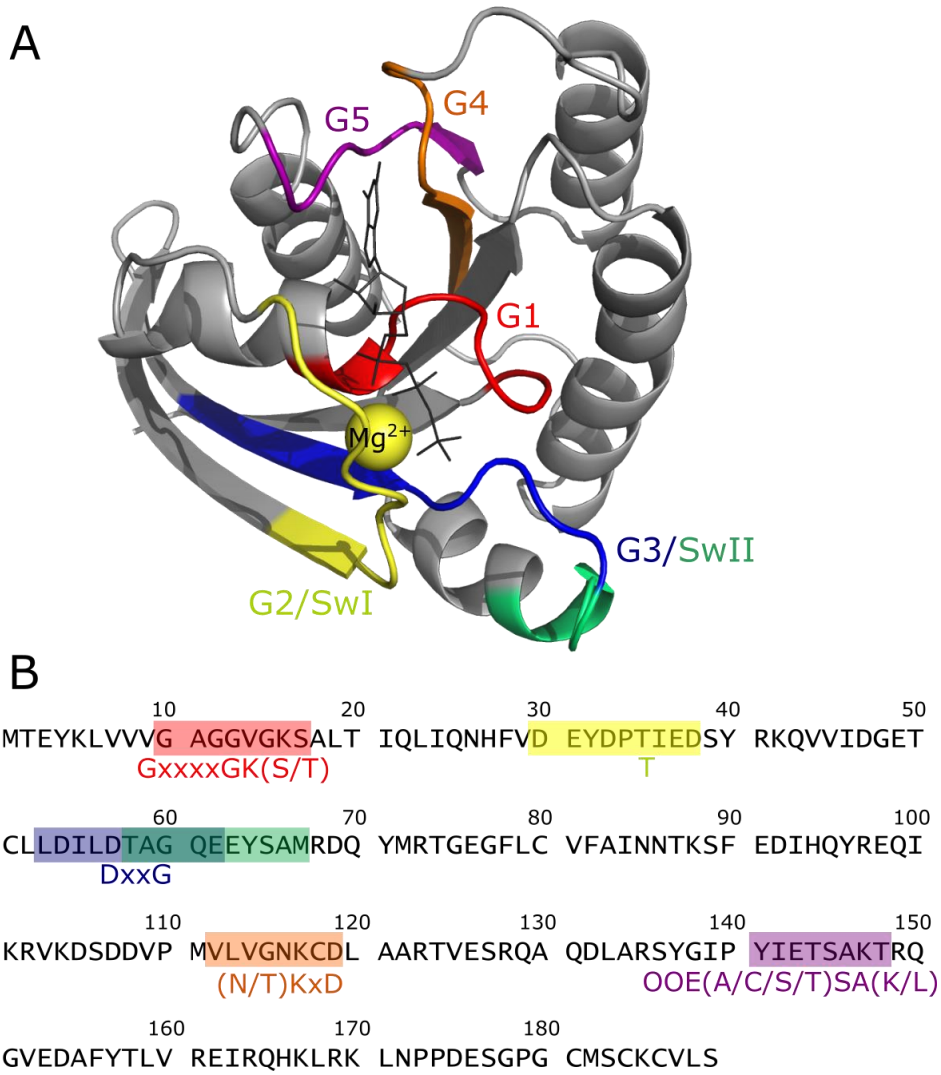


**Figure 1.2. The G domain. A.** The crystal structure of H-Ras in complex with GMPPCP, a very slowly hydrolysing analogue of GTP (PDB ID: 121P). G1 is coloured red, G2/switch I (SwI) yellow, G3 blue, switch II (SwII) green, G4 orange and G5 purple. The magnesium cation is shown as a yellow sphere. **B.** The sequence of H-Ras, with the G1-5 regions and switch II coloured as in A. The conserved motifs for each sequence are written underneath in the corresponding colour. O represents a hydrophobic amino acid.

G1, also known as the P loop (for phosphate-binding), contains the sequence GxxxxGK(S/T) and is found at residues 10-17 in Ras proteins. Several backbone amides in G1 contact the phosphate groups of GTP, as does the side-chain amine of Lys16 which forms hydrogen bonds with the β- and γ-phosphates. G2 contains a single threonine residue that is conserved among GTP-binding proteins; this critical residue (Thr35 in Ras) co-ordinates the magnesium cation through its side chain and forms a hydrogen bond with the γ-phosphate of GTP via its backbone amide. G3 (Ras residues 53-62) contains a DxxG motif. Within this motif, the

aspartate residue co-ordinates the magnesium cation while the glycine backbone amide interacts with the γ-phosphate of GTP. The G3 region also contains a highly conserved glutamine at position 61 (Ras numbering), which can co-ordinate a water molecule in a position poised to attack the terminal phosphate bond for GTP hydrolysis. The G4 motif (residues 112-119) is the main determinant of guanine nucleotide base specificity and contains the conserved sequence (N/T)KxD. The aspartate side chain forms hydrogen bonds with the guanine ring, while the asparagine and lysine residues stabilize the G1 loop. Finally, G5 (Ras residues 141-148) is comprised of the motif OOE(A/C/S/T)SA(K/L), where O represents hydrophobic amino acids. Several residues in this region stabilize the conformation of the G4 region, while the alanine (Ras residue 146) forms a hydrogen bond with the guanine base. The interactions made by small GTPases with GTP are summarised in Figure 1.3.

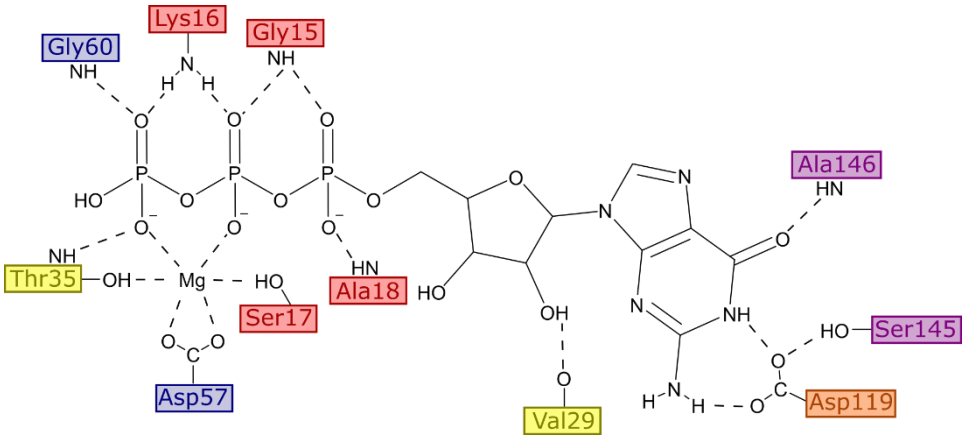


**Figure 1.3. Interactions made with GTP by the G domain.** The interactions made by Ras with GTP are shown. These interactions are conserved across all small GTPases, though residue numbering differs. Residues are coloured as in Figure 1.2. Figure adapted from Bourne *et al.* (5).

### 1.2.3 The GTPase switch

The first crystal structures of a small GTPase in the active and inactive conformations were published for H-Ras in 1990 (6). Comparison of these structures revealed the major conformational differences that give rise to their different activities. The main changes occurred in residues 30-38 and 59-67, comprising flexible regions that were termed switch I and switch II, respectively. These regions are highlighted in Figure 1.4. It is now known that

the vast majority of effector and regulatory proteins bind to one or both of these regions in order to sense the nucleotide status of the GTPase. Despite an apparent lack of sequence similarity across families, switch I and switch II sequences are highly conserved within small GTPase subfamilies.

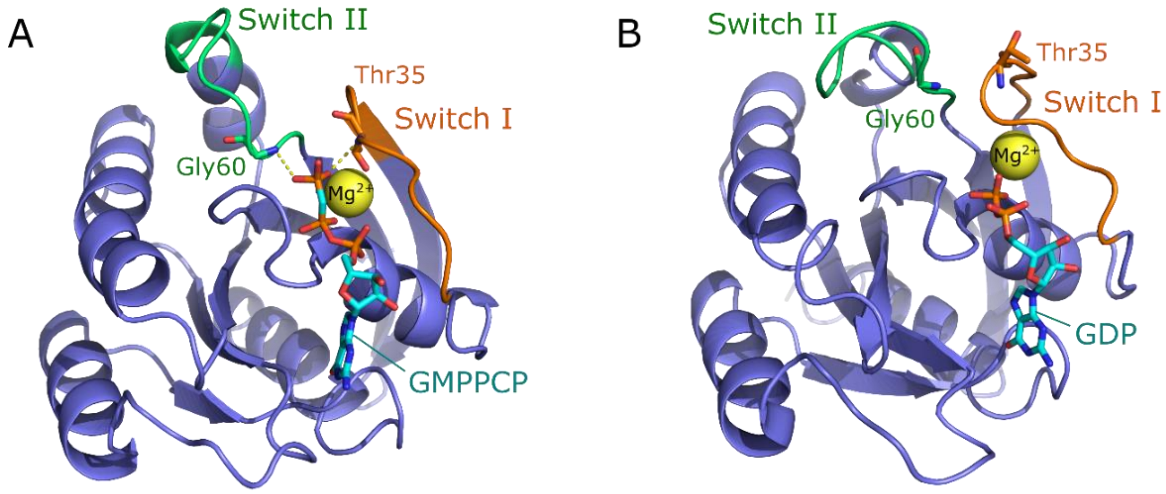


**Figure 1.4. Comparison of the active and inactive forms of H-Ras.** Conformations of active, GMPPCP-bound (**A**, PDB ID: 121P) and inactive, GDP-bound (**B**, PDB ID: 1AA9) H-Ras (blue; switch I, orange; switch II, green). The magnesium ion is represented as a sphere, and the nucleotide is shown as sticks.

Within the switch regions, residues Thr35 and Gly60 (Ras numbering) are universally conserved among the superfamily and are critical to the conformational changes observed; these residues contact the γ-phosphate of GTP in a 'loaded spring' mechanism that is released upon hydrolysis of the nucleotide (Figure 1.4). The GTP-bound state is therefore more structured, while the GDP form is considered the 'relaxed' state. This is supported by the observation that structures of the GTP-bound proteins are highly similar, while the GDP-bound structures show a greater degree of flexibility and variation between different GTPases (reviewed in (7)).

### 1.2.4 Membrane-targeting post-translational modifications

The majority of Ras and Rho family proteins terminate in a C-terminal CAAX box (C = cysteine, A = any aliphatic amino acid, X = any amino acid), which is modified at the cysteine residue by

an isoprenyl group. This modification is catalysed by farnesyltransferase (FTase) or geranylgeranyltransferase (GGTase), which add a farnesyl or geranylgeranyl isoprenoid group, respectively. The specific modification is determined by the sequence of the CAAX box.

Most Rab proteins are prenylated by GGTase II, and these proteins terminate with CC, CXC, CCX, CCXX or CCXXX sequences. Arf family proteins are not prenylated and instead are modified by myristoylation at an N-terminal glycine residue. The various modifications described serve to target the small GTPases to specific cellular membranes. These lipid anchors are often supported by a second membrane-targeting signal, for example polybasic regions made up of several lysine and arginine residues are observed for many Ras proteins, as are palmitoylation sites close to the C-terminus. Localization at cell membranes is essential for the biological activity of these small GTPases. Ran is not lipid-modified and is the only superfamily member that does not require membrane association for downstream signalling.

### 1.3 Differences in the structures of small GTPases

In addition to their relatively rigid G domain, many small GTPases contain flexible N- and C-terminal extensions. These are excluded from many published structures due to degradation of the flexible regions during purification and because they cannot be resolved by X-ray crystallography. These regions are often the sites for post-translational modifications including palmitoylation, prenylation and phosphorylation, and play a critical role in the regulation and localization of small GTPases. The structures of the small GTPases differ in these regions and some families also show differences in the G domain. The major characteristic differences are highlighted in Figure 1.5.

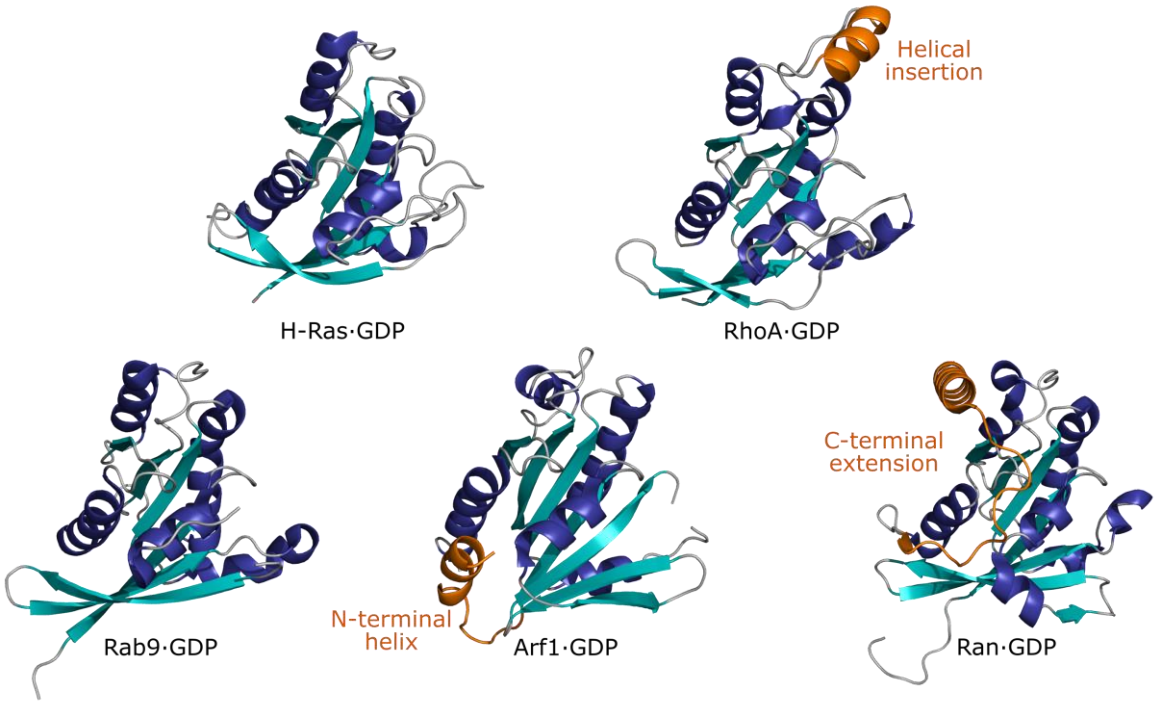


**Figure 1.5. Differences in the structures of Ras superfamily members.** Representative crystal structures from each family are shown; H-Ras·GDP (PDB ID: 1AA9), RhoA·GDP (1FTN), Rab9·GDP (1WMS), Arf1·GDP (1HVR) and Ran·GDP (3GJ0). Helices are coloured dark blue, β-strands light blue and loops grey. Structural differences compared to the core G domain structure of Ras proteins are highlighted in orange.

Arf proteins contain an N-terminal helical extension that is myristoylated at the N-terminus. This myristoyl modification is required for membrane binding and subsequent activation by GEFs (8). In GDP-bound structures the helix is held against the G domain in an auto-inhibited state (9), while in the GTP-bound state the helix is released from the G domain and can insert into the plasma membrane (10). Ran contains a helical C-terminal extension that is bound to the G domain in the GDP-bound state but is released upon GTP binding where it can interact with several binding partners (11, 12). The Rho family are distinctive as they contain a helical insertion of approximately 13 residues in the G domain (4). Rab proteins closely resemble the Ras proteins with no obvious extensions or insertions.

## 1.4 Effector proteins

Upon GEF-mediated exchange of GDP for GTP, small GTPases undergo structural rearrangements, primarily in the switch regions. These conformational changes result in the

formation of a binding surface with high affinity for their effector proteins. The presence of the interaction surface is transient, and signalling is switched off again by hydrolysis of GTP to GDP, assisted by GAPs. Each GTPase generally binds multiple effector proteins, resulting in a huge array of signalling pathways that are regulated by the small GTPases. There are currently more than 60 GTPase-effector complexes whose structures have been solved, revealing a variety of binding modes that are utilised by the effectors (reviewed in (13)). These interactions can be broadly classified by their structural elements as follows; those that bind via a β-sheet and form an extension to the β-sheet of the GTPase, interactions made via a pair of helices, effectors that bind through a pleckstrin homology (PH) domain and an 'other' group that do not fit into the aforementioned classifications (13). Examples of GTPase-effector binding modes are shown in Figure 1.6.

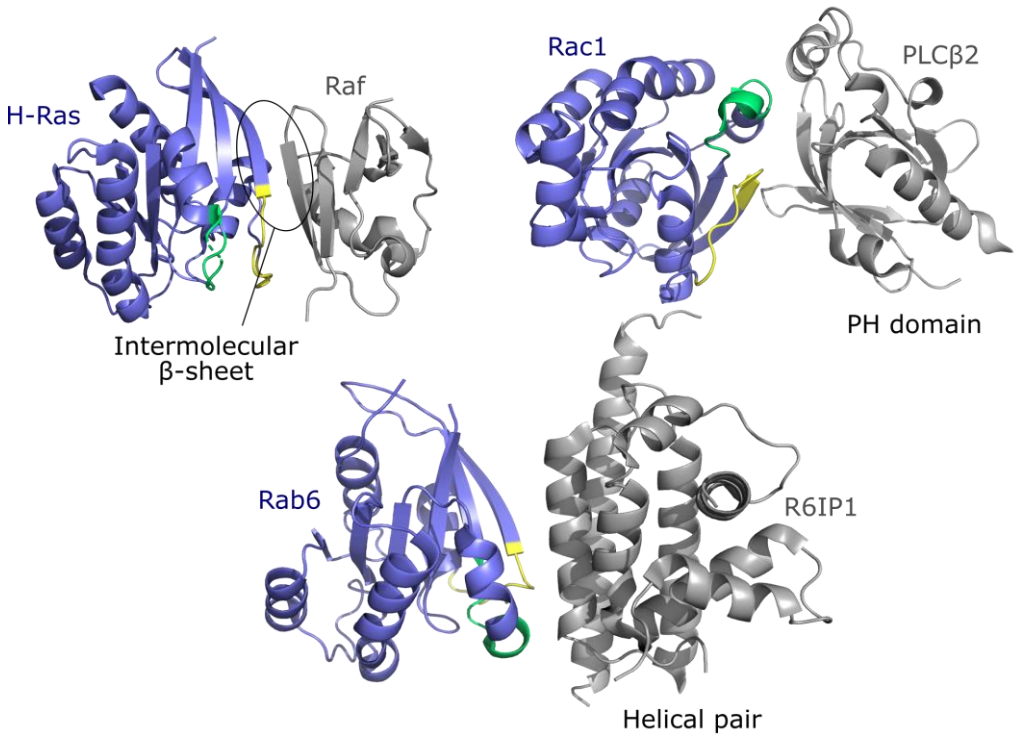


**Figure 1.6. GTPase-effector interactions.** Examples of the main structural classifications of Ras superfamily effector proteins are shown: interactions made via an intermolecular β-sheet (H-Ras/Raf, PDB ID: 4G0N), effectors that interact via a pleckstrin homology (PH) domain (Rac1/PLCβ2, 2FJU) and interactions made via a helical pair (Rab6/R6IP, 3CWZ). The small GTPase is shown in blue, with switch I coloured yellow and switch II coloured green, and the effectors are coloured in grey.

## 1.5 Ras proteins

The three *ras* genes encode four Ras proteins; N-Ras, H-Ras, and two splice variants of K-Ras, K-Ras4A and K-Ras4B. The first *ras* genes to be discovered, viral H-Ras and K-Ras, were identified in 1980s as the products of retroviral oncogenes that had been transduced from the host genome by Harvey and Kirsten rat sarcoma viruses (14, 15). Shortly after, DNA mapping and sequencing technologies allowed the identification of oncogenic *ras* genes in human tumours (16).

The Ras proteins are highly conserved throughout the G domain but exhibit significant variation in the C-terminal hypervariable region (HVR). This region contains the sites for post-translational modifications that are required for membrane localization. The Ras proteins terminate in a CAAX box, where C = cysteine, A = an aliphatic amino acid and X = Ser or Met; the cysteine residue is the target for prenylation by farnesyltransferase (FTase). In addition to farnesylation, a second membrane signal is required for stable membrane association (17, 18). For K-Ras4A, N-Ras and H-Ras, this second signal comes in the form of additional cysteine residues that are palmitoylated, while K-Ras4B contains a polybasic region of six lysine residues that interact with negative phosphate head groups in the phospholipid bilayer. The differences in the C-terminal sequences and post-translational modifications of the Ras proteins are shown in Figure 1.7.

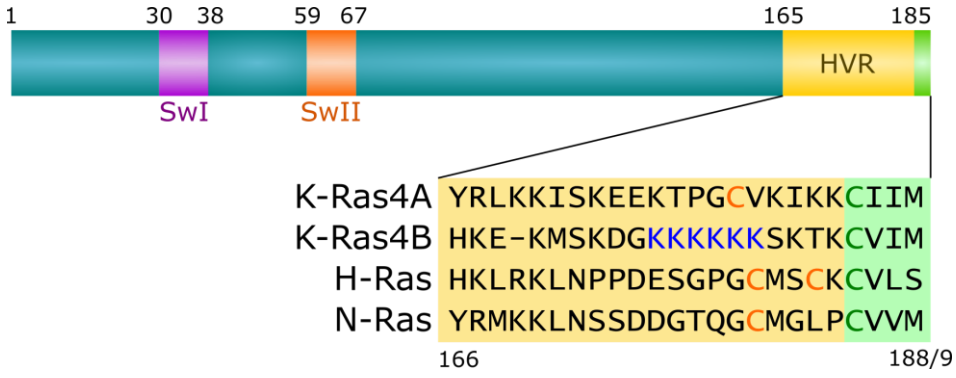


**Figure 1.7. Variation at the C-termini of Ras proteins.** All Ras proteins terminate in a CAAX box in which the cysteine residue (green) is modified by FTase. For stable membrane association, a second signal is required: in K-Ras4A, H-Ras and N-Ras, additional cysteine residues are modified by palmitoylation (orange), while K-Ras4B contains a polybasic region comprised of six lysine residues (blue) to aid membrane association. SwI, switch I; SwII, switch II; HVR, hypervariable region.

Following farnesylation, several additional processing steps are required for membrane-targeting of Ras proteins. The three C-terminal residues are cleaved by Ras-converting endopeptidase I (RCEI), leaving the farnesylated cysteine at the C-terminus (19). This residue is then methylated by isoprenylcysteine carboxylmethyltransferase (ICMT) (20, 21). All of these modifications are required for stable membrane association and activity of Ras proteins. The process is summarised in Figure 1.8.

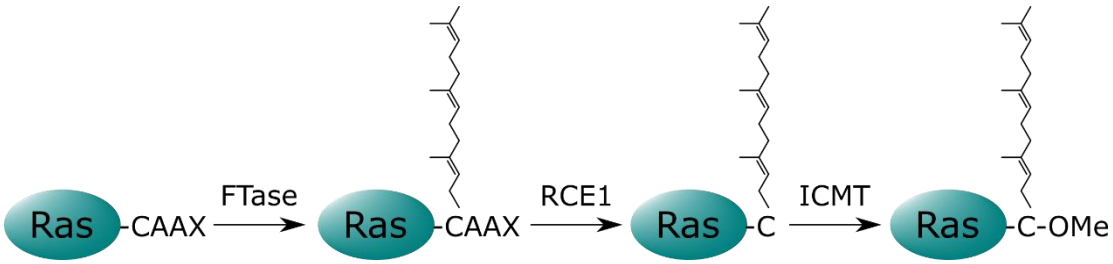


**Figure 1.8. Post-translational processing of Ras proteins.** Ras proteins terminate in a CAAX box (C = Cys, A = aliphatic amino acid, X = Ser or Met). The cysteine residue of the CAAX box is prenylated by farnesyltransferase (FTase), catalysing the addition of a 15-carbon lipid moiety. The three C-terminal residues are then cleaved by Ras-converting endopeptidase I (RCEI) and a methyl group is appended to the C-terminus by isoprenylcysteine carboxylmethyltransferase (ICMT).

### 1.5.1 Ras activation

The Ras proteins are activated in response to growth factor stimulation (22). Binding of growth factors to their receptors stimulates rapid dimerization and autophosphorylation at intracellular tyrosine residues (23, 24). The Grb2 adaptor protein binds specific phosphorylated tyrosines on the receptor via its SH2 domain. Grb2 mediates recruitment of the RasGEF, son of sevenless 1 (SOS1), to the plasma membrane where it can activate membrane-bound Ras by mediating exchange of GDP for GTP (25). The process of SOS1-mediated activation is shown in Figure 1.9. While SOS1-mediated exchange is the most-studied form of Ras activation, several other RasGEFs exist and are activated in very different ways (22).

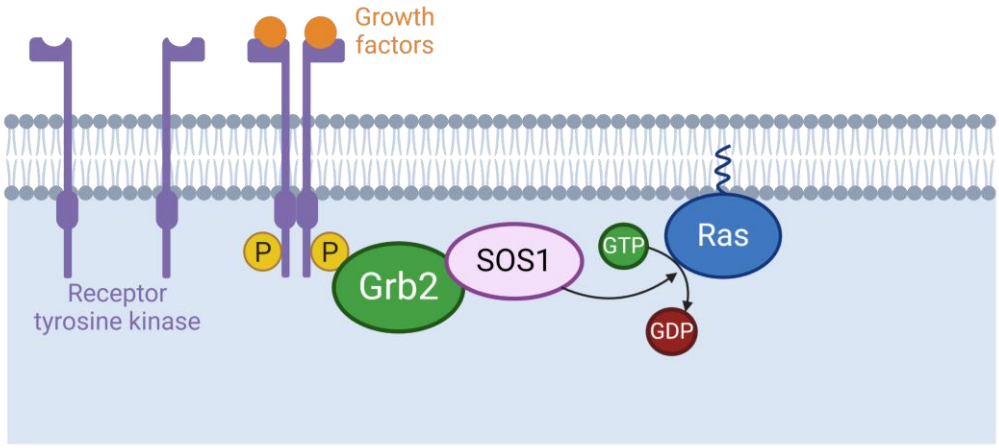


**Figure 1.9. Activation of Ras by SOS1.** Growth factor binding to the target receptor tyrosine kinase (RTK) results in dimerization and autophosphorylation of the receptors. Grb2 binds specific phosphorylated tyrosines on the receptor via its SH2 domain and recruits SOS1 to the plasma membrane. SOS1 is then in proximity to membrane-bound Ras and can catalyse the exchange of GDP for GTP on Ras, allowing it to adopt its active state. Figure created with BioRender.com.

### 1.5.2 Effector pathways

Following activation by SOS1, the Ras proteins bind and activate several downstream effector proteins. Through these many signalling pathways, the Ras proteins regulate cellular proliferation, survival and numerous other processes. The major effector pathways controlled by Ras proteins are summarised in Figure 1.10.

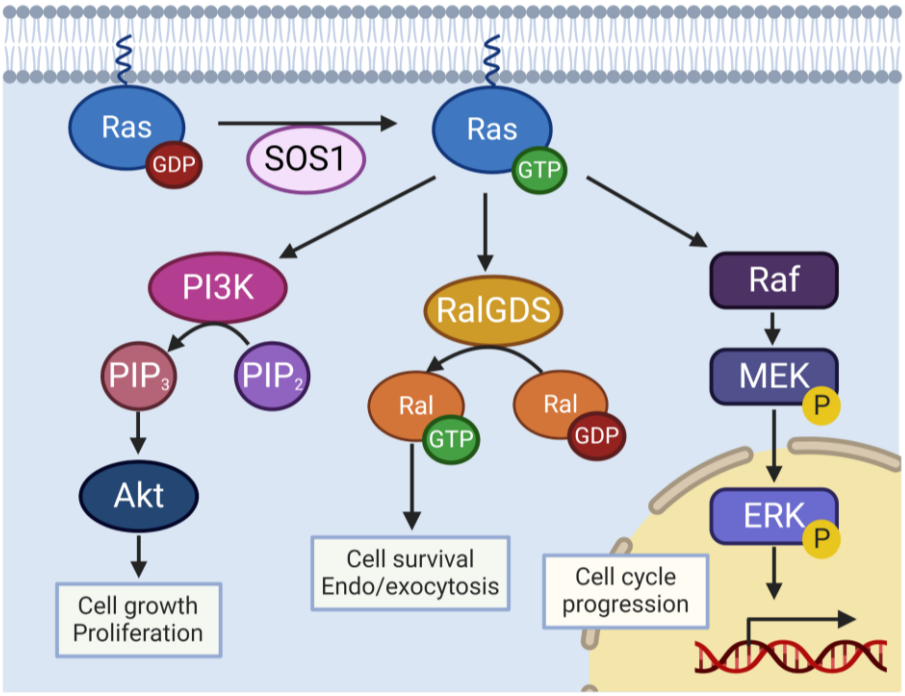


**Figure 1.10. Major Ras effector pathways.** Upon activation by SOS1, Ras proteins can interact with multiple downstream effectors, including PI3K, RalGDS and Raf. Activation of PI3K results in the conversion of $PIP_2$ to $PIP_3$, in turn activating Akt to phosphorylate a range of targets controlling cell growth and proliferation. Binding to RalGDS catalyses the exchange of GDP for GTP on the Ral proteins. Signalling through Ral effectors controls cell survival, exo- and endocytosis. Ras association with Raf activates the MAPK (mitogen-activated protein kinase) signalling pathway, resulting in the phosphorylation by ERK of transcription factors that control cell cycle progression. Figure created with BioRender.com.

The first Ras effector to be characterised was the Raf serine/threonine kinase (26, 27). Upon Ras activation, the Raf proteins undergo dimerization, leading to their activation. This begins a mitogen-activated protein kinase (MAPK) signalling cascade in which Raf phosphorylates and activates MEK (mitogen-activated protein kinase kinase), which in turn phosphorylates ERK (mitogen-activated protein kinase). Activated ERK can phosphorylate several targets in the cytoplasm and the nucleus, including transcription factors that control cell cycle progression.

The PI3K pathway is also activated downstream of Ras (28). Upon activation, PI3K converts phosphatidylinositol (4,5)-bisphosphate ($PIP_2$) to phosphatidylinositol (3,4,5)-trisphosphate ($PIP_3$). $PIP_3$ then binds and leads to the activation of Akt, resulting in the phosphorylation of a range of targets affecting cell survival and proliferation.

Active Ras proteins also bind RalGDS, a GEF for the Ral small GTPases: RalA and RalB. Upon activation, the Ral proteins engage a panel of effector proteins involved in cell proliferation, survival and the regulation of endo- and exocytosis (29). The RalGEF-Ral pathway will be discussed in detail in section 1.7. In addition to the three main effector pathways, many other effectors for Ras proteins have been identified including Tiam1, PLCε, Af6, Nore1 and Rin1 (26).

### 1.5.3 Role of Ras proteins in cancer

The *ras* genes are well-known as the most commonly mutated oncogenes in human cancer, occurring in approximately 20% of human cancers and with higher incidences in pancreatic (88%), lung (33%) and colorectal cancers (55%) (30). K-Ras is the most frequently mutated *ras* gene, accounting for 75% of all Ras-mutant cancers, followed by N-Ras (17%) and H-Ras (7%). The vast majority of Ras mutations occur at positions 12, 13 and 61, although the frequency of mutations at each position varies greatly between the isoforms (30). The positions of these mutations on the structure of Ras are shown in Figure 1.11. Mutations to these residues result in constitutive activation of the Ras protein due to impaired intrinsic and GAP-mediated hydrolysis (16, 31). This deregulated signalling through downstream effector pathways leads to uncontrolled cell growth and proliferation, resulting in the formation of tumours.

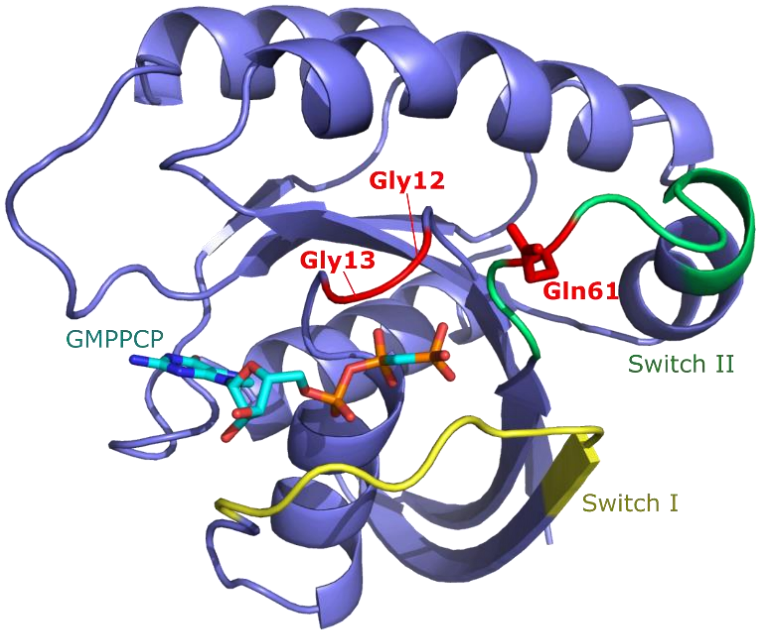


**Figure 1.11. Commonly occurring Ras mutations.** The positions of the most commonly occurring Ras mutations, at positions 12, 13 and 61 are highlighted in red on the structure of H-Ras bound to GMPPCP (PDB ID: 121P). Mutations at these positions impair intrinsic and GAP-stimulated GTP hydrolysis.

## 1.6 Attempts to target Ras therapeutically

Despite their pivotal role in cancers being known for nearly four decades, there are currently no approved therapeutics that target Ras proteins directly. While intense efforts have been made in this area, several features of Ras proteins make them challenging to target through traditional methods of drug discovery, leading them to be long considered 'undruggable'. However, in recent years, several innovative approaches to target Ras proteins have been developed and will be explored in the following sections.

In contrast to the success that has been attained with ATP-competitive inhibitors for kinases, the picomolar affinity exhibited by small GTPases for their nucleotides (32), along with high intracellular GTP concentrations of ~1 mM, makes the nucleotide binding site of these proteins an intractable target for competitive inhibitors. Disruption of GTPase interactions with their regulators or effector proteins has also proven challenging as these conventional protein-protein interactions (PPIs) are mediated by relatively large, smooth surfaces that lack distinct binding pockets for small molecules. Attempts to inhibit post-translational processing have also failed due to the emergence of compensatory mechanisms (33).

### 1.6.1 Disruption of membrane localization

Inhibition of membrane association to disrupt Ras signalling was one of the earliest avenues to be explored. Farnesyltransferase inhibitors (FTIs) were developed to block prenylation of the Ras C-terminus and hence the membrane association that is required for transformation (34). Unfortunately, FTIs failed in clinical trials and it was later discovered that K-Ras and N-Ras, the isoforms most commonly mutated in human cancers, can undergo alternative prenylation by GGTase I in the presence of FTIs (33). Dual inhibition of both enzymes is not expected to be feasible due to their large number of targets, which is likely to lead to toxic side effects. Unlike the other Ras isoforms, H-Ras cannot undergo alternative prenylation by GGTase I and could therefore be targeted by competitive FTIs (33). The use of FTIs to target certain H-Ras mutant cancers is currently being investigated in the clinic (35, 36).

Novotny *et al.* have recently reported an alternative method to mislocalize Ras proteins; they developed neo-substrates of FTase which modify K-Ras but do not allow for subsequent membrane attachment (37). Their neo-substrates could be covalently added to K-Ras by FTase at the cysteine residue of the CAAX box in place of the typical farnesyl modification. This modification prevented further processing and membrane attachment, resulting in cytoplasmic localization of K-Ras. This approach circumvents issues previously seen with FTIs as this modified K-Ras cannot be alternatively prenylated by GGTase I, offering a promising new avenue to target Ras signalling. The mechanism of action is summarised in Figure 1.12.

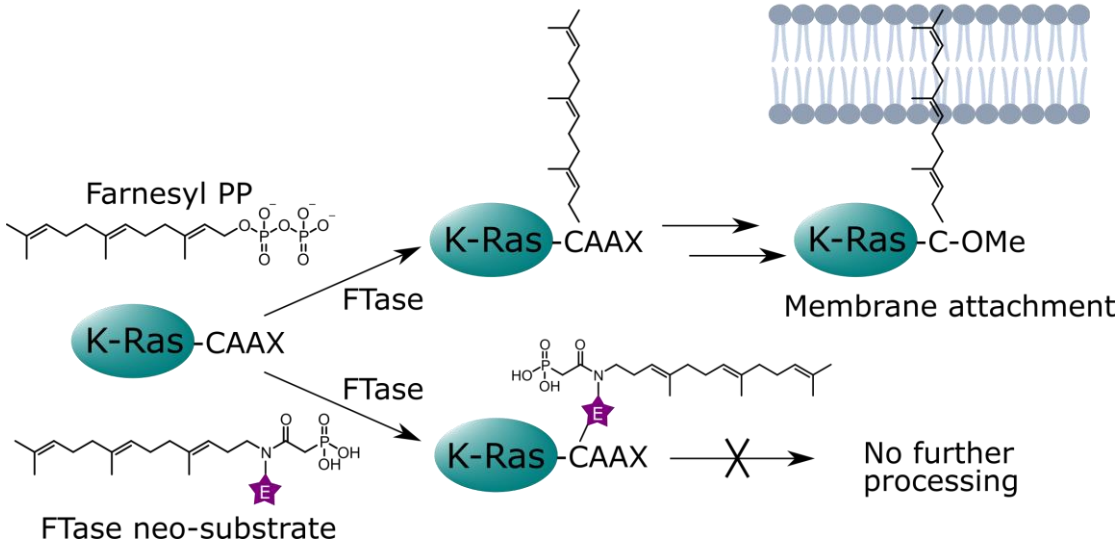


**Figure 1.12. Neo-substrates for FTase developed by Novotny *et al*.** FTase catalyses the addition of farnesyl pyrophosphate (PP) to a cysteine residue in the CAAX box of K-Ras. This is followed by further processing, resulting in membrane attachment of K-Ras via the lipid anchor. The neo-substrates developed by Novotny *et al.* resemble farnesyl PP but contain an electrophile (E) that reacts with the cysteine residue in the presence of FTase. This modification prevents any further modification of K-Ras and therefore prevents subsequent membrane attachment.

### 1.6.2 Peptide inhibitors of Ras

Peptides offer an enticing opportunity for the inhibition of PPIs as they offer excellent selectivity and target binding affinity even at relatively smooth protein surfaces, due to the large area that they occupy. In this way they retain many of the advantages of larger biologics, while their smaller molecular weight enables the possibility of cell entry. Initially peptides were limited to extracellular targets, however developments in the use of cell-penetrating peptides and research into intrinsic properties that invoke cell uptake have opened up the peptide druggable space to encompass intracellular proteins including Ras.

#### 1.6.2.1 Inhibitors of the Ras-SOS1 interaction

Peptides have been used to target the interaction of Ras proteins with the RasGEF, SOS1, hence blocking Ras activation. Patgiri *et al*. noted that within the helical hairpin region of SOS1, the majority of contacts with K-Ras are made by one helix, αH (Figure 1.13A) (38). Computational models combined with mutagenesis data revealed that residues 929-944 were the most critical for binding. They designed a peptide based on this sequence and utilised a

hydrogen bond surrogate (HBS) approach in which the hydrogen bond between the backbone carbonyl of the N-terminal residue and the amine of the N + 4$^{th}$ residue is replaced with a covalent bond to stabilize a helical conformation of the peptide (39). The resulting peptide, HBS3 (Figure 1.13B), had an affinity of 28 µM for nucleotide-free Ras and was able to inhibit SOS1-mediated exchange of GDP for GTP *in vitro*.

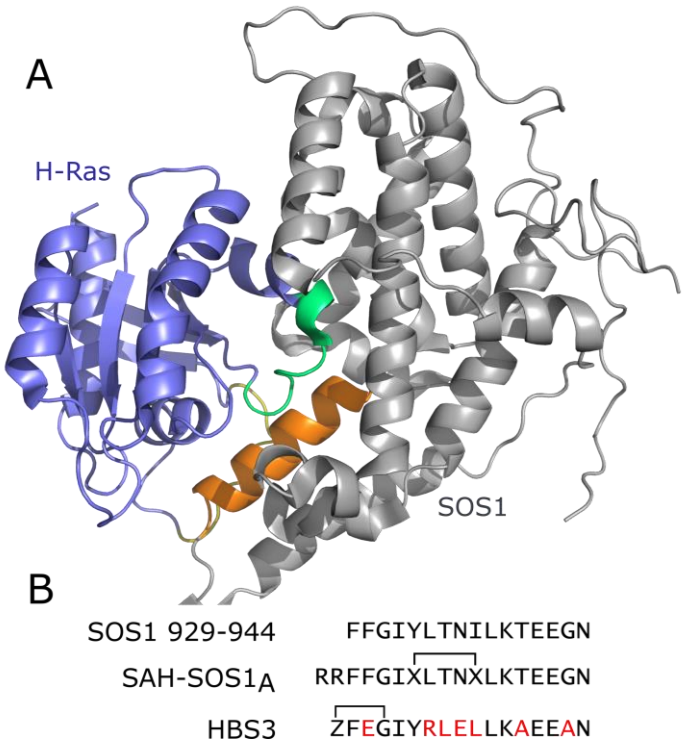


**Figure 1.13. Helical peptides targeting the Ras-SOS1 interaction. A.** Crystal structure of nucleotide free H-Ras (blue; switch I, yellow; switch II, green) in complex with SOS1 (grey, PDB ID: 1NVW). Residues 929-944 of SOS1 are coloured in orange. **B.** Peptides generated based on SOS1. X, (*S*)-pentenylalanine; Z, 4-pentenoic acid. Substitutions from the SOS1 sequence are shown in red.

Walensky and colleagues also generated peptides based on the same helical portion of SOS1, instead using all-hydrocarbon peptide stapling to stabilize a helical structure (40). Their lead peptide, SAH-SOS1$_A$ (Figure 1.13B) bound wild-type and mutant forms of K-Ras with affinities between 60 and 100 nM and was shown to block intrinsic nucleotide exchange, however it was not reported whether the peptides could also inhibit SOS1-mediated exchange. The validity of this peptide as a K-Ras inhibitor has recently been brought into question, as when Ng *et al.* thoroughly interrogated the binding of the peptide, they found it to be non-specific

(41). This study highlighted important considerations for the validation of peptides in orthogonal assays.

### 1.6.2.2 Macrocyclic Ras inhibitors derived from naïve selections

A group at Takeda in Japan have developed cyclic peptide inhibitors of the K-RasG12D mutant using phage display to screen naïve libraries. From these selections they identified a disulphide-linked cyclic peptide, KRpep-2d (Figure 1.14A), which displayed a low nanomolar affinity for K-RasG12D and impressive selectivity over wild-type K-Ras (42). The peptide decreased phospho-ERK levels downstream of Ras in a K-RasG12D mutant cancer cell line but had no effect in a K-RasG12C mutant background, demonstrating selectivity for the targeted mutant. The group went on to solve the crystal structure of KRpep-2d in complex with K-RasG12D·GDP (43). Despite being observed to inhibit GEF-mediated exchange, the peptide binding site was found to be distinct from the SOS1 binding interface. Instead, KRpep-2d occupies an allosteric site on K-Ras, adjacent to switch II, and forces switch II into a conformation that is unfavourable for binding SOS1 (Figure 1.14B and C).

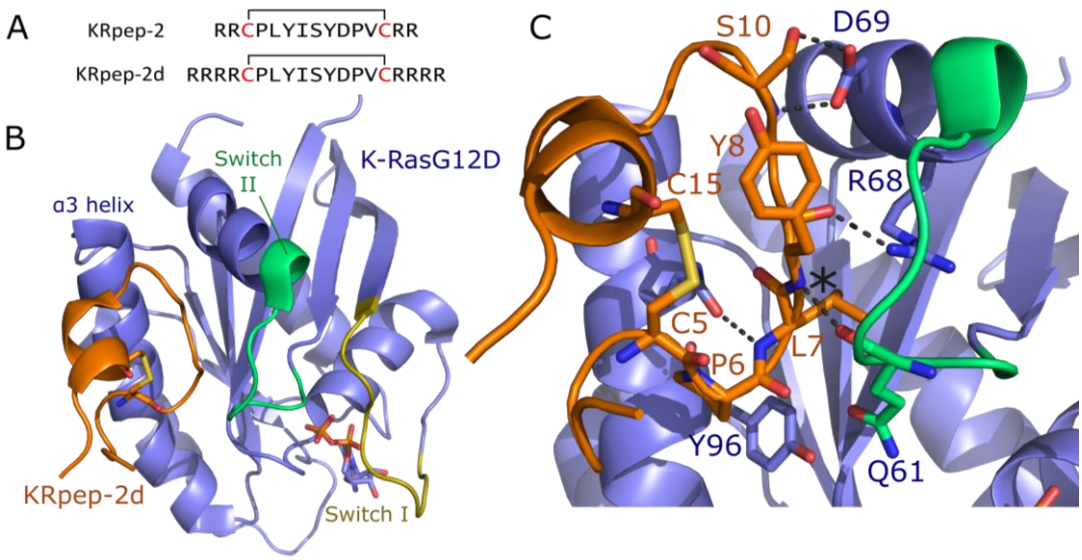


**Figure 1.14. Cyclic peptide KRpep-2d binding to K-Ras. A.** Sequences of KRpep-2 and KRpep-2d. Cysteine residues that cyclize the peptide are highlighted in red. **B.** Crystal structure of KRpep-2d bound to K-RasG12D·GDP (PDB ID: 5XCO). K-Ras is shown in blue, with switch I (yellow) and switch II (green) highlighted. The GDP nucleotide is shown as sticks. The peptide (orange) binds at a site proximal to switch II and the α3 helix. **C.** Zoom of the structure with contacts formed between KRpep-2d and K-Ras shown as dashed lines, including a hydrogen bond between the backbone NH of KRpep-2d Tyr8 and the backbone carbonyl of Gln61 on K-Ras (indicated by *).

The Pei group has generated several cyclic peptides targeting K-RasG12V using synthetic libraries. Their first library incorporated a rapamycin analogue or 'rapalog', a minimal motif to recruit FK502-binding protein 12 (FKBP) (44, 45). The recruitment of the 12 kDa FKBP protein was used to create a steric block which extended further than the small peptide and therefore could prevent effector binding if oriented correctly. The most promising peptide identified, compound 12 (Figure 1.15A), had a $K_d$ of 0.83 µM for K-RasG12V and was able to inhibit a panel of Ras-effector interactions, although no cellular activity was observed due to poor uptake of the peptide.

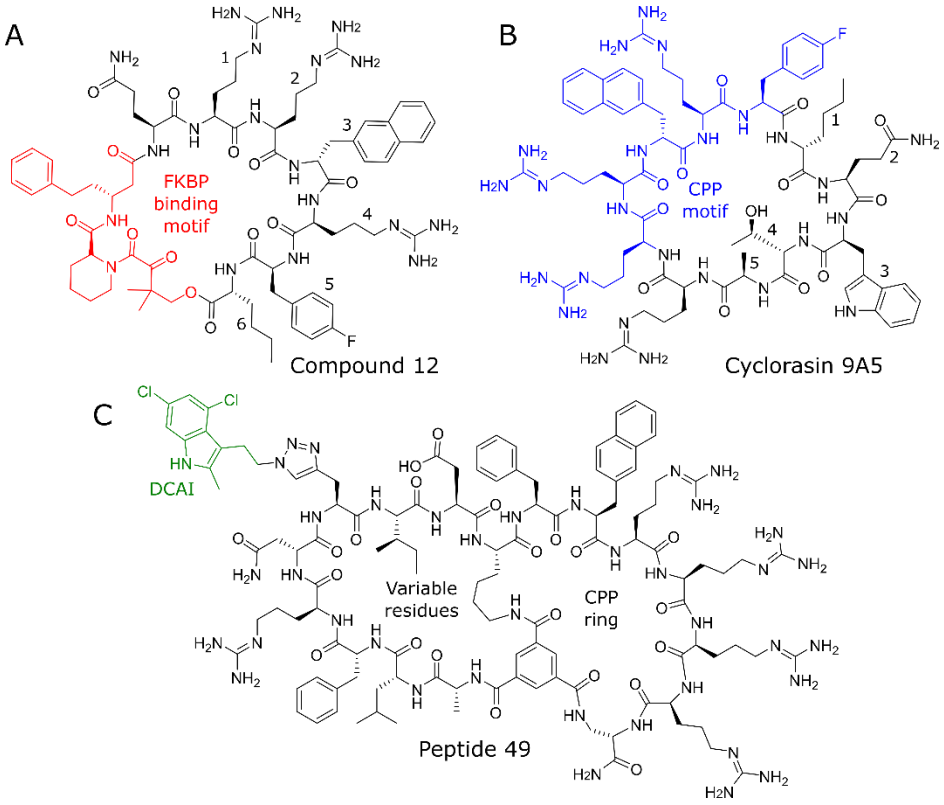


**Figure 1.15. Macrocyclic Ras inhibitors derived from synthetic screens. A.** Compound 12 identified from a screen of cyclic peptides incorporating a FKBP binding motif (red). Amino acid positions varied in the screen are labelled 1-6. **B.** Structure of Cyclorasin 9A5, a cyclic peptide identified from a library of peptides containing a CPP sequence identified previously (blue) and up to 5 variable amino acid positions (labelled 1-5). **C.** Structure of an optimized hit from a bicyclic library screen, peptide 49. DCAI, 4,6- dichloro-2-methyl-3-aminoethylindole, a K-Ras inhibitor (green).

The apparent lack of cellular uptake for compound 12 was surprising as it contained an Arg-Arg-Nal-Arg-Fpa (Nal = D-β-naphthylalanine, Fpa = L-4-fluorophenylalanine) sequence which

closely resembled potent cell-penetrating peptides (CPPs) previously identified by the group (46). A second synthetic cyclic library to search for intrinsically cell penetrant K-RasG12V inhibitors was constructed incorporating the Arg-Arg-Nal-Arg-Fpa core sequence (47). A hit from this selection was optimized to give a cell-permeable peptide, Cyclorasin 9A5 (Figure 1.15B), which displayed diffuse cytosolic localization. However, like the all-hydrocarbon stapled peptide SAH-SOS1$_A$, the binding of this peptide was independently shown to be non-specific (41).

The same group also used a synthetic library of bicyclic peptides to identify inhibitors of K-RasG12V (48, 49). In one such library they generated a scaffold in which one ring encompassed a cyclic CPP previously identified by the group, FΦR$_4$, where Φ is L-2-napthylalanine (46), and the second ring contained five variable positions to generate target binding affinity. A previously identified K-Ras small molecule inhibitor, 4,6-dichloro-2-methyl-3-aminoethylindole (DCAI), was coupled to the peptides using click chemistry. The optimized peptide 49 (Figure 1.15C) was shown to be competitive with the Raf RBD but displayed little preference for the nucleotide state of K-RasG12V. This is surprising given that Raf binds at the switch regions on Ras which change conformation dramatically depending on whether K-Ras is bound to GDP or GTP.

### 1.6.3 Covalent inhibitors of K-RasG12C

There has been remarkable success recently in generating small molecule inhibitors for the K-RasG12C mutant, as Shokat and colleagues identified a small pocket beneath switch II which they were able to exploit to generate covalent inhibitors targeting the Cys12 residue (50). Crystal structures of the modified K-RasG12C revealed the presence of a binding pocket which was not visible in the known structures of K-RasG12C and is instead induced upon compound binding (Figure 1.16A). The pocket is only formed in the GDP-bound K-RasG12C, and the presence of GTP was found to significantly decrease compound binding.

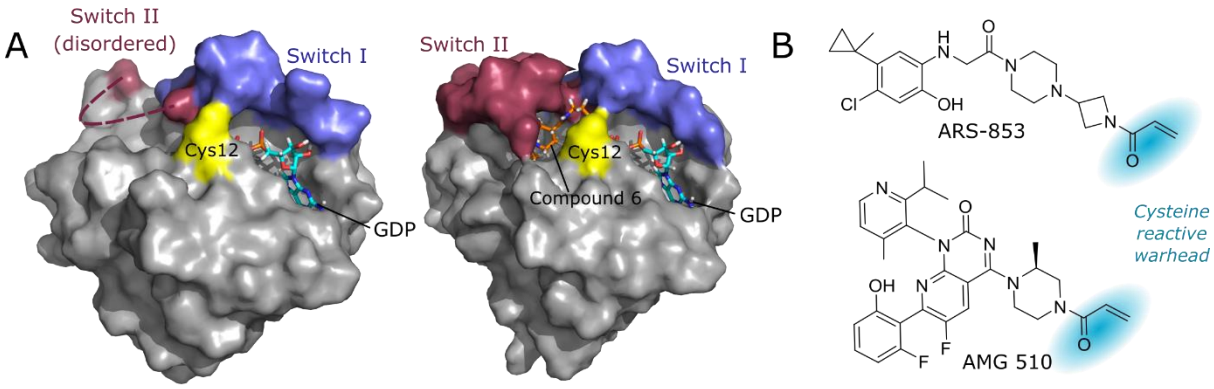


**Figure 1.16. Covalent inhibitors of K-RasG12C. A.** Structures of K-RasG12C·GDP alone (PDB ID: 4L8G) and in complex with a fragment covalently bonded to Cys12 (4LV6) reveal a binding pocket that is formed upon fragment binding. K-RasG12C is shown in grey; switch I (30-38), blue; switch II (59-67), mauve; Cys12, yellow; GDP, cyan sticks; compound 6, orange sticks. **B.** Covalent inhibitors of the K-RasG12C mutant. The warhead able to form a covalent bond with the Cys12 residue is highlighted in blue.

Patricelli *et al.* generated a series of compounds targeting this novel pocket and identified a covalent inhibitor, ARS-853 (Figure 1.16B), with improved potency (51). In this work, they challenged the previously held view that K-RasG12C is 'locked' in the active, GTP-bound state, and instead showed the mutant to be fast-cycling, revealing a therapeutic opportunity to target the inactive state of the protein. The group have reported a second series of inhibitors with *in vivo* efficacy in mouse models and oral bioavailability (52). Amgen have also developed a series of covalent inhibitors exploiting this same binding pocket of K-RasG12C and their inhibitor (AMG 510, Figure 1.16B) has passed Phase I clinical trials (53, 54).

The use of covalent inhibitors to target PPIs offers many advantages: they benefit from non-equilibrium kinetics, enabling the possibility of complete target occupancy even for compounds with modest reversible binding affinities (55). Additionally, covalent inhibitors cannot be displaced by competition with native binding partners and substrates. However, their application is limited to reactive residues at therapeutically relevant sites, for example mutants that result in an exposed cysteine residue. G12C mutations in K-Ras-driven cancers are relatively infrequent, where G12D and G12V mutations predominate (30, 56). A different picture is seen in lung cancers, however, where G12C mutations are the most common due to G:C>T:A transversions associated with mutagens found in tobacco smoke (57).

### 1.6.4 Inhibition of Ras dimerization

For years there has been conflicting data as to whether Ras functions as a monomer or if it needs to form higher order structures for its activity. There is now mounting evidence that Ras needs to form dimers or clusters in a cell in order to signal (reviewed in (58)). The α4 and α5 helices, which are distal from the switch regions, have been implicated as the drivers of dimer formation, as the vast majority of active Ras crystal structures dimerise via these helices (59). Inhibition of this interface using a monobody, a small synthetic protein based on a fibronectin type III domain, slowed tumour growth and progression in a mouse model bearing K-Ras mutant tumours (59, 60).

Designed ankyrin repeat proteins (DARPins) have also been used to inhibit Ras dimer formation through an interaction involving the α3-α4 helices of K-Ras, which have also been implicated as a possible interface for dimer formation (61, 62). Bery *et al.* used phage display with DARPin libraries to identify inhibitors of K-Ras, and an X-ray structure of one of their hits revealed that the DARPin interacts with the α3-α4 helices of K-Ras (63). The DARPin was able to inhibit mutant K-Ras dimerization as well as inhibiting K-Ras/Raf interactions, leading to a decrease in signalling.

These insights provide a novel opportunity to inhibit Ras signalling through disruption of multimer formation, however the approach may be limited, as a dimer-targeting tool is unlikely to be able to discriminate between wild-type and mutant Ras proteins.

### 1.6.5 Targeting pathways downstream of Ras

Difficulties in targeting Ras directly have led many to turn to inhibiting targets downstream of Ras instead. These attempts have mainly focussed on the Raf and PI3K pathways that contain several kinases amenable to ATP-competitive small molecule inhibition.

Many inhibitors have been developed targeting proteins within the Raf-MEK-ERK pathway, which is the best-characterised effector pathway of Ras. Raf is a key therapeutic target in itself, as activating BRaf mutations are found in around 18% of human cancers (COSMIC) and 40% of melanomas. Of these, the vast majority are V600E mutations. Two ATP-competitive inhibitors of BRaf are approved for the treatment of BRafV600E-mutant cancers including

melanomas (reviewed in (64)). However, these inhibitors have been ineffective in the treatment of Ras-mutant cancers due to an unexpected paradoxical activation of the Raf-MEK-ERK pathway in response to wild-type Raf inhibition (65, 66). Several MEK inhibitors have also been approved for the treatment of BRaf mutant melanomas, either alone or in combination with Raf inhibitors (67). These compounds are typically allosteric inhibitors rather than competing for ATP binding. While these inhibitors have been beneficial in the treatment of BRaf-mutant cancers, no therapeutic benefit has been seen in the treatment of Ras-mutant cancers. This is believed to be due to increased signalling through the PI3K and Raf pathways upon MEK inhibition (68, 69).

PI3K is another highly desirable cancer target, with mutations occurring in 20% of breast cancers (COSMIC). Several inhibitors for components of the PI3K pathway have been evaluated in the clinic, including ATP-competitive inhibitors for PI3K and mTOR (70). As is the case for MEK inhibitors, the use of PI3K pathway inhibitors as single agents to treat Ras-mutant cancers has been ineffective due to the multitude of signalling pathways that are upregulated and feedback mechanisms within the pathways. Combination trials to assess the efficacy of blocking components from both pathways are currently underway (71–74), however preliminary results have suggested that the combination is too toxic (75, 76).

Inhibition of the RalGEF-Ral pathway downstream of active Ras has been relatively underexplored to date, despite mounting evidence of the critical importance of this pathway for the survival of several Ras-mutant cancers (77). Ras activates a RalGEF (RalGDS), which in turn activates the Ral proteins, members of the Ras family of small GTPases (78). As this pathway involves protein-protein interactions mediated by small GTPases, targeting the pathway is likely to face many of the same challenges associated with targeting Ras directly. The biology of the RalGEF-Ral pathway and therapeutic attempts to target the Ral proteins will be explored in detail in the following sections.

### 1.7 Ral proteins

The two Ral (Ras-like) proteins, RalA and RalB, are members of the Ras family of small GTPases. They were first identified in 1986 through a simian cDNA library search for Ras-related genes, due to their sequence homology with Ras (>50%) (79). The Ral proteins are 206

amino acids in length and are highly similar proteins with 82% overall sequence identity. Their structures have been solved alone and in complex with several effector proteins, revealing a predictably high degree of structural similarity between the two proteins. Both proteins contain a flexible N-terminal extension of 11 residues, which is absent from Ras proteins, followed by the highly conserved G domain and a flexible C-terminal hypervariable region (HVR). Like many Ras superfamily proteins, they are lipid-modified at their C-terminus and this modification is required for their localization at cellular membranes (80).

All GEFs, GAPs and effector proteins that have been identified to date are shared by the Ral GTPases. Interactions made with these binding partners primarily occur at the switch regions, which are 100% identical in RalA and RalB. As for all Ras superfamily proteins, the switch regions are the sites of the largest conformational changes upon nucleotide exchange and hydrolysis. Additional contacts are made with other regions of the G domain (residues 12-176) of the Ral proteins, which are also highly similar with 88% sequence identity.

Despite their structural similarity, the Ral proteins have divergent and non-overlapping roles in normal and cancer cell biology (77). These differences arise partly from their distinct C-terminal regions, which drive differential localization of the proteins.

### 1.7.1 Regulation of Ral proteins

There are seven known RalGEFs, four of which (RalGDS, Rgl1, Rgl2 and Rgl3) are direct effectors of Ras (77). Active Ras recruits these GEFs to the plasma membrane where they are brought into proximity with the Ral proteins. The other RalGEFs (RalGPS1, RalGPS2 and Rgl4) are activated by mechanisms independent of Ras (81). Following Ras activation, RalGEFs activate the Ral proteins, which are then able to bind their downstream effector proteins. Two proteins have been identified with GAP activity for the Ral proteins, termed RalGAP1 and RalGAP2 (82). These proteins serve to switch off Ral signalling as expected by aiding hydrolysis of GTP to GDP. The regulation of Ral proteins downstream of Ras is summarised in Figure 1.17.

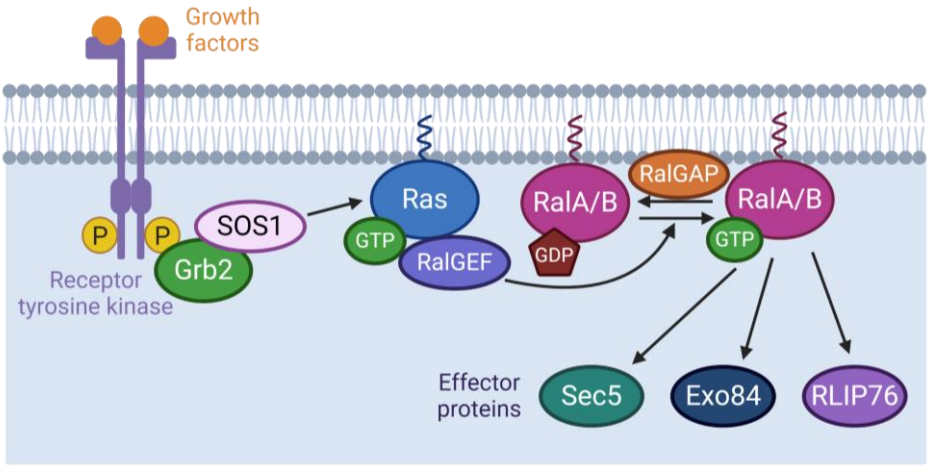


**Figure 1.17. Regulation of Ral signalling.** Upon activation by SOS1, catalysing the exchange of GDP for GTP, Ras can bind and activate several RalGEFs. The RalGEFs are then able to catalyse the exchange of GDP for GTP and activate Ral proteins. In the GTP-bound form the Ral proteins can engage downstream effector proteins including Sec5, Exo84 and RLIP76. Signalling is turned off by RalGAP-catalysed hydrolysis of GTP to GDP. Figure created with BioRender.com.

### 1.7.2 Post-translational modifications

Like Ras, the Ral proteins terminate in a CAAX box (RalA – CCIL, RalB – CCLL), in which the first cysteine residue is modified by prenylation. The X residue determines the prenyltransferase specificity (83) and while Ras proteins are modified by FTase (X = Met or Ser) the Ral proteins are targets for GGTase I (X = Leu), which catalyses the addition of a 20-carbon geranylgeranyl lipid to the first cysteine residue. As for Ras proteins, the three C-terminal residues are then cleaved by RCEI, leaving the prenylated cysteine at the C-terminus. This cysteine is subsequently methylated by ICMT (80). This process is required for correct membrane localization of the Ral proteins (80), which in turn is critical for their activity. In addition to the C-terminal processing and lipidation, the HVRs of Ral proteins are rich in lysine and arginine residues that can interact with the negative phosphate lipid head groups in the phospholipid bilayer, thereby acting as second membrane-anchoring signals (Figure 1.18).

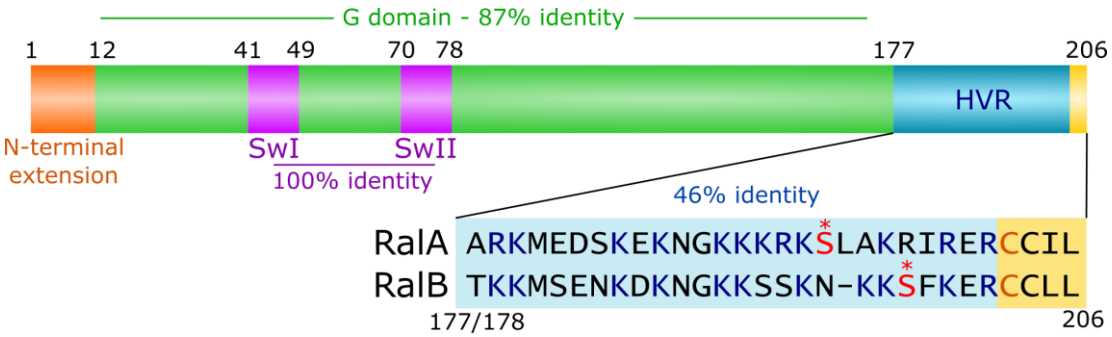


**Figure 1.18. Comparison of the C-terminal HVRs of Ral proteins.** RalA and RalB share the same overall structure with a flexible N-terminal extension of 11 amino acids, followed by the G domain (87% identity) and a flexible C-terminal hypervariable region (HVR). The HVR is the site of most variation between the proteins (46% identity) and contains the sites of post-translational modification. Ral proteins are modified by GGTase I at the cysteine residue of the CAAX box (orange). The HVR is rich in arginine and lysine residues (blue) to aid membrane attachment. RalA and RalB are phosphorylated at Ser194 and Ser198, respectively, and these phosphorylation sites are coloured red and indicated by a star (*).

Phosphorylation of the hypervariable region of the Ral proteins also plays a key role in their activity and localization. RalA is phosphorylated by Aurora kinase A at Ser194 (Figure 1.18), resulting in relocalization of RalA from the plasma membrane to internal membranes and increased activation and interaction with RLIP76 (84, 85). RalB is phosphorylated by protein kinase C (PKC) at Ser198; this modification results in the translocation of RalB from the plasma membrane and differential effector engagement (86, 87).

### 1.7.3 Ral effector proteins

Ral proteins engage their effector proteins at the nucleotide-sensitive switch regions, utilising either one or both switches for the interaction. These regions are identical between the Ral proteins, therefore it is not surprising that for those that have been measured, highly similar *in vitro* affinities of the Ral proteins for their effectors have been found.

#### 1.7.3.1 RLIP76

The first Ral effector to be discovered was RLIP76 (Ral-interacting protein 76 kDa, also known as RalBP1 for Ral-binding protein 1), which was found to contain a RhoGAP domain with activity for Rac1 and Cdc42 (88–90). RLIP76 binds to Ral proteins at both switch regions via a well-ordered coiled-coil domain that is juxtaposed but distinct from the RhoGAP domain (91).

Binding to Ral proteins does not affect the GAP activity of RLIP76 *in vitro* (88), however active Ral proteins have been shown to recruit RLIP76 to the membrane and subsequently increase the GAP activity for its membrane-associated targets in cells (84, 92). In addition to its role as a GAP, RLIP76 has been shown to interact with several proteins involved in endocytosis (93, 94), including the AP2 complex (95), REPS1/2 and Epsin (96–98), indicating a role for Ral signalling in the regulation of endocytosis. These interactions were found to be made with the N-terminal region of RLIP76 that is predicted to be disordered, or with the C-terminal domain that is predicted to form coiled-coils (94). The domain architecture and sites of interaction for RLIP76 are shown in Figure 1.19.

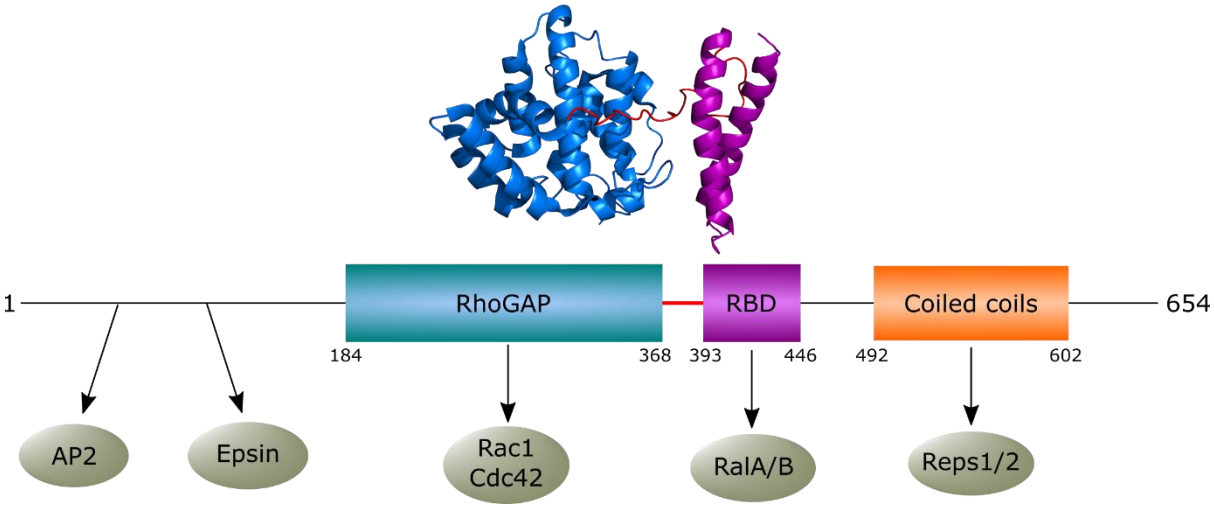


**Figure 1.19. The domain structure of RLIP76 and sites of interaction.** RLIP76 is comprised of an N-terminal disordered domain of ~180 residues, followed by the RhoGAP (blue) and Ral-binding domains (RBD, purple). The structure of this di-domain has been solved and is displayed in the corresponding colours (PDB ID: 2MBG). The C-terminal region of RLIP76 (approx. 492-602) is predicted to form coiled-coils. Figure adapted from Mott and Owen (94).

RLIP76 has been found to be upregulated in several cancers including bladder and ovarian cancers (99, 100), and has been shown to be essential for the survival of several cancer types (101). Roles for RLIP76 as an ATP-dependent transporter have also been identified, with substrates including glutathione conjugates and chemotherapeutic agents (101).

#### 1.7.3.2 Sec5/Exo84

The best characterised effectors of Ral are Sec5 (EXOC2) and Exo84 (EXOC8), members of the octameric exocyst complex (102–104). The exocyst complex is responsible for targeting and tethering secretory vesicles to specific regions of the plasma membrane. Activation of Ral proteins is required for the full assembly of the exocyst complex (105), which in turn mediates cell migration and the regulation of exocytosis.

Independent roles for the complexes of RalB with Exo84 and Sec5 have also been identified. RalB interacts with Exo84 in a subcomplex of the exocyst in response to cellular nutrient starvation and promotes the induction of autophagy (106). In contrast, the interaction between RalB and Sec5 has been shown to play a role in the innate immune response: upon activation of Toll-like receptors, the RalB/Sec5 complex was shown to recruit and activate TBK1 to support the host immune response (107). This pathway was also shown to be chronically activated in cancer cell lines harbouring activating K-Ras mutations.

#### 1.7.3.3 Other Ral effectors

Ral proteins have several other known binding partners, including the transcription factor ZONAB (ZO-1-associated nucleic acid-binding protein). RalA has been shown to activate ZONAB in a cell density-dependent manner (108). Filamin, an actin-crosslinking protein, is another known effector and associates with RalA during filopodia formation (109). Ral proteins also interact with the second messenger signalling molecules phospholipase C-$\delta$1 (PLC) and phospholipase D1 (PLD1) (110, 111), These interactions are primarily made with the N-terminal extension of Ral proteins and in the case of PLD1 are not nucleotide sensitive.

### 1.7.4 Ral proteins in cancer

Interest in the RalGEF-Ral pathway increased after it was found that despite the lack of transforming ability in murine cells, RalGDS, a RalGEF and direct effector of Ras, was more potent in transforming human cells than Raf or PI3K (112). Since then, the RalGEF-Ral pathway has been implicated in many Ras-driven cancers including pancreatic, colorectal and lung cancers (29, 77). Unlike Raf and PI3K, relatively few Ral pathway mutations have been

identified in human cancers, however the RalGEF pathway was shown to be the most commonly activated Ras effector pathway in pancreatic tumours (113).

Despite their high degree of sequence and structural similarity, Ral proteins show divergent and non-overlapping roles in cancer. Constitutively activated RalA is able to transform human cells and has been shown to be vital for anchorage-independent growth of cancer cells (113–115). RalB is not transforming but has been shown to play a role in invasion, metastasis (116), and the avoidance of apoptosis in tumour cells (102, 117), while proliferation of non-cancerous cells was unaffected by RalB knockdown (115).

Specific Ral-effector interactions have also been implicated in these observations, as RalA mutants that were defective in binding to Sec5 or RLIP76 reduced anchorage-independent growth by up to 70% (114), while the interaction of RLIP76 with RalB was required for invadopodia formation (116). The involvement of Ral-effector interactions in transmitting oncogenic Ras signalling suggests that the disruption of Ral-effector interactions could be an effective therapeutic target in Ras-driven cancers. This is supported by the observation that overexpression of the RLIP76 RBD, blocking Ral-effector interactions, inhibited anchorage-independent growth in cancer cell lines (115).

Phosphorylation of Ral proteins has also been shown to be important for their oncogenic potential (29). Cell lines expressing a RalA mutant deficient in phosphorylation (S194A) showed reduced anchorage independent growth (85). There were similar findings for RalB, as a S198A mutant, unable to be phosphorylated by PKC, reduced anchorage-independent growth, cell migration and metastasis in bladder cancer cells (86).

## 1.8 Targeting the Ral pathway

The Ral proteins interact with their effectors and regulatory proteins through protein-protein interactions and therefore, like Ras, are challenging therapeutic targets. A direct Ras inhibitor is likely to be highly toxic to cells due to the large number of downstream pathways that are controlled by this master regulatory protein. Mutant-specific inhibitors would be highly desirable for selective targeting of cancer cells but will be difficult to produce in most cases, with the exception of the successful G12C inhibitors as described in section 1.6.3. Inhibition

of the Ral pathway downstream of Ras would provide a bespoke treatment for cancers that rely on this pathway for survival and is likely to produce fewer side effects. In addition, it has been shown that non-cancerous cells do not rely on the Ral pathway for survival, therefore this approach could result in the selective killing of cancerous cells (115).

Several attempts have been made to target the Ral proteins via disruption of Ral localization, inhibition of effector interactions and stabilization of the inactive state. These approaches are described in the following sections.

### 1.8.1 Stabilization of Ral·GDP

Yan *et al*. analysed the structures of RalA·GMPPNP and RalA·GDP and identified a small binding pocket in the GDP-bound protein that is absent in the active form (Figure 1.20) (118). This pocket is located near switch II and the nucleotide binding site, therefore they postulated that a molecule binding at this site could stabilize the inactive form of RalA, preventing its activation. They docked 500,000 individual compounds at this site using *in silico* virtual screening and identified 88 hits which were then characterised biochemically. A series of derivatives based on the top compounds was generated and the lead compounds, RBC8 and BQU57 (Figure 1.20, $K_d$ RalA = 4.7 μM), were able to inhibit Ral-effector interactions and reduced tumour progression in an *in vivo* mouse model of lung cancer.

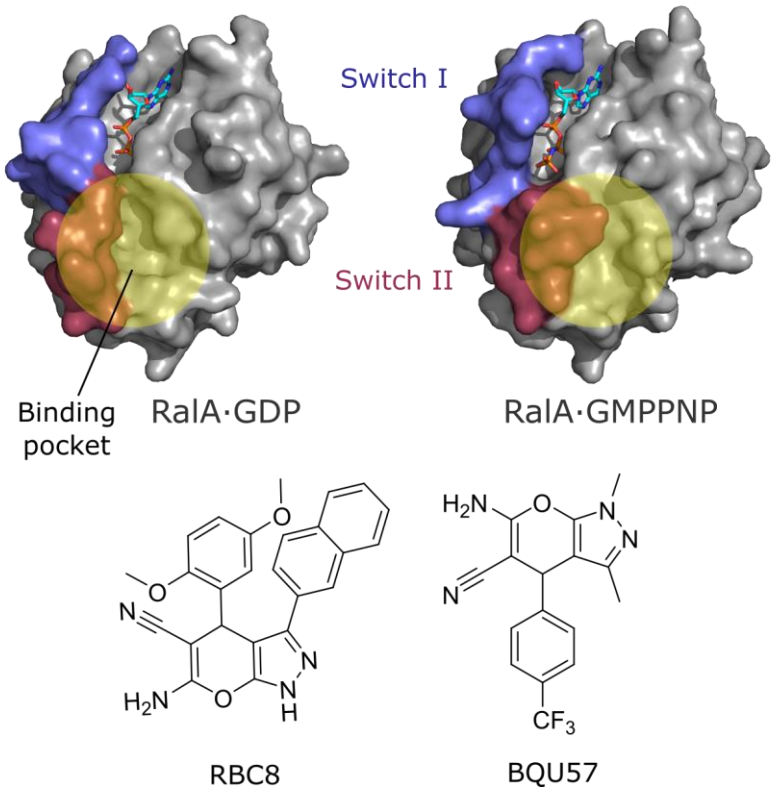


**Figure 1.20. Small molecules developed to stabilize Ral·GDP.** The structures of RalA·GDP (PDB ID: 2BOV) and RalA·GMPPNP (PDB ID: 1UAD) are shown as surfaces. There is a small binding pocket highlighted in the yellow circle that is present in the GDP but not the GMPPNP-bound conformation of RalA. The nucleotide is shown as sticks; Switch I, blue; switch II, mauve. Underneath are the chemical structures of two small molecules developed by Yan *et al.* to bind and stabilize the inactive form of Ral proteins (118).

The specificity of the inhibitor RBC8 in platelets was investigated by Walsh *et al* (119). They found that the compound successfully inhibited Ral activation in platelets by assessing Ral·GTP levels in effector pulldown assays. However, off-target effects were also seen in the concentration range required for Ral inhibition: they observed similar effects on platelet aggregation and integrin activation for both RalA/B double knockout platelets and those derived from wild-type mice following treatment with the inhibitor.

### 1.8.2 Covalent inhibition at Tyr82

While there has been success generating covalent inhibitors for G12C-mutant K-Ras, there are no cysteine residues on Ral proteins that are amenable for covalent targeting. However, several approaches have been developed to generate covalent inhibitors targeting other residues including tyrosine, histidine, serine and lysine (120, 121). Bum-Erdene *et al.* recently

screened a library of aryl-sulfonyl fluorides with the aim of covalently modifying Tyr82 on Ral proteins, which is located within the effector binding region (122). They assessed Rgl2-mediated nucleotide exchange following incubation with the library compounds using a fluorescence-based assay and identified a compound that was able to inhibit nucleotide exchange by covalent modification of Tyr82. This compound is shown in Figure 1.21. A crystal structure of the inhibitor in complex with GDP-bound RalA revealed that the inhibitor occupies a small binding pocket that is not present in the native structures, suggesting an induced fit mechanism (Figure 1.21). The inhibitor displayed selectivity for Ral proteins over related K-Ras, despite conservation of the tyrosine residue (Tyr71 in Ras). This demonstrates that the non-covalent interactions formed by the molecule with additional residues on Ral impart selectivity, providing a promising starting point for the development of specific covalent inhibitors to target the Ral proteins.

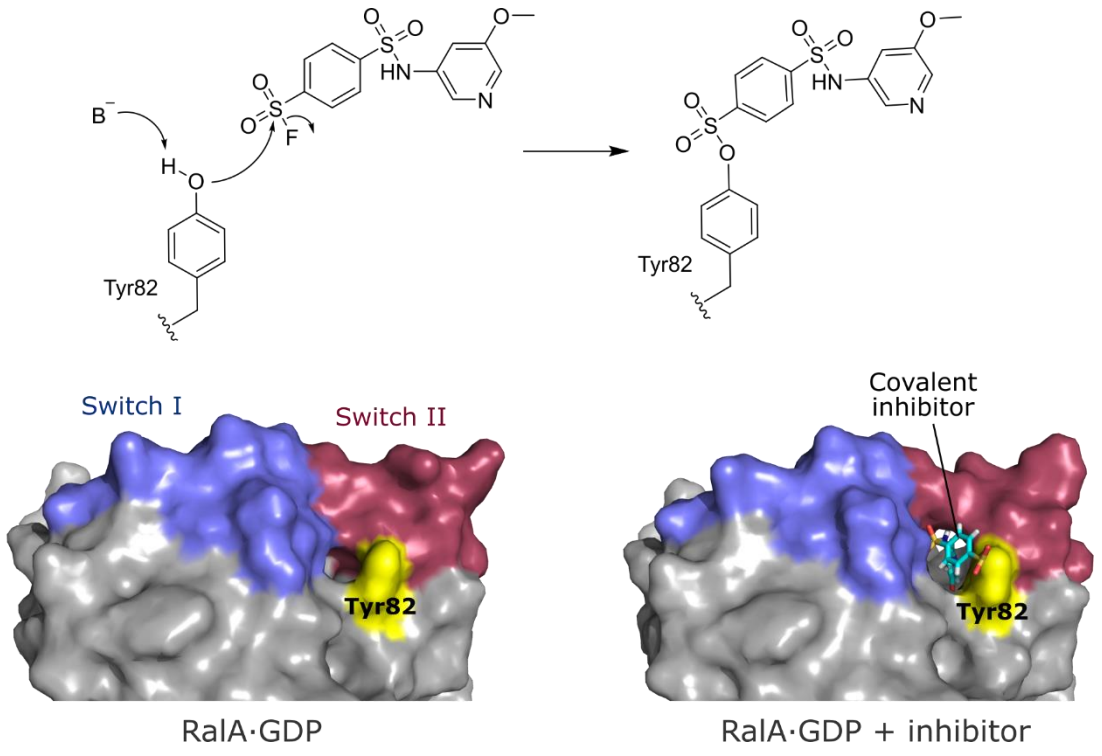


**Figure 1.21. Covalent inhibition of Ral proteins at tyrosine 82.** Tyrosine residues react with aryl sulfonyl fluorides via the reaction mechanism shown. $B^-$ = base. Comparison of the structures of RalA·GDP (PDB ID: 6P0J) and RalA·GDP in complex with the inhibitor (PDB ID: 6P0I) reveals that the covalent inhibitor binds in a pocket that is not fully formed in the unbound structure.

### 1.8.3 Targeting Ral localization

Like Ras proteins, the Ral proteins are prenylated at a C-terminal cysteine residue and this modification is essential for their correct localization and biological functioning. While Ras is modified by FTase I, Ral proteins are targets for GGTase I. Inhibition of FTase I to mislocalize Ras proteins proved ineffective, as the major isoforms, K-Ras and N-Ras, could be alternatively prenylated by GGTase I (33). In contrast, when GGTase I is inhibited, the Ral proteins are not alternatively prenylated and are mislocalized (117). Falsetti *et al.* examined the effects of GGTase inhibitors on pancreatic cancer cells and observed reduced proliferation, induction of apoptosis and a reduction in anchorage-independent growth. These effects were found to be related to Ral localization using Ral constructs that could be farnesylated, thereby restoring their localization: re-expression of farnesylated RalB in the presence of GGTase inhibition reduced apoptosis, while addition of farnesylated RalA increased anchorage-independent growth. While these results suggest that GGTase inhibitors could be effective for inhibition of Ral proteins, there are concerns over toxicity due to the large number of targets modified by GGTase I, including many Rho and Rab family members (123). Despite these concerns, Phase I clinical trials involving GGTI-2418 (a GGTase I inhibitor) showed that the inhibitor was not toxic at the doses investigated (124), suggesting that this approach could be viable for targeting cancers that are reliant on Ral proteins for survival.

### 1.8.4 Disruption of Ral-effector interactions

The Ral effectors RLIP76, Exo84 and Sec5 utilise many shared residues on Ral proteins for binding. Therefore, an inhibitor targeting this region of the Ral proteins has the potential to block all downstream effector signalling. The residues involved in binding the different Ral effectors are highlighted in Figure 1.22.

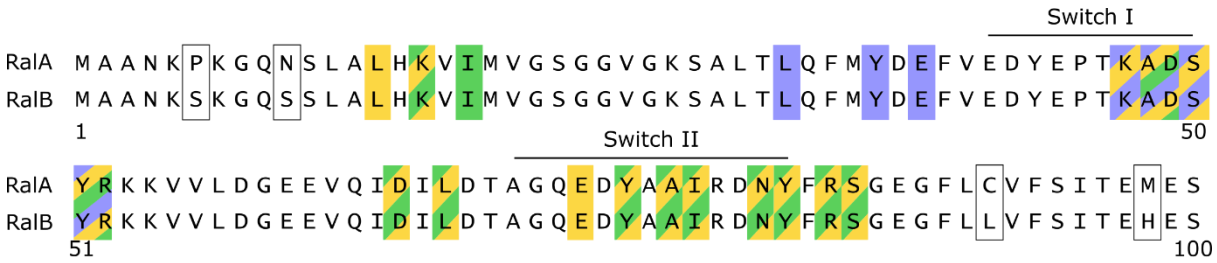


**Figure 1.22. Ral residues involved in effector protein binding.** A sequence alignment of RalA and RalB residues 1-100 is shown. Residues that differ between the two sequences are boxed and those that contact the effector proteins are coloured as follows: Exo84, yellow; Sec5, blue; RLIP76, green. Sec5 makes contacts with residues contained in and surrounding switch I, while Exo84 and RLIP76 contact both switch I and II. Figure adapted from Mott and Owen (93).

Work carried out in the lab previously sought to inhibit these Ral-effector interactions using stapled peptides. The NMR structure of RalB in complex with the RLIP76 Ral-binding domain (RBD) was used to guide the design of the peptides (91, 125). This structure revealed that RLIP76 interacts with RalB through a coiled-coil domain where more than 80% of the contacts with Ral are made through the C-terminal (α2) helix. The α2 helix was therefore used as a template to generate a series of peptides containing all-hydrocarbon staples with the aim of maintaining the helical structure. Chemical stapling successfully produced peptides with greater helicity and improved target binding compared to the unstapled parent sequence. The tightest-binding peptide identified, based on residues 423-446 of the RBD, displayed a $K_d$ of 5 µM for RalB and was selective for active Ral. This binding was shown to be competitive with two Ral effectors, RLIP76 and Sec5. The stapled peptide could enter HEK293T cells and inhibited autophagy, a RalB-dependent process, in a GFP-LC3 assay. The sequence of the best-binding peptide and the location of the sequence within the RBD are shown in Figure 1.23.

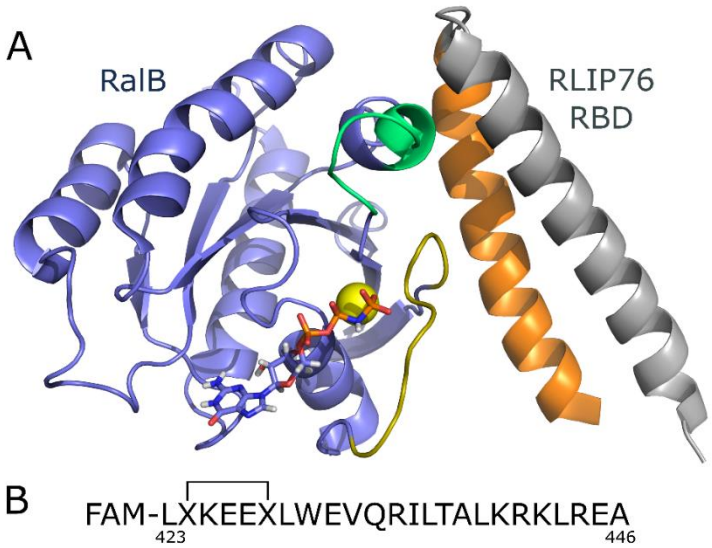


**Figure 1.23. Inhibition of Ral GTPases using stapled peptides. A.** The NMR structure of RalB·GMPPNP (blue; switch I, yellow; switch II, green) in complex with the RLIP76 RBD (grey; residues 423-446, orange. PDB ID: 2KWI). GMPPNP is shown as sticks and the $Mg^{2+}$ cation is displayed as a yellow sphere. **B.** The sequence of the tightest binding peptide identified based on the RLIP76 RBD is shown. Residues marked 'X' comprise the chemical staple. X, (*S*)-pentenylalanine; FAM, 5-carboxyfluorescein.

The work described in this thesis matured these lead peptides and improved their drug-like properties, including their binding affinity for Ral proteins, selectivity over related GTPases and peptide solubility.

## 1.9 Peptides to disrupt PPIs

As discussed in section 1.6.2, several features of peptides make them excellent agents for the inhibition of PPIs, including their exquisite target affinity and selectivity at relatively featureless surfaces. Attempts to target the Ras superfamily using peptides have been reviewed recently (126), and their use more generally as therapeutics will be discussed in the following sections.

### 1.9.1 Macrocycles

Macrocyclization of peptides is one strategy that has been employed for targeting intracellular proteins (for a recent review see (127)). Small cyclic peptides are typically resistant to proteases and have higher target affinities due to their reduced conformational

freedom. The peptides are often identified from *de novo* selections in which several approaches have been implemented for cyclization. Cysteine residues have been introduced at specific positions to invoke cyclization through disulphide bond formation or cysteine-reactive linkers can be introduced to produce monocyclic or bicyclic peptides (128). Alternatively, the RaPID selection, which can include unnatural amino acids, has been used to incorporate chloroacetylated tryptophan residues into the peptide sequence; these residues react with neighbouring cysteines resulting in a cyclic structure (129). Finally, the SICLOPPs method utilises intein splicing to generate cyclic peptide libraries in cells (130). These approaches have been successful in producing high affinity binders for a wide range of protein targets and the merits of the relative selection methods will be compared in section 1.10.

### 1.9.2 Stabilized helices

While macrocyclic binders are often derived from *de novo* peptide libraries, an alternative strategy involves mimicking existing binding motifs from PPI interfaces. Analysis of available Protein Data Bank (PDB) structures revealed that more than 60% of known PPIs contain a helix in the interaction interface (131), therefore mimicry of this critical binding motif presents an opportunity for inhibitor design. However, when helical peptide sequences are isolated from the parent protein, they often lose secondary structure and binding affinity. Chemical stabilization of α-helical peptide structures has emerged as an elegant solution to generate rigid, high affinity peptides with improved drug-like properties.

The most commonly used example of $\alpha$-helix stabilization is the all-hydrocarbon staple introduced by Verdine and colleagues (132, 133), although many other strategies exist and are summarised in Table 1.1 (134, 135). With careful staple positioning, the stabilized helical structures can have improved affinity due to a reduced entropic penalty upon binding, while in certain instances the staple itself can also interact favourably with the target protein (136). The incorporation of unnatural amino acids and increased secondary structure often improve the proteolytic stability of the peptides and can also facilitate cell permeability (137, 138).

*Table 1.1. Commonly used helix-stabilization chemistries.*

| Method | Cross-linking reaction | Ref |
|---|---|---|
| All-hydrocarbon stapling | 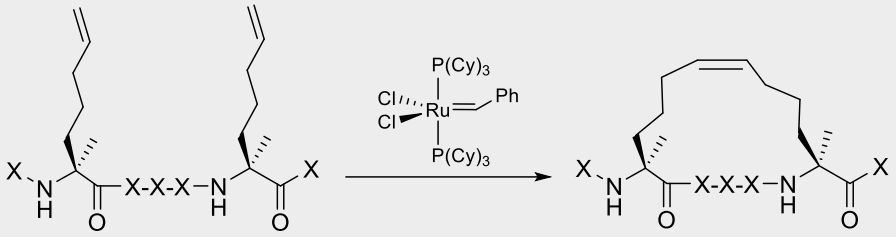 | (132) |
| Bis-thioether formation | 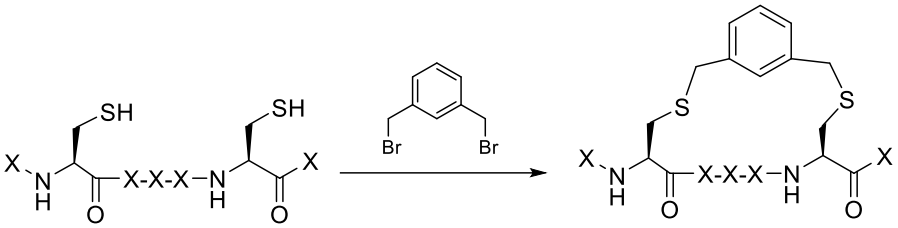 | (139) |
| Lactamization | 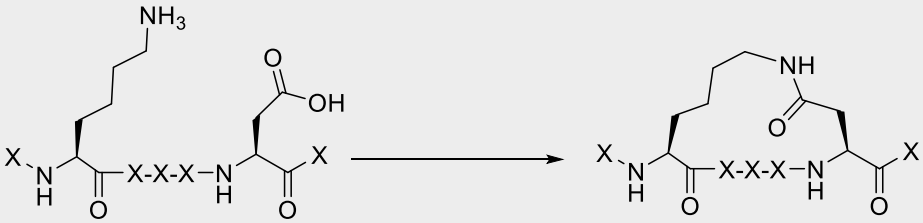 | (140) |
| Perfluoroaryl-cysteine $S_NAR$ | 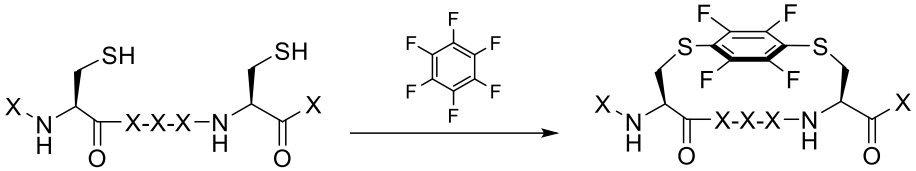 | (141) |
| Thiol-ene coupling | 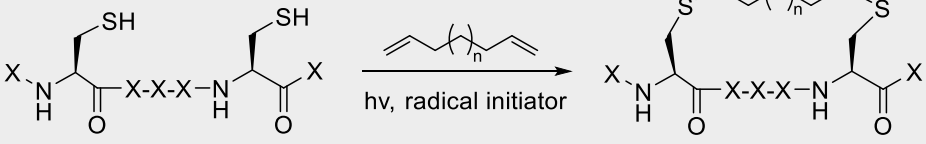 | (142) |

| | | |
|---|---|---|
| Hydrogen bond surrogate | 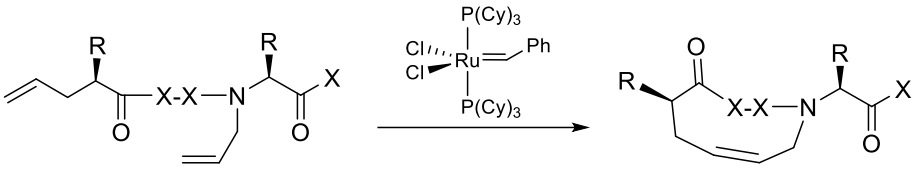 | (39) |
| Triazole 'click' reaction | 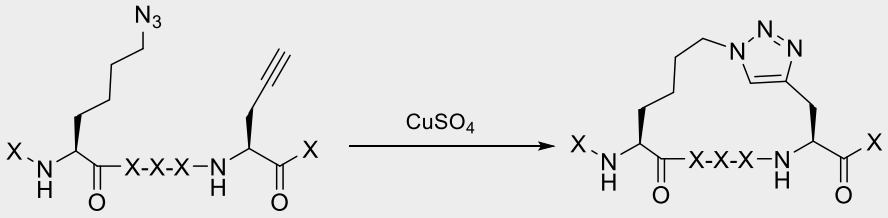 | (143) |

### 1.9.2.1 All-hydrocarbon stapled peptides

The all-hydrocarbon stapling method was first introduced by Verdine and colleagues in 2000 (133). They introduced olefin-containing amino acids with varying side chain lengths at *i*, *i* +4 and *i*, *i* +7 positions of a peptide and covalently linked the residues by a Grubbs ring closing metathesis (RCM). They identified several linker lengths that resulted in increased helicity of the peptides, however an 11 carbon linker for an *i*, *i* +7 spacing was found to produce the greatest improvement in helicity and an 8 carbon linker was optimal for *i*, *i* +4 spacings. Their work built upon the work of Blackwell and Grubbs in 1998, who demonstrated that the covalent linkage of *O*-allyl serine residues using Grubbs RCM stabilized a helical peptide structure (144). In 2004, Walensky and colleagues were the first to apply this approach to inhibit an important biological interaction when they developed helical peptides based on the BID BH3 domain to target Bcl-2 family proteins and activate apoptosis (145). Their stapled peptide was found to have improved target binding affinity and dramatically enhanced proteolytic stability compared to the wild-type sequence. They also showed that the peptide was able to enter cells, a characteristic of peptide stapling that was previously unknown.

Since those early studies there has been great interest in the use of stapled peptides to target a wide range of interactions (reviewed in (146)). Particular success has been achieved in generating peptides that re-activate p53 (147–151). These peptides act through mimicry of

p53 binding to Mdm2 and Mdmx, an interaction mediated by a 15 residue helical segment of p53 (Figure 1.24A) (152). Binding of the peptides to Mdm2 and Mdmx increases the amount of free p53 available to carry out its role as a tumour suppressor. Crystal structures of a stapled peptide, SAH-p53-8, bound to Mdm2 revealed that in addition to stabilizing a helical structure, the hydrocarbon staple is able to increase target binding affinity through formation of hydrophobic interactions with the target protein (Figure 1.24B-D) (136, 147). Another peptide based on p53, ALRN-6924, was the first stapled peptide to enter clinical trials and is currently in Phase II trials (153, 154).

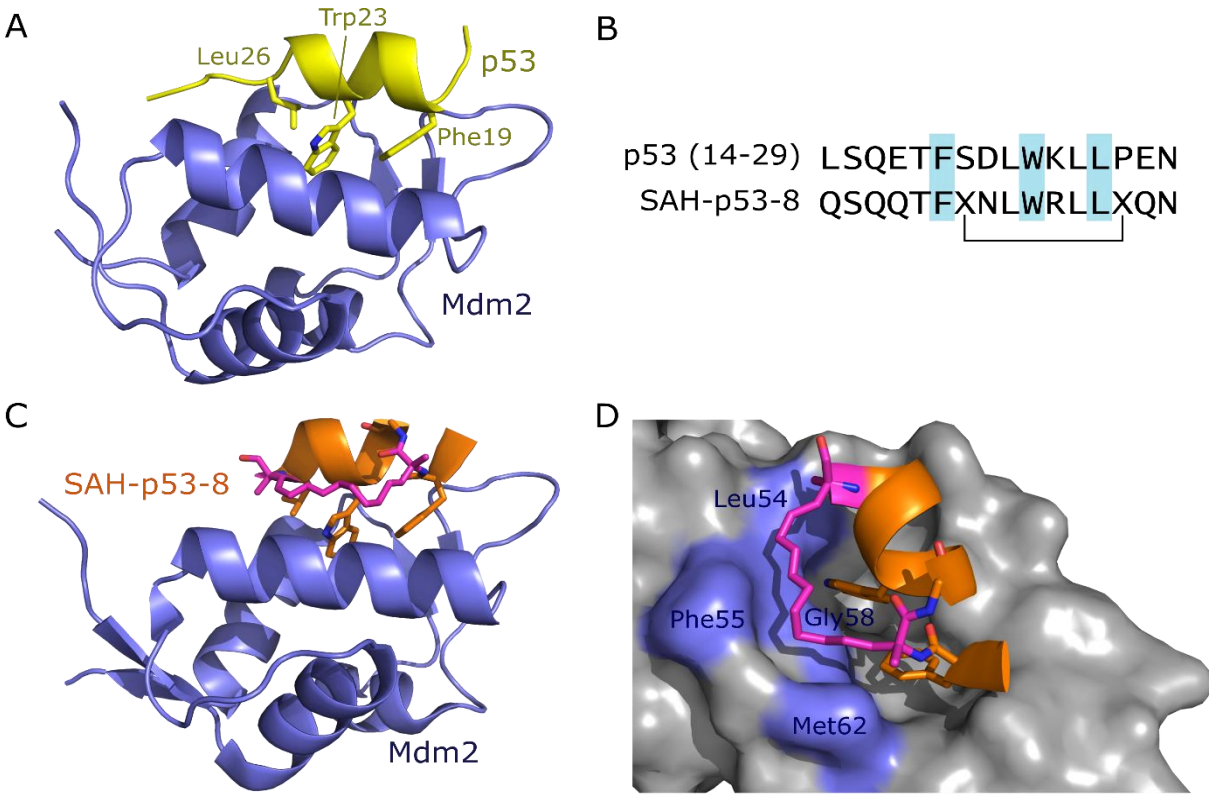


**Figure 1.24. Stapled peptides mimicking p53 binding to Mdm2/Mdmx. A.** The crystal structure of the p53 helix (residues 14-29) bound to Mdm2 (PDB ID: 1YCR). Mdm2 is shown in blue and the p53 helix is shown in yellow. Three hydrophobic residues of p53, Phe19, Trp23 and Leu26, are essential for binding Mdm2 and are shown as sticks. **B.** Sequences of $p53^{14-29}$ and the stapled peptide SAH-p53-8 are shown. The conserved hydrophobic residues that are essential for binding are highlighted in pale blue. X = staple positions. **C.** Crystal structure of the stapled peptide SAH-p53-8 bound to Mdm2 (PDB ID: 3V3B). Mdm2 is shown in blue and the stapled peptide in orange, while the staple itself is coloured pink and shown as sticks. The conserved hydrophobic residues are shown as sticks and are found in the same orientation as in the p53:Mdm2 structure. **D.** A surface view of Mdm2 (grey) shows close contact with the staple, which is able to form hydrophobic interactions with several Mdm2 residues: Leu54, Phe55, Gly58 and Met62 (blue). The all-hydrocarbon staple is shown in pink as sticks.

### 1.9.3 Cell permeability of peptides

Selections with large DNA libraries can be used to identify high affinity peptide binders for almost any protein of interest, however the hits are often not cell permeable and this confers a major limitation on the use of peptides for intracellular targets. As such, investigation into the properties of intrinsically penetrant peptides is an active area of research (reviewed in (155)). Several cell-permeable cyclic peptides exist in nature, including the immunosuppressant cyclosporin A, which is also endowed with oral bioavailability. Investigation into these natural products has guided improvements in cellular permeability of synthetic peptides, for example by N-methylation of amide bonds (156, 157). Some groups now also incorporate cell-permeable peptide (CPP) scaffolds as part of library design (49), eliminating subsequent effort spent on hits that cannot be converted to cell penetrating analogues.

Peptides that are able to enter cells do so by two major mechanisms; direct penetration and endocytosis (158, 159). Direct penetration of peptides includes energy-independent mechanisms such as passive diffusion and membrane perturbation. Lokey and co-workers have extensively studied the properties required for passive diffusion of peptides and found that small, hydrophobic peptides with internalised intramolecular hydrogen bonds displayed optimal cellular entry (160–162). The removal of exposed polar groups, either through N-methylation of the backbone or by the formation of intramolecular hydrogen bonds, is particularly important to decrease the entropic cost of desolvation upon entry into the lipid bilayer.

Hydrocarbon stapled peptides have been shown to enter cells via an energy-dependent endocytosis mechanism (163, 164). While the exact properties determining uptake remain unclear, several features of stapled peptides have been identified which appear to correlate with improved uptake; these include a net charge of +1 and above, net hydrophobicity and the formation of an amphipathic helix (138, 163, 164).

### 1.9.4 Methods to aid cellular uptake

If a lead peptide does not possess sufficient intrinsic cellular permeability, several methods can be used to transport the peptide into the cell so that the *in vivo* activity can be studied. A

widely-used method involves appending a cell-penetrating peptide (CPP) sequence to a lead peptide (recently reviewed in (159)). These peptide sequences are typically derived from nature, though some, including polyarginine sequences, have been designed. These sequences can also be used to transport much larger cargoes into cells and some commonly used CPPs and their origins are summarised in Table 1.2.

*Table 1.2. Examples of commonly used CPPs.*

| Name | Sequence | Origin | Ref |
|---|---|---|---|
| **Tat** | GRKKRRQRRRPPQ | HIV-1 Tat protein (residues 48-60) | (165) |
| **Penetratin** | RQIKIWFQNRRMKWKK | *Drosophila melanogaster*, Antennapedia homeobox peptide $pAntp_{43-58}$ | (166) |
| **PolyArg** | $R_8$, $R_9$ | Designed | (167) |
| **pVEC** | LLIILRRRIRKQAHAHSK | Vascular endothelial cadherin (residues 615-632) | (168) |
| **MAP** | KLALKLALKALKAALKLA | Designed | (169) |
| **Transportan** | GWTLNSAGYLLGKINLKALAALAKKIL | Chimera of galanin and mastoparan | (170) |

As an alternative to CPPs, lipid formulations, hydrogels and nanoparticles have also been developed to deliver peptides to their intracellular targets (reviewed in (171)).

### 1.10 Selection methods

Peptides to inhibit PPIs are often identified using selection methods that enable the screening of vast numbers of sequence variations (up to $10^{14}$ individual sequences). The selection methods discussed here share several common features: initially, large libraries encoded by DNA or RNA are constructed to allow for recombinant protein production. Following translation of the library, the genetic information is chemically linked to the protein or peptide produced to allow deconvolution of the sequence by next generation sequencing. Constructs

with the desired properties are then isolated e.g. those that bind an immobilised target protein, and the binding sequences are identified by sequencing. While the overall concepts are shared, the methods used for linking genotype to phenotype and for isolation of hits differ greatly.

The first method described for such selections was phage display, which has been widely used for peptide and antibody selections since the application was developed in the early 1990s (172–174). In phage display, phagemids are constructed in which the library of interest is ligated to a gene encoding a phage coat protein. The library is then transformed into *E. coli* for assembly into phages, which display the library sequences on their surface as part of their coat protein.

*In cellular* selections have also been implemented. Pelletier *et al.* described a method in which the library of interest is fused to one half of murine dihydrofolate reductase (mDHFR), while the second half of mDHFR is fused to the intended target protein (175). Reconstitution of mDHFR occurs when an expressed library member binds to the target protein. The cells are cultured in in the presence of a bacterial DHFR inhibitor, and therefore require active mDHFR for propagation. A competitive selection can also be set up in which library members compete against each other: those encoding higher affinity binders will have faster reconstitution of mDHFR and hence will outcompete other library members.

SICLOPPS libraries offer an elegant method for the *in cellular* selection of cyclic peptides (130, 176, 177), utilising intein splicing to cyclize the peptides. During the library construction, the peptide sequences to be cyclized are placed between a C-terminal and an N-terminal intein domain. Upon translation, splicing of the active *cis*-intein results in cyclization of the peptide library that previously linked the two domains. When coupled to a reverse two-hybrid system, this approach enables the identification of functional inhibitors of specific protein-protein interactions, rather than solely assessing target affinity.

Both *in cellular* selections and phage display require transformation of the library into a host organism, therefore the library sizes are limited by transformation efficiencies with up to $10^6$-$10^9$ sequences screened using these methods.

*In vitro* display technologies circumvent the necessity for transformation, allowing much larger libraries (up to $10^{14}$ clones) to be assessed; such methods include CIS display and mRNA

display, among others (178–180). These technologies typically use bacterial cell lysates to provide the translation machinery required to produce the library. In CIS display, the library is fused to a gene encoding RepA, which captures the DNA from which it was translated upon recognition of a *cis* element, coupling the genetic material to the library. During mRNA display, an antibiotic (puromycin) is covalently attached to the mRNA library at the 3′ end. As translation approaches the 3′ end, the puromycin, which resembles an aminoacylated tRNA, is incorporated into the growing polypeptide chain by the ribosome, coupling the mRNA sequence information to the peptide or protein produced.

While *in vitro* methods allow the screening of far larger libraries, *in cellular* selections have the advantage of screening in a more native environment. As such, the binders identified are required to have selectivity for the target and have limited toxicity to the host organism. However, as these assays are often conducted in bacterial cells, the peptides selected can still present problems in mammalian cells.

### 1.11 Project aims

This project aimed to develop second-generation stapled peptides based on RLIP76 to inhibit the Ral GTPases, building on the lead peptide that was previously identified in the lab (see section 1.8.4). The generation of peptides to inhibit the Ral proteins would be highly valuable tools in the study of Ral biology, as there are currently no well-validated inhibitors available. There is also substantial evidence that inhibition of Ral signalling blocks tumour growth and metastasis in several Ras-driven cancers (discussed in section 1.7.4), therefore peptides that effectively inhibit Ral activity could potentially be used to disrupt oncogenic Ras signalling therapeutically.

Prior to the beginning of this project, a CIS display selection was carried out based on the RLIP76 RBD to identify sequence changes that could increase binding to Ral proteins. The work described in this thesis used the insights gained from these selections to guide the design of stapled peptides with improved affinity for Ral proteins, carry out biochemical characterisation of the peptides and assess their efficacy in cells. Specifically, the initial aims were:

1. To validate the hits identified from the CIS display selection of the RLIP76 RBD by producing selected sequences as recombinant proteins and assessing their *in vitro* affinity for Ral proteins.

2. To incorporate the best-binding sequences into second-generation stapled peptides targeting the Ral GTPases, based on the α2 helix of the RLIP76 RBD.
3. To assess the activity of the resulting peptides by: measuring their *in vitro* affinity for Ral proteins, assessing the ability of the peptides to disrupt Ral-effector complexes, interrogating the binding site of the peptides and assessing the ability of the peptides to disrupt Ral signalling in mammalian cells.

Experiments to investigate the affinity and mode of binding of RLIP76 RBD mutants from the CIS display selection are described in Chapter 2. This work led to the identification of several sequence changes that improve affinity for Ral proteins. The design of all-hydrocarbon stapled peptides based on these sequences and evaluation of the activity of the peptides is described in Chapter 3. During these investigations it became apparent that several properties of the peptides required improvement, including the solubility, specificity, and cell-penetrating ability of the peptides: progress made to improve these properties is also described in Chapter 3. Finally, an alternative method of peptide stapling, allowing for the modification of unprotected, recombinantly-produced peptides has been utilised to produce peptides targeting the Ral GTPases. These peptides were cross-linked at cysteine residues rather than requiring unnatural amino acids to form the staple. The relative activities of these peptides compared to their all-hydrocarbon stapled counterparts were assessed and are detailed in Chapter 4.

# 2 Maturation of the RLIP76 RBD

## 2.1 Introduction

The Ral-binding domain (RBD) of RLIP76 (residues 393-446) adopts a coiled-coil structure comprising two α-helices. The contacts that the RBD makes with Ral proteins, and the energetic contributions of these contacts, have been determined using combined data from an NMR structure of the RLIP76 RBD in complex with RalB and an alanine scan of the RBD (91, 181). The residues that contribute most to binding Ral proteins are shown in Figure 2.1. Approximately 80% of the contacts made with Ral proteins are contained within the α2 helix of the RBD, while contacts with the α1 helix are less extensive and are limited to the C-terminal end of the helix. Four residues within the RBD were identified that result in a complete loss of binding to RalA upon replacement with alanine; His413, Trp430, Arg434 and Thr437 (181). Of these critical contacts, three are located within the α2 helix, and only His413 is in the α1 helix.

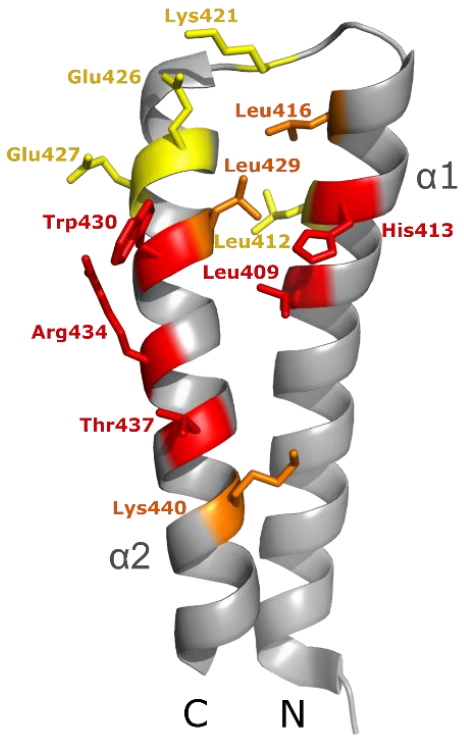


**Figure 2.1. The Ral-binding domain of RLIP76.** The NMR structure of the RLIP76 RBD is shown (PDB ID: 2KWI), with residues whose mutation to Ala disrupts binding to Ral proteins shown as sticks and coloured as follows: yellow, 2 to 5-fold weaker affinity; orange, 5 to 10-fold weaker affinity; red, > 10-fold weaker affinity. Figure adapted from Campbell *et al.* (181).

The RLIP76 RBD displays a very similar affinity for RalA and RalB ($K_d$ = 185 and 265 nM, respectively), and alanine scanning of the RBD has shown that most residues have a similar effect on the binding affinities (181). However, some differences have been identified: for example, replacement of Leu429 with alanine resulted in a 5-fold decrease in binding to RalA, while binding to RalB was reduced more than 20-fold. Arg434 was another point of differentiation: mutation to alanine resulted in a complete loss of binding to RalA, while this substitution reduced binding to RalB less than 3-fold. These results indicate that there are subtle differences in how Ral proteins interact with their effector proteins, despite the identical sequences in their effector-binding regions.

### 2.1.1 Stapled peptides based on the RLIP76 RBD

The RLIP76 RBD has been used previously as a template to generate stapled peptide inhibitors of Ral proteins (125). Two peptide sequences were designed based on each of the helices of

the RLIP76 RBD and containing all of the contacts that are made with Ral proteins by that helix: Peptide 1 comprised the entire α2 helix (residues 423-446, Figure 2.2A), while Peptide 2 contained the loop region between helices and all of the contacts made by the α1 helix (residues 408-422). As these peptides were not expected to retain a helical structure outside of the coiled-coil domain, hydrocarbon staples were incorporated into the peptides at various positions with the aim of stabilizing a helical conformation (Figure 2.2B). Optimization of the staple position was required to maximise the helicity of the peptides and to ensure that the residue replacement did not negatively affect binding. In fact in certain cases, careful positioning of the staple has been shown to improve affinity through direct interactions of the staple with the target protein (136).

A

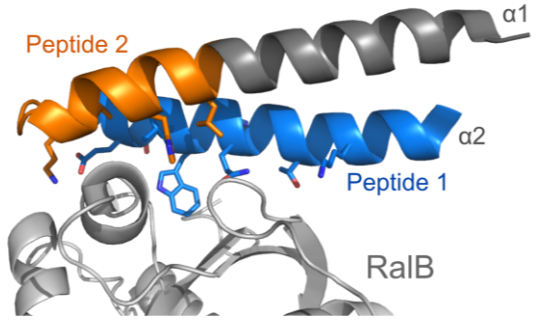


B

| Peptide | Sequence | Helicity (%) |
|---|---|---|
| Peptide 1 | LSKEERLWEVQRILTALKRKLREA | 50 |
| Peptide 2 | LLNSLHRDLQGGIKD | 4 |
| SP1 | LXKEEXLWEVQRILTALKRKLREA | 81 |
| SP2 | LSKEERLWEXQRIXTALKRKLREA | 50 |
| SP3 | LSKEEXLWEXQRILTALKRKLREA | 84 |
| SP4 | LSKEEXLWEVQRXLTALKRKLREA | 88 |
| SP5 | LXKEEXLWEVQRXLTAXKRKLREA | 87 |
| SP6 | LLNXLHRXLQGGIKD | 57 |

**Figure 2.2. Design of stapled peptides based on the RLIP76 RBD to target Ral proteins. A.** Structure of the RLIP76 RBD in complex with RalB·GMPPNP (PDB ID: 2KWI). Residues on the RLIP76 RBD that result in a decrease in binding to Ral proteins when they are replaced with alanine are shown as sticks. The sequence encompassed by Peptide 1 is shown in blue, while the sequence of Peptide 2 is shown in orange. RalB is shown in grey. **B.** Sequences of peptides based on the RLIP76 RBD. X indicates the positions of unnatural amino acids used to form all-hydrocarbon staples. Helicity values were determined by Thomas *et al.* (125). SP, stapled peptide.

From the panel of peptides containing a variety of staple positions and lengths, it was found that a peptide based on the α2 helix with a staple bridging residues 424 and 428 (SP1, Figure 2.2B) displayed the greatest affinity for Ral proteins, with a $K_d$ of 5 μM for RalB and around 6-fold weaker binding to RalA (125). This peptide bound RalB around 6-fold tighter than the non-stapled parent sequence, Peptide 1, demonstrating the utility of the all-hydrocarbon stapling method. All of the staples tested improved the helicity of the peptides to varying degrees, except for SP2 where the staple bridged central residues of the helix, replacing residues 432 and 436 (Figure 2.2B).

## 2.2 Work preceding this project

Following identification of the promising lead peptide, this project aimed to improve the affinity of SP1 for Ral proteins by optimizing the sequence. It had been shown previously, using NMR titration experiments, that a non-stapled peptide based on the α2 helix of the RLIP76 RBD (Peptide 1, Figure 2.2B) binds in a similar manner to the RLIP76 RBD, utilising many of the same residues for binding (125). It had not been possible to carry out such investigations using the stapled peptide (SP1) due to limited aqueous solubility, however it was hypothesized that the binding of this peptide was more likely to resemble the RBD than the non-stapled peptide due to its increased helical structure. It was therefore decided that the RBD could act as a convenient model to study how sequence changes affect binding to Ral proteins and any insights gained could be carried forward and incorporated into the design of stapled peptides based on this domain.

Selection technologies utilising recombinant protein expression provide a method to screen huge libraries and identify sequences that bind to a target protein, where up to $10^{14}$ sequence variations can be tested in a relatively short time. Therefore, a selection to identify amino acid substitutions within the α2 helix that can improve affinity for Ral proteins was undertaken. As the stapled peptides contain unnatural amino acids, they are not suitable templates for most selection methods utilising recombinant production, therefore the RLIP76 RBD was used as the template for the selection to identify sequences that could then be synthesized as stapled peptides.

### 2.2.1 CIS display maturation of the RLIP76 RBD

CIS display (178) was chosen as the selection method due to the large library size (up to $10^{14}$ clones) that can be tested (Figure 2.3). A library encoding the RLIP76 RBD (residues 393-446) with several variable positions was fused to the gene encoding RepA, a protein which captures the DNA which it was translated from. The library was produced by recombinant protein expression and then incubated with target Ral proteins that had been immobilised via a biotin tag. Non-binding sequences were washed off and the process was repeated over several

rounds with increasing stringency to enrich for binding sequences, which were then easily identified by next generation sequencing.

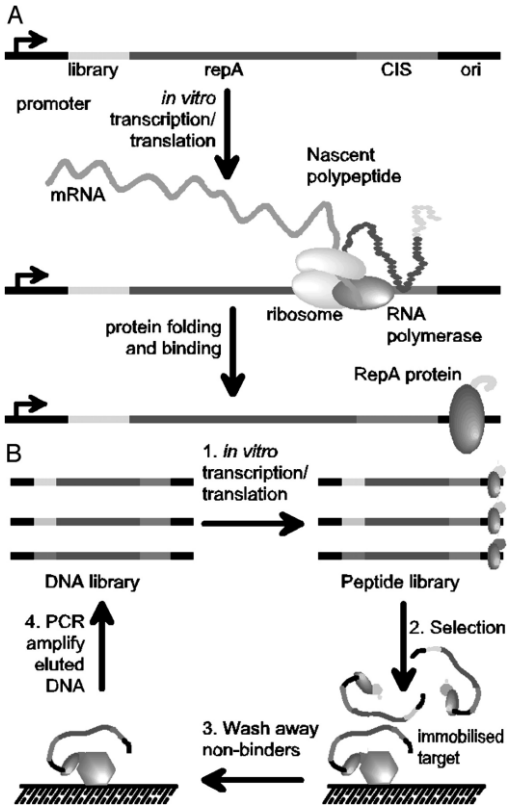


**Figure 2.3. Principles of CIS display maturation**. A library of interest is fused to a gene encoding RepA. When the protein is translated, the RepA protein captures the DNA from which it originated, allowing easy identification of binding sequences using next generation sequencing. Binding sequences are captured by the target protein immobilised on beads. Following washing to elute non-binders, the bound DNA is eluted and carried into the next round of selection. This process is repeated over several rounds to enrich for the binding sequences. Figure from Odegrip *et al.* (178).

Biotinylated RalA and RalB proteins bound to GMPPNP, a non-hydrolysable analogue of GTP, were used as target proteins in separate selections in order to identify any sequences that bound one isoform selectively. In the selections, up to 10/24 positions of the RLIP76 RBD were allowed to change, and these positions are shown in Figure 2.4. Only residues in the α2 helix as contained in the lead peptide (residues 423-446) were matured, and within that helix only those on the Ral-binding surface of the helix that have the potential to form interactions with Ral were allowed to alter. Trp430 was retained in all selections, as this residue has been shown to be critical for binding Ral proteins and mutation at this position to alanine ablates

binding to RalA and RalB (181). Both helices of the RLIP76 RBD were included in the selection to maintain the helical secondary structure of the domain.

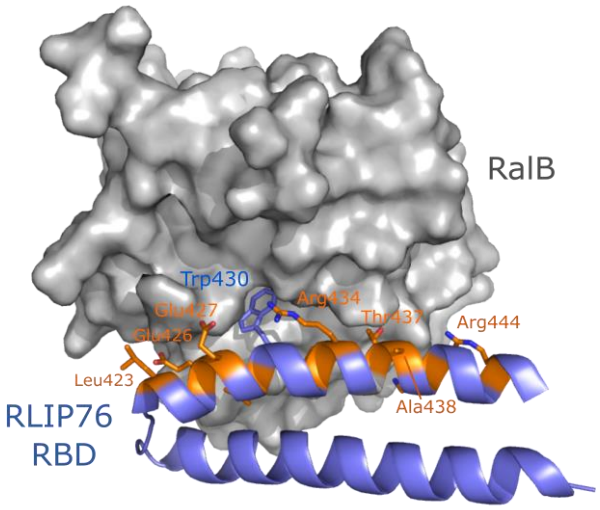


**Figure 2.4. Amino acid positions allowed to alter in the CIS display selections.** The RLIP76 RBD is shown in blue, while the 10/24 positions in the α2 helix that were allowed to alter are shown as orange sticks. Trp430, an amino acid essential for binding Ral proteins, occupies a deep binding pocket on RalB and is shown as blue sticks. RalB is shown as a grey surface (PDB ID: 2KWI).

In the first maturation library, 8 positions were subject to selection and were allowed to alter to any amino acid (Table 2.1), while the second library contained 10 positions that could be varied. Positions 426 and 433 in the second library could include any amino acid, though other positions could only be replaced by a subset of amino acids with the aim of retaining desirable properties such as hydrophobicity (NTT codon) and polarity or basicity (MRV codon, Table 2.1).

*Table 2.1. Codon assignment in maturation libraries designed for CIS display selection.*

| Position | L423 | E426 | E427 | L429 | Q433 | R434 | T437 | A438 | K440 | R444 |
|---|---|---|---|---|---|---|---|---|---|---|
| Library 1 | - | NNK[1] | NNK | NNK | NNK | NNK | NNK | - | NNK | - |
| Library 2 | RVK[2] | NNK | RVK | NTT[3] | NNK | RVK | NWW[4] | RVK | MRV[5] | MRV |

[1]NNK encodes (with relative frequencies): Cys, Asp, Glu, Phe, His, Ile, Lys, Met, Asn, Gln, Trp, Tyr, 2x Ala, 2x Gly, 2x Pro, 2x Thr, 2x Val, 3x Leu, 3x Arg, 3x Ser
[2]RVK encodes: Asp, Glu, Lys, Asn, Arg, Ser, 2x Ala, 2x Gly, 2x Thr
[3]NTT encodes: Phe, Ile, Leu, Val
[4]NWW encodes: Asp, Glu, Phe, His, Lys, Asn, Gln, Tyr, 2x Ile, 2x Val, 3x Leu
[5]MRV encodes: His, Asn, Ser, 2x Lys, 2x Gln, 5x Arg
N = A/T/C/G, K = T/G, R = A/G, V = A/C/G, T = T, W = A/T, M = A/C

Initial selections with each target, RalA or RalB, included only sequences from library 1, while subsequent selections included equimolar amounts of libraries 1 and 2 (Table 2.2). Each selection was carried out with and without an 'off-rate' step, in which the bound complexes were incubated with non-biotinylated target protein followed by a washing step to remove proteins not bound to the beads. The aim of this step was to remove peptides with faster off-rates which would dissociate and bind to the non-biotinylated Ral protein, thereby enriching for peptide sequences that were less likely to dissociate from the bead-bound complexes.

*Table 2.2. Summary of selections used to identify matured RLIP76 RBD sequences binding to RalA and RalB.*

| Selection | Target | Library used | Off-rate washing |
|---|---|---|---|
| 1 | RalB | 1 | Yes |
| 2 | RalB | 1 | No |
| 3 | RalB | 1 & 2 | Yes |
| 4 | RalB | 1 & 2 | No |
| 5 | RalA | 1 | Yes |
| 6 | RalA | 1 | No |
| 7 | RalA | 1 & 2 | Yes |
| 8 | RalA | 1 & 2 | No |

Each selection was carried out over four rounds to enrich for binding sequences, with increased stringency in later rounds achieved by decreasing the amount of biotinylated Ral target protein (round 1 and 2, 25 nM; round 3, 5 nM; round 4, 2.5 nM). A peptide cluster analysis tool was used to identify mutations that frequently occurred together and the three most commonly occurring clusters are listed in Table 2.3.

*Table 2.3. Amino acid clusters identified from CIS display.*

| Cluster | L423 | E426 | E427 | L429 | Q433 | R434 | T437 | A438 | K440 | R444 |
|---|---|---|---|---|---|---|---|---|---|---|
| **1** | - | L | S/T | X* | T/H | L | R | - | P | - |
| **2** | - | W | D | A | S | X | X | - | R | - |
| **3** | - | - | X | - | L | - | - | - | R | - |

* X denotes no preference.

While some individual amino acid changes might produce an effect on binding in isolation, it was considered likely that the changes need to be included together, as they appeared in the selection, in order to exert an effect. Therefore, when analysing hits from these selections it was important to look at entire sequences that were selected and clusters of mutations that commonly appeared together, rather than the effects of individual substitutions.

## 2.3 Recombinant production of RLIP76 RBD constructs

This work aimed to identify and characterise sequences from the CIS display selection that improve affinity for Ral proteins. Several of the top hits were produced recombinantly from *E. coli* to validate the hits from the selection by measuring their *in vitro* affinities for Ral proteins. The sequences selected were those that appeared with the highest frequencies whilst ensuring that representatives from each cluster identified in section 2.2.1 were included. The sequences that were produced as recombinant proteins are listed in Table 2.4.

*Table 2.4. RLIP76 RBD constructs produced recombinantly.*

| Name | Sequence[a] |
|---|---|
| Wild-type-His | RLIP76(393-422, C411S)-LSKEERLWEVQRILTALKRKLREANSSGRQISGHHHHHHGS |
| Wild-type | RLIP76(393-422, C411S)-LSKEERLWEVQRILTALKRKLREA |
| HLR | RLIP76(393-422, C411S)-LSKEHRLWEVLRILTALRRKLREA |
| SMLR | RLIP76(393-422, C411S)-LSKESRMWEVLRILTALRRKLREA |
| DVLR | RLIP76(393-422, C411S)-LSKEDRVWEVLRILTALRRKLREA |
| NTR | RLIP76(393-422, C411S)-LSKNERLWEVTRILTALRRKLREA |
| SDT | RLIP76(393-422, C411S)-LSKSDRLWEVTRILTALKRKLREA |
| LTHTLKP | RLIP76(393-422, C411S)-LSKLTRHWEVTLILKALPRKLREA |
| WDASQSR | RLIP76(393-422, C411S)-LSKWDRAWEVSQILSALRRKLREA |
| WDASTAY | RLIP76(393-422, C411S)-LSKWDRAWEVSTILAALYRKLREA |
| WNASELR | RLIP76(393-422, C411S)-LSKWNRAWEVSEILLALRRKLREA |
| LTTLR-His | RLIP76(393-422, C411S)-LSKLTRLWEVTLILRALKRKLREANSSGRQISGHHHHHHGS |

[a] Underlined residues indicate variations from the wild-type RBD sequence.

A construct containing the RLIP76 RBD (residues 393-446, C411S) in pGEX-HisP, herein referred to as the wild-type RBD, was already available in the lab. This construct contains an N-terminal GST fusion protein which is cleavable by HRV-3C protease and a non-cleavable 6x His-tag at the C-terminus. A His-tagged form of the wild-type RLIP76 RBD was produced but for most other variants a stop codon was introduced by site-directed mutagenesis after Ala446 to remove the C-terminal His-tag. The mutations shown in Table 2.4 were added to the wild-type construct using site-directed mutagenesis as described in the methods.

A small-scale expression trial was carried out to establish the optimal conditions for protein expression. Bacterial cultures were grown and then induced at 37 °C for 5 h or at 20 °C

overnight. The cells were lysed, and the soluble proteins were separated from insoluble material to determine which condition produced the most soluble protein. The expression trial for the wild-type construct is shown in Figure 2.5.

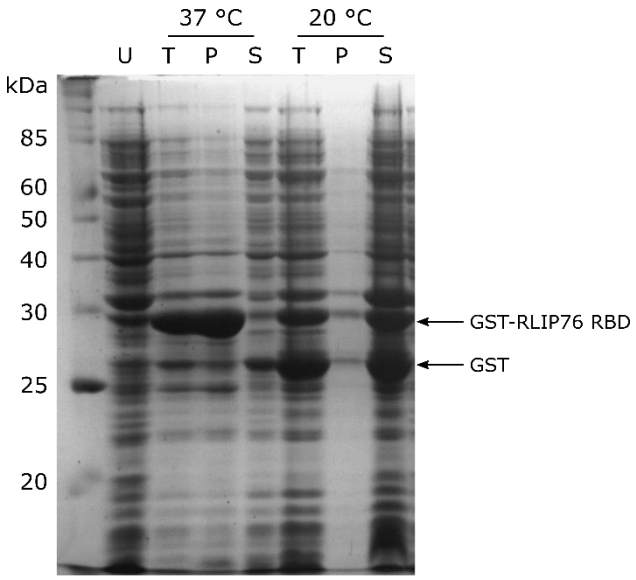


**Figure 2.5. Test expression of GST-RLIP76 RBD (residues 393-446, C411S) in BL21 *E. coli*.** U – uninduced, contains a sample of BL21 cells that have not been induced with IPTG. T – total, shows cellular contents of BL21 cells expressing GST-RLIP76 RBD after induction with 0.1 mM IPTG at 37 °C for 5 hours, or at 20 °C overnight as indicated. These induced samples have been split into a pellet sample (P) containing the insoluble proteins and the supernatant (S) containing the soluble proteins.

Most of the protein produced at 37 °C was present in the insoluble fraction, while far more soluble protein was present following induction at 20 °C overnight. This was despite the increased amount of free GST observed after induction at 20 °C, which is likely due to degradation of the RLIP76 RBD fusion protein.

Large-scale cultures were grown and induced at 20 °C overnight. Following cell lysis, the GST-RLIP76 RBD proteins were immobilised on glutathione agarose beads and non-bound proteins were washed off, leaving the purified fusion protein on the beads (Figure 2.6A). The RLIP76 RBD was released from the GST tag by cleavage with HRV-3C protease and collected by washing the beads with buffer (Figure 2.6B). Finally, the cleaved protein was purified by size exclusion chromatography (Figure 2.6C and D).

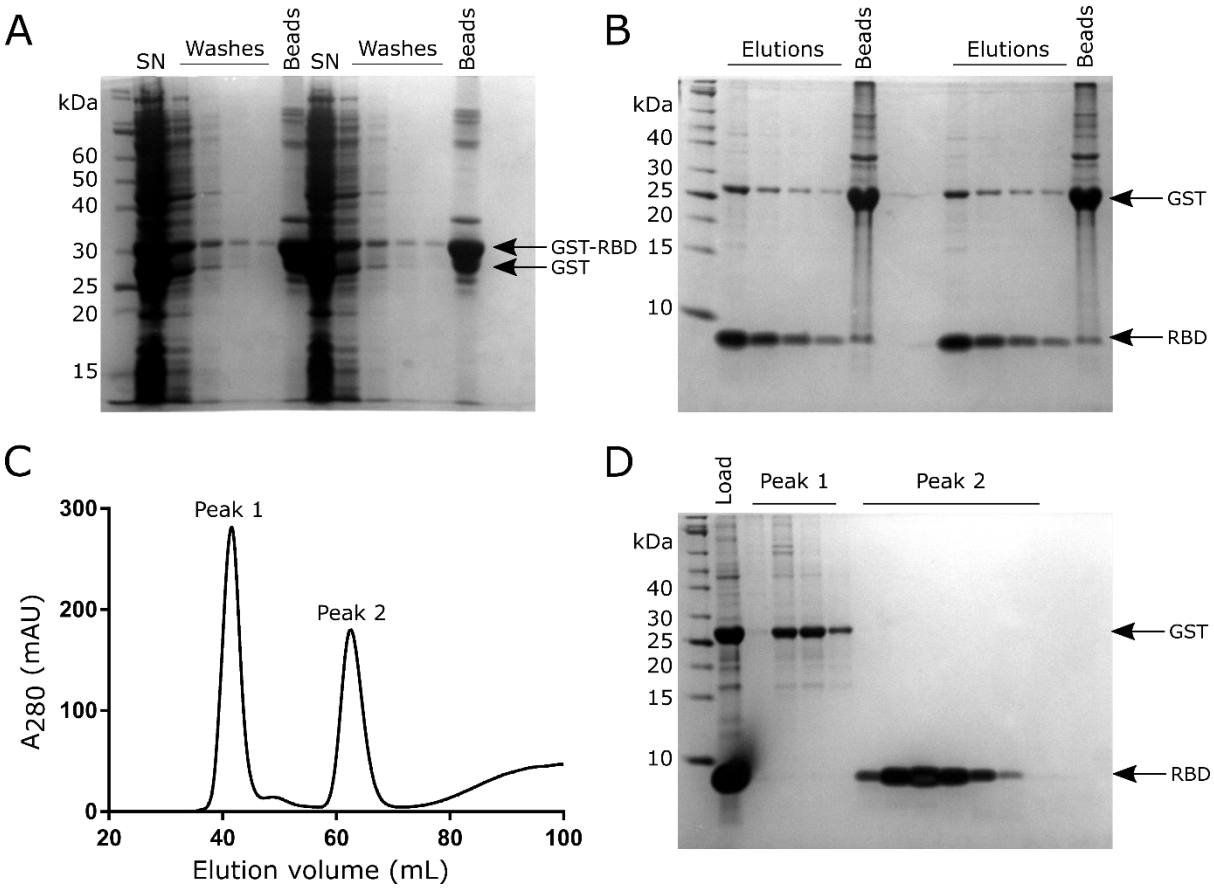


**Figure 2.6. Large scale expression and purification of GST-RLIP76 RBD (393-446, C411S). A.** Samples taken from the supernatants of cell lysates from 1.5 L BL21 cells expressing GST-RLIP76 RBD after incubation with glutathione agarose beads (SN) and from washes with buffer + 0.1% Triton. The sample labelled 'beads' shows the bead slurry following the washes, containing immobilised GST-tagged RLIP76 RBD (GST-RBD, MW = 33 kDa). A smaller species is also present at > 25 kDa, which is likely GST that the fusion protein has been cleaved from. **B.** Samples taken from elutions with purification buffer following overnight cleavage with HRV-3C protease. The free RLIP76 RBD is observed below the 10 kDa marker (MW = 6.9 kDa). Small amounts of GST are also detached from the beads during elution. A bead sample taken following the elutions shows GST immobilised on the beads and a small amount of the RBD still present. **C.** Chromatogram from purification of the RLIP76 RBD on a Superdex 30 size exclusion column. **D.** SDS-PAGE analysis of samples of protein loaded onto the S30 column (load) and fractions from peaks labelled peak 1 and peak 2 in C. The RLIP76 RBD is visible under the 10 kDa marker and has eluted with high purity at around 65 mL elution volume (peak 2). Peak 1 contains larger protein aggregates and GST.

The mutants were expressed as for the wild-type fusion protein and were all purified in a good yield and with high purity except for the LTHTLKP construct. Following HRV-3C cleavage, the LTHTLKP RBD precipitated and no soluble protein was obtained after size exclusion purification. This precipitation was likely caused by a disruption to the coiled-coil structure following the introduction of a helix-breaking proline residue, causing the protein to unravel and aggregate.

A proline residue at position 440 was selected for with high frequency in the CIS display selection and there were a large number of similar sequences containing a K440P substitution. A consensus sequence was identified by analysis of the sequence clusters (Table 2.3, Cluster 1 - E426L/E427T/ Q433T/R434L/T437R/K440P). This cluster sequence was produced with a lysine residue in place of proline, as in the wild-type RBD, in order to measure the affinity contribution of the remainder of the cluster. The mutant lacking the proline residue was produced as a His-tagged construct (LTTLR-His), remained soluble during purification, and was produced in good yield.

## 2.4 Preparation of Ral proteins

The Ral proteins used in this study are truncated at the C-terminus (RalA residues 1-184, RalB residues 1-185) for ease of purification, as it has been noted previously that the C-terminus is unstructured and prone to degradation. It has been confirmed that these truncations do not affect the binding affinity of Ral proteins for their effectors, as all binding contacts are contained in the G-domain which has been preserved (181). The proteins used in this work also contain a single point mutation, Q72L, equivalent to Q61L in Ras, that impairs the intrinsic hydrolysis of the nucleotide so that they can be studied in their active conformation. These constructs are herein referred to as RalA and RalB.

RalA and RalB were produced as N-terminal MBP fusions with a His-tag preceding the MBP protein. Following large-scale expression and cell lysis, the fusion proteins were purified by affinity chromatography using Ni-NTA agarose beads. The Ral proteins were then cleaved from the His-tagged MBP with thrombin and eluted from the beads by washing with buffer. Ral proteins were then purified using size exclusion chromatography. An example purification is shown in Figure 2.7.

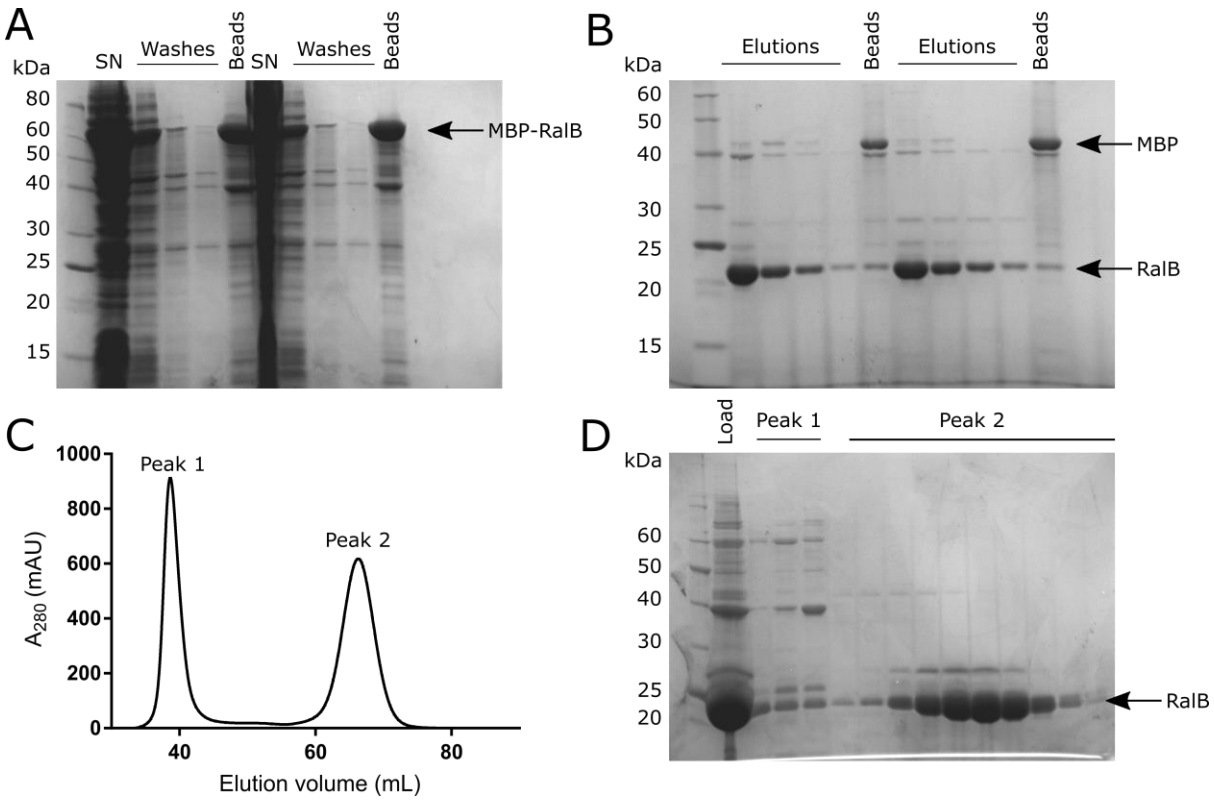


**Figure 2.7. Purification of Ral proteins. A.** SDS-PAGE analysis of samples taken from Ni-NTA bead washes following incubation with lysate of BL21(DE3) cells expressing MBP-RalB. SN, supernatant. Protein immobilised on the beads is visible in the 'beads' sample. **B.** Samples taken from elutions with buffer following overnight thrombin cleavage, and a bead sample following the elutions to show any remaining bound protein. **C.** Chromatogram from a Superdex S75 size exclusion purification of MBP-RalB. **D.** Samples taken from column fractions corresponding to peaks 1 and 2 are shown in C. RalB has a predicted molecular weight of 21.5 kDa and runs just below the 25 kDa marker.

Following purification, the nucleotide status of the Ral proteins was assessed by precipitating the protein and analysing the bound nucleotide by high performance liquid chromatography (HPLC) using an anion exchange column. The different formal charges of the nucleotides result in different retention times on the anion exchange column and standards containing purified nucleotides were run to allow identification of the peaks (Figure 2.8). Despite the presence of the Q72L mutation in the Ral proteins, some of the protein produced was still bound to GDP. Therefore, the bound nucleotide was exchanged for GMPPNP, a very slowly hydrolysable analogue of GTP that has been widely used for the study of active small GTPases. The efficiency of the exchange was assessed using HPLC, and the resulting protein was found to be 100% GMPPNP-bound. An example chromatogram is shown in Figure 2.8.

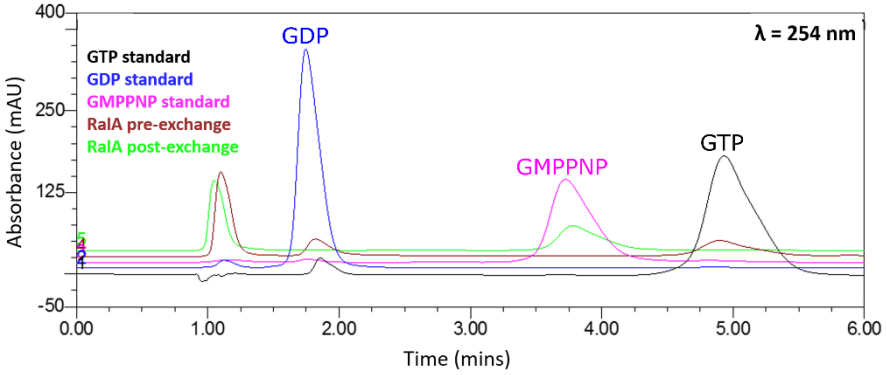


**Figure 2.8. HPLC analysis of nucleotides bound to RalA pre- and post-nucleotide exchange for GMPPNP.** Standards of GTP, GDP and GMPPNP were also run for identification of bound nucleotides. RalA pre-exchange (brown) contains a mixture of GTP and GDP, while the post-exchange sample (green) contains only GMPPNP. The peak observed at one minute for RalA samples contains buffer components that are not retained by the anion exchange column.

## 2.5 The binding affinity of RLIP76 RBD mutants to Ral proteins measured by scintillation proximity assays

The strength of the interactions between the RLIP76 RBDs and Ral proteins were measured using scintillation proximity assays (SPAs). In these assays, fluoromicrospheres coated with Protein A are used to attach an anti-His antibody for immobilisation of a His-tagged RLIP76 RBD. Prior to performing the assay, the Ral protein was radiolabelled by exchanging the bound nucleotide for $^{3}$H-GTP. When a complex is formed between the immobilised RLIP76 RBD and the labelled Ral protein, the radiolabelled protein is brought into proximity with the bead and scintillant within the fluoromicrospheres is excited by the β-emission of the $^{3}$H to produce a photon of light, which can be detected. The process is summarised in Figure 2.9. This signal is measured over a range of Ral concentrations to establish a $K_d$ value for the interaction.

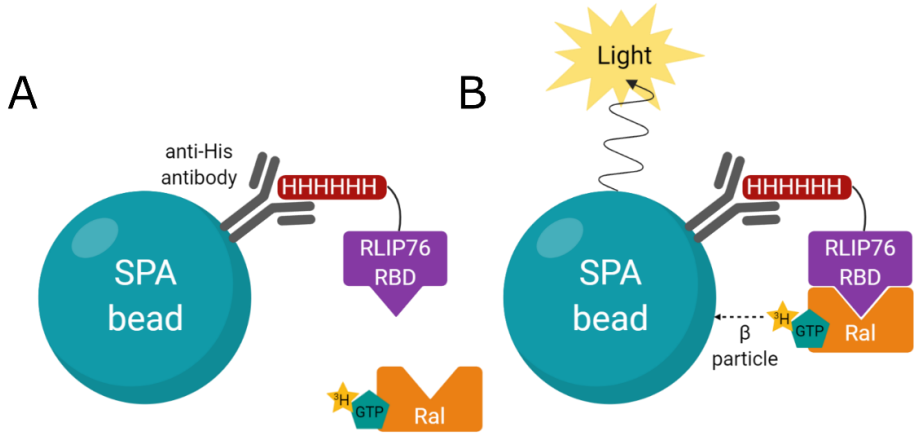


**Figure 2.9. Scintillation proximity assays (SPAs) to measure interactions between Ral proteins and their effectors. A.** His-tagged RLIP76 RBD constructs are immobilised on Protein A-coated fluoromicrospheres via an anti-His antibody. **B.** When the Ral protein labelled with [$^3$H]-GTP comes into close contact with the fluoromicrosphere i.e. when bound to the immobilised effector protein, the short-range beta emissions from the tritium excite scintillant fluid within the bead and a photon of light is produced. Figure created with BioRender.com.

### 2.5.1 Direct binding measurements

The direct binding of RalA and RalB to His-tagged wild-type RLIP76 RBD was measured to check protein quality. $K_d$ values of 45 and 54 nM were measured for RalA and RalB respectively, which are close to the previously reported values of 264 and 209 nM (181). The apparent differences in the measured and previously determined $K_d$ values may be due to the method used to determine the radiolabelled protein concentration: Bradford assays were used and are variable depending on the protein used for calibration, which is often BSA. In these experiments, non-radiolabelled RalB whose concentration had been determined by absorbance at 280 nm was used to produce a standard curve for the Bradford assay (data not shown). Examples of these direct measurements are shown in Figure 2.10.

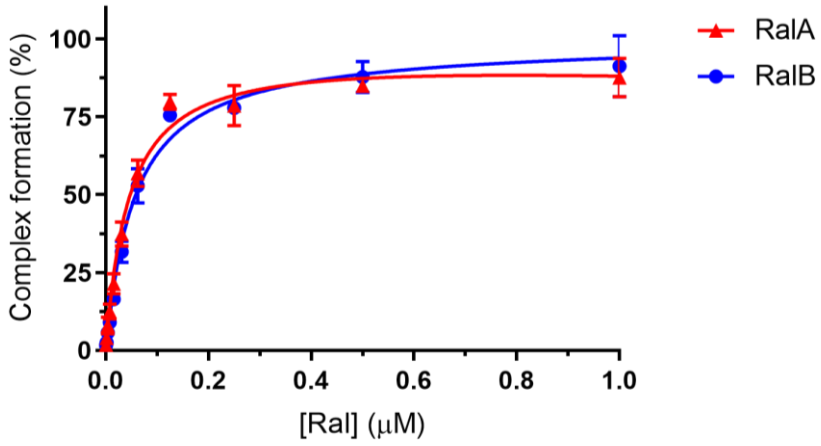


**Figure 2.10. Direct binding measurements of RalA and RalB to His-tagged RLIP76 RBD in SPAs.** The indicated concentration of [$^3$H]GTP-labeled Ral protein was incubated with His-tagged wild-type RLIP76 RBD (80 nM). The signal was corrected by subtraction of the background signal from parallel measurements containing no RLIP76 RBD. The data was fitted to a binding isotherm to give an apparent $K_d$ value and the maximum signal at saturating Ral concentrations as described previously (181). The data and curve fits are displayed as a proportion of this maximal signal: $K_d$ RalA, 45 ± 6 nM; RalB, 54 ± 10 nM. n = 2.

The His-tagged LTTLR mutant was also tested in direct binding assays and did not show measurable binding to RalA (Figure 2.11). This could suggest that the Pro residue that was selected at position 440 as part of Cluster 1 was critical for binding, perhaps by opening up the structure to make different residues available for binding. Alternatively, the unstructured RBD may have been selected for as a false positive by interacting with the bead surface or Ral proteins non-specifically.

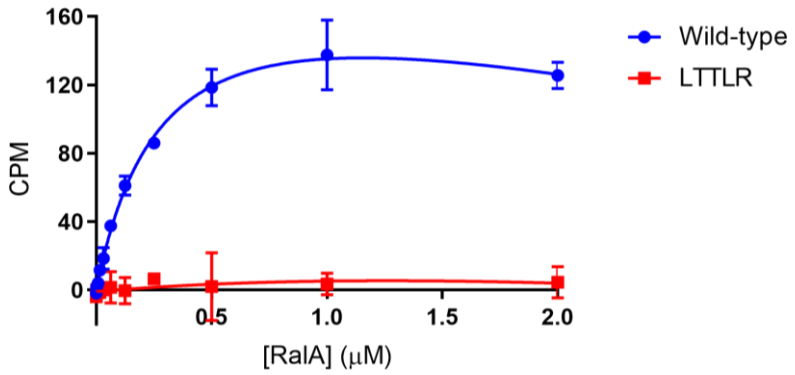


**Figure 2.11. Direct binding of the wild-type RLIP76 RBD and the LTTLR mutant to RalA, measured using scintillation proximity assays.** The indicated concentration of [$^3$H]GTP-labelled Ral protein was incubated with His-tagged wild-type or LTTLR RLIP76 RBD (80 nM). The signal was corrected by subtraction of the background signal from parallel measurements containing no RLIP76 RBD. The data was fitted to a binding isotherm to give apparent $K_d$ values as described previously (181): $K_d$ wild-type, 177 ± 16 nM; LTTLR, no binding. CPM, counts per minute. n = 2.

In this experiment, the wild-type RLIP76 RBD curve appears to curve down at 2 μM RalA. This is likely a result of the overall scintillation counts being very low, therefore the subtraction of the no RLIP76 RBD control experiment produces greater variability due to the low signal. The overall counts are affected by the extent of radiolabelling of the GTPase, and the line curving down was not observed in other experiments using a well-labelled GTPase where the overall signal was much higher.

### 2.5.2 Competition SPAs

SPA competition experiments were used to measure the binding of the other RLIP76 RBD mutants to RalA and RalB. In these experiments, a complex between the His-tagged wild-type RBD and RalA or RalB is allowed to form on the beads and unlabelled RLIP76 RBD is then titrated in, as shown in Figure 2.12. If binding is competitive, the signal decreases with increasing unlabelled RBD as Ral proteins are removed from proximity with the bead. Competition experiments were used as a greater range of $K_d$ values can be measured by this method, allowing weaker interactions to be quantified.

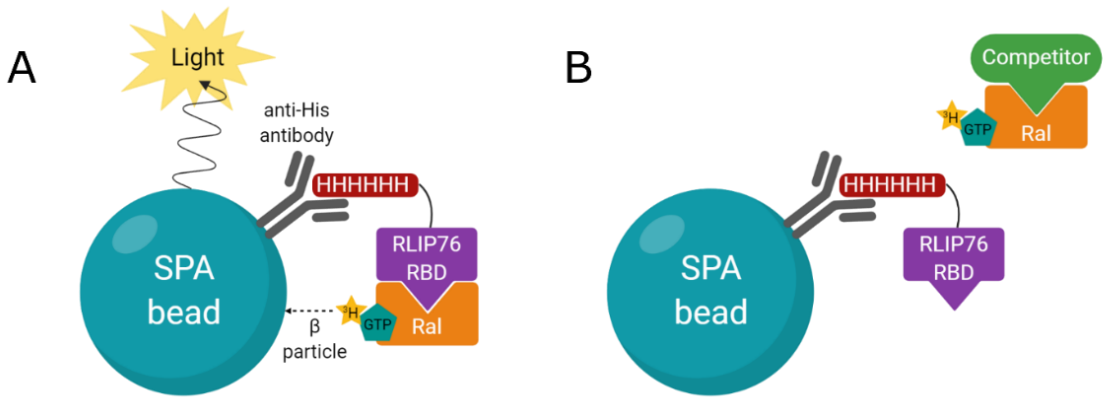


**Figure 2.12. SPA competition experiments to measure Ral-effector interactions. A.** A signal is produced when [$^3$H]GTP-labelled Ral is brought into proximity with a fluoromicrosphere SPA bead by interaction with an immobilised effector protein. **B.** Addition of a protein or peptide which binds an overlapping site on Ral proteins displaces the Ral protein from the bead surface, leading to a reduction in the measured signal. Figure created with BioRender.com.

The results of competition experiments measuring the binding of the panel of mutant RBDs to RalA and RalB are shown in Figure 2.13 and the calculated affinities are listed in Table 2.5. Affinity calculations incorporate the measured $K_d$ of the Ral/RLIP76 RBD complex on the beads, obtained from direct measurements (section 2.5.1).

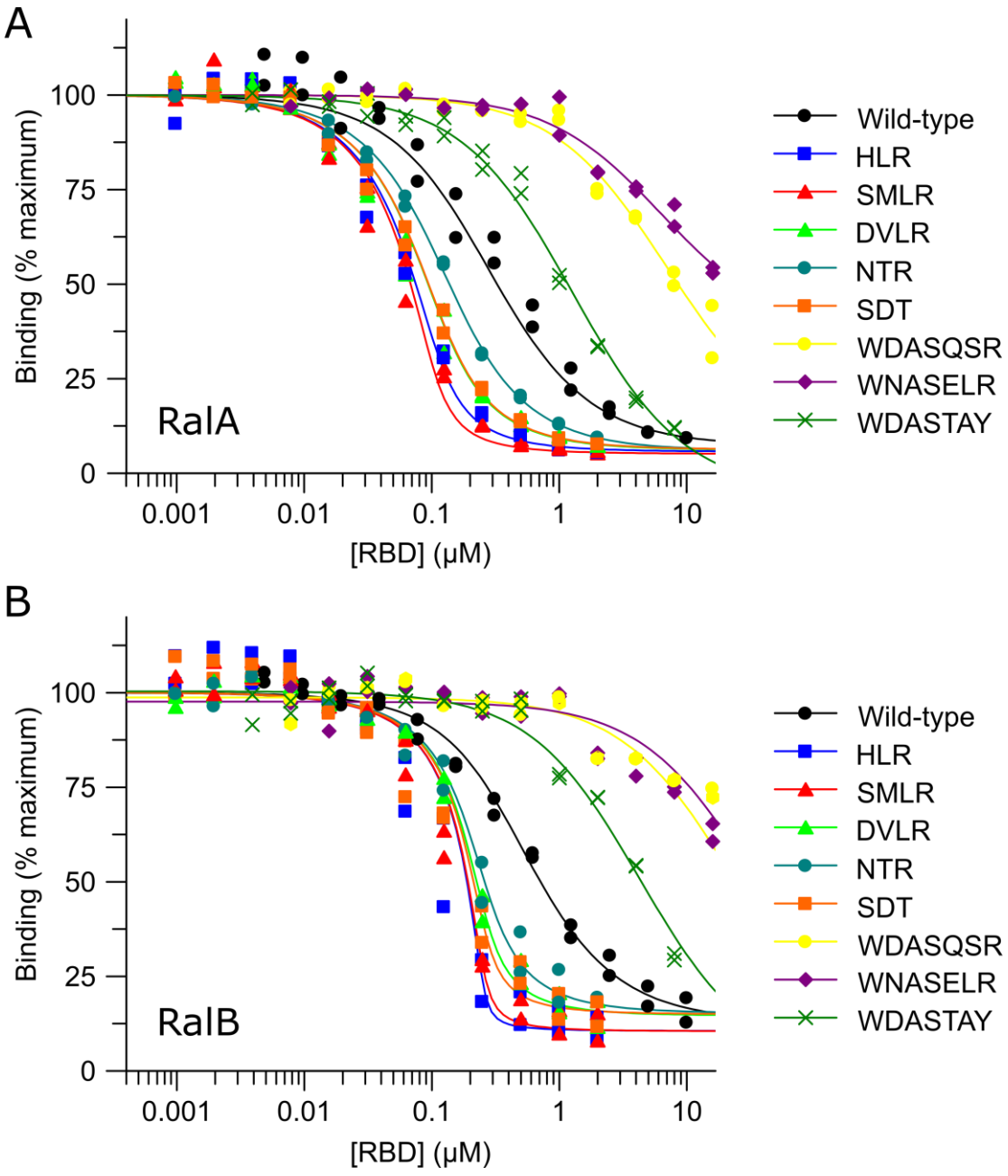


**Figure 2.13. Binding of mutant RLIP76 RBDs to Ral proteins measured by SPA competitions.** Mutant RBDs at the concentrations indicated were titrated into fixed concentrations of [$^3$H]-GTP RalA (**A**) or RalB (**B**) and His-tagged RLIP76 RBD (wild-type) immobilised on SPA beads. The data were fitted to an isotherm describing competitive binding to yield apparent $K_d$ ($K_i$) values for the mutant RBDs as described previously (182). Data and fits are displayed as a percentage of the maximum SPA signal measured for each condition. The measured $K_d$ values are listed in Table 2.5.

*Table 2.5. Affinities of RLIP76 RBD mutants for RalA and RalB measured by SPA competition.*

| Sequence name | RLIP76 RBD sequence[a] | $K_d$ RalA (nM)[b,c] | Fold change | $K_d$ RalB (nM)[b,c] | Fold change |
|---|---|---|---|---|---|
| Wild-type | LSKEERLWEVQRILTALKRKLREA | 96 ± 17 | - | 109 ± 16 | - |
| HLR | ....H.....L......R...... | 5 ± 3 | ↓19 | 1 ± 2 | ↓109 |
| SMLR | ....S.M...L......R...... | 3 ± 3 | ↓32 | 2 ± 2 | ↓55 |
| DVLR | ....D.V...L......R...... | 12 ± 4 | ↓8 | 7 ± 2 | ↓16 |
| NTR | ...N......T......R...... | 29 ± 4 | ↓3 | 13 ± 4 | ↓8 |
| SDT | ...SD.....T............. | 12 ± 4 | ↓8 | 4 ± 4 | ↓27 |
| WDASQSR | ...WD.A...SQ..S..R...... | 3020 ± 720 | ↑31 | 6970 ± 930 | ↑64 |
| WNASELR | ...WN.A...SE..L..R...... | 2750 ± 850 | ↑29 | 10350 ± 2250 | ↑95 |
| WDASTAY | ...WD.A...ST..A..Y...... | 530 ± 70 | ↑6 | 1200 ± 140 | ↑11 |

[a] Only residues 423-446 of the RLIP76 RBDs are listed, the constructs encompass residues 393-446.
[b] The mean $K_d$ is reported from two experiments.
[c] Error reported is from curve fitting.

Non-tagged wild-type RLIP76 RBD was used in a self-competition to check that the affinities measured by both methods were comparable. The affinities measured by SPA competition were estimated as 96 nM for RalA and 109 nM for RalB, which agree with the affinities measured in direct experiments (45 and 54 nM, section 2.5.1). All of the mutants tested displayed very similar affinities for RalA and RalB, which was unsurprising given that the two proteins have identical sequences in their effector binding regions.

Five of the eight mutants tested displayed higher affinity for Ral proteins than the wild-type RBD, with the tightest binding mutants, HLR and SMLR, exhibiting more than 20-fold improved affinity. These mutants shared the substitutions Q433L and K440R, which comprised a frequently occurring consensus sequence identified from the selection (Cluster 3, section 2.2.1). This suggests that these two mutations are driving the improved binding affinity, while a number of additional substitutions can be tolerated at positions 427 and 429. The DVLR mutant, containing the same consensus, bound slightly more weakly than the HLR and SMLR

mutants but still with 8 to 16-fold improved affinity compared to the wild-type sequence. The mutation of Gln433 to threonine was observed in two of the mutants displaying higher affinity: NTR and SDT, suggesting that this mutation could also be driving an improvement in binding.

The WDASQSR, WNASELR and WDASTAY mutants all showed reduced binding compared to the wild-type RBD, despite these sequences being selected with high frequency in the CIS display selection. To assess whether the RBDs were selected for as a result of binding to another site on the Ral proteins, the WDASQSR mutant was produced as a His-tagged construct to measure the direct binding affinity. The WDASQSR mutant displayed very weak binding to RalA (Figure 2.14), suggesting that the selection of this sequence was a false positive result.

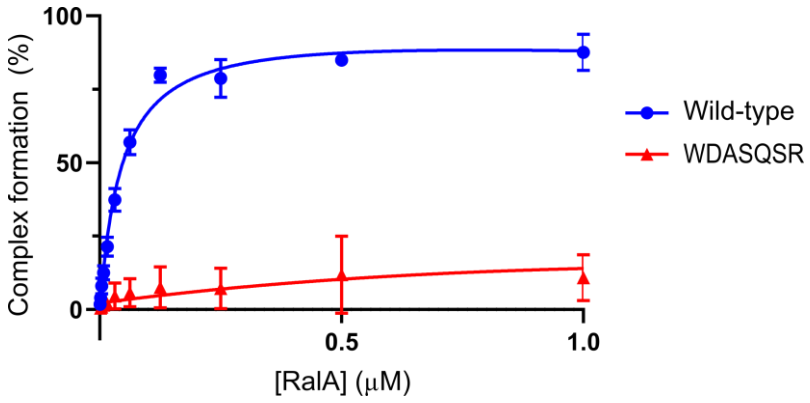


**Figure 2.14. Direct binding of the wild-type RLIP76 RBD and the WDASQSR mutant to RalA, measured using scintillation proximity assays.** The indicated concentration of [$^3$H]GTP-labelled RalA was incubated with His-tagged wild-type or WDASQSR RLIP76 RBD (80 nM). The signal was corrected by subtraction of the background signal from parallel measurements containing no RLIP76 RBD. The data was fitted to a binding isotherm to give an apparent $K_d$ value and the maximum signal at saturating Ral concentrations as described previously (181): wild-type, 45 ± 6 nM; WDASQSR, binding was too weak to fit. CPM, counts per minute. n = 2.

The identification of these false positive hits may have arisen due to the low enrichment of specific binding sequences identified in the selection. As the wild-type RLIP76 RBD template already displays a high affinity for Ral proteins and only specific residues were allowed to alter in the selection, it is perhaps unsurprising that only a few sequences with improved affinity were identified. The relatively low abundance of sequences with very high affinity for Ral

proteins may have allowed for weaker binders such as the WDASQSR, WNASELR and WDASTAY mutants to be retained through multiple rounds of selection.

### 2.6 Secondary structure estimation by circular dichroism

The addition of mutations into the RLIP76 RBD could disrupt the coiled-coil structure and therefore impact binding affinity. To assess whether the coiled-coil structure had been affected, circular dichroism (CD) was used to estimate the secondary structure of selected mutants and the wild-type RBD, and the results are shown in Figure 2.15. Helical proteins give rise to a characteristic trace in CD spectra containing a double dip with minima at 208 and 222 nm. The helical content of a protein or domain can be estimated by measuring the absorbance at 208 and 222 nm, with a more helical protein giving rise to greater negative values.

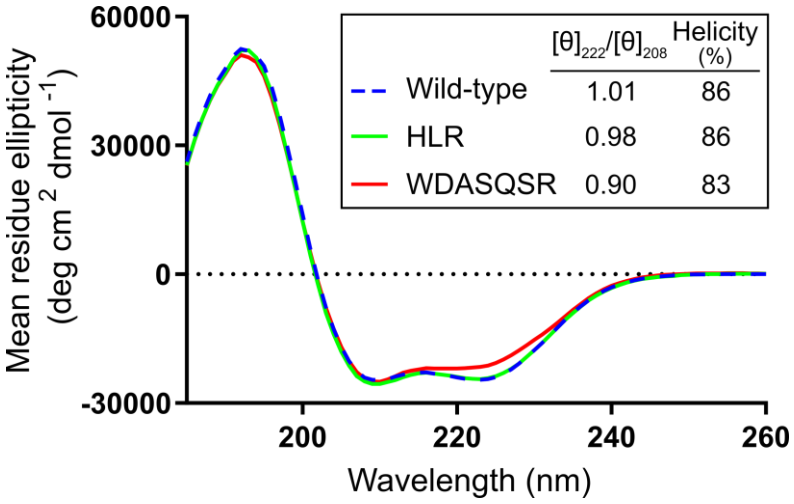


**Figure 2.15. CD spectra of RLIP76 RBD variants.** CD data are reported as mean residue ellipticities (deg cm$^2$ dmol$^{-1}$, θ) over the wavelength range 260-185 nm. The calculated ratios of the mean residue ellipticities at 222/208 nm are shown in the inset. The helical content of each RBD was determined using the CDSSTR method with reference Set 3 and DichroWeb (183–185).

Coiled-coil content can be estimated from the $[\theta]_{222}/[\theta]_{208}$ ratio, where θ is the mean residue ellipticity at the indicated wavelength: coiled-coils give values of approximately 1.0 while single α-helices give values closer to 0.8 (186, 187). All three of the proteins tested displayed the characteristic double dip at 208 and 222 nm indicating a helical secondary structure, and the calculated helicities were very similar between the mutants and the wild-type RBD (83-

86%). There were differences, however, in the estimated coiled-coil content of the mutants: the addition of seven mutations in the instance of WDASQSR changed the $[\theta]_{222}/[\theta]_{208}$ ratio from 1.01 for the wild-type RBD to 0.90, suggesting that the coiled-coil structure is disrupted, while the addition of three mutations to produce the HLR mutant had a minimal effect on the overall structure ($[\theta]_{222}/[\theta]_{208}$ = 0.98).

## 2.7 Dissecting the drivers of improved binding

During the CIS display selection performed here, multiple amino acid changes can occur simultaneously, so families of mutations that occur together are identified. In order to determine the contribution of individual mutations in the best-binding 'HLR' sequence, each mutation was reverted individually to the wild-type amino acid. The constructs listed in Table 2.6 were prepared using site-directed mutagenesis of the His-tagged RLIP76 RBD plasmid and the proteins were produced as described in section 2.3 and the methods.

*Table 2.6. RLIP76 RBDs produced recombinantly for the analysis of individual sequence substitutions.*

| Name | RLIP76 RBD sequence[a] |
|---|---|
| Wild-type-His | RLIP76(393-422, C411S)-<br>LSKEERLWEVQRILTALKRKLREANSSGRQISGHHHHHHGS |
| HLR-His | RLIP76(393-422, C411S)-<br>LSKE<u>H</u>RLWEV<u>L</u>RILTAL<u>R</u>RKLREANSSGRQISGHHHHHHGS |
| LR-His | RLIP76(393-422, C411S)-<br>LSKEERLWEV<u>L</u>RILTAL<u>R</u>RKLREANSSGRQISGHHHHHHGS |
| HL-His | RLIP76(393-422, C411S)-<br>LSKE<u>H</u>RLWEV<u>L</u>RILTALKRKLREANSSGRQISGHHHHHHGS |
| HR-His | RLIP76(393-422, C411S)-<br>LSKE<u>H</u>RLWEVQRILTAL<u>R</u>RKLREANSSGRQISGHHHHHHGS |
| L-His | RLIP76(393-422, C411S)-<br>LSKEERLWEV<u>L</u>RILTALKRKLREANSSGRQISGHHHHHHGS |

[a] Residues that differ from the wild-type RBD sequence are underlined.

Affinities of the mutants for Ral proteins were measured using isothermal titration calorimetry (ITC). An example of the data obtained is shown in Figure 2.16, and the measured $K_d$ values for RalA and RalB are listed in Table 2.7 and Table 2.8, respectively. The $K_d$ measured for RalB and the wild-type RLIP76 RBD (2.7 μM) is in close agreement with the previously reported value of 1.9 μM, which was also measured by ITC (125). The interactions between Ral proteins and the wild-type RLIP76 RBD were driven by a favourable enthalpic term (ΔH) which outweighs the entropic cost of binding (ΔS), as has been observed previously (125). While the binding affinity of the RLIP76 RBD to RalA has not been measured by ITC previously, it has been consistently observed that the affinities of RalA and RalB for the RLIP76 RBD are very similar (181), as was seen here ($K_d$ 2.3 μM RalA and 2.7 μM RalB). The $K_d$ values measured by ITC differ from those measured using SPAs (ITC $K_d$ values were around 20-fold weaker for the wild-type RBD), therefore comparing across these methods was avoided.

The variation in $K_d$ values measured using different assays may be due to the different features of the assays. In SPA experiments, one component is immobilised on beads and therefore may be presented in a particular orientation that is favourable or unfavourable to binding and the beads are pelleted at the bottom of the well giving rise to a 2D surface for binding with an increased local concentration of the immobilised component. In contrast, ITC measurements are performed with both components free in solution. SPAs may therefore estimate a tighter binding affinity because a protein bound to the immobilised component may be in very close proximity to another immobilised binding partner when released, meaning it forms another complex more quickly than if all components were free in solution. This should be controlled for by using the lowest possible concentration of the immobilised component that gives rise to a reasonable assay window.

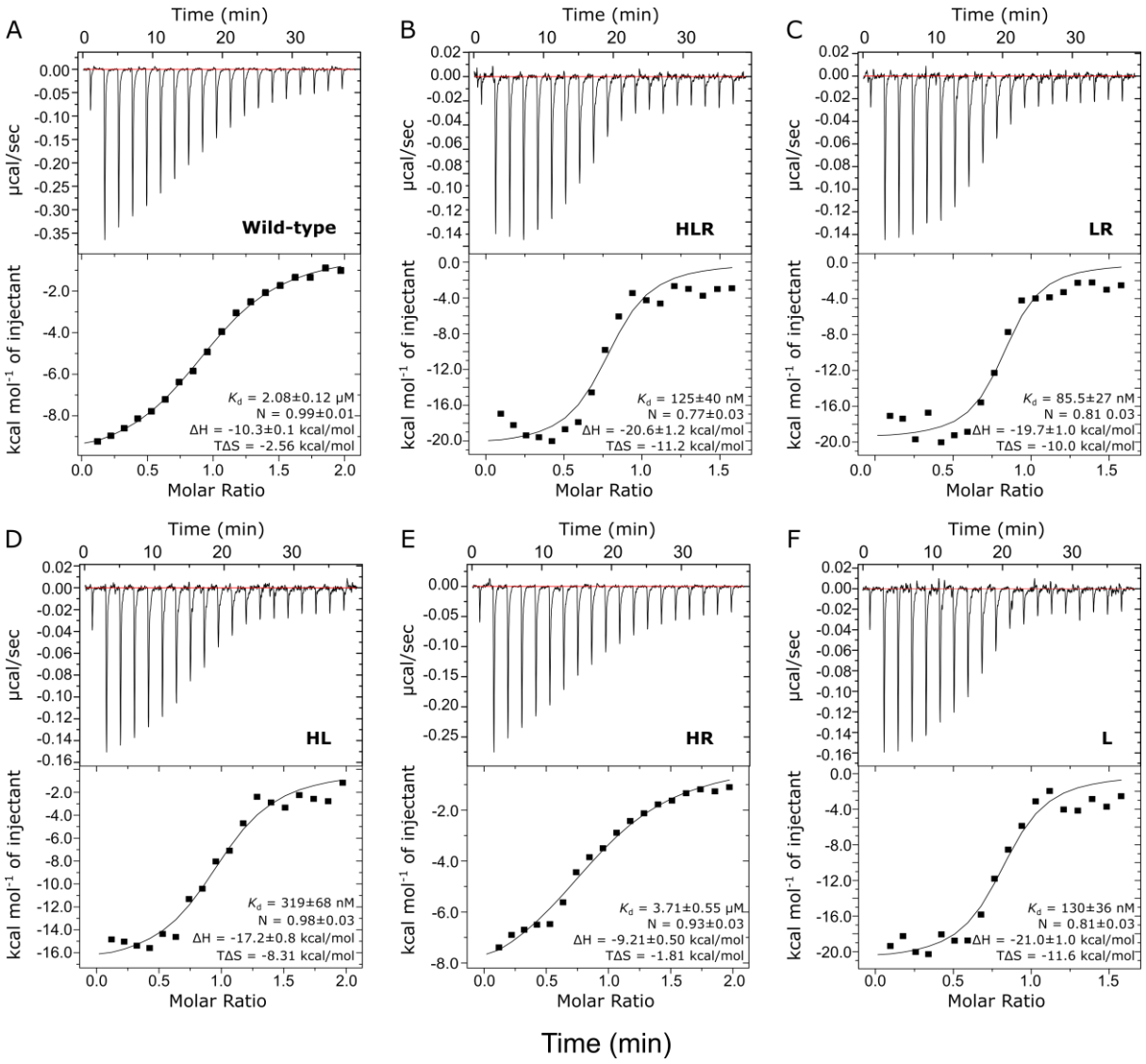


**Figure 2.16. ITC experiments measuring the interactions between selected RLIP76 RBD mutants and Ral proteins.** Shown are representative ITC data from titrations of RalB·GMPPNP into the indicated RLIP76 RBDs. The top panel of each graph shows the raw data relating to the heat change associated with each injection of RalB into the RBD. In the bottom panel, the peaks have been integrated to calculate the heat change associated with each injection. The data was fit using Origin software to a single state binding model with a least-squares fit, and the parameters for the fit for individual experiments are shown in each panel.

*Table 2.7. Binding parameters obtained from ITC for RalA titrated into selected RLIP76 RBDs.*

| Name | $K_d$ RalA (nM)[a] | N value[a] | ΔH (kcal mol$^{-1}$)[a] | TΔS (kcal mol$^{-1}$) |
|---|---|---|---|---|
| Wild-type-His | 2280 ± 250 | 0.90 ± 0.02 | -10.9 ± 0.3 | -3.25 |
| HLR-His | 299 ± 88 | 0.88 ± 0.05 | -21.4 ± 1.6 | -12.5 |
| LR-His | 82 ± 27 | 0.61 ± 0.03 | -27.2 ± 1.6 | -17.5 |
| HL-His | 412 ± 86 | 0.99 ± 0.04 | -21.3 ± 1.1 | -12.6 |
| HR-His | 1170 ± 104 | 0.79 ± 0.02 | -43.9 ± 1.7 | -35.8 |
| L-His | 99 ± 29 | 0.84 ± 0.03 | -21.3 ± 1.0 | -11.7 |

[a] Error from curve fitting for a single experiment.

*Table 2.8. Binding parameters obtained from ITC for RalB titrated into selected RLIP76 RBDs.*

| Name | $K_d$ RalB (nM)[a] | N value[a] | ΔH (kcal mol$^{-1}$)[a] | TΔS (kcal mol$^{-1}$)[a] |
|---|---|---|---|---|
| Wild-type-His | 2720 ± 640 | 1.00 ± 0.01 | -10.5 ± 0.2 | -2.89 ± 0.33 |
| HLR-His | 96.2 **±** 29.1 | 0.89 ± 0.12 | -17.7 ± 2.9 | -8.12 ± 3.08 |
| LR-His | 132 ± 46 | 0.81 ± 0.00 | -21.0 ± 1.3 | -11.6 ± 1.5 |
| HL-His | 224 ± 94 | 0.83 ± 0.15 | -19.5 ± 2.3 | -10.3 ± 2.0 |
| HR-His | 4350 ± 630 | 0.99 ± 0.06 | -9.05 ± 0.16 | -1.72 ± 0.08 |
| L-His | 110 ± 19 | 0.75 ± 0.06 | -22.4 ± 1.4 | -12.9 ± 1.3 |

[a] Data reported are the mean values from two independent experiments ± one standard deviation.

The E427H mutation was found to be deleterious for binding to RalA, as the E427H/Q433L double mutant bound less tightly than the Q433L single mutant ($K_d$ 412 nM vs 99 nM), and the E427H/Q433L/K440R triple mutant bound less tightly than the Q433L/K440R double mutant ($K_d$ 299 nM vs 82 nM). For RalB the differences were less pronounced, as the E427H/Q433L/K440R triple mutant bound with a similar affinity to the Q433L/K440R double

mutant ($K_d$ 96 nM vs 132 nM, with overlapping errors), though the E427H mutation still did not improve binding in this case.

The Q433L mutation resulted in the greatest improvement in binding, as adding this mutation alone into the RLIP76 RBD increased the binding affinity more than 20-fold to RalA and RalB ($K_d$ 2280 vs 99 nM for RalA, and $K_d$ 2720 vs 111 nM for RalB). This substitution may have been expected to give a more favourable entropic contribution (TΔS) due to the replacement of a polar residue with a hydrophobic side chain: however, this was not the case and the improvement in affinity for the Q433L mutant was due to a 2-fold increase in the favourable enthalpic contribution. Furthermore, the Q433L substitution actually increased the entropic cost of binding by 3 to 4-fold. This suggests that the Q433L mutation in the RBD has a more nuanced effect on binding than simply forming hydrophobic interactions with the Ral proteins, perhaps by altering the presentation of other RBD residues.

The K440R mutation appeared to confer a minimal improvement in binding to Ral proteins, as the E427H/Q433L/K440R triple mutant bound with only slightly higher affinity than the E427H/Q433L double mutant to RalA and RalB. The effect was not as pronounced as for the Q433L mutation and this is not surprising as the physicochemical properties of lysine and arginine are very similar: they are both cationic residues of similar side chain length. Arginine, however, does extend slightly further than lysine and has the potential to form more than one hydrogen bond, which could result in improved affinity.

The E427H/K440R (HR) double mutant lacking a Q433L substitution actually decreased binding to RalB by around 2-fold compared to the wild-type RLIP76 RBD. This demonstrated that these mutations are only beneficial when included with the Q433L substitution, as was selected for in the CIS display selection. This decrease was driven by a les enthalpically favourable interaction with RalB. The result for the HR double mutant looked strikingly different for RalA, increasing the binding affinity by around 2-fold compared to the wild-type RLIP76 RBD. The interaction increased the favourable enthalpic contribution by approximately 4-fold compared to the wild-type RBD, however this was offset by a much less favourable entropic contribution. These results show that there are subtle differences in the effector binding regions of the Ral proteins despite their identical sequences in this region, as has been shown previously (181).

## 2.8 Structural basis for improved binding

To investigate how the mutations improve binding to Ral proteins, structural data was obtained for the tightest-binding HLR and SMLR mutants in complex with RalB using X-ray crystallography.

### 2.8.1 RalB/RLIP76 RBD (HLR) mutant complex

Initially, an attempt was made to solve the structure of the RLIP76 RBD (E427H/Q433L/K400R) mutant in complex with active, GMPPNP-bound RalA and RalB. The protein complexes were prepared by incubating RalA or RalB with an excess of the RLIP76 RBD, followed by size exclusion chromatography (Figure 2.17). The RBD was added in excess as this is separated more easily from the complex due to the large difference in molecular weight.

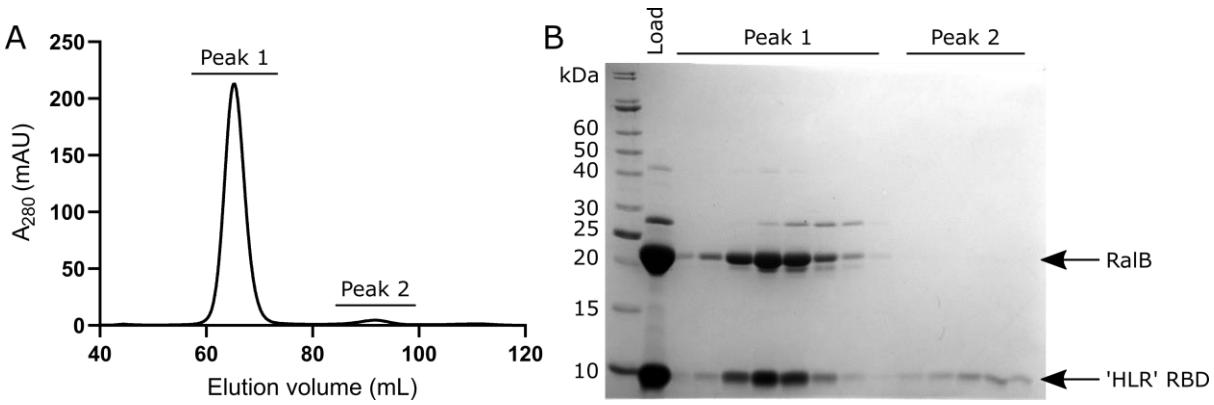


**Figure 2.17. Purification of the RalB/HLR RBD complex. A.** Chromatogram obtained after running the mixture of RalB and HLR RBD on a Superdex S75 column. **B.** SDS-PAGE analysis of fraction contents corresponding to peaks labelled in A. RalB and the HLR RBD co-elute in Peak 1, while excess free HLR RBD is present in Peak 2.

RalB and the HLR RLIP76 RBD co-eluted from the column, indicating stable complex formation, as confirmed by the presence of both species in a symmetrical peak at an earlier elution volume than the free HLR RLIP76 RBD. These complexes were then used to set up

crystallisation trials at two concentrations (10 and 5 mg $mL^{-1}$) with a range of commercially available screens, followed by incubation at 20 °C.

Large crystals were obtained for RalB in complex with the HLR RBD (Figure 2.18), while no crystals were observed for the conditions containing RalA. The RalB/HLR RBD crystals diffracted to 1.5 Å resolution and the experimental parameters are detailed in Table 2.9. The structure was determined by molecular replacement using the NMR structure of RalB·GMPPNP in complex with the wild-type RLIP76 RBD (PDB ID: 2KWI) as a search model as described in the methods.

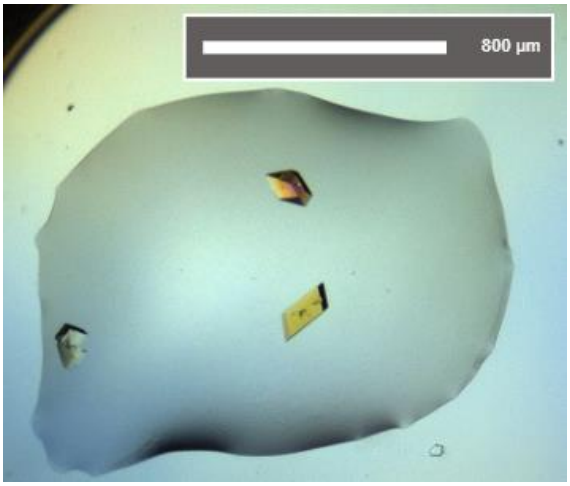


**Figure 2.18. Crystals obtained for the RalB/HLR RBD complex that were used for subsequent structure determination by X-ray crystallography.** The image was taken for the 10 mg $mL^{-1}$ condition after 8 days incubation at 20°C. The well contained 0.1 M Bicine pH 9 and 30% w/v PEG 6K.

*Table 2.9. Data Collection and Refinement Statistics for RalB·GMPPNP in complex with the RLIP76 RBD HLR mutant.*

| **Data collection** | |
|---|---|
| PDB identifier | 6ZQT |
| Resolution (Å) | 50.4-1.51 (1.55-1.51) |
| Space group | P 1 $2_1$ 1 |
| Cell dimensions | |
| a,b,c (Å) | 47.5, 77.4, 66.4 |
| α,β,γ (°) | 90, 90.3, 90 |
| Total reflections | 569,182 (24,662) |
| Redundancy | 7.6 (4.5) |
| Completeness (%) | 99.7 (98.7) |
| $I/\sigma$ | 18.3 (1.2) |
| Wilson B-factor (Å$^2$) | 24.5 |
| **Refinement** | |
| $R_{work}/R_{free}$ (%) | 18.9/22.1 (33.6/36.3) |
| No. of protein atoms | 3686 |
| No. of ligand atoms | 72 |
| No. of water molecules | 362 |
| RMSD bond length (Å) | 0.005 |
| RMSD bond angles (°) | 0.75 |
| Ramachandran statistics | |
| In favoured regions (%) | 97.1 |
| In allowed regions (%) | 2.9 |
| Outliers (%) | 0 |
| Mean B-factor (Å$^2$) | 34.5 |

[a] The numbers in parentheses represent values for the highest resolution shell.

The structure generated was compared with the NMR structure of RalB in complex with the wild-type RLIP76 RBD (PDB ID:2KWI) (91) to assess how the mutations could increase the affinity for RalB. In the wild-type RBD structure Gln433 does not form extensive contacts with RalB (Figure 2.19A), while the side chain of Leu433 in the HLR mutant packs closely with RalB and contributes to a hydrophobic network involving several Ral residues (Ala48/Leu67/Tyr82) and Trp430 of RLIP76 (Figure 2.19B). The ITC experiments described in section 2.7 also demonstrated that the Q433L mutation had the greatest contribution to increased binding, improving the affinity by more than 20-fold alone.

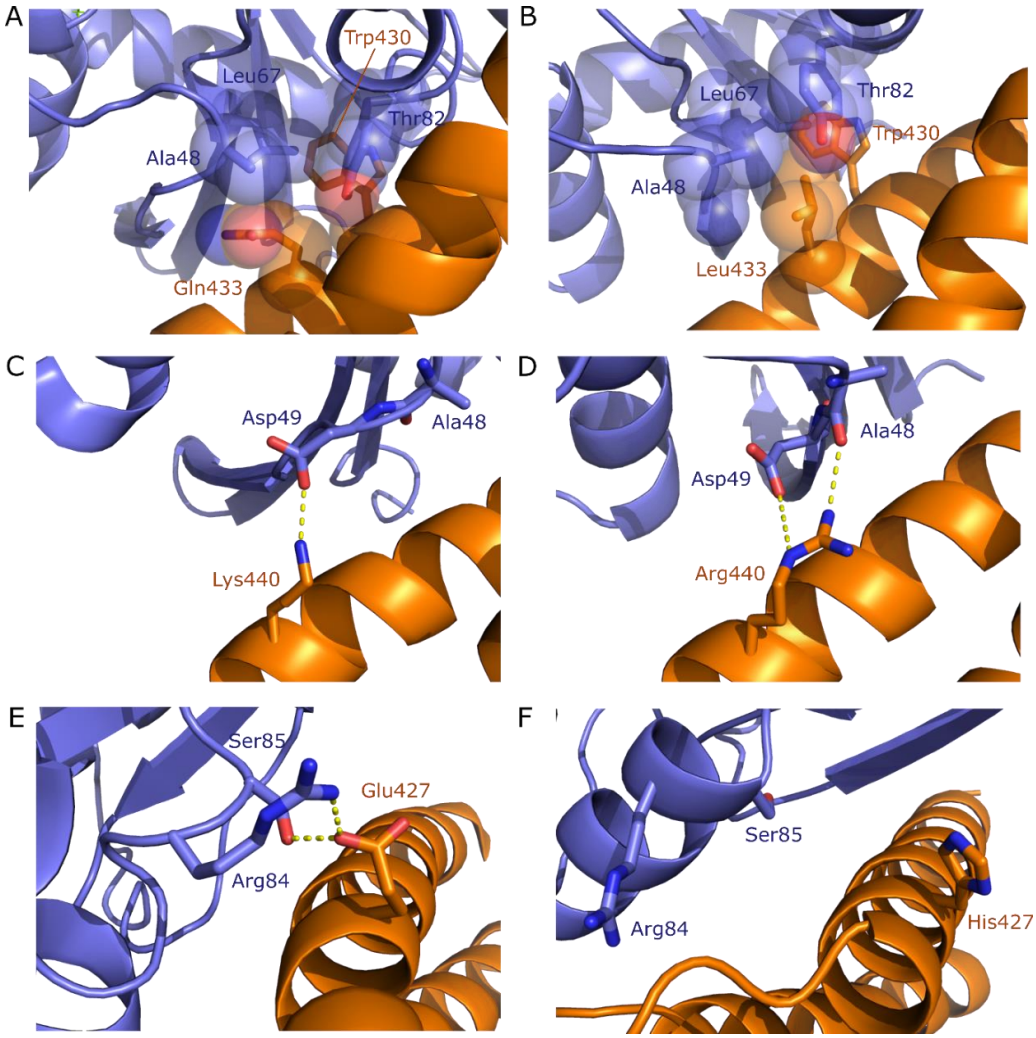


**Figure 2.19. Detailed view of RalB:RLIP76 RBD interactions.** Panels **A**, **C**, and **E** show zoomed detail of the wild-type RBD structure (PDB ID: 2KWI), while **B**, **D** and **F** show the HLR mutant structure (PDB ID: 6ZQT).

In the wild-type RBD structure, Lys440 forms a hydrogen bond with RalB Asp49 (Figure 2.19C) and this interaction has been shown to be critical for binding to Ral proteins, as replacement of Lys440 with alanine reduced the affinity 10-fold (181). Replacement of Lys440 with arginine allows the H-bond to be maintained in addition to forming a hydrogen bond with the backbone carbonyl of Ala48 (Figure 2.19D). This additional interaction is made possible by a reorganisation of switch I, which may be mediated by the replacement of Gln433 with leucine. This K440R mutation exerts only a minimal improvement in binding of the RBD to Ral proteins, as evidenced by ITC experiments (section 2.7).

The replacement of Glu427 with histidine breaks a salt bridge formed with RalB without forming any new interactions (Figure 2.19E and F), which explains why the E427H mutation

was shown to be detrimental to Ral binding by ITC (section 2.7). The Q433L and K440R mutations were selected far more frequently in the selection, while a range of amino acids were selected for at positions 427 and 429, suggesting that several substitutions at these positions are tolerated rather than the substitutions driving high affinity binding.

### 2.8.2 RalB/RLIP76 RBD (SMLR) mutant complex

Given the success had forming high quality crystals for the RalB/RLIP76 (HLR) complex, other high affinity RLIP76 RBD mutants were also trialled for crystallization. The SMLR and SDT mutants were purified in complex with RalB as described for the RalB/RLIP76 RBD (HLR) complex (section 2.8.1). Both protein complexes co-eluted from the gel filtration column, indicating stable complex formation. The SMLR mutant complex produced a number of large crystals under the same conditions that had been successful for the HLR mutant (Figure 2.20A), and smaller crystals were observed for a second condition (Figure 2.20B). No crystals of the SDT mutant complex were formed.

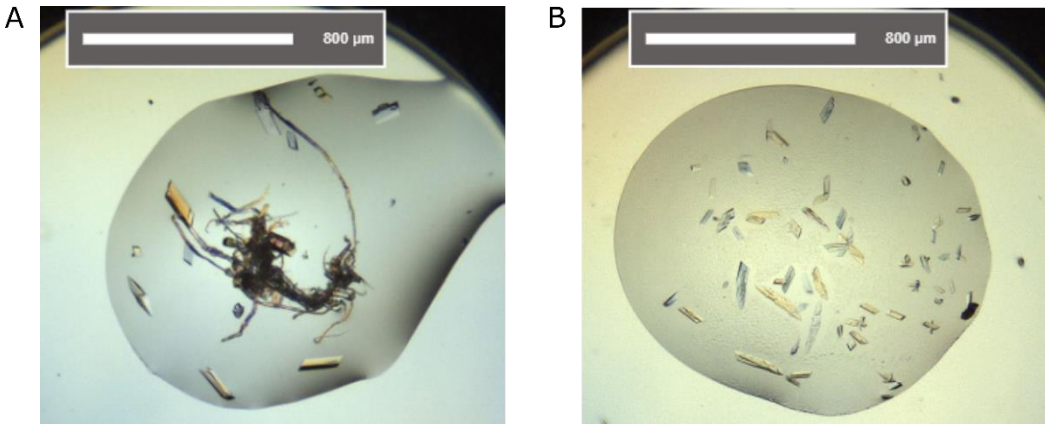


**Figure 2.20. Crystals obtained for RalB in complex with the SMLR RLIP76 RBD mutant.** The images were taken following 5 days of incubation at 20 °C with 10 mg $mL^{-1}$ complex. **A.** Well contains 0.1 M Bicine pH 9 and 30% w/v PEG 6K, the same conditions that produced crystals for the RalB/HLR RBD complex. These crystals were used for subsequent structure determination by X-ray crystallography. **B.** Smaller crystals were also observed in a well containing 0.1 M Tris-HCl pH 8 and 30% w/v PEG 6K.

The structure of the RalB/RLIP76 RBD (SMLR) mutant complex was solved to 1.5 Å and the experimental details are listed in Table 2.10. The structure was highly similar to that of the HLR mutant complex, with an RMSD of only 0.1 Å between the two structures (Figure 2.21).

The only differences in sequence between the two RBD variants are at positions 427 and 429; neither of these positions form direct contacts with RalB and so do not affect the overall structure or binding affinity. This is in line with the observation that the two RLIP76 RBD mutants (HLR and SMLR) have very similar affinities for RalB (1 and 2 nM respectively) as measured by SPA competition (section 2.5.2).

*Table 2.10. Data Collection and Refinement Statistics for RalB·GMPPNP in complex with the RLIP76 RBD SMLR mutant.*

| | |
|---|---|
| **Data collection** | |
| PDB identifier | 6ZRN |
| Resolution (Å) | 65.8-1.48 (1.56-1.48) |
| Space group | P 1 $2_1$ 1 |
| Cell dimensions | |
| a,b,c (Å) | 47.2, 77.5, 65.8 |
| α,β,γ (°) | 90, 90.1, 90 |
| Total reflections | 1,159,648 (176,059) |
| Redundancy | 14.8 (15.4) |
| Completeness (%) | 100.0 (100.0) |
| $I/\sigma$ | 8.0 (1.3) |
| Wilson B-factor (Å$^2$) | 19.3 |
| **Refinement** | |
| $R_{work}/R_{free}$ (%) | 20.1/23.9 (34.9/36.1) |
| No. of protein atoms | 3725 |
| No. of ligand atoms | 78 |
| No. of water molecules | 244 |
| RMSD bond length (Å) | 0.006 |
| RMSD bond angles (°) | 0.80 |
| Ramachandran statistics | |
| In favoured regions (%) | 96.9 |
| In allowed regions (%) | 3.1 |
| Outliers (%) | 0 |
| Mean B-factor (Å$^2$) | 30.8 |

[a] The numbers in parentheses represent values for the highest resolution shell.

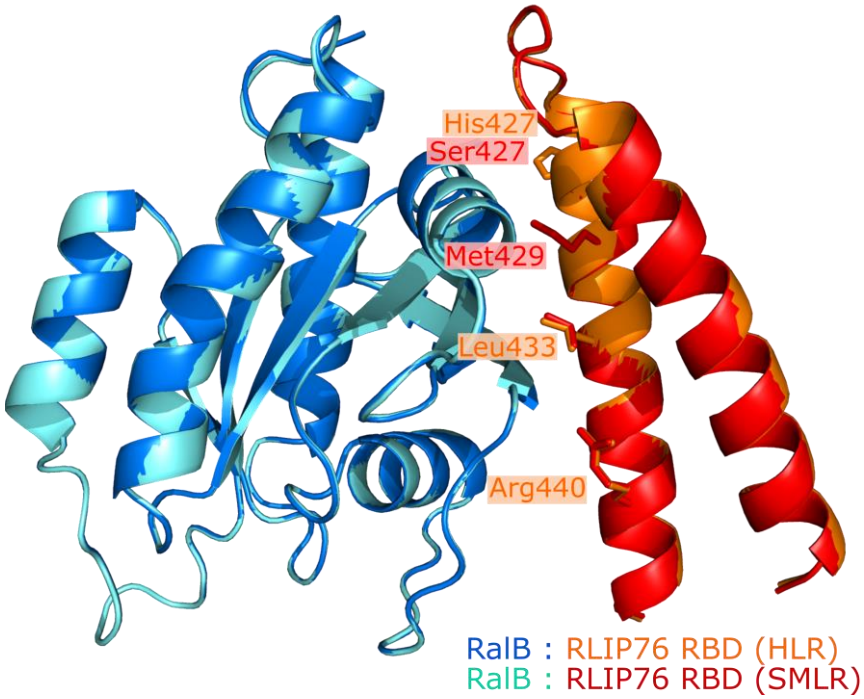


**Figure 2.21. The crystal structures of RalB·GMPPNP in complex with the RLIP76 RBD HLR and SMLR mutants reveal a high degree of similarity**. The RalB·GMPPNP/HLR complex (PDB ID: 6ZQT) is shown in blue and orange, while the RalB·GMPPNP/SMLR complex (PDB ID: 6ZRN) is shown in cyan and red. The residues that have been mutated from the wild-type RLIP76 RBD are shown as sticks.

## 2.9 Specificity of mutant RLIP76 RBDs for Ral GTPases

As the intention was to use the information from these mutant RBDs to guide the design of therapeutic peptides targeting the Ral proteins, retention of target selectivity was important. Amongst small G proteins, RLIP76 is considered to be a specific effector for RalA and RalB. To test for selectivity over the closely related Ras proteins, the RLIP76 RBD mutants were assayed for binding to K-Ras Q61L in an SPA competition assay. K-Ras shares approximately 50% similarity with Ral proteins and is found within the same family. Raf is a well-characterised effector protein for K-Ras, therefore GST-Raf RBD in complex with [$^{3}$H]-GTP K-Ras was immobilised on Protein A beads via an anti-GST antibody and was then competed off with non-tagged Raf RBD as an internal control, or with the mutant RLIP76 RBDs. The results are shown in Figure 2.22 and affinities obtained are listed in Table 2.11.

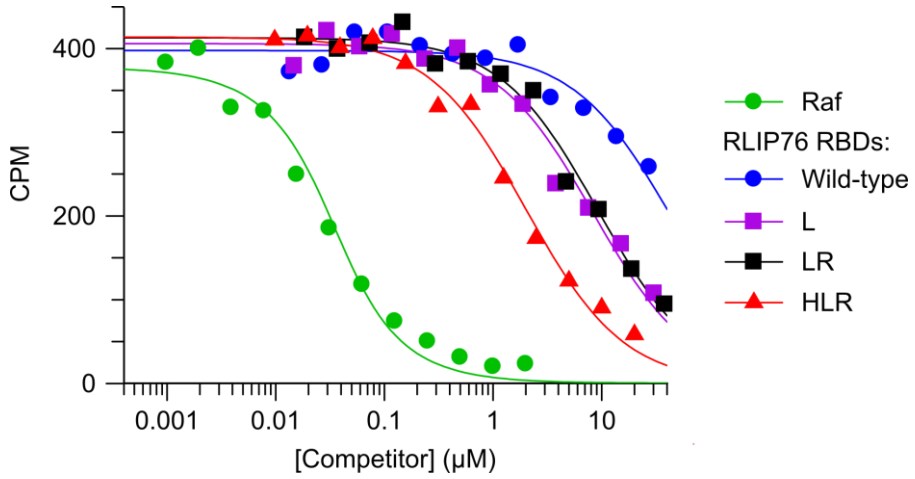


**Figure 2.22. SPA competition experiments to measure binding of RLIP76 RBDs to K-Ras**. Indicated RBDs and Raf were titrated into fixed concentrations of [$^3$H]-GTP K-Ras and GST-Raf RBD immobilised on SPA beads. The data were fitted to an isotherm describing competitive binding to yield apparent $K_d$ ($K_i$) values for the mutant RBDs as described previously (182), and the values obtained are listed in Table 2.11. n = 1.

*Table 2.11. Affinities measured from SPA competition experiments with immobilised Raf RBD and $^3$H-GTP K-Ras.*

| Protein | $K_d$ K-Ras (μM)[1] |
|---|---|
| Raf RBD | 0.0069 ± 0.0016 |
| **RLIP76 RBDs:** | |
| Wild-type-His | 18.1 ± 3.1 |
| L-His (Q433L) | 3.43 ± 0.45 |
| LR-His (Q433L/K440R) | 3.80 ± 0.41 |
| HLR-His (E427H/Q433L/K440R) | 0.827 ± 0.081 |

[1] Error from curve fitting.

The affinity of non-tagged Raf RBD for K-Ras was estimated to be 7 nM, which is comparable to the previously published value of 40 nM (188), and demonstrates that the proteins used were of good quality.

The wild-type RLIP76 RBD displayed very weak binding to K-Ras ($K_d$ 18.1 μM), which was expected as RLIP76 is not an effector of Ras. Addition of the Q433L mutation increased binding to K-Ras 5-fold, suggesting that this mutant may be able to form additional hydrophobic interactions with Ras, as was observed for RalB in the co-crystal structure. The K440R mutation made very little difference to the K-Ras affinity, as was the case for binding

to Ral proteins in ITC experiments (section 2.7). Interestingly, while the E427H mutation made very little difference to the binding affinity for Ral proteins, addition of this mutation to the LR double mutant to produce the HLR triple mutant increased binding to K-Ras a further 4-fold. Therefore, when generating therapeutic peptides towards Ral proteins based on this sequence, it may be preferable to exclude the E427H mutation as this could reduce binding to other GTPases and hence improve selectivity.

While addition of the three HLR mutations increased binding of the RLIP76 RBD for K-Ras by more than 20-fold, this binding was still very weak compared to the values observed for Ral proteins ($K_d$ 827 nM for K-Ras vs 5 nM for RalA and 1 nM for RalB, section 2.5.2), demonstrating that the sequence still displays considerable selectivity for Ral proteins. This suggests that a peptide based on the HLR sequence is likely to have a good therapeutic window for targeting the Ral GTPases as the binding of the HLR RBD mutant to K-Ras was 160 to 800-fold lower than to the Ral proteins.

## 2.10 Discussion

The aim of this work was to identify sequences based on the Ral-binding domain of RLIP76 with improved affinity for Ral proteins and maintained selectivity over closely related GTPases to inform the design of therapeutic stapled peptides. Prior to this project, a selection was performed using the RLIP76 RBD to identify amino acid substitutions that can improve binding to Ral proteins. Stapled peptides are an unsuitable starting point for a selection utilising recombinant protein expression due to the presence of unnatural amino acids, therefore the RLIP76 RBD was used as the template for selection. The RBD has been used as a convenient tool for biochemical manipulation in this project and the insights gained were used to generate stabilized peptides based on this domain.

In the design of the CIS display selection, variable positions were chosen based on their proximity to Ral, with only those able to form contacts with Ral being allowed to alter. Residues essential for binding e.g. Trp430 were not altered, as it had been shown previously that mutation of this residue to alanine ablates binding to Ral proteins (181). Trp430 occupies a defined binding pocket on Ral, therefore it is unlikely that a substituted residue could produce an improved fit and binding affinity. Allowing fewer positions to alter in a selection

means that more of the possible sequence space can be covered for the selected positions, increasing the chance of producing a high affinity binder. Rationally reducing the number of amino acids that can appear in each position, as in library 2, also served to reduce the total number of sequences, while retaining sequences that were more likely to produce high affinity binders.

The frequency of occurrence of each hit in this selection was relatively low compared to what has been observed using CIS display for other selections. None of the binding sequences were greatly enriched, suggesting modest improvements in one sequence over another. This could be because the RLIP76 RBD sequence is close to its optimal sequence for binding to Ral proteins and cannot be greatly improved by changes to the selected residues. During the selection, only 10/24 positions on the α2 helix were allowed to alter and the overall coiled-coil structure was supported by the presence of the non-modified α1 helix. This meant that sequences were constrained to the coiled-coil structure and therefore the potential to form new interactions with Ral proteins was limited. Rather than using a known effector for affinity maturation to inform peptide design, a naïve selection using a library of peptides could be used to produce a greater diversity of possible binding modes.

This work aimed to validate the hits from the selection by producing the sequences as recombinant proteins and assessing their binding to Ral proteins in biochemical assays. Three clusters of mutations appearing with the highest frequency (Table 2.3) were identified from the selection. Cluster one contained a proline residue in place of Lys440, however it was not possible to produce sequences containing this mutation as the proteins aggregated, suggesting that the RBD has become unstructured. Proline is known to be a helix-breaking amino acid and was therefore likely to be responsible for the loss of structure. A construct containing the rest of the mutations identified in cluster one, with Lys440 instead of proline was purified and this RBD mutant (LTTLR) did not show any binding to Ral proteins (Figure 2.11), suggesting this cluster was either identified as a false positive result, or that the proline residue was critical for binding. These disordered, proline-containing proteins may have been selected due to non-specific binding to the beads or another component of the assay.

The second sequence cluster identified, cluster 2 (Table 2.3), contained five amino acid changes occurring together with high frequency. The sequences related to this cluster

(WDASQSR, WNASELR and WDASTAY) that were produced and tested all bound RalA and RalB with lower affinity than the wild-type RBD sequence in SPA competition experiments. To test whether the sequence could bind a different site on Ral with higher affinity, hence explaining the selection, a His-tagged version of the WDASQSR mutant was produced to assess direct binding. The sequence did not show appreciable binding to Ral proteins in a direct assay, so was likely selected for specifically but as a lower affinity sequence. CD experiments showed that the inclusion of these seven mutations decreased the coiled-coil structure of the RLIP76 RBD, which could have contributed to a loss of affinity.

The selection was successful in identifying mutants with improved affinity for the Ral proteins, as the tightest binding RBDs exhibited more than a 20-fold increase in affinity. The two best-binding sequences assayed, along with several other hits from the selection, contained Q433L and K440R mutations (cluster 3, Table 2.3), while positions 427 and 429 appeared as a variety of amino acids. ITC experiments demonstrated that the Q433L mutation alone gave the greatest increase in binding, while the K440R mutation gave a more modest improvement. Substitutions at positions 427 and 429 had little effect, suggesting that a range of amino acids could be well-tolerated in this position. Elucidation of the structure of two mutants containing the Q433L mutations revealed that the leucine residue can form extensive hydrophobic interactions with RalB, which appears to be the driver for the improvement in binding. Arg440 is able to form an additional hydrogen bond with RalB compared to the lysine at this position in the wild-type structure. The residues at positions 427 and 429 did not appear to form any interactions with RalB and the two overall structures of these mutants were nearly identical. In conjunction with the ITC experiments described in section 2.7, the structural evidence confirms that these positions are not necessary for driving high affinity interactions.

While making changes to the RLIP76 RBD, it is important that selectivity for Ral proteins is maintained. Increasing the mutational load of the RLIP76 RBD from the single Q433L mutant to the HLR triple mutant increased off-target binding to K-Ras, therefore peptides designed to target Ral selectively should include fewer mutations to retain more selectivity. The E427H mutation could be excluded, as this does not enhance binding to Ral proteins but does increase off-target binding to K-Ras.

Biochemical, biophysical and structural analysis of the products from the CIS display selection has led to the identification of useful amino acid substitutions to include in second-generation stapled peptides targeting the Ral proteins. While this selection explored a huge range of natural amino acid combinations, it is possible that the inclusion of unnatural amino acids could also aid binding affinity. Replacement of tryptophan with chlorotryptophan in Mdm2-binding peptides has resulted in peptides with improved affinity, due to the chloro moiety extending deeper into the binding pocket and forming more extensive contacts with the target (189). Such a replacement may also benefit Ral-binding peptides as binding is mediated by a critical tryptophan residue (Trp430). The Q433L mutation in the RLIP76 RBD was shown to be most beneficial in improving binding by making increased hydrophobic contacts with Ral, therefore it is possible than an unnatural hydrophobic amino acid could be used in this position to form even stronger or more extensive hydrophobic contacts with Ral proteins. The crystal structures of mutant RBDs in complex Ral could be used as helpful starting points to model unnatural amino acid substitutions and predict which may form favourable contacts.

# 3 Stapled peptides targeting the Ral GTPases

## 3.1 Introduction

As discussed in Chapter 1, an inhibitor of the Ral GTPases would be highly valuable to assess the utility of inhibiting the Ral pathway to disrupt oncogenic Ras signalling. The Ral pathway has been shown to play a critical role in the survival of several Ras-mutant cancer types, including pancreatic and colorectal cancers (reviewed in (77)). Like Ras, the active Ral proteins interact with their effectors through protein-protein interactions utilising a smooth, shallow surface that is difficult to target through traditional drug discovery methods. Peptides are an effective modality to target such surfaces, as these biologics can offer exquisite target binding and selectivity at large, relatively featureless interfaces.

Previous work carried out in the lab has demonstrated that stapled peptides based on residues 423-446 of the Ral effector RLIP76 can bind and inhibit Ral proteins (125). In this work, a variety of staple lengths and positions were trialled and it was found that a peptide containing an all-hydrocarbon staple bridging positions 424-428 gave rise to the tightest binding affinity for Ral proteins, with a $K_d$ for RalB of 5 μM.

Chapter 2 described how a maturation selection was carried out on the Ral-binding domain (RBD) of RLIP76, with the aim of identifying sequences that bind more tightly to Ral proteins to inform the design of second-generation stapled peptides. Here, the insights gained from the selection and other work involving the RLIP76 RBD have been used to improve several important drug-like properties of the stapled peptides, including target affinity, selectivity and cell entry.

## 3.2 Peptides generated from selection sequences

Four of the most enriched sequences from the CIS display selection described in Chapter 2 provided templates for the design of a series of stapled peptides based on residues 423-446 of the RLIP76 RBD. The two staple positions that gave rise to the highest affinity binders identified previously were incorporated into each sequence and a fluorescein tag was added to the N-termini of the peptides for assessment of binding affinities by fluorescence

polarization (125). The staples were formed using (*S*)-pentenylalanine residues that were covalently linked by Grubbs' ring closing metathesis. A reversed sequence containing a central staple was also generated to act as a negative control in binding experiments. These peptides were purchased from a commercial source and are listed in Table 3.1.

*Table 3.1. Stapled peptides (Eurogentec) based on sequences identified by CIS display maturation of the RLIP76 RBD.*

| Peptide name[a] | Sequence[b] |
|---|---|
| Non-stapled | FAM-LSKEERLWEVQRILTALKRKLREA |
| SP1 | FAM-LXKEEXLWEVQRILTALKRKLREA |
| SP2 | FAM-LSKEERLWEXQRIXTALKRKLREA |
| Reversed sequence | FAM- AERLKRKLATXIRQXEWLREEKSL |
| LTNTLKP-SP1 | FAM- LXKLTXNWEVTLILKALPRKLREA |
| LTNTLKP-SP2 | FAM- LSKLTRNWEXTLIXKALPRKLREA |
| LSHTLRP-SP1 | FAM- LXKLSXHWEVTLILRALPRKLREA |
| LSHTLRP-SP2 | FAM- LSKLSRHWEXTLIXRALPRKLREA |
| WDASQSR-SP1 | FAM- LXKWDXAWEVSQILSALRRKLREA |
| WDASQSR-SP2 | FAM- LSKWDRAWEXSQIXSALRRKLREA |
| HLR-SP1 | FAM- LXKEHXLWEVLRILTALRRKLREA |
| HLR-SP2 | FAM- LSKEHRLWEXLRIXTALRRKLREA |

[a] SP1, staple position 1 bridging residues 424 and 428 (RLIP76 numbering); SP2, staple position 2 bridging 432 and 436.
[b] Sequence variations from the 'wild-type' peptide (SP1) are underlined. X, (*S*)-pentenylalanine; FAM, 5-carboxyfluorescein.

### 3.3 Fluorescence polarization to assess peptide binding

Fluorescence polarization (FP) is a technique that is widely used in the process of drug discovery to quantify protein-ligand interactions. In this assay, a fluorophore is excited with plane-polarized light and the emitted light is measured in two planes: one that is parallel ($I_{\parallel}$) *to* the polarized light used for excitation and another that is perpendicular ($I_{\perp}$). The extent of

polarization (P) is linked to the amount of light detected in each of these planes by equation 1:

$$P = \frac{I_{\parallel} - I_{\perp}}{I_{\parallel} + I_{\perp}} \qquad \text{(Equation 1)}$$

The observed polarization is linked to the rotational diffusion rate of the fluorophore being measured. For example, a small molecule in a solution of low viscosity will rotate on a timescale that is far shorter than the excitation lifetime of the fluorophore (typically ns), therefore the emitted light will be randomly distributed between the planes ($I_{\parallel} = I_{\perp}$) and resulting polarization is zero. As the size of the fluorescent species or the viscosity of the solution increases, the speed of rotation of the fluorophore decreases. As the rotational diffusion rate approaches and exceeds the excitation lifetime of the fluorophore, the amount of emitted light measured in the parallel ($I_{\parallel}$) and perpendicular ($I_{\perp}$) planes is no longer evenly distributed and polarization is retained (Figure 3.1).

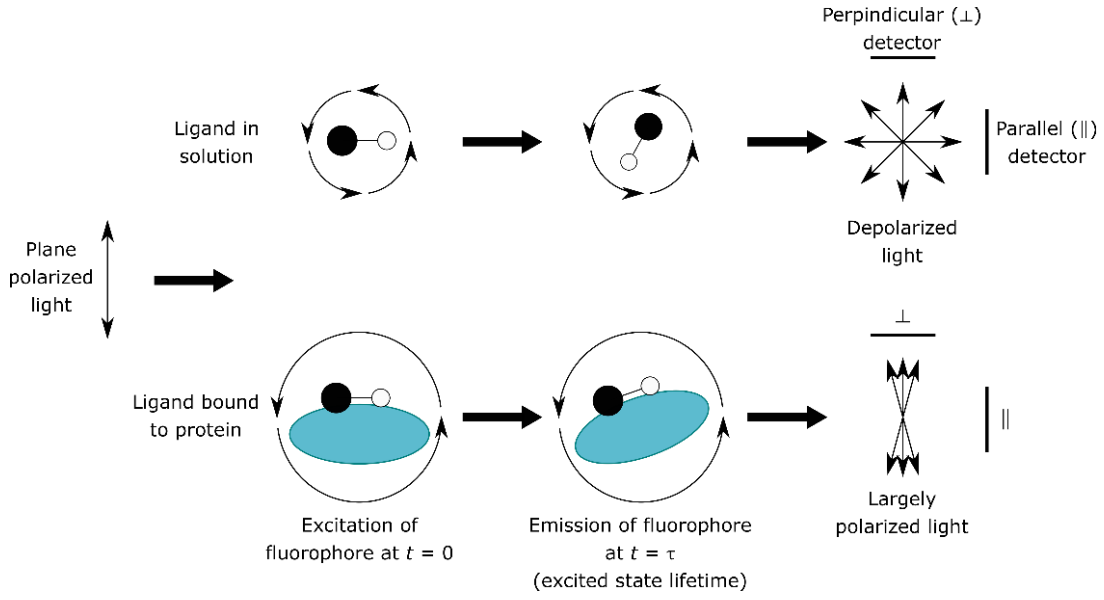


**Figure 3.1. Principles of fluorescence polarization.** A small molecule or peptide (black circle) linked to a fluorophore (white circle) is excited by plane polarized light. During the lifetime of the excited state (τ), the free molecule rotates significantly, and the emitted light is depolarized. When the fluorescent entity is bound to a larger molecule e.g. a protein (blue ellipse), it rotates much less during the excitation lifetime and much of the polarization of the light is retained. The emitted light is detected at parallel (‖) and perpendicular (⊥) planes to the initial polarized light. Figure reproduced from Moerke (190).

When a small fluorescent ligand binds a larger molecule e.g. a protein, the rotational diffusion of the complex is reduced compared to the free fluorophore and an increase in polarization is observed. As such, affinity can be assessed by titrating a protein into a fixed concentration of fluorescent ligand. The assay window is determined by the difference in rotational diffusion of the free fluorophore and the bound complex, therefore the fluorophore should be attached to the smaller binding partner in order to maximise this measurable difference.

### 3.4 Binding of stapled peptides to the Ral GTPases

The binding of the panel of stapled peptides to active Ral proteins was measured by FP, using a fixed concentration of fluorophore-conjugated peptide and increasing concentrations of the Ral protein. The Ral proteins contained a Q72L mutation that prevents nucleotide hydrolysis, ensuring that they were studied in their active form. Additionally, the bound nucleotides were exchanged for GMPPNP, a very slowly hydrolysable analogue of GTP, prior to use. The results are shown in Figure 3.2 and the $K_d$ values obtained are listed in Table 3.2.

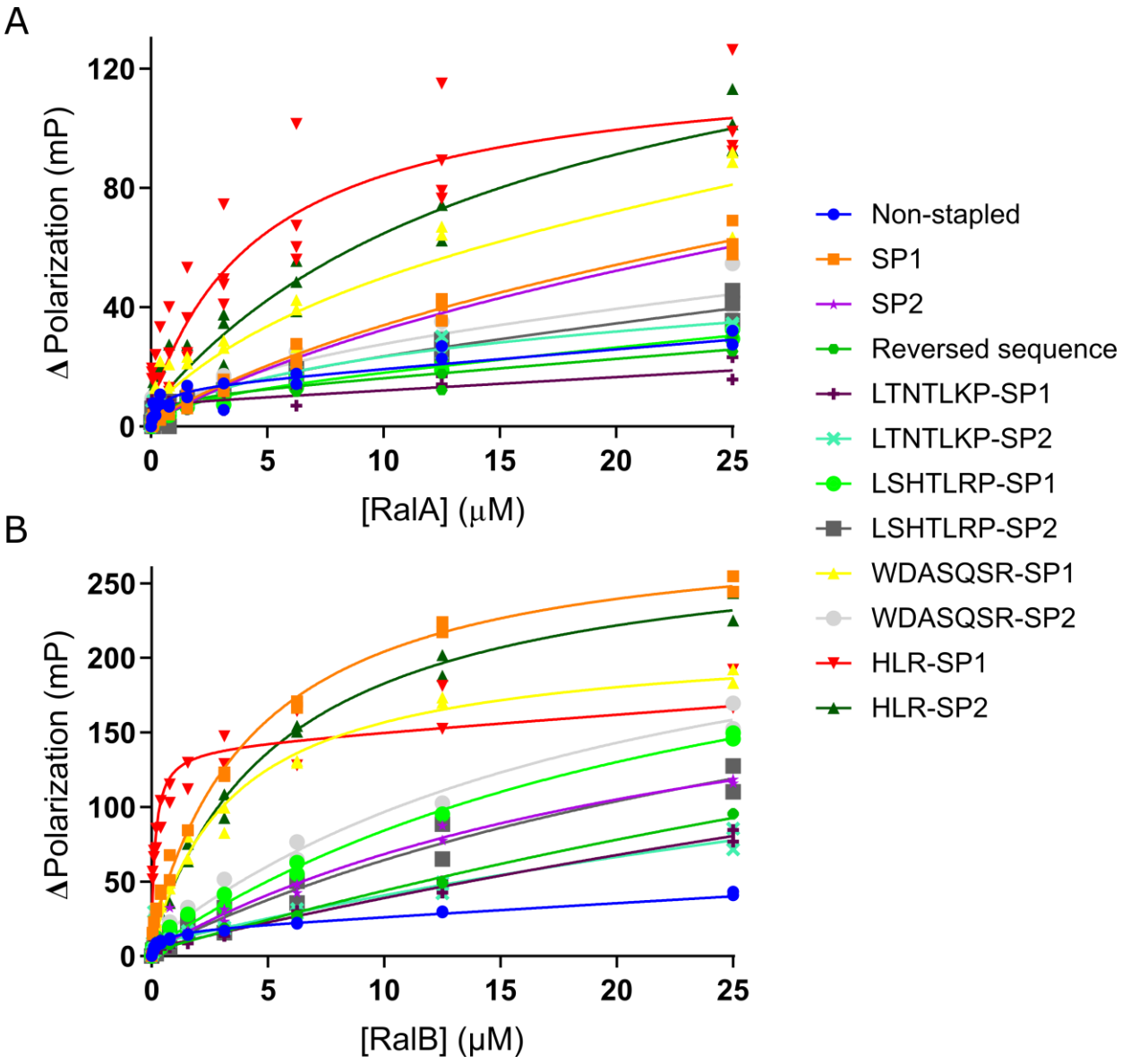


**Figure 3.2. Binding of stapled peptides to Ral proteins.** FP data for direct binding of 20 nM FAM-labelled stapled peptides to varying concentrations of RalA·GMPPNP (**A**) or RalB·GMPPNP (**B**). Data were fitted to a single-site binding model using non-linear regression analysis in GraphPad Prism. Individual data points are displayed as symbols and the fit lines as solid coloured lines corresponding to the data point colours. SP1, staple position 1; SP2, staple position 2; mP, millipolarization units. n ≥ 2 for all conditions.

*Table 3.2. Affinities of peptides for Ral proteins measured by FP.*

| Peptide name | $K_d$ RalA (μM)[a] | $K_d$ RalB (μM)[a] |
|---|---|---|
| Non-stapled | - | - |
| SP1 | 17.2 ± 9.2 | 4.68 ± 0.64 |
| SP2 | 16.3 ± 10.2 | 25.3 ± 18.1 |
| Reversed sequence | - | - |
| LTNTLKP-SP1 | - | - |
| LTNTLKP-SP2 | - | - |
| LSHTLRP-SP1 | - | 31.4 ± 10.8 |
| LSHTLRP-SP2 | - | 35.1 ± 33.2 |
| WDASQSR-SP1 | 8.68 ± 7.57 | 3.47 ± 0.68 |
| WDASQSR-SP2 | - | 24.8 ± 11.7 |
| HLR-SP1 | 4.70 ± 2.04 | 0.159 ± 0.047 |
| HLR-SP2 | 14.8 ± 8.0 | 5.60 ± 0.80 |

[a] Values for peptides showing equal or lower polarization changes than the negative control peptide were deemed 'non-binders' and measured $K_d$ values are not included as indicated by '-'.

HLR-SP1 showed the largest apparent improvement in binding to Ral proteins over the SP1 parent peptide, with a 30-fold improvement in binding to RalB (160 nM vs 4.7 μM), and a 3-fold improvement in binding to RalA (4.7 μM vs 17 μM). This agreed with the findings in the context of the RLIP76 RBD, where the HLR mutations gave rise to a 20-fold improvement in binding compared to the wild-type sequence (sections 2.5 and 2.7).

In these experiments, several differences between the binding of the peptides and the RLIP76 RBDs were revealed. For example, the HLR-mutant RLIP76 RBD affected binding to RalA and RalB equally (section 2.5), while the HLR-mutant peptide (HLR-SP1) had a much larger impact on binding to RalB than to RalA (30-fold vs 3-fold). In addition, the wild-type and HLR-mutant RBDs do not discriminate between the Ral proteins and bind with near-identical affinity to RalA and RalB. The peptides, however, show much greater binding affinity for RalB. This suggested that the peptides may not binding in the same way as the α2 helix of the RBD and may instead be binding non-specifically.

There was also variability between the data repeats e.g. HLR-SP1 for RalA, suggesting that another factor was influencing the apparent binding affinities. It was later shown that increasing the incubation time prior to reading the plate led to tighter $K_d$ estimates and a greater maximum signal (see section 3.4.2), demonstrating that a non-specific effect was confounding these results.

The WDASQSR mutations were also tested in the context of the RLIP76 RBD and were found to significantly decrease binding to Ral proteins (section 2.5). In this context however, the WDASQSR-SP1 peptide appears to bind Ral proteins with around 2-fold greater affinity than the wild-type sequence (SP1), again suggesting that this stapled peptide bound to Ral proteins in a different manner to the coiled-coil RBD containing the same residues. It was important to establish the mode of binding of the peptides, as any therapeutic peptides would be required to inhibit Ral-effector interactions in order to disrupt Ral signalling.

The LTNTLKP and LSHTLRP sequences could not be tested within the RLIP76 RBD due to aggregation issues during purification, which was believed to be due to the presence of a helix-breaking Pro residue in both cases. As stapled peptides, these sequences reduced binding to Ral proteins compared to the SP1 parent peptide and showed similar changes in polarization to the reversed sequence.

### 3.4.1 Peptide selectivity for Ral proteins over related small GTPases

In order to assess the selectivity of the peptides for Ral proteins over closely related small GTPases, a panel of small GTPases was prepared. RhoA (1-186, F25N/Q63L) and Cdc42 (1-184, Q61L) were produced as described in the methods, while Rac1 (1-187, Q61L) and K-Ras (1-169) were available in the lab as purified proteins. The bound nucleotides of all GTPases were exchanged for GMPPNP prior to use in fluorescence polarization assays. These proteins will herein be referred to as RhoA, Cdc42, Rac1 and K-Ras.

The results from fluorescence polarization assays measuring the binding between the SP1 and HLR-SP1 stapled peptides and the panel of small GTPases are shown in Figure 3.3 and the measured $K_d$ values are listed in Table 3.3.

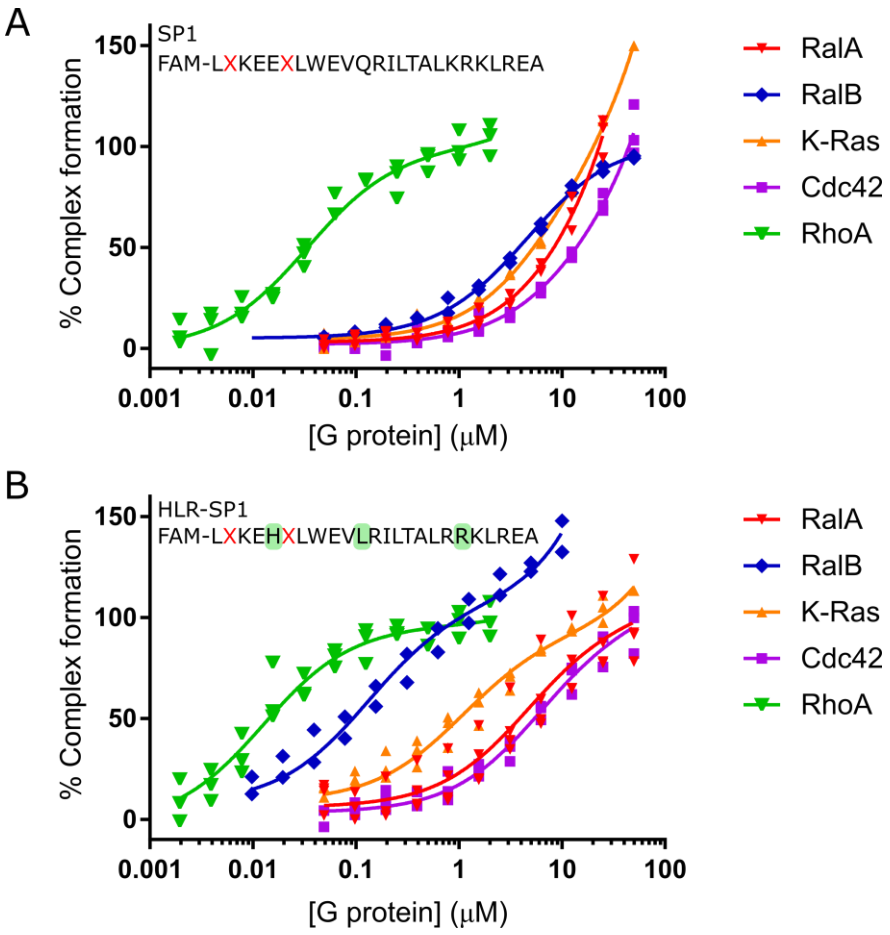


**Figure 3.3. Binding of SP1 and HLR-SP1 peptides to a panel of small GTPases**. FP data for direct binding of 20 nM FAM-labelled SP1 (**A**) and HLR-SP1 (**B**) to varying concentrations of the indicated small GTPases. Data were fitted to a single-site binding model using non-linear regression analysis in GraphPad Prism, and the $K_d$ values obtained are listed in Table 3.3. Data and curve fits are displayed as a percentage of the calculated saturated FP signal in each assay. n ≥ 2 for all conditions, and individual results are displayed as symbols. The peptide sequences are shown, and variations from the SP1 sequence are highlighted in green. X, (*S*)-pentenylalanine; FAM, 5-carboxyfluorescein.

*Table 3.3. Affinities of SP1 and HLR-SP1 peptides for a panel of small GTPases measured by FP.*

| GTPase | $K_d$ SP1 (μM)[a] | $K_d$ HLR-SP1 (μM)[a] |
|---|---|---|
| RalA | 17.2 ± 9.2 | 4.68 ± 0.64 |
| RalB | 4.70 ± 2.04 | 0.159 ± 0.047 |
| K-Ras | 8.18 ± 1.99 | 1.06 ± 0.20 |
| Cdc42 | 13.0 ± 7.4 | 6.11 ± 1.67 |
| RhoA | 0.0338 ± 0.0054 | 0.0125 ± 0.0022 |

[a] Error from curve fitting.

Several of the binding curves did not reach saturation and instead continued to rise with a linear slope indicating a non-specific binding effect e.g. for K-Ras, Cdc42 and RalA with SP1. The equation used to calculate the binding affinities takes this slope into account and estimates the maximum binding that is observed without the non-specific effect, hence some curves exceed the predicted 100% complex formation. In some conditions e.g. HLR-SP1 with RalB, it is clear that two binding events are taking place, as the curve appears to saturate before rising again in a linear fashion.

Both peptides appeared to bind RhoA with far greater affinity than that displayed for the Ral proteins. The peptides were not expected to bind RhoA, as the RLIP76 RBD from which the peptides were derived does not bind to RhoA (data not shown). This observation, in combination with the unusual curve shapes, suggested that non-specific interactions made by the peptides were responsible. Later experiments confirmed that non-specific binding was confounding the results of these FP experiments and that the peptides were not genuine RhoA binders.

### 3.4.2 Investigations into non-specific binding

When performing the FP assays, it was observed that the magnitude of the signal changed depending on the incubation time before reading. This was investigated using the SP1 peptide and RalB, measuring the same wells after increasing incubation times, and the results are shown in Figure 3.4. The FP signal increased over time and the mid-point of the curve shifted to the left, indicating a tighter binding affinity. The peptide-RalB complex is unlikely to need so long to equilibrate, therefore the increase in signal over time is likely due to a non-specific effect, such as binding of the peptide to the wells of the plate, that accumulates over time.

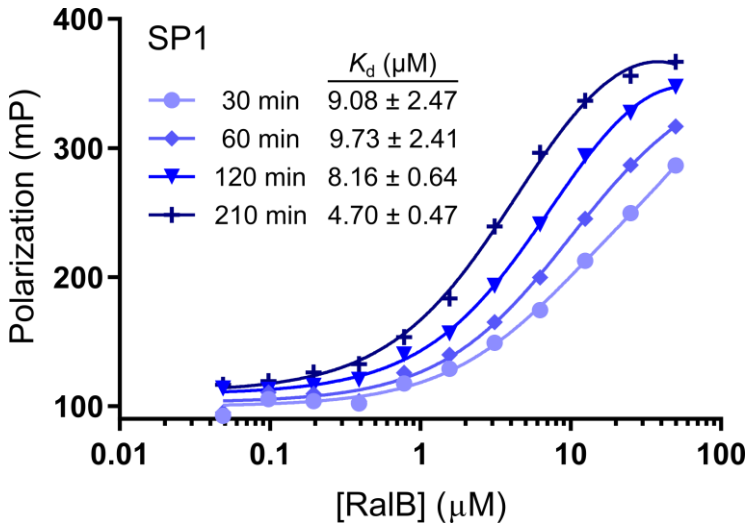


**Figure 3.4. FP measurements of SP1/RalB samples increase over time.** FP data for direct binding of 20 nM FAM-labelled SP1 to varying concentrations of RalB·GMPPNP after 30, 60, 120 or 210 minutes incubation at room temperature. Data were fitted to a single-site binding model using non-linear regression analysis in GraphPad Prism. mP, millipolarization units. n = 1.

The phenomena of increasing signal over time has been observed previously in FP assays (41): Ng *et al.* observed an increase in fluorescence polarization over time for certain fluorescently-labelled peptides in the absence of a binding partner, indicating binding of the peptides to the well surfaces. However, this effect was not observed when using coated plates such as those used in these assays. The increases in polarization observed here may instead be due to an aggregation event.

The variable maxima in the FP experiments following saturation of the signal also suggested that there was an issue with non-specific binding (see Figure 3.2). Peptides that were aggregating or sticking to the plate surface prior to the addition of protein would exhibit a higher starting polarization value due to decreased conformational freedom and would therefore be affected to a lesser extent upon binding to a target protein. In these experiments, the peptides alone did show varying polarization values when compared to fluorescein with a pre-defined polarization value of 35 mP (data not shown).

The presence of non-specific binding in the assay meant that it was important to establish whether the peptides were binding to Ral proteins at all, or whether the observed binding curves were in fact false positive results. RalB alanine mutants were used to ascertain whether the peptides were binding at their intended binding site. Several RalB proteins with alanine

mutations known to disrupt binding to the RLIP76 RBD were available in the lab: Y36A, E38A and Y51A mutants were selected as all of these mutants reduced affinity for the RLIP76 RBD by more than 5-fold, and the Y51A mutation resulted in a complete loss of binding (181). The bound nucleotides of these mutants were exchanged for GMPPNP and the binding to the SP1 peptide was assessed using fluorescence polarization. The results are shown in Figure 3.5.

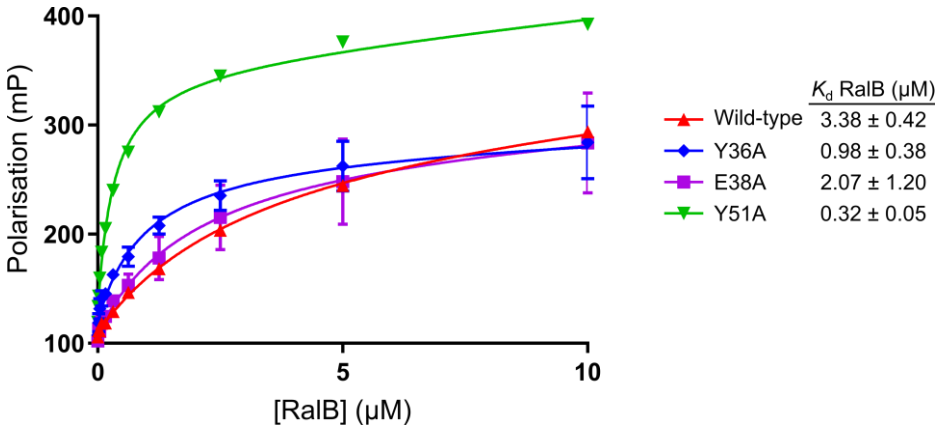


**Figure 3.5. Binding of SP1 to RalB alanine mutants.** FP data for direct binding of 20 nM FAM-labelled SP1 to varying concentrations of wild-type or alanine variants of RalB·GMPPNP. Data were fitted to a single-site binding model using non-linear regression analysis in GraphPad Prism. mP, millipolarization units. n = 2 for Y36A/E38A and n = 1 for Y51A/wild-type RalB.

None of the RalB mutants tested resulted in a loss of binding to the peptide and, surprisingly, the Y51A mutant appeared to bind much more tightly, with a greater change in polarization. This suggests that the peptide is not binding at the expected binding site on RalB, i.e. the binding site of the RLIP76 RBD, as a decrease in binding to the RalB mutants would then be expected. Therefore, the observed binding was likely due to non-specific effects. This meant that the affinities that had been measured using this method were not reliable, and an alternative method needed to be found.

### 3.4.3 Assessing peptide binding in SPA competitions

As an alternative to the FP assays, SPA competition experiments were attempted to measure the binding affinities of the peptides for Ral proteins. The peptides were poorly soluble in aqueous solution, therefore the experimental set up had to be modified to include detergent

(Tween20) to aid peptide solubility. To assess whether the presence of detergent would affect the measured signal or affinity of the interactions, different concentrations of Tween20 were tested in SPA competitions using the wild-type RLIP76 RBD and RalB. The results are shown in Figure 3.6.

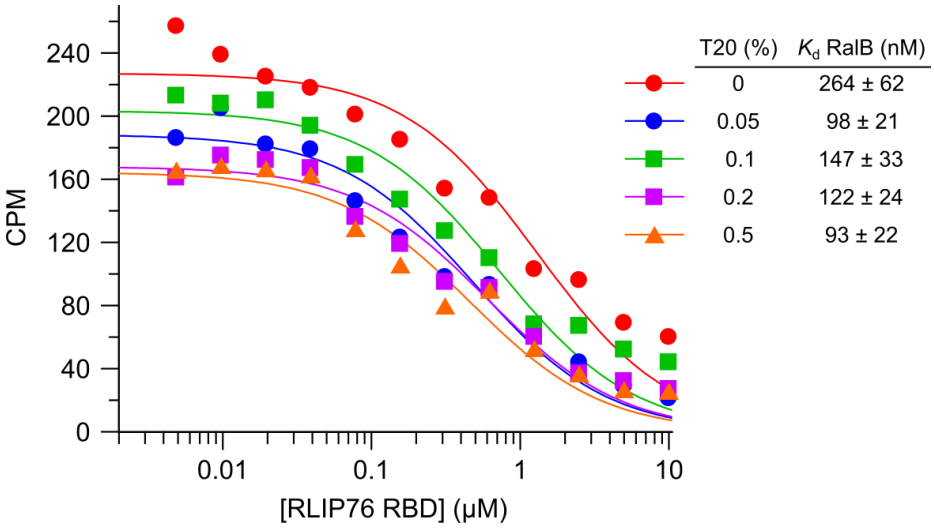


**Figure 3.6. Effect of Tween20 concentration on the SPA competition measurement between the RLIP76 RBD and RalB.** Wild-type RLIP76 RBD was titrated into fixed concentrations of [$^3$H]GTP·RalB and His-tagged wild-type RLIP76 RBD in the presence of varying Tween20 (T20) concentrations in competitions SPAs. The data were fitted to an isotherm describing a pure competition model as described previously to give an apparent $K_d$ ($K_i$) values for the RBD (182): 0%, 264 ± 62 nM; 0.05%, 98 ± 21 nM; 0.1%, 147 ± 33 nM; 0.2%, 122 ± 24 nM; 0.5%, 93 ± 22 nM. CPM, counts per minute. n = 1.

All of the Tween20 concentrations tested (0.05-0.5%) produced curves with a similar maximum signal and a similar $K_d$ for RalB (93-147 nM), suggesting that the presence of Tween20 did not adversely affect binding at these concentrations. The 0% Tween20 condition gave a higher $K_d$ than was usually observed ($K_d$ = 264 nM, typically ~100 nM). However, it is evident from the data in Figure 3.6 that the data is not particularly good for the 0% Tween data set, suggesting that this $K_d$ is not necessarily accurate. It was therefore decided that it would be suitable to include Tween20 in the assays to assess binding of hydrophobic peptides.

A final concentration of 0.25% Tween20 was included in SPA competition experiments to measure binding of selected peptides to RalB and the results are presented in Figure 3.7.

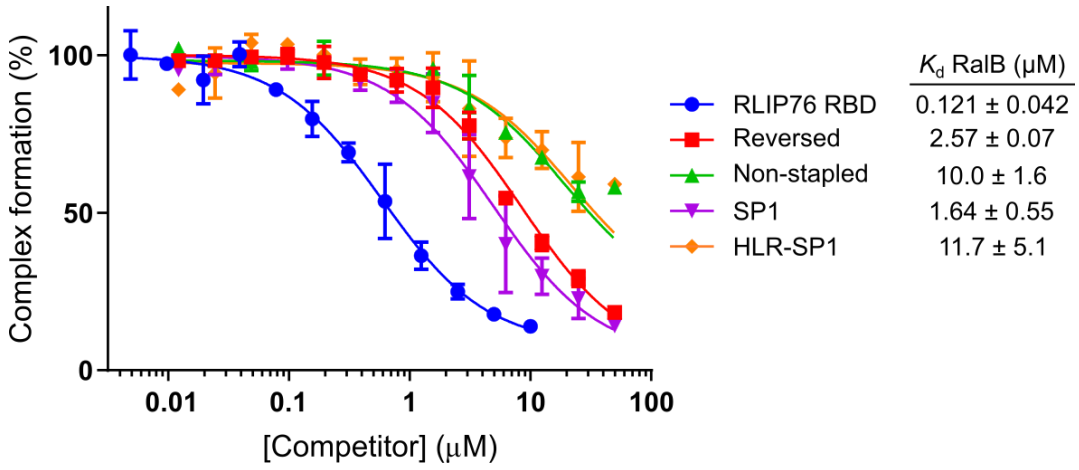


**Figure 3.7. Disruption of the RalB-RLIP76 RBD interaction by hydrophobic peptides.** Increasing concentrations of the indicated peptides were titrated into fixed concentrations of [$^3$H]GTP·RalB and His-tagged wild-type RLIP76 RBD in the presence of 0.25% Tween20 in competition SPAs. The data were fitted to an isotherm describing a pure competition model as described previously to give apparent $K_d$ ($K_i$) values for the peptides (182): $K_d$ RLIP76 RBD, 0.121 ± 0.042 μM; reversed sequence, 2.57 ± 0.07 μM; non-stapled, 10.0 ± 1.6 μM; SP1, 1.64 ± 0.55 μM; HLR-SP1, 11.7 ± 5.1. Mean $K_d$ values and standard deviations are reported. n = 2.

The SP1 peptide bound with an apparent $K_d$ of 1.6 μM for RalB. However some issues were revealed in this experiment, as the reversed sequence peptide, designed to be a negative control in binding experiments, appeared to bind with a similar affinity of 2.6 μM. HLR-SP1 bound with a weaker affinity than the SP1 peptide ($K_d$ = 11.7 μM), despite the same sequence substitutions giving a 20-fold improvement in binding in the context of the RLIP76 RBD (sections 2.5 and 2.7). Together, these data suggested that these peptides were not binding in an analogous manner to the RBD that they are based on, making the results difficult to interpret any further. It was therefore thought necessary to reconsider the design of the peptides.

### 3.5 Improving peptide solubility

It was suspected that the non-specific interactions seen in the *in vitro* binding assays might be a result of the hydrophobic nature of the peptides, as many of the stapled peptides were highly insoluble in aqueous buffer (< 2 μM). Coiled-coils, such as the RLIP76 RBD, are held together by hydrophobic residues at the centre of the two helices. When the sequence of the α2 helix was isolated, as in the stapled peptides, hydrophobic residues that would normally be buried at the coiled-coil interface became solvent exposed (Figure 3.8A and B). In addition,

the N-terminal staple position (424-428, SP1) replaced serine and arginine residues in the wild type sequence with the all-hydrocarbon staple, adding to the overall hydrophobicity of the peptide.

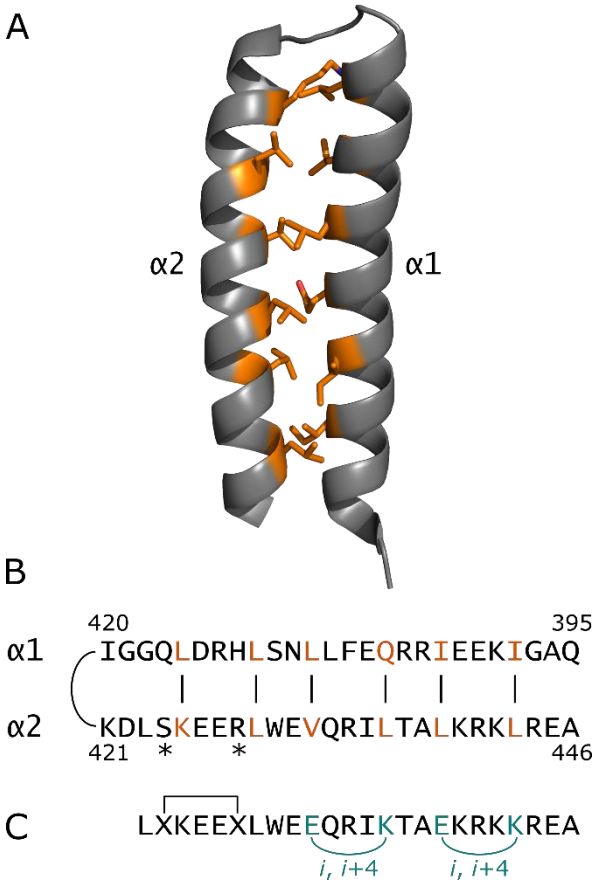


**Figure 3.8. Coiled-coil stabilizing interactions in the RLIP76 RBD. A**. Structure of the RLIP76 RBD (PDB: 2KWI) with residues forming interactions at the coiled-coil interface coloured in orange and shown as sticks. **B**. Sequence of the RLIP76 RBD with interactions at the coiled-coil interface shown as lines. The residues replaced by (*S*)-pentenylalanine to form a chemical staple in are starred (*). Residues are coloured as in A. **C**. Proposed peptide sequence with engineered solubility. Glutamate and lysine residues are used to replace hydrophobic residues, and were placed with *i*, *i* + 4 spacing to allow for the formation of helix stabilizing salt bridges. X, (*S*)-pentenylalanine.

It was hypothesized that the solubility of the peptides could be improved by replacing hydrophobic residues that did not contribute to binding with charged or polar residues. Four hydrophobic residues that would normally be present in the coiled-coil interface were replaced with alternating glutamate and lysine residues with *i*, *i*+4 spacing (Figure 3.8C). This arrangement has been shown to allow the formation of helix-stabilizing salt bridges (191). It

was deemed favourable to stabilize the helical conformation, as in several instances more helical peptides have displayed tighter binding affinities due to a reduced entropic penalty on binding, as had already been observed with peptides based on the RLIP76 RBD (125, 192). The residues selected do not normally form interactions with Ral proteins, therefore their replacement was unlikely to affect the affinity of the peptide.

Several peptides were synthesized as part of this work to investigate the effect of adding in these solubilizing salt bridges to the properties of the peptides; the peptides produced are listed in Table 3.4. For FAM-labelled peptides, a polyethylene glycol (PEG) linker was added between the peptide sequence and the N-terminal fluorescein label to aid solubility and to prevent the bulky tag from interfering with interactions made by the peptides. In addition to the peptide containing the HLR mutations (HLR-sol), a second peptide containing only the Q433L mutation was synthesized (L-sol). It had been found that increasing the number of mutations in the RLIP76 RBD, including the E427H substitution, resulted in increased off-target binding to K-Ras (see section 2.9), therefore it was anticipated that the L-sol peptide would display better selectivity towards Ral proteins. The resulting peptides were highly soluble in water (> 3 mM).

*Table 3.4. Peptides synthesized for investigations of solubilizing mutations. SP1 (Eurogentec) is included in the table for sequence comparison.*

| Peptide name | Sequence[a] | Expected masses[b] | Masses found[b] | Retention time (min)[c] | Purity (%)[c] |
|---|---|---|---|---|---|
| SP1 | FAM-LXKEEXLWEVQRILTALKRKLREA | - | - | - | - |
| HLR-sol | FAM-PEG-LXKEHXLWEELRIKTAERRKKREA | MW – 3587.2<br>1794.6/1196.7/897.8/718.4 | 1196.7/897.8/718.4 | 4.6 | 99 |
| L-sol | FAM-PEG-LXKEEXLWEELRIKTAEKRKKREA | MW – 3551.1<br>1776.6/1184.7/888.8/711.2 | 1184.7/888.7/711.2 | 5.0 | 97 |
| WT-sol | LXKEEXLWEEQRIKTAEKRKKREA | MW – 3048.6<br>1525.3/1017.2/763.2/610.7 | 1525.2/1016.9/763.1/610.8 | 3.9 | 71 |
| W430A-hyd | LXKEEXLAEVQRILTALKRKLREA | MW – 2857.5<br>1429.7/953.5/715.4/572.5 | 1429.6/953.3/715.2 | 6.9 | 82 |
| W430A-sol | LXKEEXLAEEQRIKTAEKRKKREA | MW – 2933.7<br>1467.7/978.8/734.4/587.7 | 1467.6/978.7/734.3/587.8 | 3.7 | 94 |
| HLR-hyd | LXKEHXLWEVLRILTALRRKLREA | MW – 2993.7<br>1497.9/998.9/749.4/599.7 | 998.8/749.3/599.6 | 7.0 | 73 |

[a] Sequence variations from the wild type sequence for improving affinity are underlined, while solubilizing mutations are coloured blue and are shown in bold. X, (*S*)-pentenylalanine; FAM, 5-carboxyfluorescein; PEG, polyethylene glycol linker.
[b] Expected and observed masses from LC-MS analysis. Masses are in the form m/z (mass/charge number).
[c] Retention times and purity assessed by analytical HPLC

A soluble peptide lacking the HLR mutations was also synthesized (WT-sol) to assess whether these mutations improve binding of the soluble peptides. Soluble and hydrophobic versions of peptides with Trp430 mutated to alanine (W430A-sol and W430A-hyd) were also produced to be used as negative control peptides, as this tryptophan residue has been shown to be critical for binding Ral proteins in the context of the RLIP76 RBD (181).

### 3.5.1 Peptide synthesis

The peptides were synthesized using Fmoc-based solid-phase synthesis. Synthesis commenced from the C-terminus using an automated synthesizer for all proteinogenic amino acids. (*S*)-pentenylalanine was added using manual coupling reactions, as this residue is more sterically hindered than the proteinogenic amino acids due to the additional methyl group at the Cα position (Figure 3.9A) and was therefore expected to be coupled less efficiently. The manual couplings were carried out with a more powerful activator (hexafluorophosphate azabenzotriazole tetramethyl uranium, HATU) than is used with the automated synthesis to enhance the reaction efficiency. Residues directly following (*S*)-pentenylalanine were triple-coupled using the automated synthesizer to ensure efficient coupling to the hindered amino acid. Once the N-terminal leucine residue was reached, a Grubbs ring-closing metathesis was carried out to covalently link the two (*S*)-pentenylalanine residues (Figure 3.9B).

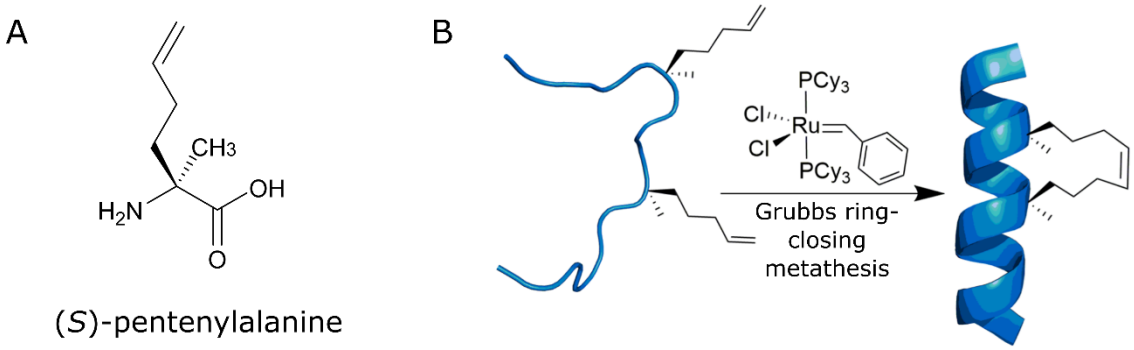


**Figure 3.9. Incorporation of all-hydrocarbon peptide staples. A**. Structure of (*S*)-pentenylalanine, the amino acid used to form the all-hydrocarbon staple. **B**. Grubbs ring-closing metathesis uses a Ruthenium catalyst to enable formation of covalent bonds between the two olefin-containing residues.

Following the ring-closing metathesis, a small-scale test cleavage followed by LC-MS analysis was used to check the quality of the crude product and the efficiency of the stapling reaction. After confirmation that the desired product was present, PEGylation was carried out using automated synthesis, followed by a manual coupling of 5-carboxyfluorescein (FAM). The colour of the resin after washing was used as an indicator of effective FAM-labelling. The finished peptide was cleaved from the resin and purified using reverse phase HPLC (Figure 3.10A). Fractions were analysed by LC-MS to identify those containing the desired peptide mass. Fractions containing the desired peptide at high purity were pooled and analysed by analytical HPLC and LC-MS (Figure 3.10B and C). The purified peptides were lyophilised for later use.

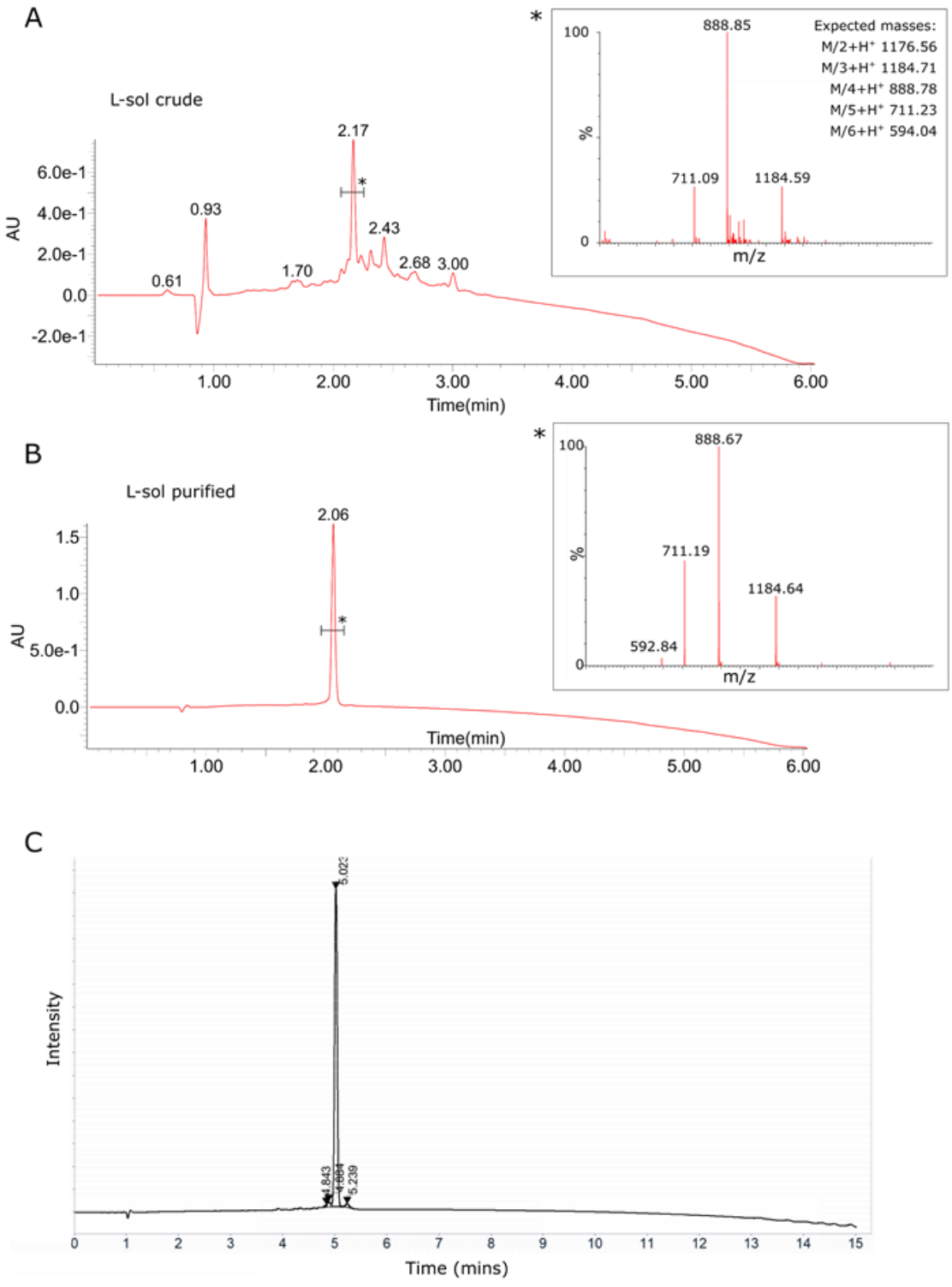


**Figure 3.10. Purification of stapled peptides. A**. HPLC trace of L-sol peptide crude mixture. The MS profile (inset) corresponds to the material found within the peak at 2.17 mins indicated by (*). **B**. HPLC trace of L-sol peptide following purification by reverse phase HPLC. The MS profile (inset) corresponds to the area surrounding the peak at 2.06 mins indicated by (*). **C**. Analytical HPLC trace of the purified L-sol peptide.

### 3.5.2 Binding of L-sol and HLR-sol to Ral proteins

The affinity of the soluble peptides HLR-sol and L-sol for Ral proteins was measured using fluorescence polarization. The results are shown in Figure 3.11, and the affinities obtained are listed in Table 3.5.

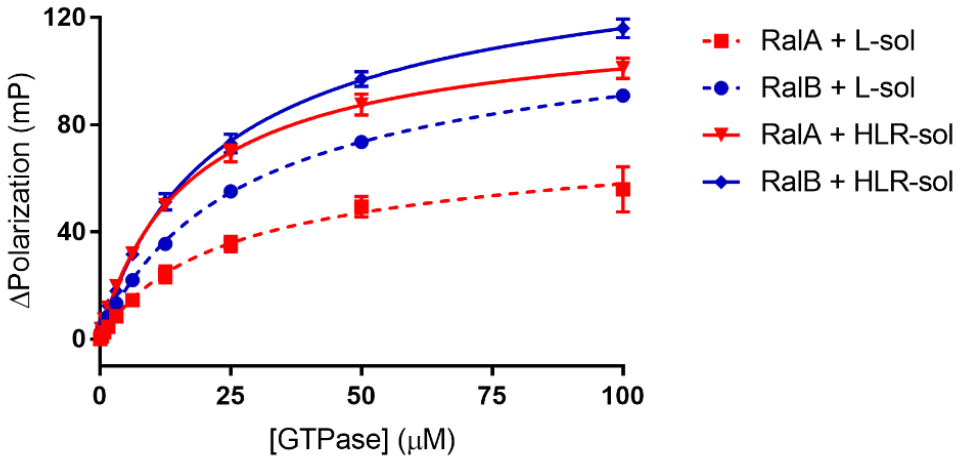


**Figure 3.11. Binding of soluble peptides to Ral proteins.** FP data for direct binding of 20 nM FAM-labelled L-sol (dashed lines) and HLR-sol (solid lines) to varying concentrations of RalA·GMPPNP (red) or RalB·GMPPNP (blue). Data were fitted to a single-site binding model using non-linear regression analysis in GraphPad Prism, and the $K_d$ values measured are listed in Table 3.5. mP, millipolarization units. n = 3.

*Table 3.5. Affinities of soluble peptides for RalA and RalB measured by FP.*

| Peptide | Sequence[a] | $K_d$ RalA (μM)[b] | $K_d$ RalB (μM)[b] |
|---|---|---|---|
| HLR-sol | FAM–PEG–LXKEHXLWEELRIKTAERRKKREA | 16.6 ± 1.3 | 21.1 ± 1.8 |
| L-sol | FAM–PEG–LXKEEXLWEELRIKTAEKRKKREA | 19.6 ± 3.9 | 24.4 ± 5.0 |

[a] Sequence variations from the wild type sequence for improving affinity are underlined, while solubilizing mutations are coloured blue and are shown in bold. X, (*S*)-pentenylalanine; FAM, 5-carboxyfluorescein; PEG, polyethylene glycol linker.
[b] Results from 3 independent experiments, error shown is from curve fitting.

The HLR-sol and L-sol peptides both bound with a very similar affinity to Ral proteins. This reflects observations made with the RLIP76 RBD, where the E427H/Q433L/K440R mutant bound RalB with a $K_d$ of 96 nM, while the Q433L only mutant had a very similar $K_d$ of 111 nM (section 2.7). The measured affinities were also very similar for RalA and RalB, which was expected as the Ral proteins are 100% identical in the region which the RLIP76 RBD, the

domain the peptides are based on, binds. Taken together these observations suggested that the peptides were binding the Ral proteins at the intended effector-binding site, as the same trends were observed using the mutant RBDs for which the binding site is known.

Notably, the peptides bind Ral proteins with affinities far lower than the corresponding RLIP76 RBD e.g. the HLR-sol peptide has a $K_d$ of 21 μM for RalB, while the HLR mutant RBD has a $K_d$ of 96 nM (section 2.7). While these values have been obtained from different assays, the difference is considerable. The peptides are based on the single α2 helix of the RLIP76 RBD and lack the α1 helix, which is known to contain some key residues for binding to Ral proteins: Campbell *et al.* showed previously that mutation of Leu409 or His413 to alanine, ablates binding to Ral proteins (181). The reduced binding of the peptides compared to the RLIP76 RBD could therefore be attributed to the absence of these key residues. It is also possible that a loss of helical secondary structure in the peptides compared to the RBD could result in a loss of binding.

### 3.6 Estimation of peptide helical content

Increased helical content of stapled peptides is thought to increase binding affinity by reducing an entropic loss upon binding (192). The helical content of the peptides used in this study was assessed using circular dichroism (CD) and the results are shown in Figure 3.12.

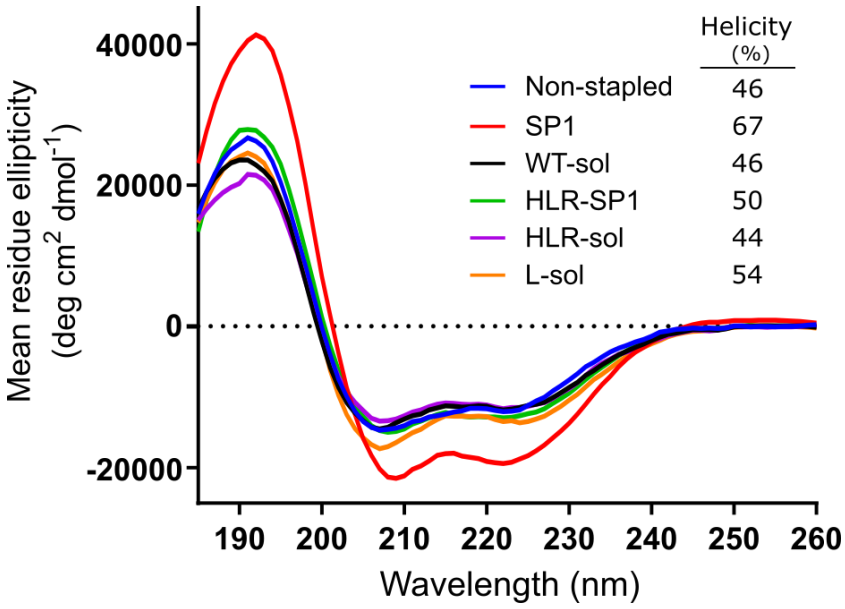


**Figure 3.12. Circular dichroism spectra of selected peptides.** CD spectra were measured over the wavelengths 260-185 nm and the reported percentage helicity (%) was estimated by the CDSSTR method and reference set 3 using Dichroweb (183–185).

The data demonstrated that introduction of a hydrocarbon staple bridging residues 424 and 428 increased the helicity of the peptide from 46% (non-stapled) to 67% (SP1), demonstrating the utility of all-hydrocarbon stapling to increase helical secondary structure, as has been shown by many others previously (137). However, the introduction of the four solubilizing mutations (WT-sol) reduces the helicity to a similar level to the non-stapled helix, demonstrating a disruption in the secondary structure.

The solubilizing mutations were inserted so that they could form two Glu-Lys salt bridges, with the aim of stabilizing a helical conformation. However, these residues replaced hydrophobic residues that could have formed helix-stabilizing interactions with several other residues in the sequence. Creamer and Rose have calculated energetic contributions for all hydrophobic residue combinations at *i*, *i* + 3 and *i*, *i* + 4 spacings (193), and the values for the pairs of residues identified in SP1 are shown in Figure 3.13. They also looked at the effect of having three leucine residues at regular spacings in the peptide sequence, e.g. *i*, *i* + 3, *i* + 7, and found that the favourable, helix-stabilizing interactions formed were greater than the sum of their parts. This is likely to also be true for other hydrophobic residues, therefore the helical conformation of SP1 is potentially supported by the network of hydrophobic

interactions on the non-binding surface of the peptide. When the solubilizing mutations were introduced, the possibility of forming any of the hydrophobic interactions was removed (Figure 3.13), therefore a loss of helicity is observed despite the helical stabilization potentially provided by Glu-Lys salt bridges (191).


**Figure 3.13. Possible hydrophobic interactions within the SP1 peptide.** *i*, *i* + 3 interactions are indicated by red dashed lines, while *i*, *i* + 4 interactions are shown as blue dashed lines. Numbers above the lines correspond to the ΔE values in kcal $mol^{-1}$ for specific interactions calculated by Creamer and Rose using model peptides (193). The solubilizing mutations in WT-sol are coloured in blue. X, (*S*)-pentenylalanine; Fam, 5-carboxyfluorescein.

The introduction of the HLR mutations into the peptide to improve affinity for Ral proteins also reduced the helicity of the peptide (50% HLR-SP1 vs 67% for SP1), giving rise to a trace similar to the non-stapled peptide. It is possible therefore that the binding of the peptides to Ral proteins could be improved if the helicity of the peptides was increased e.g. by re-optimization of the staple length and position for the HLR mutated sequence or by introduction of a second staple.

## 3.7 Role of the RLIP76 RBD α1 helix in binding

It was noted in section 2.1 that certain residues in the RLIP76 RBD that contact RalB lie on the α1 helix. As the lead stapled peptides based on the RLIP76 RBD only contain the α2 helix residues, we wanted to assess the importance of the α1 helix for binding to Ral proteins. Therefore, the key hotspots on this helix were mutated to alanine: Leu409 and His413 were selected for mutation as it has been shown previously that replacement of either residue with alanine decrease binding to Ral proteins by at least 10-fold (181). The L409A/H413A mutations were added into the wild-type and HLR mutant RBDs and the proteins were prepared as described in section 2.3. The binding of these mutant RLIP76 RBDs to RalA was

measured using competition SPAs. The results are shown in Figure 3.14 and the calculated affinities are listed in Table 3.6.

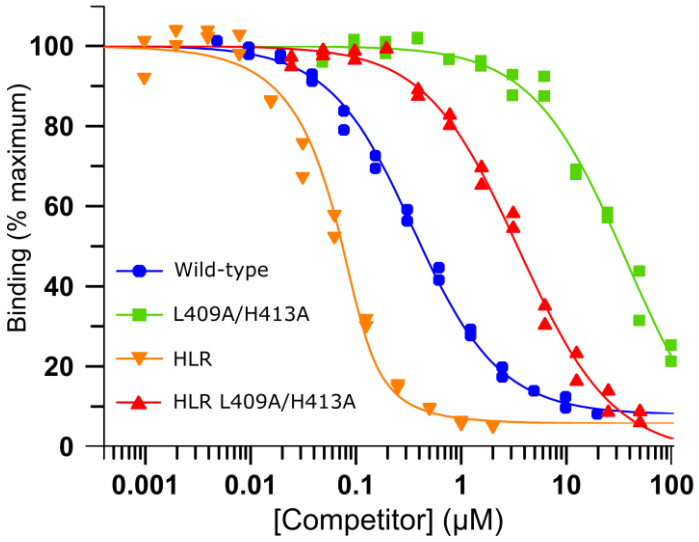


**Figure 3.14. Binding of RBD constructs with key α1 helix residues mutated to alanine.** Increasing concentrations of the indicated RBDs were titrated into fixed concentrations of [$^3$H]GTP·RalA and His-tagged wild-type RLIP76 RBD in competition SPAs. The data were fitted to an isotherm describing a pure competition model as described previously to give an apparent $K_d$ ($K_i$) values for the competing species (see Table 3.6) (182).

*Table 3.6. Affinities of mutant RBDs for RalA measured by competition SPA.*

| RLIP76 RBD | Sequence | $K_d$ RalA (μM)[a] |
|---|---|---|
| Wild-type | GPLGSETQAGIKEEIRRQEFLLNSLHRDLQGGIKD<br>LSKEERLWEVQRILTALKRKLREA | 0.128 ± 0.010 |
| L409A/H413A | GPLGSETQAGIKEEIRRQEFLANSLARDLQGGIKD<br>LSKEERLWEVQRILTALKRKLREA | 16.1 ± 3.1 |
| HLR L409A/H413A | GPLGSETQAGIKEEIRRQEFLANSLARDLQGGIKD<br>LSKEHRLWEVLRILTALRRKLREA | 1.50 ± 0.17 |
| HLR | GPLGSETQAGIKEEIRRQEFLLNSLHRDLQGGIKD<br>LSKEHRLWEVLRILTALRRKLREA | 0.005 ± 0.003 |

[a] Results from two independent experiments. The mean $K_d$ values and standard errors from curve fitting are shown.

Mutating both Leu409 and His413 to alanine resulted in a dramatic decrease in affinity for RalA, with a 120-fold decrease in the wild-type background (139 nM vs 16.6 μM) and a 280-fold decrease in the HLR mutant background (5 nM vs 1.42 μM), demonstrating the

importance of these contacts for binding to Ral proteins. The L409A/H413A RBD should reflect the maximal binding of a peptide based on the α2 helix, as the coiled-coil domain constrains this helix in an entirely helical conformation, while the isolated peptide can suffer from a loss of helicity due to the lack of supporting structure which would likely result in a decreased binding affinity.

The secondary structures of the L409A/H413A RBD mutants were assessed by CD to check whether the observed reductions in affinity were due to a loss of binding contacts or a disruption of the coiled-coil structures. The results from the CD analysis are displayed in Figure 3.15.

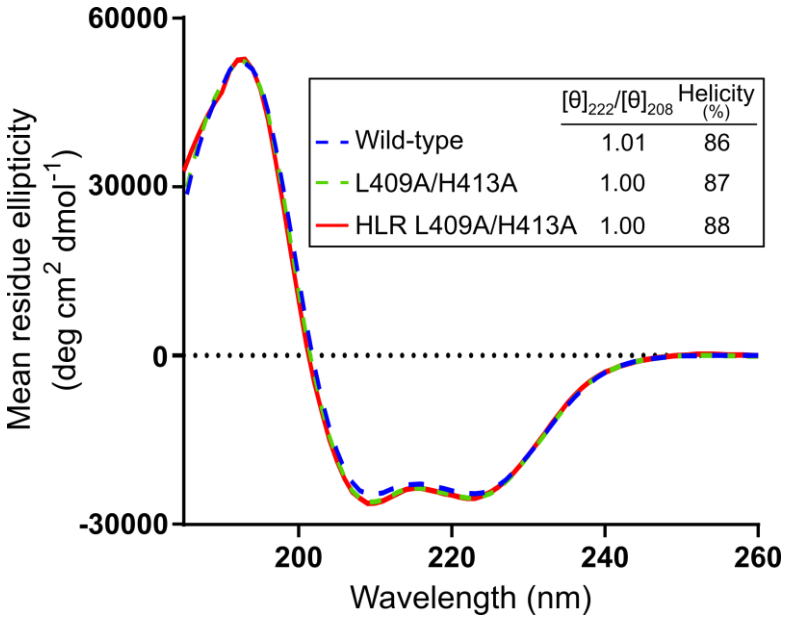


**Figure 3.15. Secondary structure of RLIP76 RBDs with key α1 helix residues mutated to alanine.** CD spectra of the wild-type RLIP76 RBD and L409A/H413A RBD mutants were measured over the wavelengths 185-260 nm with a protein concentration of 0.2 mg $ml^{-1}$. The calculated helicities and ratios of the mean residue ellipticities (θ) at 222 and 208 nm ($[\theta]_{222}/[\theta]_{208}$) are shown in the inset. The reported percentage helicity (%) was estimated by the CDSSTR method and reference set 3 using Dichroweb (183–185).

The measured helicities of the L409A/H413A mutants were near identical to the wild-type RBD (86-88%). The $[\theta]_{222}/[\theta]_{208}$ ratios, which are an indicator of coiled-coil content, also did not change appreciably when the L409A/H413A mutations were added, with a value of 1.01 for the wild-type RBD and 1.00 for the mutant RBDs, indicating that the coiled-coil structure is not disrupted upon addition of these mutations. It appeared, therefore, that the reduced

affinities of the L409A/H413A mutants were due to the side chain interactions that were lost, indicating that the α1 helix of the RLIP76 RBD plays a critical role in binding to Ral proteins.

### 3.8 Peptide selectivity

In order to assess the selectivity of the soluble peptides for Ral proteins, the binding of HLR-sol and L-sol to a panel of small GTPases was measured by fluorescence polarization. K-Ras was included in the experiment as the Ras proteins are found in the same family as the Ral proteins and are therefore very similar. All the small GTPases were studied in their active form (see section 3.4.1). The results are presented in Figure 3.16, and the $K_d$ values determined are listed in Table 3.7. The peptides demonstrated impressive selectivity for Ral proteins, with barely detectable binding to any of the other small GTPases tested.

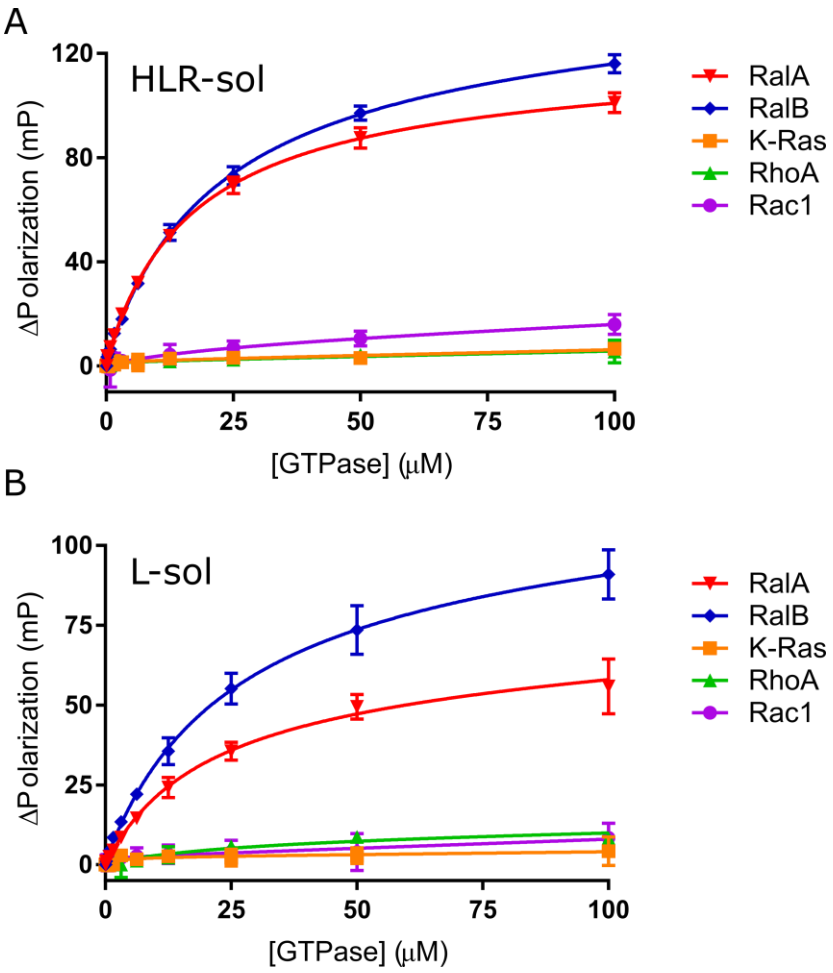


**Figure 3.16. Binding of HLR-sol and L-sol to a panel of small GTPases.** FP data for direct binding of 20 nM FAM-labelled HLR-sol (**A**) and L-sol (**B**) to varying concentrations of the indicated small GTPases. Data were fitted to a single-site binding model using non-linear regression analysis in GraphPad Prism. mP, millipolarization units. n = 3 for all conditions except for K-Ras, n = 2.

*Table 3.7. Binding of HLR-sol and L-sol peptides to a panel of GTPases measured by FP.*

| GTPase | $K_d$ HLR-sol (μM)[a] | $K_d$ L-sol (μM)[a] |
|---|---|---|
| RalA·GMPPNP | 16.6 ± 1.3 | 19.8 ± 3.9 |
| RalA·GDP | NB | NB |
| RalB·GMPPNP | 21.1 ± 1.8 | 24.4 ± 5.0 |
| K-Ras·GMPPNP[b] | NB | NB |
| RhoA·GMPPNP | NB | NB |
| Rac1·GMPPNP | NB | NB |

[a] Results from three independent experiments, the mean $K_d$ values and standard errors are listed. NB, no binding.
[b] Results from two independent experiments.

To effectively block Ral signalling, the peptides are required to target the active, GTP-bound form of Ral, as this is the state in which the effector proteins bind. It would be undesirable to also hit the inactive, GDP-bound form of Ral as this would reduce the effective concentration of peptide in the cell, reducing the effectiveness of inhibition. The Ral proteins used in this study so far were produced with a Q72L mutation to minimise hydrolysis of the bound nucleotide and the bound nucleotide had been exchanged for GMPPNP, a very slowly-hydrolysable analogue of GTP, to ensure that the protein being studied was in its active conformation. To generate GDP-bound RalA, a wild-type construct was used (residues 1-184). After protein purification, analysis of the bound nucleotide revealed that the protein was mostly GDP-bound. The protein was incubated at room temperature overnight to allow complete hydrolysis of remaining GTP to GDP, which was confirmed by HPLC.

The binding of HLR-sol and L-sol to active and inactive RalA was assessed by fluorescence polarization. The results are shown in Figure 3.17 and Table 3.7. The peptides showed no measurable binding to the GDP-bound form of RalA, indicating that they are likely binding the switch regions of Ral, as these regions are most sensitive to the nucleotide status of the protein.

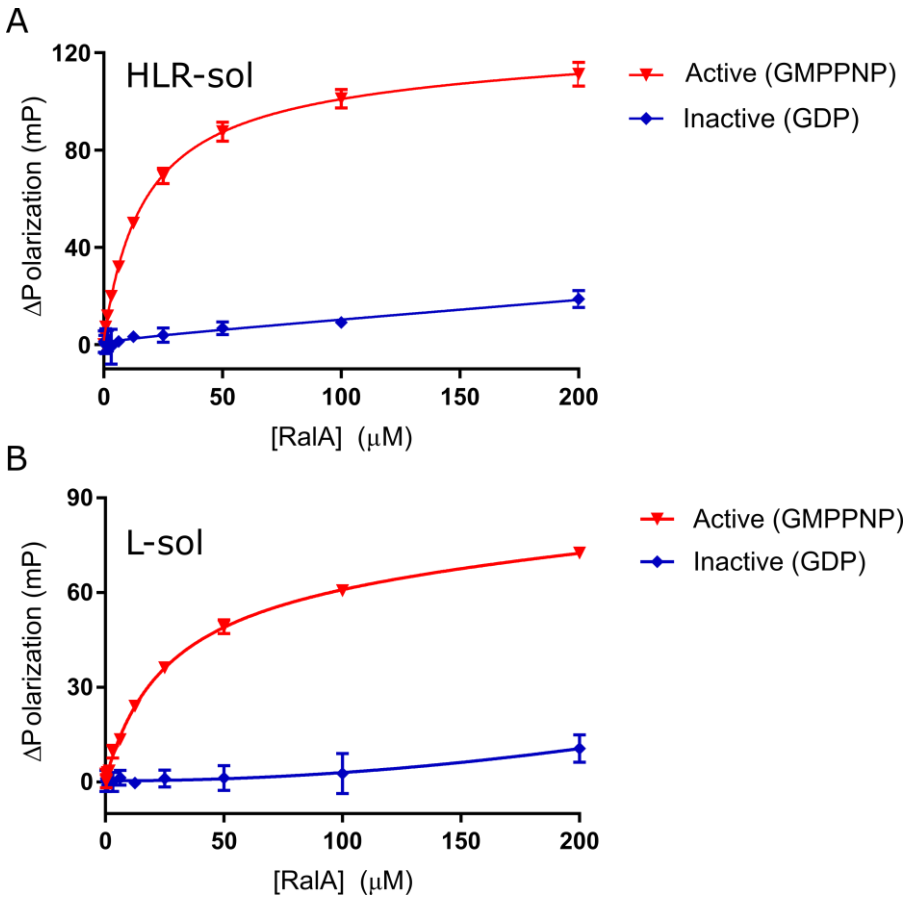


**Figure 3.17. Selectivity of HLR-sol and L-sol for GMPPNP-bound RalA.** FP data for direct binding of 20 nM FAM-labelled HLR-sol (**A**) and L-sol (**B**) to RalA·GDP and RalA·GMPPNP reveal that both peptides display selectivity for the active form of the GTPase. Data were fitted to a single-site binding model using non-linear regression analysis in GraphPad Prism, and the results are listed in Table 3.7. mP, millipolarization units. n = 3.

## 3.9 Inhibition of Ral-effector interactions

For the peptides to inhibit Ral signalling, it is essential that they bind at the same site as the effector proteins and can disrupt Ral-effector interactions. Experiments to assess the ability of the peptides to disrupt multiple Ral-effector interactions were carried out and are described in the following sections.

### 3.9.1 Disruption of Ral-effector complexes by soluble peptides

To assess whether the peptide could compete for Ral-effector interactions *in vitro*, SPA competition experiments were performed. In these assays, increasing concentrations of peptide were titrated into immobilised Ral-effector effector complexes to see whether

disruption of the complex was observed, indicating competitive binding of the peptide. The effector proteins RLIP76 and Sec5 were immobilised in this assay and the binding of the peptides were measured. The wild-type RBD was included in these experiments as an internal control. The results are shown in Figure 3.18, and the $K_d$ values obtained are listed in Table 3.8.

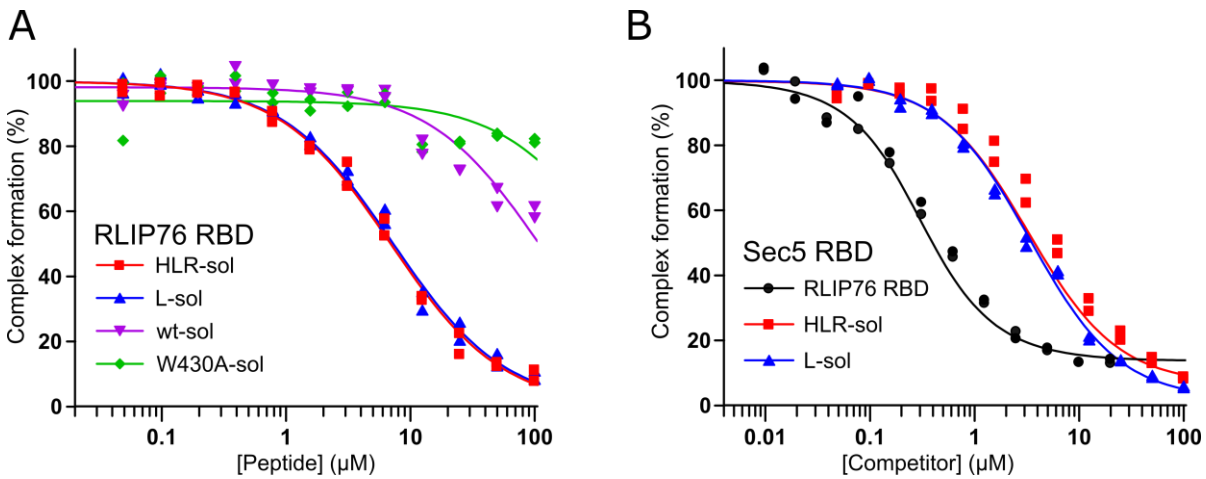


**Figure 3.18. Disruption of Ral-effector complexes by HLR-sol and L-sol.** Increasing concentrations of the indicated peptides were titrated into fixed concentrations of [$^3$H]GTP·RalA and His-tagged wild-type RLIP76 RBD (**A**) of GST-Sec5 RBD (**B**) in competition SPAs. The data were fitted to an isotherm describing a pure competition model as described previously to give an apparent $K_d$ ($K_i$) values for the peptides (see Table 3.8) (182).

*Table 3.8. Binding of stapled peptides and the RLIP76 RBD to RalA in SPA competitions.*

| Competitor | $K_d$ RLIP76-His$_6$ competition (μM)[a] | $K_d$ GST-Sec5 competition (μM)[a] |
|---|---|---|
| HLR-sol | 2.97 ± 0.29 | 1.74 ± 0.15 |
| L-sol | 3.09 ± 0.32 | 1.81 ± 0.14 |
| wt-sol | 48.6 ± 7.7 | ND[b] |
| W430A-sol | > 100 | ND |
| RLIP76 RBD | 0.096 ± 0.017 | 0.115 ± 0.030 |

[a] Results from two independent experiments. Mean $K_d$ values and curve fitting errors are shown.
[b] ND – not determined.

The soluble peptides, HLR-sol and L-sol, were able to compete with the RLIP76 RBD and Sec5 RBD for binding to RalA, demonstrating that the peptides bind at a site that overlaps with the binding sites for both of these effector proteins. The $K_d$ values for the peptides measured in the competition SPAs are around 10-fold tighter than those measured by FP. $K_d$ values measured using SPAs were considerably tighter than those measured by ITC experiments e.g. 100 nM vs 2 µM for the wild-type RLIP76 RBD as has been observed previously (125, 181). This demonstrates the necessity to use multiple methods to measure the interaction affinities and suggests that extrapolation between different assay types should be avoided.

The HLR-sol and L-sol peptides bound Ral proteins around 10-fold weaker than the wild-type RLIP76 RBD. The reduced affinity compared to the native binding partner suggests that a relatively high concentration of peptide would need to be delivered to the cytosol to observe inhibition of the complexes *in vivo*, requiring low toxicity and high cellular permeability of the sequence.

The soluble peptide lacking the HLR mutations (WT-sol) bound much more weakly than the HLR-sol and L-sol peptides, indicating that the presence of the HLR and L mutations are improving binding to Ral proteins, as was observed for the same mutations in the context of the RLIP76 RBD (section 2.7), giving further evidence that the peptides are binding in a similar manner to the RBD.

The W430A-sol peptide was designed as a negative control: a tryptophan residue known to be critical for binding to Ral proteins (Trp430 in the RBD) (181) was mutated to alanine to ablate binding. This peptide bound very weakly to RalA in SPA competitions ($K_d$ > 100 µM) and was therefore considered to be a suitable negative control for future experiments.

### 3.9.2 Disruption of Ral-effector complexes in mammalian cell lysates

The ability of the soluble peptides to disrupt Ral-effector complexes in a mammalian cell lysate was next assessed using co-immunoprecipitation experiments. Either V5-tagged RalB Q72L alone, or RalB and flag-tagged RLIP76 were transfected into HEK293T cells and RalB containing complexes were immunoprecipitated using an anti-V5 antibody. The presence of RLIP76 was probed using an anti-flag antibody and Sec5 was detected using an antibody for the endogenous protein. The results are shown in Figure 3.19. It was possible to detect flag-

tagged RLIP76 and endogenous Sec5 in complex with RalB. Addition of increasing amount of HLR-sol and L-sol peptide into the cell lysates decreased the amount of RLIP76 and Sec5 that co-immunoprecipitated with RalB (Figure 3.19A, B, D and E). This clearly demonstrates that the peptides and effector proteins share a common binding site on RalB and that the peptides have selectivity for RalB proteins, as they can bind in a complex cell lysate with all other proteins present.

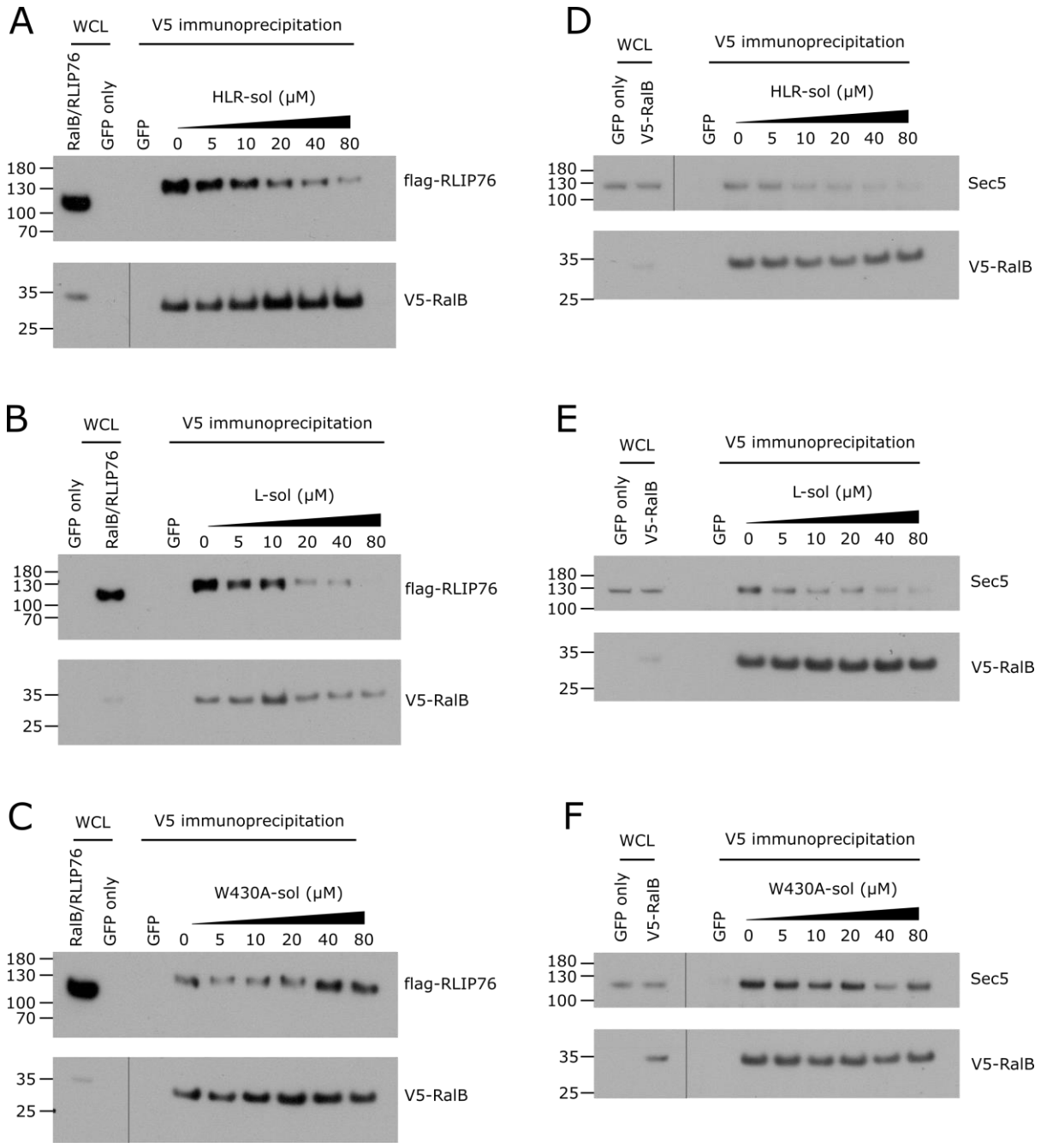


**Figure 3.19. Disruption of Ral-effector complexes by second-generation stapled peptides in a mammalian cell lysate. A-C.** The indicated concentrations of HLR-sol (**A**), L-sol (**B**) and W430A-sol (**C**) stapled peptides were added to HEK293T cell lysates transfected with GFP only or V5-tagged RalB Q72L and flag-tagged RLIP76 24 h prior to lysis. Beads coated with an anti-V5 antibody were added to the lysate mixture to precipitate RalB and any bound proteins. The presence of RalB and bound RLIP76 was assessed by probing with anti-flag (RLIP76) and anti-V5 (RalB). **D-F**. Co-immunoprecipitations were performed as above without flag-RLIP76 transfection with the indicated concentrations HLR-sol (**D**), L-sol (**E**) and W430A-sol (**F**) stapled peptides. The presence of RalB and bound Sec5 was assessed by probing with anti-Sec5 and anti-V5 (RalB). The results are representative of at least two independent repeats. WCL, whole cell lysate. Images split by a vertical grey line are composite images made up of different exposures.

The co-immunoprecipitation experiment was also carried out in the presence of the W430A-sol peptide, which was designed as a negative control peptide and displays very weak binding to Ral proteins (Figure 3.19C). The W430A-sol peptide was not able to disrupt Ral-effector complexes in the concentration range tested, indicating that the inhibition is due to a specific binding event, and that the peptides bind in an analogous manner to the RLIP76 RBD.

### 3.10 Mapping the peptide binding site by NMR

Data from the SPA competition and co-immunoprecipitation experiments indicated that the HLR-sol and L-sol peptides were binding at the effector-binding site on Ral. In order to establish the specific binding site of the HLR-sol peptide, an NMR titration with $^{15}$N-labelled RalB and increasing amounts of unlabelled peptide was carried out.

$^{15}$N-labelled RalB Q72L was produced using M9 minimal media supplemented with $^{15}NH_4Cl$ as a $His_{10}$-tagged construct from pET16b as described in the methods. The bound nucleotide was exchanged for GMPPNP prior to use and the exchange efficacy was confirmed by HPLC analysis.

Initially, an HSQC spectrum of the $^{15}$N-labelled RalB alone was recorded. In this spectrum, a peak arises for each N-H group in the labelled protein e.g. backbone amides for all residues except proline and side chain N-H groups in arginine, asparagine, glutamine and lysine residues. Subsequent HSQC spectra were recorded with increasing concentrations of unlabelled ligand (peptide) until a saturated complex was reached, as evidenced by a lack of any further shifted peaks between spectra. Upon binding of the ligand, residues that are proximal to the binding site of the ligand experience chemical shift perturbations (CSPs) due to a changing chemical environment experienced by the residue, causing the position of the peak in the HSQC to change. In this way, residues that are involved in ligand binding can be identified. The HSQC spectra of $^{15}$N-labelled RalB alone and after the addition of two molar equivalents of peptide are shown in Figure 3.20.

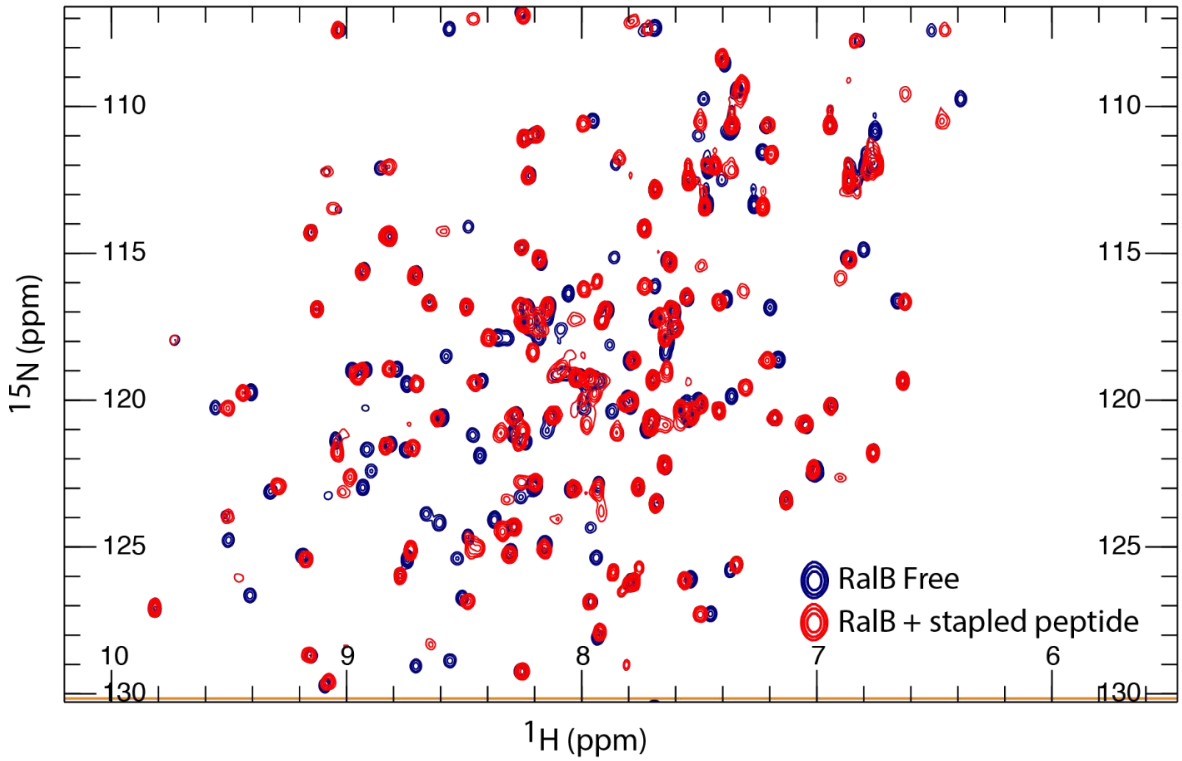


**Figure 3.20. $^{1}$H,$^{15}$N HSQC NMR spectra of 15N-labelled RalB alone (blue) and after the addition of two equivalents of HLR-sol (red).** Experiments were recorded on a Bruker 800 MHz spectrometer. Many peaks have shifted upon addition of the peptide, corresponding to residues that are part of, or proximal to, the binding site of the peptide.

Several peaks have changed position between the two spectra, indicating binding of the ligand. After the addition of two molar equivalents of peptide, no further shifts were observed and the complex appeared to be saturated. At intermediate points in such a titration i.e. when the complex is not saturated, the appearance of the spectra depends on the rate of exchange between the free and bound forms of the labelled protein, which is determined by the affinity and kinetics of the interaction. The exchange regimes are depicted in Figure 3.21. When the ligand has a high affinity for the labelled protein, the off rate ($k_{off}$) is often slower than the timescale of the experiment (typically ms) therefore the protein is observed in either the free or the bound state at ratios relating to the concentration of the ligand: this is known as slow exchange and is observable as a disappearance in the peak corresponding to the free protein, and the appearance of a peak for the bound protein (194). For lower affinity ligands, the interaction kinetics result in the ligand exchanging on and off the protein multiple times during the timescale of the experiment: this is known as fast exchange, and the peak appears

as an average result of these positions, which shifts closer to the bound position as the concentration of ligand is increased. There is a third exchange regime, known as intermediate exchange, which exists between the two timescales already discussed. This exchange regime results in the shifting and broadening of peaks, often leading to a disappearance of the peak at intermediate titration points before reappearance at the bound position.

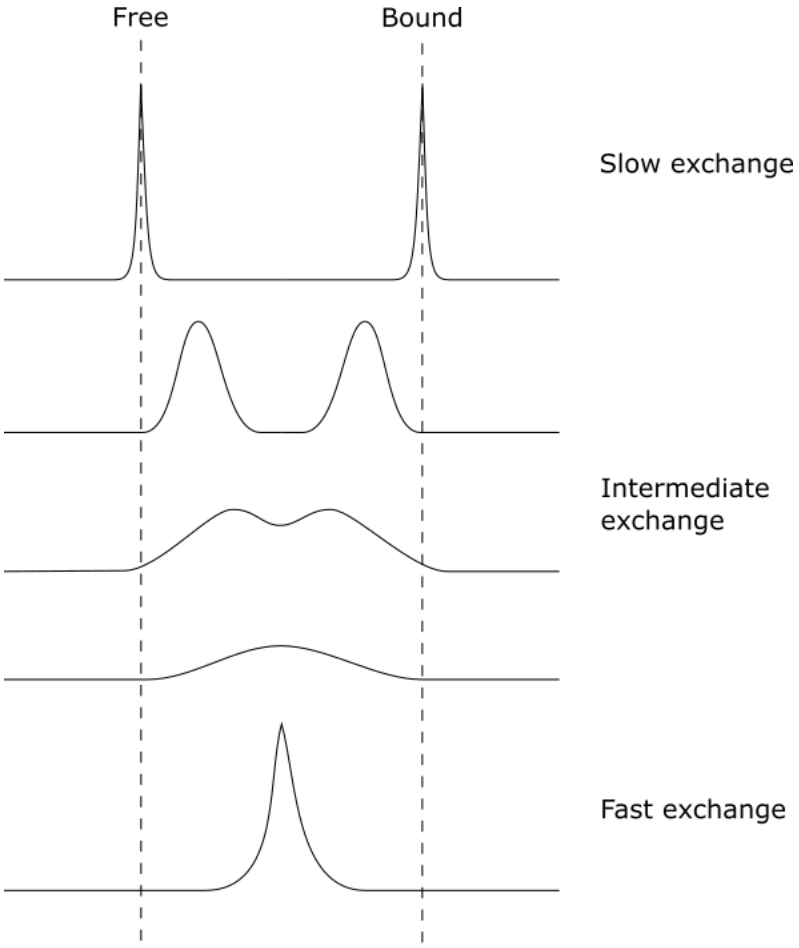


**Figure 3.21. Exchange regimes observed in NMR.** During fast exchange, the binding and release of the ligand occurs on a shorter timescale than the NMR experiment, therefore an intermediate form of a peak is observed, with the signal being averaged across the free and bound states. As the concentration of ligand is increased, the peak moves further towards the bound state. In slow exchange, the ligand comes on and off the protein much slower than the timescale of the experiment, therefore the protein is observed in either the free or the bound form and the population of each state is determined by the concentration of the ligand present. Intermediate exchange is somewhere between the two exchange regimes: as the ligand concentration increases, peaks corresponding to the free and bound forms broaden and shift, sometimes resulting in disappearance of an observable peak.

Assignments for the free and RLIP76 RBD bound forms of RalB have been published previously (195, 196), and were used to assign the free RalB spectrum in this experiment. The spectrum of RalB in complex with the HLR-sol peptide was assigned by analysing intermediate points of the titration to determine the direction of peak movement and using the RLIP76 RBD complex assignments for comparison.

The complex appeared to be in intermediate exchange, as throughout the titration peaks disappeared while shifting to a new position before reappearing in a different location. For many residues e.g. Val165, Gln153 and Leu30 (Figure 3.22A and B), the movement of the peaks could be easily tracked by following the movement of the peak using intermediate points of the titration, which were visible despite a reduction in intensity for the middle points. For other residues e.g. Met35 and Tyr 36, no peaks were visible for the intermediate points of the titration (Figure 3.22C and D), however peaks appeared for the saturated complex at positions very similar to those observed in the RLIP76 RBD complex, therefore these peaks are likely to correspond to those same residues.

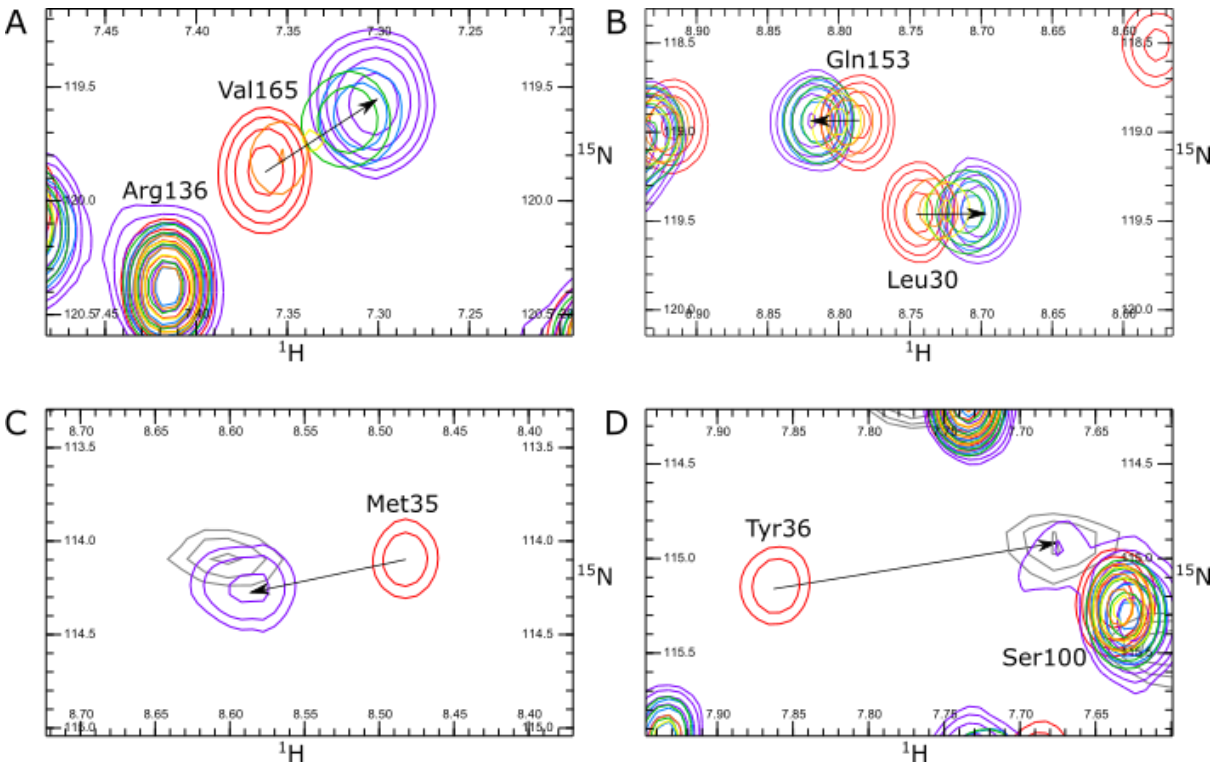


**Figure 3.22. Sections of $^{1}$H,$^{15}$N HSQC NMR spectra showing selected peak shifts from the titration of HLR-sol into $^{15}$N-labelled RalB.** The peaks are coloured as follows; red, free RalB; orange, 0.25 molar equivalents (eq) HLR-sol; yellow, 0.5 eq HLR-sol; green, 1.0 eq HLR-sol; blue, 1.25 eq HLR-sol; purple, 2 eq HLR-sol. **A** + **B**. The movement of peaks corresponding to Val165, Gln153 and Leu30 can be followed using intermediate points of the titration. The middle points (yellow) show a reduction in intensity that is indicative of an intermediate exchange regime. **C** + **D**. Met35 and Tyr36 do not have peaks at intermediate time points by which their movement can be tracked. Assignments from the previously determined RalB/RLIP76 RBD complex (grey) were instead used to identify the end-point position of these peaks.

The distances that the backbone amide peaks of RalB shifted are plotted in Figure 3.23A. Some peaks could not be traced as they had shifted too far from their original position for reliable assignment; these peaks have been given an arbitrary assignment of 0.3 ppm and are coloured in grey in the bar chart. Data is missing for multiple residues, including those for residues 43-50; these residues make up part of switch I, a region that is flexible in the free form of the protein. This flexibility means that no peaks are visible in the free spectrum for these residues due to conformational averaging, therefore no shift differences could be assigned. Several of these peaks did however appear in the complex spectra, where the residues exist in a more fixed conformation.

The residues corresponding to the peaks that shifted furthest were mapped onto the structure of RalB and are shown in Figure 3.23B. This revealed a localized region of affected residues, which is likely to represent the binding site of the peptide.

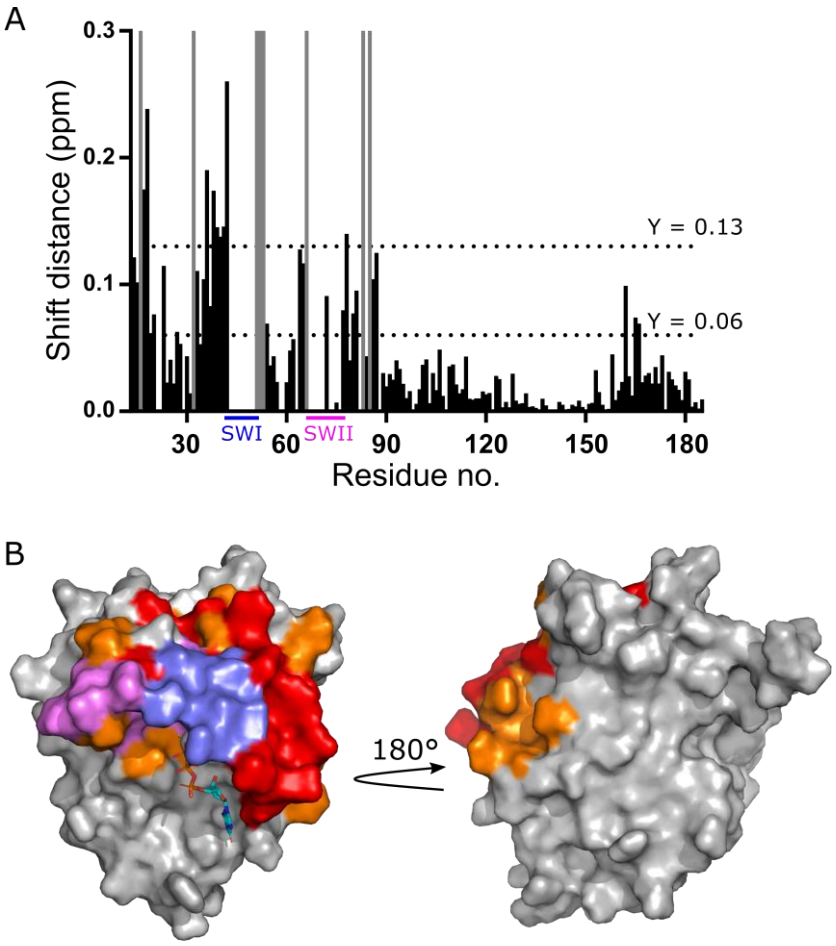


**Figure 3.23. Chemical shift perturbations for RalB after addition of HLR-sol peptide. A**. Chemical shift distances for backbone amides of RalB after addition of two equivalents of HLR-sol peptide. Peaks that have shifted too far to be reliably assigned have been given a chemical shift distance of 0.3 ppm and are shown in grey. Some switch region residues are missing from the free RalB spectrum due to their conformational flexibility, therefore shift distances cannot be assigned, and no bar is shown. 0.06 ppm marks the average chemical shift, and 0.13 ppm is the average plus one standard deviation. Y = 0.06 and 0.13 are marked by dotted lines. **B**. Residues with the largest chemical shift distances mapped onto the surface of RalB (PDB: 2KWI). Shifts greater than 0.13 ppm are displayed in red and those greater than 0.06 ppm are displayed in orange, switch I residues are coloured blue, and switch II residues are coloured purple.

The shifts were also mapped onto the known Ral-effector complex structures to determine whether the binding site of the peptide was likely to overlap with the effector binding sites. The results are shown in Figure 3.24. The shift mapping revealed significant overlap between

the binding site of the peptide and the Ral effectors, Sec5 and RLIP76. There was less overlap observed with the binding site of Exo84, though there were some residues that appeared to be shared with the two binding sites. Exo84 predominantly makes contacts with switch I, a region that could not be analysed in the titration due to the flexibility. The peptide likely also makes contacts with this region as it appears to bind in an analogous manner to the α2 helix of the RLIP76 RBD and therefore the overlap between these binding sites is likely greater than it appears in this analysis.

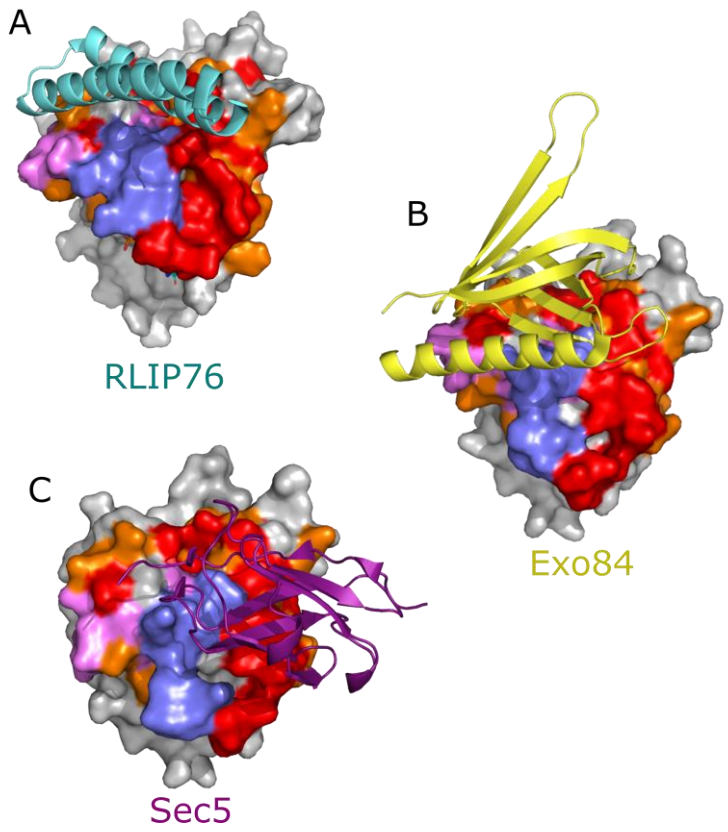


**Figure 3.24. Residues shifted on Ral upon addition of an excess of the HLR-sol peptide, mapped onto Ral-effector complex structures.** Structures of Ral with RLIP76 (**A**, PDB:2KWI), Exo84 (**B**, PDB:1ZC3) and Sec5 (**C**, PDB:1UAD) are shown, with residues that displayed shift distances greater than 0.13 ppm shown in red, and those greater than 0.06 ppm shown in orange, switch I residues are coloured blue, and switch II residues are coloured purple.

### 3.11 Cellular entry of stapled peptides

In several instances, adding an all-hydrocarbon staple into a peptide sequence has been shown to aid cellular penetration; the overall properties governing cell penetration have been

investigated, and while the findings do not apply to all stapled peptides, it has been observed that properties including a net positive charge and amphipathic helix correlated with improved cellular entry (138, 163). It has also been observed that increasing net hydrophobicity correlates with improved cellular uptake: Sakagami *et al.* found that peptides containing the olefin-containing amino acids used for chemical stapling had greater cellular uptake before the Grubbs ring-closing metathesis to form the chemical staple had occurred, which they attributed to the more hydrophobic nature of the peptides pre-stapling (164).

### 3.11.1 Assessment of cell entry with confocal microscopy

The lead peptide identified in the study prior to the work presented here was able to enter cells, as confirmed using confocal microscopy (125). The ability of the matured HLR-SP1 hydrophobic peptide to enter cells was investigated using live cell confocal microscopy in which the peptide was visualised using the fluorescein label. HEK293T cells were seeded 24 h prior to imaging and 1 µM peptide was added to the media either three or six hours prior to imaging. Dextran (10,000 MW average) was also added to the cells as an endosomal marker. Immediately prior to imaging, the cells were washed with PBS to remove non-internalized peptide and clear cell culture media was added to aid imaging. The resulting images are shown in Figure 3.25.

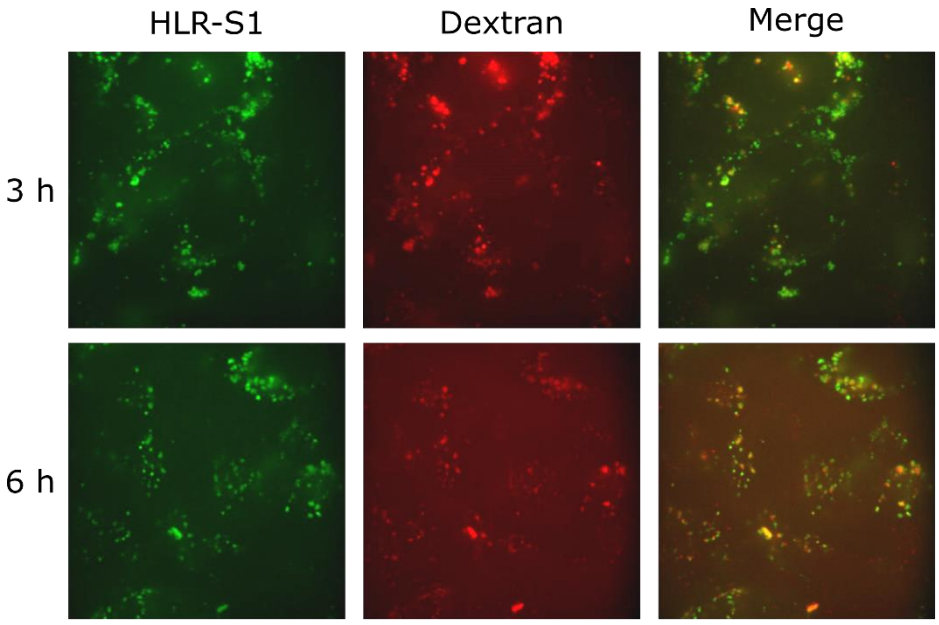


**Figure 3.25. Entry of HLR-SP1 into cells.** FAM-labelled HLR-SP1 (1 µM) and a dextran marker (Alexa Fluor™ 647, 10,000 MW) for endosomes were added to HEK293T cells for the time points indicated and cell entry was assessed by fluorescent live cell confocal microscopy. Approximately 3-5 cells are pictured in each image.

The fluorescent peptide appeared as punctate dots inside the cells, indicating that the peptide was present inside endosomes. No escape into the cytosol was observed in the timeframes investigated. The presence of the peptides in endosomes was confirmed by co-localization with the dextran marker, which has been shown to be retained in endosomes (197). A higher concentration of peptide (10 µM) was also investigated, however this appeared to be toxic to the cells and produced insoluble peptide aggregates (data not shown).

The ability of the HLR-sol and L-sol peptides to enter HEK293T cells was also investigated, however no uptake of these peptides was observed (data not shown). This suggests that the amphipathic nature of the HLR-SP1 helix or overall hydrophobicity of the peptide were important for cell entry. In order to study the effects of the soluble peptides in cells, cell-permeable sequences were therefore investigated to transport the peptides into cells.

### 3.11.2 Addition of cell-penetrating peptides to aid cell permeability

There are several options that can be used to transport peptides into cells, including electroporation, lipid delivery systems and the addition of cell-permeable tags. Here, the use

of cell-permeable peptide (CPP) tags was investigated as this approach has been used successfully previously and their ability to transport peptides into cells is well established (198).

Adachi *et al.* recently investigated a panel of well-known CPPs for cytosolic entry using a novel approach in which luciferin was conjugated to the CPPs via a disulphide linkage (199). Upon entry to the cytosol, the reducing environment causes the release of luciferin, which can then be oxidised by a cytosolically-expressed luciferase, resulting in a luminescent signal. In this study they also investigated a set of novel CPPs based on a viral protein sequence from Influenza A. The CPPs that displayed best cytosolic penetrance were conjugated to a cyclic peptide and their ability to transport the peptide cargo into the cell was assessed. They found that an octaArg (R8) motif and a novel CPP termed PF5 transported the greatest amounts of peptide into the cytosol. Therefore, these two CPPs were trialled and conjugated to our peptide.

The peptides listed in Table 3.9 were synthesized following the same procedure described in section 3.5.1 and the methods. A Gly-Ser flexible linker was included between the peptide sequence and the CPP to minimise any impact of the CPP on the structure of the Ral-binding peptide. The Q433L and K440R mutations were included in the sequence, however the E427H mutation was omitted as this substitution was thought to reduce selectivity for Ral proteins. A carboxyfluorescein (FAM) label was included at the N-terminus for visualisation of the peptides using confocal microscopy.

*Table 3.9. Synthesis of CPP-conjugated peptides.*

| Peptide name | Sequence[a] | Expected masses | Masses found | Retention time (min) | Purity (%) |
|---|---|---|---|---|---|
| LR-R8 | FAM-PEG-LXKEEXLWEELRIKTAERRKKREA-GS-RRRRRRRR | MW - 4972.8 1558.6/1244.2/995.6/831.5/711.6 | 1244.1/995.5/711.6 | 5.3 | 88 |
| LR-PF5 | FAM-PEG-LXKEEXLWEELRIKTAERRKKREA-GS-TRVLKRWKLF | MW – 5051.9 1685.0/1264.0/1011.4/844.7/722.9 | 1684.5/1263.8/1011.3/722.5 | 5.7 | 72 |

[a] Sequence variations from the wild type sequence for improving affinity are underlined, while solubilizing mutations are coloured blue and are shown in bold. X, (*S*)-pentenylalanine; FAM, 5-carboxyfluorescein; PEG, polyethylene glycol linker.

### 3.11.3 Cellular entry of modified peptides

The cellular entry of the CPP-conjugated peptides, LR-R8 and LR-PF5, was investigated using confocal microscopy with fixed HEK293T cells and the results are shown in Figure 3.26. The cells were treated with varying concentrations of peptides three hours before the cells were washed with PBS, fixed with paraformaldehyde and imaged as described in the methods. In these experiments, cells were fixed prior to visualisation to allow more conditions to be analysed.

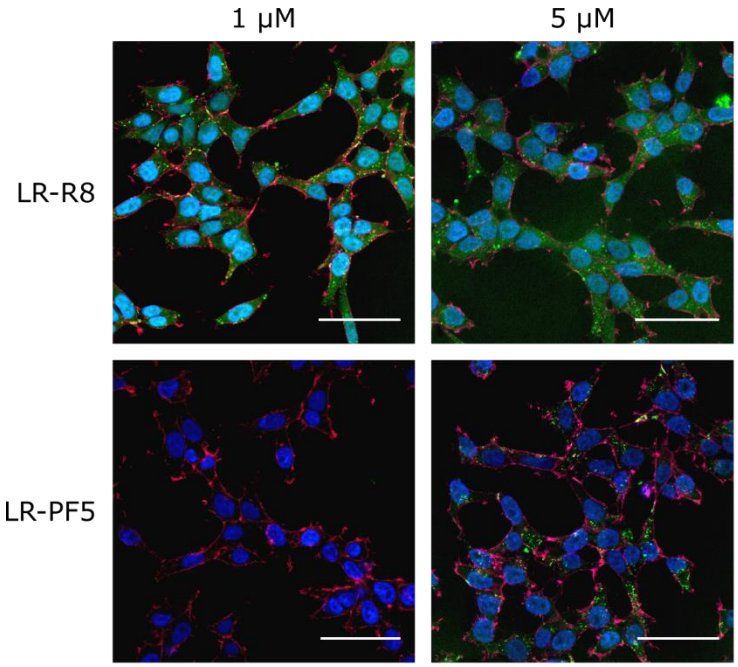


**Figure 3.26. Cellular entry of CPP-conjugated peptides into cells.** Peptides at the doses indicated were added into HEK293T cell media 3 h prior to fixing with paraformaldehyde. Images were recorded using fluorescent confocal microscopy. Representative images from three independent experiments are shown; Green, fluorescein; blue, DAPI nuclear stain; red, phalloidin-alexa647 conjugate. Scale bars represent 50 µm.

The R8-conjugated peptide displayed diffuse cytosolic staining at both concentrations tested, along with some puncta suggesting endosomal localization. The PF5-conjugated peptide did not show any cellular entry at 1 µM but did show entry in the 5 µM condition, however this staining was punctate and no escape of peptide from endosomes into the cytosol was observed. A longer incubation time of 6 h also did not show any cytosolic staining. Therefore, the octaArg peptide appeared to be a better candidate to assess the cellular activity of the peptides. Care must be taken, however, when analysing confocal images from fixed cells: it has been shown previously that the fixing process can disrupt endosomes so that the peptides appear to be cytoplasmic (200, 201). Therefore, phenotypic assays are required to confirm that the peptides are able to reach their target within cells.

### 3.11.4 Binding of CPP-conjugated peptides to Ral proteins

After appending a CPP to the peptides it was necessary to re-test the binding to Ral proteins, to assess whether the CPP had impacted the binding. Fluorescence polarization assays were used to measure binding to the Ral proteins as described in section 3.4. During these

experiments, the fluorescence intensity varied greatly throughout the titration when it should stay relatively constant, indicating a change in chemical environment of the fluorophore. This was likely due to non-specific binding to the plates. In an attempt to reduce this non-specific binding, different amounts of Tween20 and BSA were added to the assay mix and the results are shown in Figure 3.27.

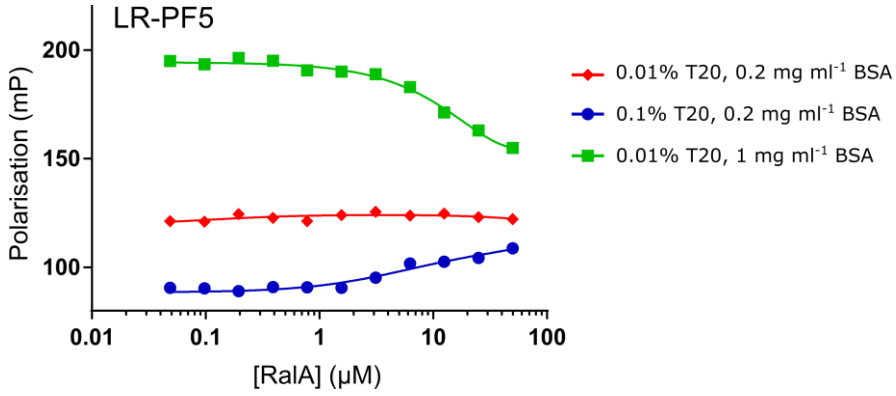


**Figure 3.27. Optimization of FP experiments for CPP-conjugated peptides binding to Ral proteins.** FP data for direct binding of 20 nM FAM-labelled LR-PF5 to RalA·GMPPNP in the presence of varying concentrations of Tween20 (T20) and BSA. Data were fitted to a single-site binding model using non-linear regression analysis in GraphPad Prism. mP, millipolarization units. n = 1.

At low concentrations of Tween20 (0.01%) no peptide binding to Ral proteins was observed, however the fluorescence intensity varied significantly under this condition. At the higher Tween20 concentration (0.1%) a binding curve was apparent, albeit with a very small assay window.

In these experiments, the machine was calibrated using the peptide alone in 0.01% Tween20 and 0.2 mg $mL^{-1}$ BSA at 120 mP, and all three rows were read with this calibration. A drop in starting fluorescence polarization was observed when the Tween20 concentration was increased to 0.1%, suggested that the fluorophore was more mobile. This could indicate that the Tween20 was preventing the peptide from sticking to itself or the plate and therefore was more available to bind the target. An increase in polarization was observed when the BSA concentration was raised to 1 mg $mL^{-1}$. This could indicate that the peptide is sticking to the BSA, as this large protein (62 kDa) would cause an increase in polarization if bound to the peptide. The 1 mg $mL^{-1}$ BSA condition loses polarization as the amount of RalA is increased, suggesting that the peptide is then transferred from the larger BSA to the smaller Ral protein.

The condition containing 0.1% Tween20 and 0.2 mg $mL^{-1}$ BSA appeared to be the best condition, however the assay window observed was far smaller than has been seen previously. Fluorescence polarization assays measure the difference in the rotational diffusion of a fluorophore by measuring the difference between emitted parallel (∥) and perpendicular (⊥) light following excitation with polarized light. When the ligand-conjugated fluorophore binds a protein target, the rotational diffusion is altered, and this is measured by a change in polarization. Therefore, the assay window is determined by the difference in rotation between the free and bound ligand. The reduction in assay window, therefore, is likely due to the increased size of the CPP-conjugated peptides, which will exhibit less rotational diffusion than the peptides without a CPP. The CPPs are linear flexible extensions and therefore will affect the rotation more than a compact folded structure of equivalent molecular weight. To improve the assay window a larger binding partner could be utilised to increase the rotational difference between the free and bound form of the peptide.

The Ral proteins used previously were produced as His-MBP fusions, followed by cleavage of the MBP protein to produce tag-less Ral. To increase the size of the Ral protein, RalA was purified with the MBP fusion protein attached. Instead of purifying the Ral protein on Ni-NTA beads followed by enzymatic cleavage, the His-MBP-RalB fusion was purified on a Ni-NTA column and eluted with imidazole. The fusion protein was purified further using size exclusion chromatography and the bound nucleotide was exchanged for GMPPNP.

This MBP-RalA protein was used to assess binding of the CPP-conjugated peptides and the results are shown in Figure 3.28. The fusion protein successfully increased the binding window observed in the assay, however non-specific binding was still observed despite the presence of Tween20, as evidenced by a linear slope rather than saturation. The binding was measured in the presence and absence of BSA and no changes were observed, therefore BSA was excluded from subsequent assays. Using MBP-RalA, both CPP-conjugated peptides bound with a similar affinity to the HLR-sol peptide, demonstrating that the CPPs had not negatively or positively impacted binding *in vitro*.

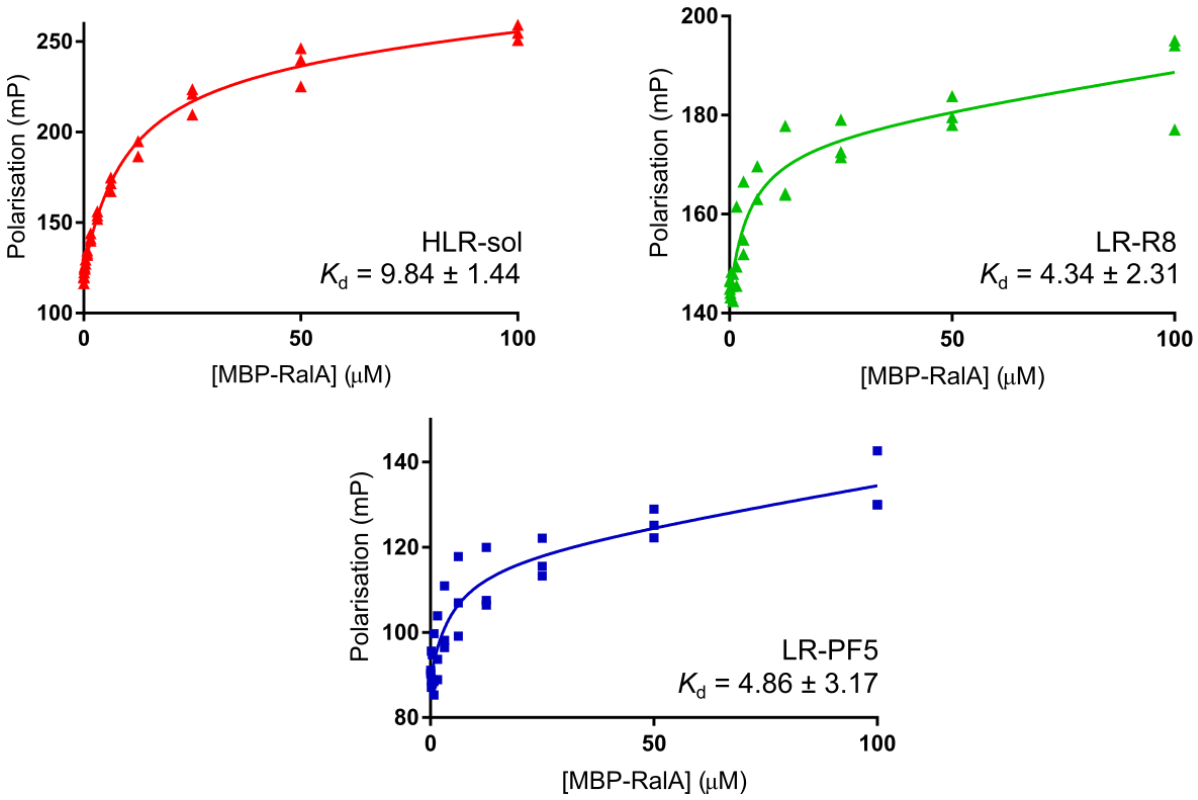


**Figure 3.28. Binding of HLR-sol and CPP-conjugated peptides to MBP-RalA.** FP data for the direct binding of 20 nM FAM-labelled HLR-sol (upper left), LR-R8 (upper right) and LR-PF5 (lower) to MBP-RalA. All conditions contained 0.1% Tween20. n = 3, and all individual results are displayed. Data were fitted to a single-site binding model using non-linear regression analysis in GraphPad Prism. $K_d$ HLR-sol = 9.84 ± 1.44 μM, $K_d$ LR-R8 = 4.34 ± 2.31 μM, $K_d$ LR-PF5 = 4.86 ± 3.17 μM. mP, millipolarization units.

The binding of CPP-conjugated peptides was also assessed using co-immunoprecipitation assays to compare the competitive binding of HLR-sol, LR-R8 and LR-PF5 in a mammalian cell lysate. The assay was set up as described in section 3.9.2, with the peptides added into the cell lysates during incubation with anti-V5 coated beads. The results are shown in Figure 3.29.

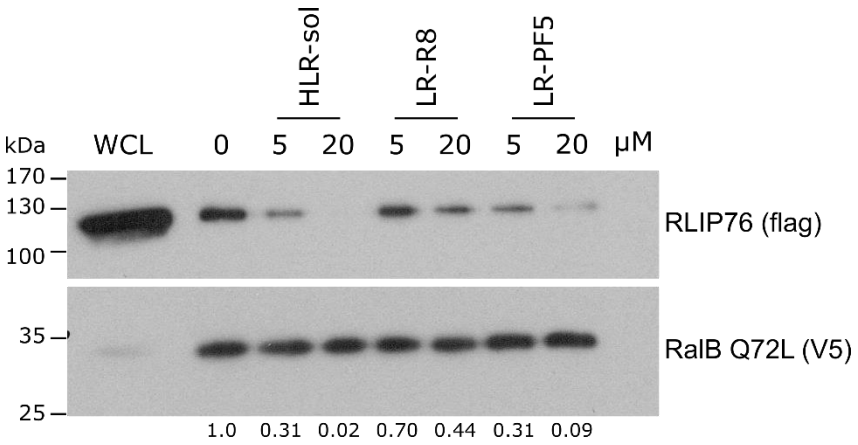


**Figure 3.29. Disruption of RalB-RLIP76 complexes by CPP-conjugated peptides in cell lysates.** The indicated concentrations of HLR-sol, LR-R8 and LR-PF5 were added into HEK293T cell lysates that had been transfected with flag-RLIP76 and V5-RalB Q72L 24 hours prior to lysis. Beads coated with an anti-V5 antibody were added to the lysate mixture to precipitate RalB and any bound proteins. The presence of RalB and bound RLIP76 was assessed by probing with anti-flag (RLIP76) and anti-V5 (RalB). Densitometry values quantifying the ratio of RLIP76:RalB relative to the no peptide condition are displayed underneath the corresponding condition. The result shown is representative of two independent experiments. WCL, whole cell lysate.

Both CPP-conjugated peptides appeared to inhibit the RalB-RLIP76 interaction to a lesser extent than the HLR-sol sequence. However, it was noted during the experiment that the CPP-conjugated peptides precipitated at high concentrations. This was particularly evident for the LR-R8 peptide, which is the likely reason that this peptide appeared to inhibit Ral-effector interactions to a lesser extent. Therefore, the concentrations of the peptides in the lysates could not be reliably estimated and this would affect their apparent ability to disrupt the RalB-RLIP76 interaction.

### 3.11.5 Co-immunoprecipitation experiments with dosed cells

The ability of the peptides to enter cells and disrupt Ral-effector complexes was next assessed using co-immunoprecipitation experiments in which the peptides were dosed into cell culture media three hours prior to cell lysis. The results are presented in Figure 3.30. Both peptides, LR-R8 and LR-PF5, were able to inhibit RalB-Sec5 interactions at the highest concentration tested (20 μM), while inhibition was also observed for 5 μM dosing of the LR-R8 peptide. Similar levels of inhibition were observed at 20 μM peptide concentrations, suggesting a similar amount of each peptide was able to enter the cells.

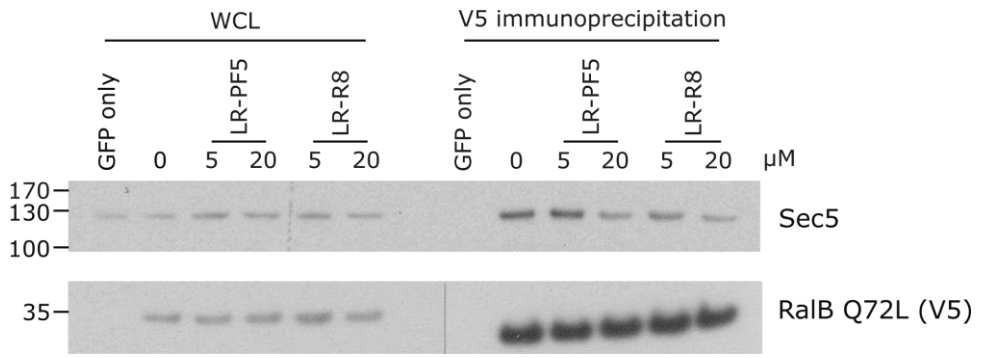


**Figure 3.30. Disruption of Ral-effector complexes by CPP-conjugated peptides added to live cells.** Complexes of V5-tagged RalB Q72L and Sec5 were precipitated from HEK293T cell lysates following 3-hour dosing with CPP-conjugated peptides at the indicated concentrations. The result is representative of two independent experiments. WCL, whole cell lysate.

When assessing the cell entry of the peptides using confocal microscopy, the PF5-conjugated peptide appeared to be less able to enter cells and was present in endosomes, therefore it is surprising that this peptide was able to inhibit Ral-effector interactions to the same extent as the LR-R8 peptide. During this experiment, however, endosomes would be lysed prior to pulling out the Ral-effector complexes, therefore the peptide could have been released from endosomes. To understand whether the peptides are able to reach Ral proteins in the cytosol, phenotypic experiments assessing Ral activity inside cells would be required.

## 3.12 Discussion

This work aimed to improve the affinity of a lead stapled peptide (SP1), based on the α2 helix from the Ral-binding domain of RLIP76, containing an all-hydrocarbon staple. Chapter 2 described how CIS display was used to identify mutations in the RLIP76 RBD that could improve affinity for Ral proteins, and the sequences from this selection formed the basis for the design of a series of stapled peptides (Table 3.1).

From this original panel of peptides, it appeared that the HLR-SP1 peptide gave the greatest improvement in binding to Ral proteins with a $K_d$ for RalB of 160 nM measured by FP, which was around a 30-fold improvement in binding compared to the WT-SP1 parent peptide. This peptide contained the same sequence substitutions that were shown to improve affinity in the context of the RLIP76 RBD; E427H, Q433L and K440R, therefore it was initially assumed that the peptide was binding in an analogous manner to the RLIP76 RBD.

Analysis of the selectivity of the peptides SP1 and HLR-SP1 against a panel of small GTPases indicated some issues, as the peptides appeared to bind RhoA with far greater affinity than the Ral GTPases, raising questions over the specificity of the binding observed. Addition of detergent could have been a simple method to eradicate non-specific hydrophobic binding, however adding a small amount of Tween20 (0.01%) into the assays produced variable results, making it difficult to draw conclusions from the data obtained (data not shown). Several pieces of evidence pointed to the conclusion that these peptides were binding to the GTPases non-specifically via the hydrophobic back face of the peptides. Firstly, the peptides displayed very different affinities for RalA and RalB, while the effector binding region of these two proteins is identical; the RLIP76 RBD, both in the wild-type and HLR-mutant forms, displays near identical affinity for RalA and RalB. Secondly, when key residues on RalB known to be involved in binding to RLIP76 were mutated to alanine, the binding to the peptides was not negatively affected as would have been expected for peptides binding at this interface. Additionally, when the hydrophobic residues on the back face of the peptide were replaced with soluble salt bridges (HLR-sol), the binding observed to other GTPases was eradicated and the resulting peptide bound RalA and RalB with near identical affinities, which were lower than had been seen previously for the hydrophobic HLR-SP1 peptide using FP.

When the hydrophobic peptides were tested in SPA competition experiments in the presence of detergent, the HLR-SP1 peptide showed very weak binding while the SP1 peptide displayed an affinity for Ral proteins that was very similar to the HLR-sol and L-sol peptides, despite binding more tightly in FP experiments. All this data together suggests that the hydrophobic peptides are not binding as expected, making any results using these peptides difficult to interpret.

In the complex of the wild-type RLIP76 RBD with Ral, more than 80% of contacts are made via the α2 helix and these contacts are preserved in the peptides used in this study (91, 181). However, alanine scanning analysis of the RLIP76 RBD identified five hotspot residues whose mutation to alanine dramatically decreased binding to Ral proteins and two of these residues (Leu409 and His413) are located in the α1 helix (181), which does not form part of the peptide sequence. Constructs of the RLIP76 RBD in which Leu409 and His413 were mutated to alanine were engineered in this study and this construct was used to determine the maximal binding affinity that could be obtained by the α2 helix contacts alone. The presence of the α1 helix

means that the coiled-coil structure is maintained, therefore the α2 helix is held in a helical structure. When studying the stapled peptides which were not 100% helical, it was not possible to discern how much this loss of helicity affected the binding affinity, therefore the RBD construct with L409A/H413A mutations can act as a model for a 100% helical peptide based on the α2 helix.

The wild-type and HLR-mutant α2 helix sequences were tested within these constructs with the key α1 helix contacts removed. Inclusion of L409A and H413A mutations to the wild-type RLIP76 RBD resulted in a great loss of affinity for RalA ($K_d$ 16 μM vs 140 nM). These results suggest that the maximum affinity that could be obtained using a peptide based on the wild-type residues of the RLIP76 RBD α2 helix is 16 μM, which is around 115-fold weaker than the RLIP76 RBD binding affinity. The $K_d$ of the previous lead peptide (SP1) for RalB was estimated to be 5 μM by ITC, only 2-fold weaker than the RLIP76 RBD affinity measured by ITC ($K_d$ ~ 2 μM) (125). The investigations in this work suggest that the previously assigned $K_d$ for SP1 is unreliable and was likely due to non-specific binding effects. Therefore, it was not possible to compare the binding affinities of the second-generation peptides to those published previously.

Adding the HLR mutations (E427H/Q433L/K440R) into the L409A/H413A background improved affinity more than 10-fold ($K_d$ = 1.4 μM), however this value was far weaker than the HLR-mutant RBD with α1 contacts preserved ($K_d$ = 5 nM). The $K_d$ value of 1.4 μM for the HLR-mutant with α1 contacts removed represents an estimate for the maximum affinity of a 100% helical stapled peptide based on this sequence, assuming no favourable contacts are made by the staple. The $K_d$ measured for the HLR-sol peptide by SPA competition was 2.8 μM, around 2-fold weaker. This value is very close to the estimated maximum affinity, despite the loss of helicity that was observed in CD experiments when the HLR or solubilizing mutations are added into the peptide. Based on these assumptions, a more helical peptide could only result in up to 2-fold improved affinity, therefore different solubilizing mutations or staple positions to improve helicity were not investigated further.

The soluble peptides HLR-sol and L-sol were able to disrupt Ral proteins interacting with their effectors; Sec5 and RLIP76, as shown by SPA competition experiments and co-immunoprecipitations. The binding site of the HLR-sol peptide was confirmed by carrying out

an NMR titration with $^{15}$N-labelled RalB and increasing concentrations of unlabelled peptide. This experiment identified many residues involved in binding to the peptide which are also common to binding the effector proteins, and the apparent binding site of the peptide overlapped well with the known interfaces determined in the structures of Ral-effector complexes.

It was hypothesized that a peptide containing only the Q433L single mutation, rather than the HLR triple mutations, would have improved selectivity for Ral proteins over related GTPases, based on experiments with the RLIP76 RBD in section 2.9. When the peptides HLR-sol and L-sol were tested against a panel of small GTPases in FP experiments, they displayed very similar selectivity for Ral proteins, and both showed almost no detectable binding to the other GTPases. The maximum concentrations of proteins that can be used in these assays is limited by the aqueous solubility of the GTPases, therefore it is possible that differential selectivity of the peptides could have been observed at higher concentrations of the GTPases. Therefore, when designing the CPP-conjugated peptides to be used in cellular assays, the E427H substitution was not included.

Two CPPs were conjugated to the peptide of interest to assess their ability to transport the peptide into the cytosol of mammalian cells. The peptides were tagged with an N-terminal fluorescent label so that they could be visualised using confocal microscopy. The two CPPs, R8 and PF5, were both able to transport the peptide into the cell at the higher concentration (5 µM) tested, while the R8 sequence also showed uptake in the 1 µM condition. The R8 CPP produced mostly diffuse cytosolic staining, with some indication of peptide trapped in endosomes by the presence of punctate staining. However, this could have been an artefact of fixing the cells, as has been observed previously (200, 201). The PF5 sequence, however, showed only punctate staining, suggesting that very little endosomal escape had occurred. Therefore, the R8 CPP performed best at transporting the peptides to the cytosol.

The binding of these CPP-modified peptides to Ral proteins was assessed to check whether binding was disrupted by the presence of the CPP. FP assays to assess binding were not straightforward, as non-specific binding and a very small assay window were observed using the typical experimental conditions. Different concentrations of Tween20 and BSA were tested and it was found that adding 0.1% Tween20 into the assay helped to reduce non-

specific binding, while the addition of small amounts of BSA had no effect. The PF5 peptide is a hydrophobic sequence and therefore non-specific binding could be reduced with detergent, while the R8 sequence is highly cationic, therefore could have benefitted from increased salt concentrations in the assay. RalA fused to His-MBP was produced to improve the assay window in these assays by increasing the size difference between the free and bound peptide. This larger protein successfully increased the assay window, allowing more reliable results to be produced. The binding of the HLR-sol peptide to MBP-RalA was also assessed under these new conditions and these *in vitro* experiments revealed that the CPP-conjugated peptides displayed a very similar affinity to the HLR-sol peptide (all $K_d$ values 4-10 µM).

When the CPP-conjugated peptides were tested for their ability to disrupt Ral-effector complexes in a mammalian cell lysate, both peptides showed reduced disruption of the RLIP76-RalB complex compared to the HLR-sol peptide, which was likely due to the poor peptide solubility at high concentrations. Therefore, it was difficult to compare relative abilities to disrupt Ral-effector interactions in this assay.

If the presence of the CPP sequences was causing a disruption to binding, other CPP sequences could be investigated. Alternatively, the CPP could be attached to the peptide via a cleavable linkage e.g. a disulphide bond that is reduced upon entry into the cytosol. This approach was employed by Adachi *et al.* when they investigated uptake of a panel of CPPs, although it was not reported whether the CPP sequence was actually removed inside the cytosol (199).

The CPPs are flexible extensions to the peptide that are likely to be susceptible to proteolysis. This is unlikely to cause issues, as the sequences do not appear to contribute to the binding affinity, and they are unlikely to be degraded before reaching their intended location in the cytosol. To decrease the likelihood of degradation, a cyclic CPP such as those developed by Pei and co-workers could be used (202, 203), as these rigidified structures are much more stable to proteolysis. The sequences also contain unnatural amino acids that protect them further from proteases.

The peptides generated in this work have a relatively low affinity for the Ral proteins compared to the native effector proteins, with around 10 to 20-fold weaker binding. The affinity obtained is not likely to be suitable for a competitive inhibitor to be used

therapeutically, as very high intracellular concentrations of peptide would be required to see a sustained effect on Ral signalling.

The peptides identified in this study could however be used as a starting point for the development of a covalent inhibitor for Ral proteins, with a warhead installed to covalently modify the Ral protein. Covalent inhibitors do not require binding affinities to be as strong as typical inhibitors, as once the covalent bond is formed, this irreversible modification holds the inhibitor in place at the binding site. Bum-Erdene *et al.* recently designed covalent inhibitors targeting Tyr82 on Ral proteins, using an aryl sulfonyl fluoride group as the reactive warhead (122). The compounds generated are unlikely to have selectivity for Ral proteins in a complex cell mixture due to their limited complexity, however the study demonstrates the possibility of targeting this tyrosine residue on Ral for covalent inhibition. This tyrosine residue is situated very close to the predicted binding site of the peptides generated in this study: Tyr82 forms a hydrogen bond with His413 in the RLIP76 RBD structure and this residue is located in the α1 helix of the RBD which is lacking in the peptides. While the peptide is unlikely to make direct contact with Tyr82, if it is binding in a similar manner to the α2 helix of the RLIP76 RBD, then the Tyr82 residue is situated only a few angstroms away. Therefore, if a warhead could be installed into the peptide at an appropriate position to reach the Tyr82 residue, this could potentially be used as a covalent inhibitor of Ral proteins with target selectivity installed in the peptide sequence.

An alternative approach could involve converting the peptide into a proteolysis targeting chimera (PROTAC). The PROTAC approach aims to hijack the cell's degradation pathways and involves conjugation of a small molecule to recruit an E3 ubiquitin ligase to a ligand targeting a protein of interest (POI) e.g. a Ral-binding peptide (204). These chimeric molecules aim to bring together the POI and an E3 ubiquitin ligase in such a way that the POI is ubiquitinated and targeted for degradation. Once ubiquitination has occurred, the PROTAC molecule is free to target another POI and hence their action is catalytic. Therefore, binding is not required to be as strong as for sustained inhibition of a POI, as the degradation event only needs to occur once for removal of the target. Evidence has shown that certain cancer cells, and not healthy cells, rely on Ral proteins for survival (115), hence targeted degradation of Ral proteins could be a promising approach in the treatment of such cancers. The peptides generated in this work could be converted into PROTAC molecules to degrade Ral proteins *in vivo*, though some

serendipity is required for this approach, as not all POIs can form favourable complexes with and be ubiquitinated by the E3 ligases that have well-characterised ligands for recruitment.

In summary, this work has resulted in the development of stapled peptides targeting the Ral GTPases with improved properties compared to the previous lead peptide. These include improved solubility and impressive selectivity for the active form of Ral proteins over the GDP-bound state and closely related small GTPases. Addition of a CPP has facilitated effective transport of the peptides into the cytosol where they can access their intended targets. These optimized peptides could be used as starting points for covalent inhibitors or PROTACs for therapeutic use or as tools to study Ral biology *in vivo*.

# 4 Recombinant peptide production

## 4.1 Introduction

The all-hydrocarbon peptide stapling approach has proven successful in generating helical, cell-permeable and protease-resistant peptides, but many additional methodologies for chemical stabilization of a helical structure have been developed (reviewed in (205)). Several of these strategies involve the covalent linkage of cysteine residues in unprotected peptides, thereby removing the requirement for incorporation of unnatural amino acids into the peptide sequences (135, 206). These approaches enable the modification of sequences produced by recombinant peptide expression, allowing for the production of long and synthetically challenging sequences.

One simple and effective approach involves the use of dibromo-containing cross-linkers; these reagents react with cysteine residues under aqueous conditions, requiring only a basic pH for reactivity (206, 207). Jo *et al.* exploited this chemistry to develop helical calpain inhibitors; they trialled a series of thiol-reactive cross-linkers with short peptides containing cysteine residues at *i*, *i* + 4 positions and investigated their relative helicities (139). The reagents that successfully cross-linked the peptides are shown in Figure 4.1. They found that cross-linking with the dibromo-*m*-xylene linker (compound 2) gave rise to the most helical peptides.

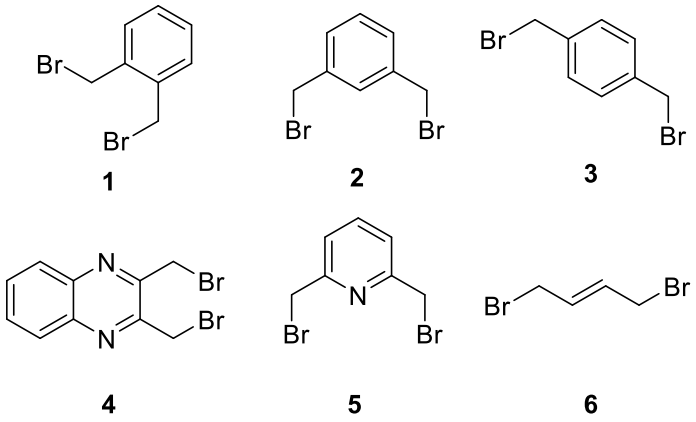


**Figure 4.1. Thiol-reactive cross-linkers for the generation of helical peptides.** Compounds 1-6 were used by Jo *et al.* to generate cysteine cross-linked peptides (139). 1, dibromo-*o*-xylene; 2, dibromo-*m*-xylene; 3, dibromo-*p*-xylene; 4, 2,3-bis(bromomethyl)quinoxaline; 5, 2,6-bis(bromomethyl)pyridine; 6, (*E*)-1,4-dibromobut-2-ene.

## 4.2 Aims

Technology to allow production of recombinant peptides that could be stabilized in a helical conformation using dibromo-*m*-xylene to cross-link cysteine residues at *i*, *i* + 4 spacings was considered advantageous for this project. This would allow production of peptides easily in house, without a complex chemistry set up. This chapter describes the production of a series of peptides based on the α2 helix of the RLIP76 RBD (residues 423-446), parallel to those described in Chapter 3 in which the all-hydrocarbon staples have been replaced with cross-linked cysteine residues.

Following production of the peptides, the properties and activities of the peptides were compared with their all-hydrocarbon stapled counterparts to assess whether this approach could be used to replace the synthetic peptides described in Chapter 3. Here the helical propensities of the recombinant peptides, their *in vitro* affinities for the Ral proteins and their ability to disrupt Ral-effector complexes were investigated.

## 4.3 Recombinant peptide production

Firstly, it was necessary to identify a method to produce the desired peptide sequences. Due to the highly flexible nature of the unmodified peptides, they are susceptible to proteolytic degradation and can be challenging to produce as soluble fusion partners.

### 4.3.1 GB1-fusion peptides

The first attempt to produce the peptides recombinantly utilised pOP5BP, a vector generated by Hyvönen *et al.* (unpublished). The pOP5BP vector contains an 8x His-tagged GB1 domain at the N-terminus, followed by an HRV-3C protease recognition site and a C-terminal Avi tag (Figure 4.2). The small size of the GB1 domain (B1 domain of the *Streptococcus* protein G, 56 residues) facilitates high yields of a small fusion partner, which in this case is the peptide sequence (208, 209). The Avi tag (15 residues) can be biotinylated by the enzyme BirA in the presence of biotin, allowing for immobilisation of the purified peptide for biochemical analysis. The desired peptide sequence was cloned into the pOP5BP vector following the HRV-3C recognition site using overlapping oligos, as described in the methods.

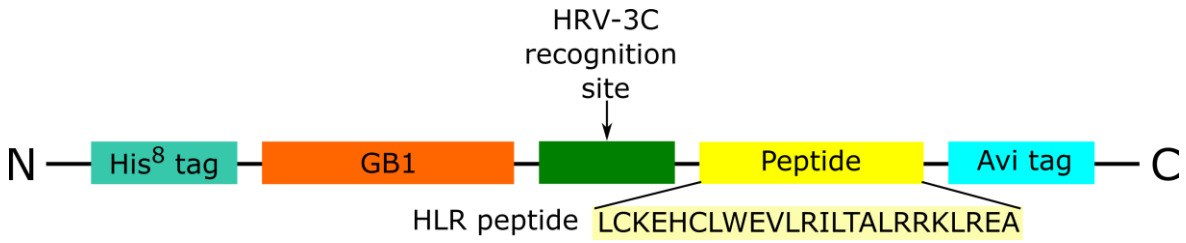


**Figure 4.2. Schematic of the pOP5BP vector.** The Pop5BP vector contains an N-terminal 8x His-tag (teal), followed by the B1 domain from *Streptococcus* protein G (GB1, orange). The peptide sequence (yellow) is separated from the GB1 domain by an HRV-3C protease recognition element (green). There is a 15-residue Avi tag (cyan) C-terminal to the peptide sequence that can be biotinylated by the enzyme BirA in the presence of biotin. The sequence of the HLR peptide cloned into pOP5BP is shown.

The aim was to produce the HLR peptide (Figure 4.2) as a soluble fusion protein and then cleave with HRV-3C protease to yield the Avi-tagged peptide. The GB1-peptide fusion was co-expressed with BirA and the growth media was supplemented with biotin to facilitate biotinylation of the Avi tag by BirA. The fusion protein was purified by affinity chromatography utlising binding of the His-tag to an $Ni^{2+}$-NTA column (Figure 4.3A and B), eluted with imidazole and subjected to cleavage with HRV-3C protease. The cleaved products were then purified by size exclusion chromatography using a Superdex S30 gel filtration column (Figure 4.3C). Following incubation with HRV-3C protease, there was no mass change in the protein observed by SDS-PAGE analysis and no evidence of the desired peptide cleavage product at

~4 kDa (Figure 4.3D). This suggested that the HRV-3C protease cleavage was unsuccessful or that the peptide had been degraded prior to cleavage.

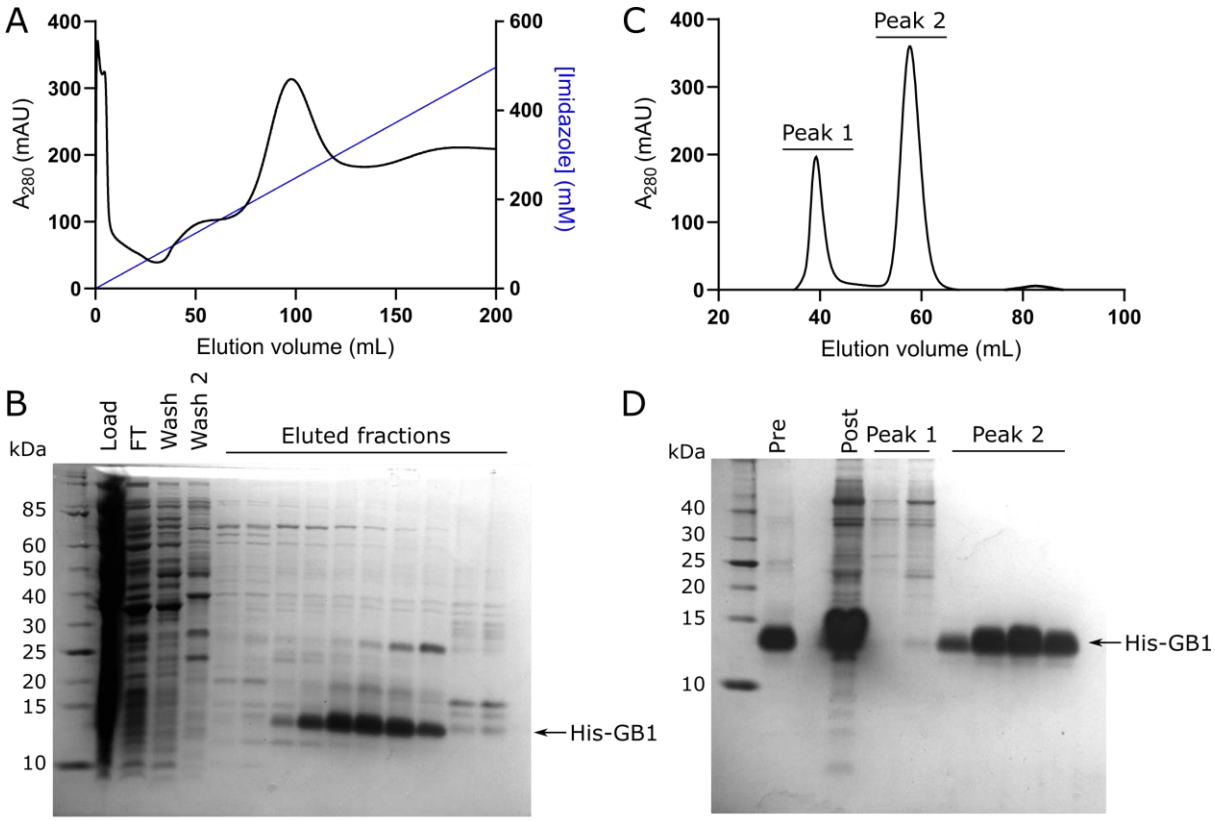


**Figure 4.3. Purification of a GB1-HLR peptide fusion. A**. Chromatogram showing elution of His-GB1 fusion protein from a Ni-NTA column with increasing concentrations of imidazole (right axis). **B**. SDS-PAGE analysis of samples from Ni-NTA purification. Load, sample of supernatant loaded onto column; FT, column flow-through; Wash, sample from column washing with purification buffer; Wash 2, sample from column washing with purification buffer supplemented with 20 mM imidazole; Eluted fractions, proteins eluted from the column with increasing concentrations of imidazole. The arrow shows the band predicted to contain the His-tagged GB1 domain (9.5 kDa) **C**. Chromatogram from Superdex S30 gel filtration purification, following overnight cleavage with HRV-3C protease. **D**. SDS-PAGE analysis of samples from gel filtration purification: Pre, sample of protein before cleavage with HRV-3C protease; post, sample of protein after HRV-3C cleavage which was loaded onto the column; eluted fractions, fractions corresponding to Peaks 1 and 2 in chromatogram C.

A small-scale expression trial of the construct was carried, out with samples taken at various time points to determine whether the GB1-peptide fusion was being degraded prior to cleavage. A western blot probed with an anti-His antibody was used to ensure that the correct band was identified (Figure 4.4). The intact fusion protein was observed running above the

15 kDa marker in all 'total' cell lysate samples, containing both soluble and insoluble proteins but was only visible in the soluble fraction for one hour following induction with isopropyl β-D-1-thiogalactopyranoside (IPTG) at 37 °C, while a small amount was present after induction at 20 °C for 16 hours. Following prolonged incubation at 37 °C, only a band with a smaller molecular weight was visible in the soluble fraction, indicating that the fusion protein was susceptible to proteolysis and was therefore short-lived. A large-scale preparation following induction at 37 °C for only one hour was attempted but still no intact fusion protein was obtained. It was surmised that the flexible and unstructured nature of the peptide makes it too susceptible to proteolysis to allow purification.

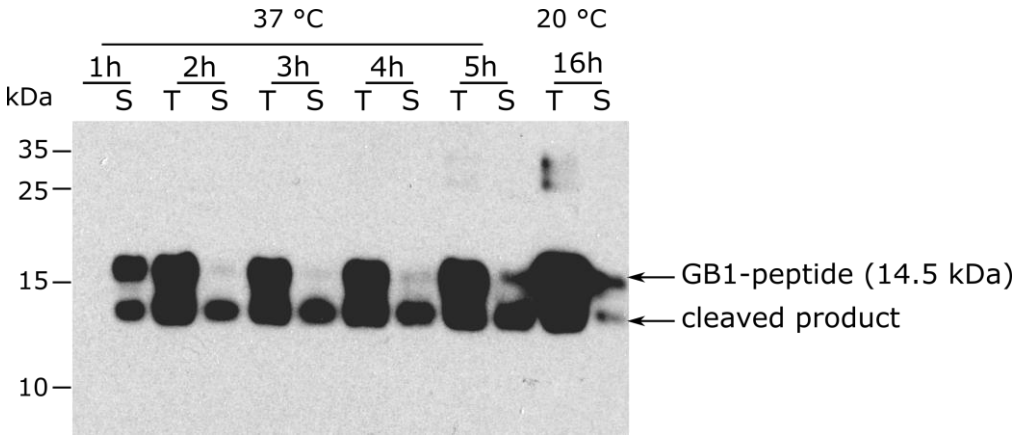


**Figure 4.4. Expression trial of the GB1-peptide fusion.** A western blot probed with an anti-His antibody shows samples taken at various time points following induction with 1 mM IPTG at the temperatures shown. T – total contents of *E. coli* cells following lysis, S – soluble proteins, those present in the supernatant following centrifugation of *E. coli* lysates. The intact GB1-peptide fusion protein (14.5 kDa) is visible above the 15 kDa marker, while a smaller cleavage product is observed below the 15 kDa marker.

There appeared to be intact GB1-peptide fusion present in the 'total' lysis sample for all conditions trialled, but not in the soluble fractions, suggesting that some of the fusion protein was present in insoluble inclusion bodies. A preparation of inclusion bodies was therefore attempted as described in the methods, however no protein at the correct molecular weight for the fusion protein was identified in the purified inclusion bodies following several buffer washes. Samples from the inclusion body preparation are shown in Figure 4.5.

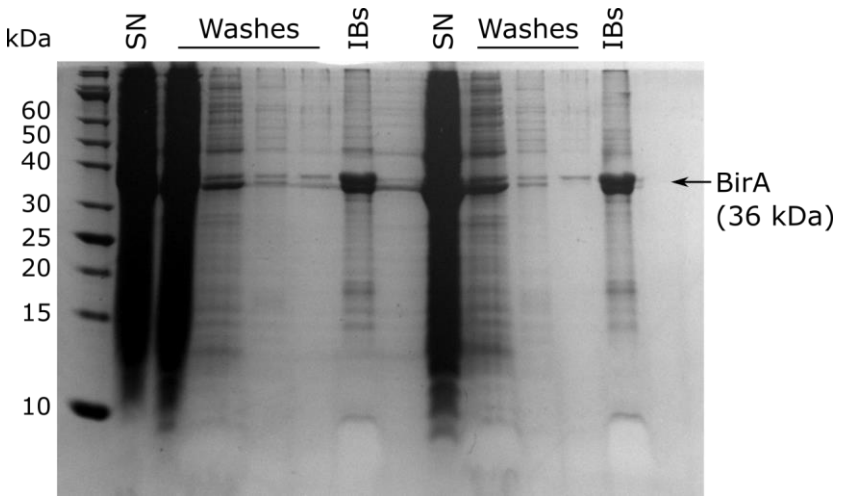


**Figure 4.5. Inclusion body preparation of the GB1-HLR peptide fusion.** SDS-PAGE analysis of samples taken during the inclusion body preparation: SN, supernatant following lysis and centrifugation of *E. coli* cells; Washes, supernatants from washes of the cell pellet; IBs, inclusions bodies after resuspension of the cell pellet in 6 M Gdn-HCl. Only BirA (36 kDa) is observed in the purified inclusion bodies in appreciable quantities. No GB1-HLR peptide fusion (14.5 kDa) was observed in any of the samples analysed.

### 4.3.2 KSI-fusion peptides

Following the difficulties encountered in producing the peptide as a soluble fusion partner, a protocol designed to direct the peptide into inclusion bodies was attempted. pET31b (Novagen) was used to produce a KSI-HLR peptide fusion with a C-terminal His-tag. The ketosteroid isomerase (KSI) protein is highly insoluble and drives the fusion product into inclusion bodies where it is protected from proteases.

#### 4.3.2.1 Cloning the peptide into pET31b

The HLR peptide sequence was cloned into the pET31b vector using overlapping oligos as described in the methods. The vector is designed to facilitate peptide cleavage with cyanogen bromide (CNBr) at methionine residues, therefore there are methionine residues located before and after the cloning site in the vector. Due to safety issues concerning the use of CNBr, an Asp-Pro motif was inserted between the peptide sequence and the KSI fusion protein to act as an acid-labile cleavage site (210–212). The KSI protein contains an additional Asp-Pro sequence that would give rise to a peptide of similar molecular weight once cleaved, so this aspartate residue was mutated to glutamate to avoid difficulties in separating the cleavage products. A schematic of the fusion protein produced is shown in Figure 4.6.

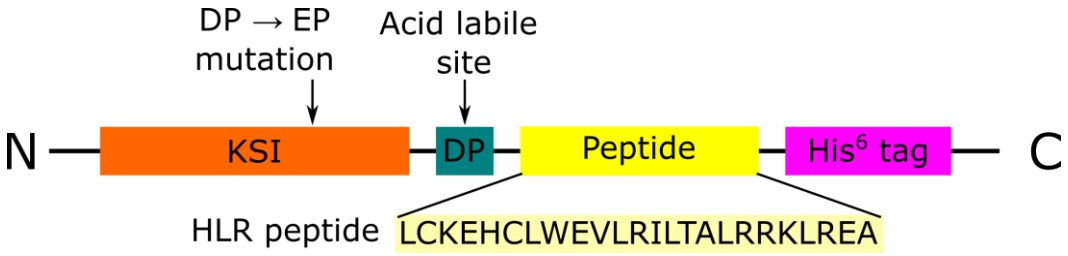


**Figure 4.6. Production of a KSI-HLR peptide fusion from pET31b.** pET31b encodes the ketosteroid isomerase (KSI) protein N-terminal to the cloning site and a 6x His-tag at the C terminus. The HLR peptide was cloned into the vector using overlapping oligos and an Asp-Pro motif was also included as an acid-labile cleavage site. As the KSI protein contains an additional Asp-Pro motif, this site was mutated to Glu-Pro to avoid difficulties in separating the cleavage products.

#### 4.3.2.2 KSI-peptide expression trials

Trial expressions of the construct in BL21(DE3) cells were carried out using varying amounts of IPTG for induction and different growth times following induction (Figure 4.7). The KSI-peptide fusion was found almost exclusively in the cell pellet following expression and cell lysis, demonstrating that it was insoluble and located in inclusion bodies. Expression of the fusion protein was observed even in the absence of IPTG induction, presumably due to a loss of repression in the BL21(DE3) cells used, and there was also very little difference in the amount of expression observed for the two IPTG concentrations tested. The cell pellet, and hence total amount of protein, increased with an increased length of expression, therefore final conditions of 1 mM IPTG for 6 hours were selected for large scale expression. Lysozyme was used to assist cell lysis and was hence visible in the soluble fraction of the bacterial lysates.

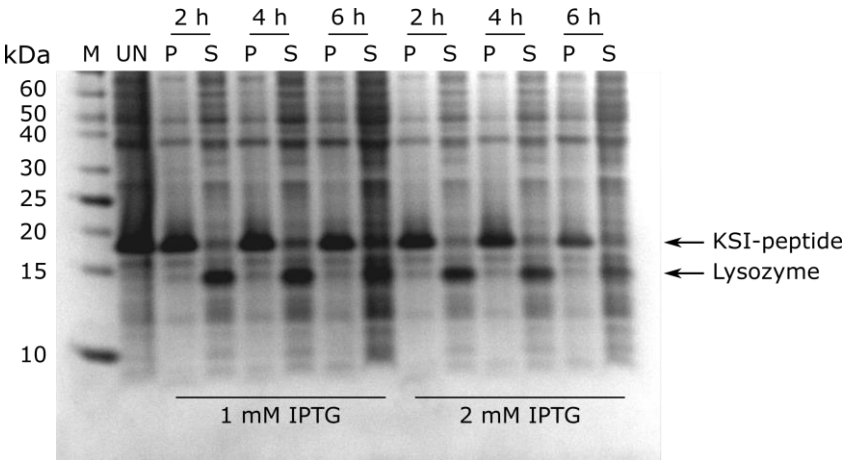


**Figure 4.7. Expression trial of the KSI-peptide fusion.** SDS-PAGE analysis of samples taken from trial expressions: UN, uninduced; P, cell pellet; S, soluble fraction. The expected molecular weight of the KSI-peptide fusion is 18.3 kDa and lysozyme is 14.3 kDa. The KSI-peptide fusion is observed in the cell pellet and is therefore likely present in inclusion bodies.

#### 4.3.2.3 KSI-peptide large scale expression

A large-scale expression of the construct was carried out and, following lysis, the cell pellet was washed several times with buffer to clean the inclusion bodies. The pellet was then resuspended in 6 M guanidine to solubilize the inclusion bodies containing the KSI-peptide fusion (Figure 4.8A). The fusion protein was purified by $Ni^{2+}$-NTA affinity chromatography utilising the C-terminal His-tag (Figure 4.8B and C). Two bands were seen by SDS-PAGE analysis following elution with 300 mM imidazole: the strongest appeared around the expected weight for the fusion protein (18.3 kDa) and a second, less prominent, band at approximately the weight of a KSI-peptide fusion dimer (36.6 kDa). This dimer is likely observed due to insufficient amounts of reducing agent in the sample buffer. The peptide contains exposed cysteine residues and therefore can form disulphide-bonded dimers and higher oligomeric structures.

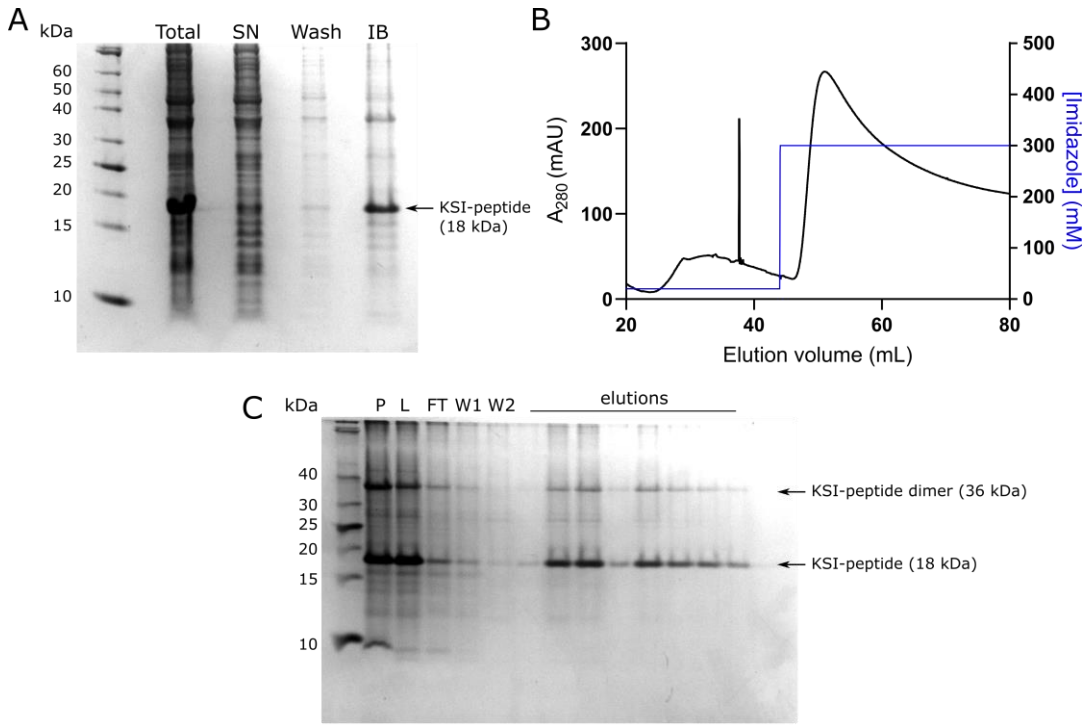


**Figure 4.8. Purification of KSI-HLR peptide fusion from inclusion bodies. A**. SDS-PAGE analysis of samples from large scale expression: Total, total cellular contents following lysis; SN, soluble proteins that remain in the supernatant following centrifugation; Wash, contents of final wash of pellet following centrifugation; IB, contents of inclusion bodies after solubilizing the pellet in 6 M Gdn-HCl. **B**. Chromatogram from $Ni^{2+}$-NTA affinity chromatography of KSI-peptide fusion in 6 M Gdn-HCl. The fusion protein, containing a C-terminal 6x His-tag, was eluted with 300 mM imidazole (right axis). **C**. SDS-PAGE analysis of samples from affinity chromatography: P, samples remaining in pellet after solubilization in 6 M Gdn-HCl; L, sample loaded onto column; FT, column flow-through; W1, wash with purification buffer to remove unbound proteins; W2, wash with purification buffer + 20 mM imidazole to remove weakly associated proteins; elutions, fractions taken following column washing with 300 mM imidazole to elute His-tagged proteins.

### 4.3.2.4 Dual preparation of tagged and tag-less peptides

The results shown in section 4.3.2.3 demonstrated that the pET31b vector could be used to successfully isolate a KSI-peptide fusion protein from inclusion bodies. It was decided that it would be useful to additionally generate peptides without a His-tag for use in assays such as SPA competitions. A second construct was therefore engineered in pET31b containing two peptide sequences, separated from each other and the KSI fusion by Asp-Pro residues for cleavage with dilute acid (Figure 4.9).

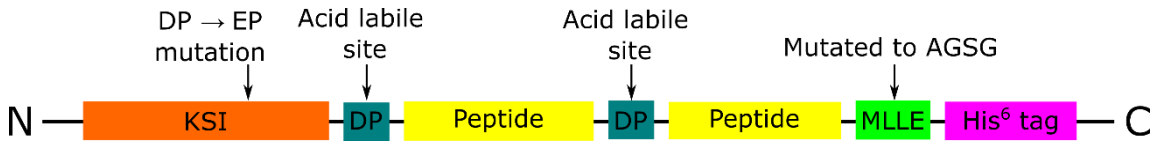


**Figure 4.9. KSI-peptide fusion containing two peptide sequences in pET31b.** The peptide sequence was inserted into the pET31b vector as described for the single peptide, however an additional peptide sequence was also included. These peptides were separated by an Asp-Pro motif to cleave between the two with dilute acid. The residues between the second peptide and the C-terminal His-tag were mutated to Ala-Gly-Ser-Gly to provide a flexible linker between the peptide and the tag. The peptides listed in Table 4.1 were produced from these constructs.

Four residues remained between the second peptide and the His-tag following cloning into the pET31b vector: Met-Leu-Leu-Glu (Figure 4.9). The need to immobilise the peptide via the His-tag for some downstream applications had been anticipated and therefore a flexible linker was more desirable than the bulky residues that were currently in place. Four of these residues were therefore mutated to Ala-Gly-Ser-Gly, where Ala is the final residue of the second peptide sequence and the remaining residues were to form the flexible linker. Fusion proteins were expressed and purified as described for the construct containing a single peptide sequence in the previous section.

The peptide sequences listed in Table 4.1 were prepared using this method. The sequences selected were those described in Chapter 3 that displayed the highest affinity for Ral proteins, with cysteine residues for cross-linking replacing the hydrocarbon staple residues. The peptide sequences also contain the Glu-Lys salt bridges for improved solubility, as described in Chapter 3. Additionally, there was an extra proline residue at the N-terminus and an aspartate at the C-terminus for the non-tagged peptides remaining from the acid cleavage site.

*Table 4.1. Peptides produced recombinantly as KSI-fusions.*

| Peptide | Sequence[a] |
|---|---|
| csHLR | PLC$_s$KEHC$_s$LWEELRIKTAERRKKREAD |
| csHLR-His | PLC$_s$KEHC$_s$LWEELRIKTAERRKKREAGSGHHHHHH |
| csLR | PLC$_s$KEEC$_s$LWEELRIKTAERRKKREAD |
| csLR-His | PLC$_s$KEEC$_s$LWEELRIKTAERRKKREAGSGHHHHHH |

[a] Cs – cysteine (for cross-linking). Substitutions identified by CIS display to improve the sequence affinity compared to the wild-type RLIP76 RBD sequence are underlined, while solubilizing mutations are shown in bold and coloured blue.

### 4.3.3 Peptide stapling with dibromo-*m*-xylene

Following purification of the fusion protein by $Ni^{2+}$-NTA affinity chromatography, a cross-linking reaction with dibromo-*m*-xylene was carried out (Figure 4.10). The reaction required a basic pH (approximately 8.0) to ensure that the cysteine residues were not protonated and were therefore reactive. A reducing agent was also required to ensure that the cysteine residues are not engaged in disulphide bonds, which would prevent them from reacting with the linker. Tris(2-carboxyethyl)phosphine (TCEP) was used for this purpose as other commonly used reducing agents such as dithiothreitol (DTT) and β-mercaptoethanol contain thiol groups that could also react with the linker. Following acid hydrolysis to release the peptide from KSI, the extent of stapling was assessed using matrix-assisted laser desorption/ionization mass spectrometry (MALDI-MS). 100% stapled product was observed for peptides incubated with the cross-linking agent overnight.

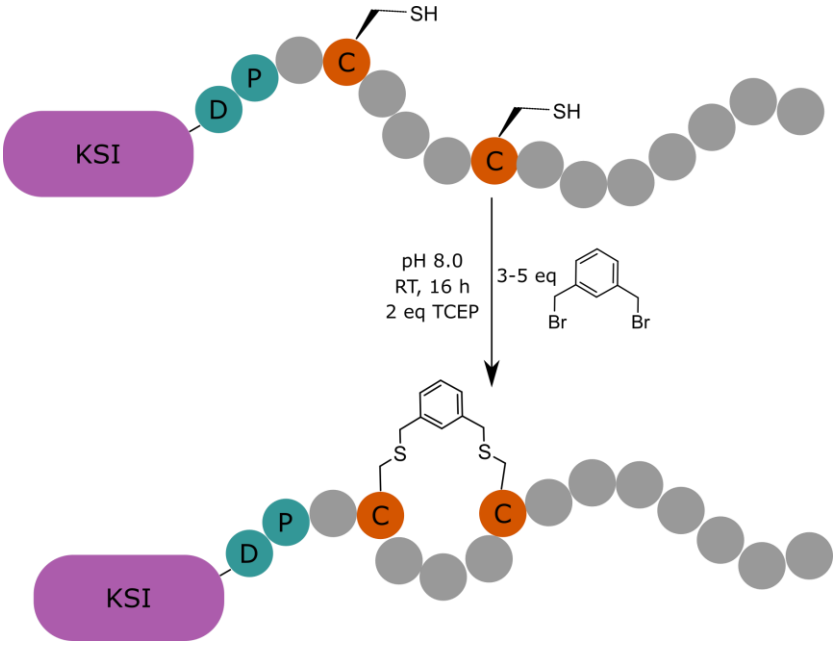


**Figure 4.10. Reaction conditions for cross-linking peptides with dibromo-*m*-xylene.** The KSI-peptide fusion in 6 M Gdn-HCl with 50 mM Tris-HCl pH 8.0 was mixed with 3-5 equivalents dibromo-*m*-xylene, 2 equivalents TCEP and stirred overnight at room temperature, giving rise to the cross-linked product.

### 4.3.4 Acid hydrolysis to cleave labile Asp-Pro bonds

The cross-linked peptides were cleaved from the KSI fusion protein by adjusting the pH to approximately 1.0 with acid, prior to heating the mixture to 85 °C for five hours, following the method described by Gavit and Better to cleave acid labile Asp-Pro bonds (212). Following hydrolysis, the mixture was dialysed into pH 7.0 buffer, causing the KSI to precipitate while the peptide sequences remained soluble.

### 4.3.5 Purification of cleaved peptides

SDS-PAGE analysis of the hydrolysed samples revealed that very little intact fusion protein was left following the five-hour hydrolysis reaction (Figure 4.11). However, small amounts of incomplete hydrolysis products were observed, with a band corresponding to the mass of the KSI protein with a single peptide attached (17 kDa) and another for the two peptides that had been cleaved from the KSI but not from each other (7 kDa). Following dialysis into buffer, only the cleaved peptides remained in solution, while any KSI-containing fragments precipitated and were separated (Figure 4.11).

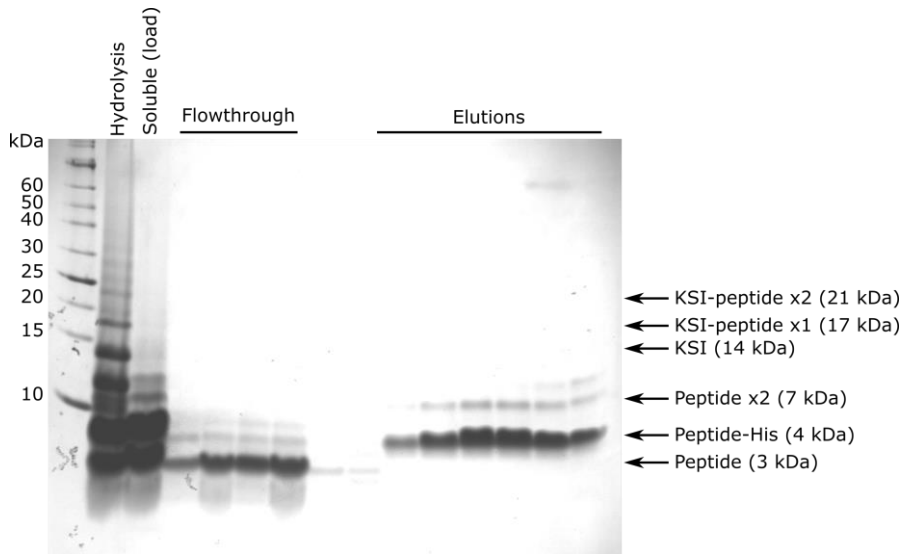


**Figure 4.11. Purification of cleaved peptides, csLR and csLR-His.** SDS-PAGE analysis of the mixture following hydrolysis (hydrolysis), and of soluble proteins following dialysis into buffer (soluble). These were loaded onto a $Ni^{2+}$-NTA column. The flow-through shows samples of proteins that did not stick to the column and the samples labelled 'elutions' correspond to fractions eluted from the $Ni^{2+}$-NTA column with imidazole.

The soluble peptides were loaded onto a $Ni^{2+}$-NTA affinity column. The non-tagged peptide did not stick to the column and was found in the flow-through, while the His-tagged peptides were retained and were subsequently eluted with imidazole (Figure 4.11). The non-tagged peptides were slightly contaminated with the His-tagged peptide and as these peptides are unlikely to be separated by size-exclusion chromatography, the flow-through was collected and passed back over the $Ni^{2+}$-NTA column to remove any remaining His-tagged peptide.

Finally, the peptides were purified further by size exclusion chromatography on a Superdex S30 column to remove any larger contaminants (Figure 4.12). The peptides were effectively separated from other species and the resulting fractions contained very few visible contaminants.

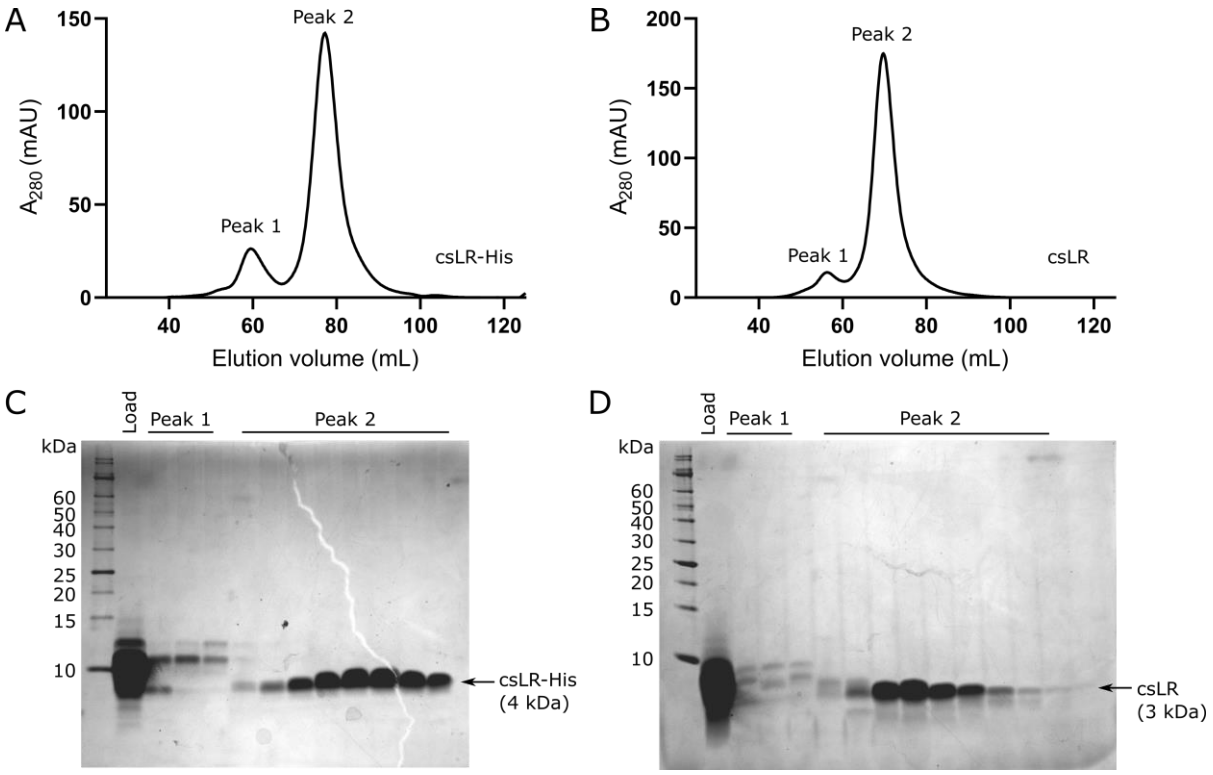


**Figure 4.12. Size exclusion purification of cleaved peptides.** The peptides were purified using a Superdex S30 column. **A** and **B** show the chromatograms obtained from the purifications of the csLR-His and csLR peptides, respectively. SDS-PAGE analysis of the eluted fractions for both the His-tagged (**C**) and non-tagged (**D**) csLR-sol peptides are shown. The peptides are found in the largest peak (peak 2) in each instance.

## 4.4 Binding of recombinant peptides in SPA competitions

Binding affinities of the dibromo-*m*-xylene peptides, csLR and csHLR, to RalB were measured in SPA competition experiments. The results are shown in Figure 4.13 and the calculated $K_d$ values are listed in Table 4.2.

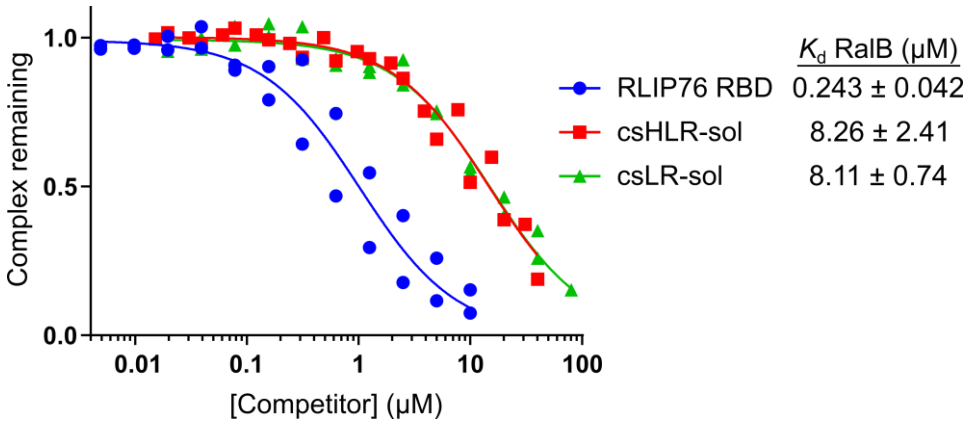


**Figure 4.13. Binding of dibromo-*m*-xylene peptides to RalB in SPA competition experiments.** The RLIP76 RBD (blue), csHLR-sol peptide (red) and csLR-sol peptide (green) were titrated into fixed concentrations of [$^3$H]GTP·RalB and His-tagged RLIP76 RBD immobilised on SPA beads. The data were fitted to an isotherm describing competitive binding to yield apparent $K_d$ ($K_i$) values for the competitors as described previously (182). Data and fits are displayed as a fraction of the maximum SPA signal measured for each condition, and the calculated $K_d$ values are listed in Table 4.2.

*Table 4.2. Comparison of $K_d$ values obtained by SPA competition experiments with dibromo-m-xylene peptides and an all-hydrocarbon stapled synthetic peptide.*

| Peptide | Sequence[a] | $K_d$ Ral (μM) |
|---|---|---|
| HLR-sol | FAM–PEG–LXKEHXLWEELRIKTAERRKKREA | 2.97 ± 0.29 (RalA) |
| csHLR | PLC$_s$KEHC$_s$LWEELRIKTAERRKKREAD | 8.26 ± 2.41 (RalB) |
| csLR | PLC$_s$KEEC$_s$LWEELRIKTAERRKKREAD | 8.11 ± 0.74 (RalB) |

[a]Cs – cysteine (cross-linked). Residues that have been included to improve affinity compared to the wild-type RLIP76 RBD sequence are underlined, while solubilizing mutations are shown in bold and coloured blue. FAM, 5-carboxyfluorescein; PEG, polyethylene glycol linker.

The csHLR and csLR peptides bound RalB with similar affinities, with $K_d$ values of 8.3 and 8.1 μM, respectively. This was in agreement with previous experiments, demonstrating that the E427H mutation in the RLIP76 RBD has little effect on the affinity for RalB (section 2.7). Both peptides were able to compete with the RLIP76 RBD, demonstrating that they occupy a shared binding site.

The affinities of the cysteine cross-linked peptides were 2 to 3-fold weaker than those obtained for their hydrocarbon stapled counterpart: the HLR-sol peptide displayed a $K_d$ of 3.0 μM for RalA in SPA competitions (Table 4.2, section 3.9.1). It is reasonable to compare this

value for RalA with affinities measured for RalB and the cysteine cross-linked peptides, as FP experiments showed that the affinities of the HLR-sol hydrocarbon stapled peptide were very similar for RalA and RalB (section 3.5.2). Additionally, all experiments using the same sequences in the context of the RLIP76 RBD showed near identical results with RalA and RalB (section 2.5 and 2.7).

Binding affinities of the csHLR-sol and csLR-sol peptides for RhoA, a related small GTPase, were also measured using SPA competitions, and the results are shown in Figure 4.14. Both peptides bound more weakly to RhoA than to RalB, the intended target, with $K_d$ values of 13 µM for csHLR and 47 µM for csLR. The csLR peptide bound around 4-fold more weakly than the csHLR peptide, suggesting that introducing fewer changes in the sequence compared to that of the wild-type RLIP76 RBD can increase selectivity for Ral proteins, as was also seen in section 2.9.

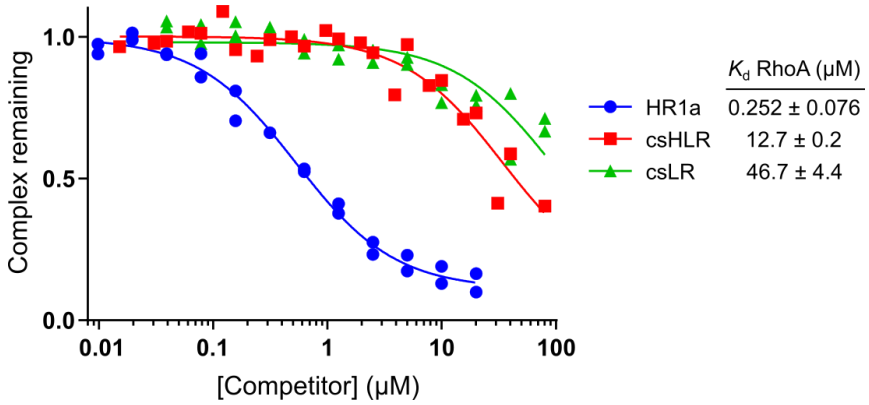


**Figure 4.14. Off-target binding of dibromo-*m*-xylene peptides to RhoA.** The HR1a domain from the RhoA effector PRK1 (blue), csHLR-sol peptide (red) and csLR-sol peptide (green) were titrated into fixed concentrations of [$^3$H]GTP·RhoA and His-tagged HR1a immobilised on SPA beads. The data were fitted to an isotherm describing competitive binding to yield apparent $K_d$ ($K_i$) values for the competitors using GraphPad Prism. Data and fits are displayed as a fraction of the maximum SPA signal measured for each condition, and standard errors are reported: $K_d$ HR1a, 252 ± 76 nM; csHLR, 12.7 ± 0.2 µM; csLR, 46.7 ± 4.4 µM. n = 2.

## 4.5 Inhibition of complexes in mammalian cells

The ability of the csHLR peptide to disrupt Ral-effector complexes in a mammalian cell lysate was next assessed using co-immunoprecipitation experiments as described in section 3.9.2. A representative western blot is shown in Figure 4.15. At the concentrations measured, the csHLR-sol peptide was unable to inhibit the interaction of RalB with RLIP76, while the

hydrocarbon stapled analogue (HLR-sol) was able to disrupt complexes at similar concentrations (see section 3.9.2).

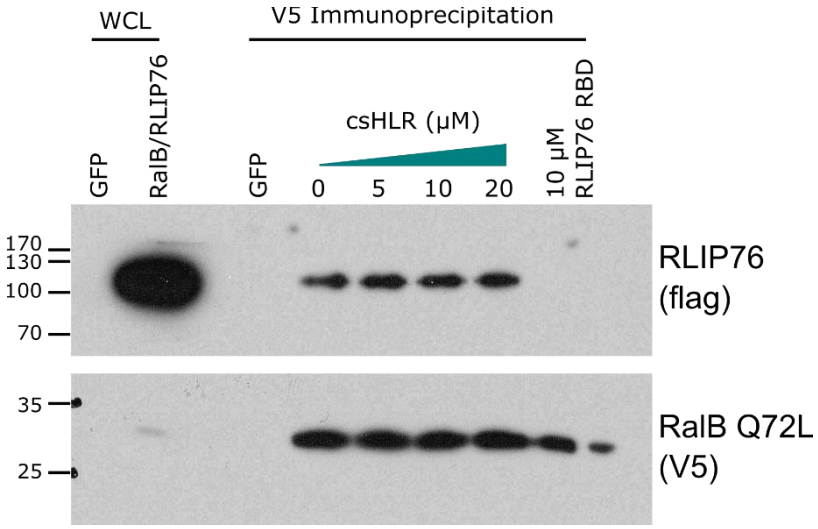


**Figure 4.15. Co-immunoprecipitation of RalB/RLIP76 complexes from HEK293T cell lysates in the presence of increasing amounts of csHLR peptide.** HEK293T cells were transfected with RalB Q72L-V5 and RLIP76-flag or GFP 24 hours before lysis. The csHLR peptide and RLIP76 RBD were added into the cell lysates at the concentrations indicated. Beads coated with an anti-V5 antibody were added to the lysate mixture to capture RalB and any bound proteins. Presence of RalB/RLIP76 complexes was assessed by western blotting, probing with anti-flag (RLIP76) and anti-V5 (RalB). WCL, whole cell lysate; GFP, green fluorescent protein. The result is representative of two independent repeats.

## 4.6 Secondary structure evaluation

The helical content of the csLR peptide was also assessed using circular dichroism (CD) and the resulting data is shown in Figure 4.16. The dibromo-*m*-xylene linked csLR peptide lacked any helical secondary structure, as is normally indicated by minima at 208 and 222 nm and a positive signal at wavelengths less than 200 nm. Instead it exhibited a profile more characteristic of a random coil, with an estimated helicity of 22%. This was much less helical than the HLR-sol peptide containing an all-hydrocarbon staple, which was estimated to be 44% helical (see section 3.6).

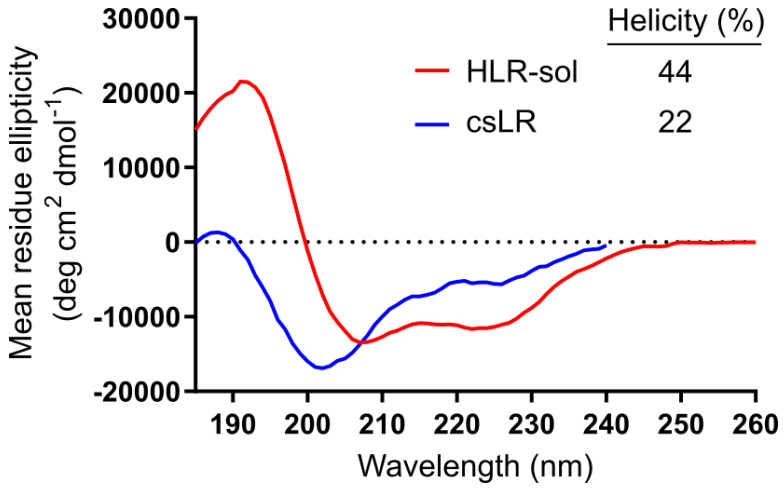


**Figure 4.16. CD spectra of cysteine cross-linked and dibromo-*m*-xylene stapled peptides.** The CD spectra of the dibromo-*m*-xylene linked csLR peptide (blue) and the HLR-sol peptide containing an all-hydrocarbon staple (red) were measured in the range 185-260 nm. CD data are reported as mean residue ellipticity (deg $cm^2$ $dmol^{-1}$, θ). HLR-sol exhibits much greater helicity as evidenced by the characteristic minima at 208 and 222 nm. the reported percentage helicity (%) was estimated by the CDSSTR method and reference set 3 using Dichroweb (183–185).

Aside from the staple composition, the sequences of the two peptides are largely similar, although the csLR peptide has an additional proline at the N-terminus and an aspartate at the C-terminus as artefacts from the acid cleavage sites. It is possible that these sequence differences could be causing a loss of helicity, however it is more likely that the *m*-xylene cross-link is less effective than the all-hydrocarbon staple at stabilizing a helical structure.

In addition to covalently linking the residues at *i*, *i* + 4 positions, the (*S*)-pentenylalanine amino acids used to form the hydrocarbon staple contain a methyl group at the Cα position, as shown in Figure 4.17. This di-substituted position does not occur in natural amino acids and has been shown to induce a helical conformation, even without covalent linkage of the amino acids, by favouring backbone torsion angles associated with helices. This has been observed for other di-substituted amino acids including α-amino isobutyric acid (Aib) (213). As the m-xylene staple bridges two cysteine residues lacking a di-substituted Cα, this additional helix stabilization is not present and this may explain why the recombinantly produced peptide has a less helical structure.

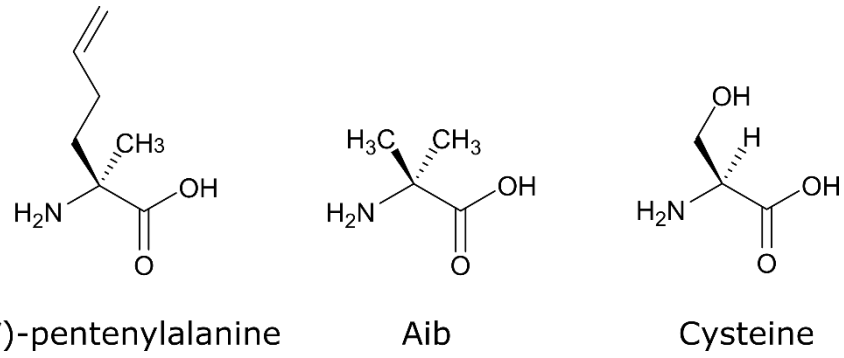


**Figure 4.17. Structures of di-substituted amino acids.** (*S*)-pentenylalanine and Aib contain an additional methyl group at the alpha carbon when compared to the proteinogenic amino acids. The structure of Cysteine is shown for comparison.

## 4.7 Discussion

An effective method was developed for producing recombinant peptides using cysteine cross-linking chemistry with a dibromo-*m*-xylene linker, resulting in the production of peptides that can bind to Ral proteins and inhibit Ral-effector interactions *in vitro*.

Initial attempts to produce the peptides as soluble GB1 fusions encountered problems, as the unstructured sequence was very susceptible to proteolysis and the peptide sequence was not intact for long enough to purify the GB1-peptide fusion. Switching to the modified pET31b vector, which generates a KSI-peptide fusion circumvented these issues by directing the peptide fusions to inclusion bodies where they are protected from proteases. This approach resulted in high yields of the fusion product that could be purified from the inclusion bodies.

Reaction of the KSI-peptide fusion protein with dibromo-*m*-xylene resulted in complete cysteine cross-linking at the desired sites, with no side products observed. It would be possible to form intermolecular cross-links between peptides or to add multiple dibromo-*m*-xylene cross-linkers to a single peptide, however the reaction conditions followed had been previously optimized to reduce the possibility of these side reactions occurring (206). Keeping the concentration of the KSI-peptide fusion relatively low (< 1 mM) meant that intramolecular bond formation was far more likely to occur than cross-linking between peptides. Additionally, using the cross-linker at only three equivalents in excess meant that the chance of forming doubly-substituted peptides was low, while keeping the linker concentration high enough that the reaction can still occur in a relatively short time frame. While the literature

has shown that the reaction goes to completion within an hour (206), longer incubations were used here to ensure that the reaction had gone to completion, as the MALDI-MS analysis to check stapling was not performed until after the subsequent hydrolysis reaction to release the peptides.

The pET31b vector encodes for methionine residues at either end of the peptide cloning site for cleavage using cyanogen bromide (CNBr). Due to safety concerns using this reagent, labile Asp-Pro bonds were employed here, before and between the peptide sequences, for cleavage in dilute acid. The acid hydrolysis was found to be highly effective, as very little intact fusion protein was present after the five-hour incubation, however some very low amounts of incomplete hydrolysis products were observed. Regardless, the majority of peptides were cleaved in this timescale and this method can be carried out on the benchtop, in contrast to the CNBr method which requires a fumehood and specialist safety training, making this a far preferable alternative. The cleaved peptides were isolated at high purity using $Ni^{2+}$-NTA affinity followed by size exclusion chromatography.

Modification with dibromo-*m*-xylene only induced very low levels of helicity in the peptides, as indicated by circular dichroism analysis (see section 4.6). The resulting peptides displayed a mostly random coil signature with an estimated 22% helicity, while the same sequences produced synthetically with an all-hydrocarbon staple exhibited much greater levels of helicity (~ 44% for HLR-sol). This loss of helicity may explain the drop in affinity for Ral GTPases in the *in vitro* binding experiments (section 4.4), as several sources have reported a positive correlation between peptide helical content and binding affinity (145, 151), due to a decreased entropic cost on binding. Many other helix stabilization chemistries involving thiol-reactive linkers have been identified (135) and could be investigated to produce more helical peptides using recombinant production.

The cysteine cross-linked peptide, csHLR, was not able to inhibit Ral complexes in a mammalian cell lysate at the concentrations tested (section 4.5), which was likely due to their reduced affinity for Ral proteins. To progress this project, it was therefore decided to move forwards with the all-hydrocarbon stapled peptides. Despite this, the robust method developed here to produce peptides from *E. coli* has been established as a lab resource and has already been useful in progressing other peptide projects.

# 5 Conclusions and future directions

## 5.1 Conclusions

The overarching aim of this project was to improve the properties of a lead stapled peptide based on RLIP76 to target the Ral GTPases. Specifically the project aimed to: identify sequence changes within RLIP76 that can improve affinity for Ral proteins (Chapter 2); to use those sequences to generate stapled peptides with higher affinity for Ral proteins (Chapter 3); to measure the activity of the peptides, using biochemical and biophysical assays to determine their binding affinities and ability to disrupt Ral-effector interactions (Chapter 3); and finally, to assess whether the peptides can enter mammalian cells and disrupt Ral signalling (Chapter 3). In addition to the primary goals, a method to produce constrained helical peptides using a recombinant system was also developed as part of this work (Chapter 4).

These aims have been addressed and discussed in detail within Chapters 2-4. Chapter 2 described how sequence substitutions within the RLIP76 RBD that can increase the affinity for Ral proteins were identified using CIS display and how the effect of the substitutions on the binding affinity was rigorously analyzed using multiple *in vitro* assays. X-ray crystal structures of the mutants revealed the interactions responsible for high affinity binding. Work detailed in Chapter 3 aimed to transfer the sequence substitutions identified in Chapter 2 to the lead stapled peptide targeting the Ral proteins. Investigations using these peptides revealed unexpected problems with non-specific binding, however the peptides were successfully redesigned to improve their solubility and selectivity for the Ral GTPases. Affinities of these second-generation peptides for Ral GTPases were measured and their binding site on RalB was determined by NMR. CPPs were appended to the peptides to study their effects in mammalian cells: the resulting peptides were able to enter cells and disrupt Ral-effector interactions. Chapter 4 described an effective system for the recombinant production of peptides that were cross-linked at cysteine residues.

This project has achieved its primary goal of using the RLIP76 RBD as a model to improve the properties of stapled peptides targeting the Ral GTPases. The RBD was used to interrogate vast numbers of possible sequences, the best of which were successfully transferred into stapled peptides with greatly improved affinity for Ral proteins. Modifications to the peptide

sequence to improve the physical properties without affecting binding were guided by the structure of the RLIP76 RBD in complex with RalB, resulting in the design of peptides with far superior solubility and selectivity compared to the previous lead peptide. For the peptides to form the basis for an effective therapeutic however, their activity and cell-penetrating properties will still need to be improved: further investigations that could be carried out to address these issues are described in the following sections.

## 5.2 Future directions

### 5.2.1 Further improving the peptide activity

The peptides produced in this work displayed modest affinity for the Ral proteins, albeit with excellent selectivity. As discussed in Chapter 2, their activity could be improved by maturing the peptides into covalent inhibitors or PROTACs. A reactive tyrosine residue is available on the surface of the Ral proteins, which lies close to the peptide binding site, therefore installation of an electrophilic warhead, such as those identified by Meroueh and colleagues (122), on this face of the peptide could transform the peptides into covalent inhibitors. This approach would allow for effective inhibition without the requirement for nano- and picomolar binding affinities, as the binding event would need only to occur once, with the covalent modification that ensued then allowing the effect to be sustained.

Effective PROTACs have also been developed using inhibitors with micromolar affinities for their target protein (214). Their mechanism of action involves catalytic degradation of the target protein rather than requiring sustained engagement, enabling the PROTAC to be effective at sub-stoichiometric quantities (204). For an efficient PROTAC to be developed, target selectivity is critical to avoid off-target effects. The peptides developed in this work are highly selective for active Ral proteins and therefore their activity may be enhanced using a PROTAC approach.

### 5.2.2 Improving cellular permeability

The previous lead peptide (SP1) displayed cellular permeability, however once the changes described in Chapter 3 were applied to improve the selectivity and solubility of the peptides,

it was no longer cell-permeable. This is likely due to the addition of two Glu-Lys salt bridges on the back face of the peptide. These salt bridges replaced hydrophobic residues and it has been shown previously that hydrophobic stapled peptides and those with an amphipathic helix enter cells more effectively (138, 164). It could be valuable to try more combinations of residues on the back face of the peptides to see whether the cellular penetration could be improved while maintaining solubility. For example, a single Glu-Lys salt bridge or substitution with small polar residues could be investigated.

It was shown in Chapter 2 that appending an octa-Arg CPP to the peptides allowed the peptides to be transported to the cytosol of mammalian cells, however only two CPP sequences were assessed as part of this study. It would therefore be useful to test other CPP sequences to see whether higher levels of the current peptides could be transported into the cell. A helical CPP such as penetratin (166) may additionally be able to improve the peptide affinity through stabilization of the helical secondary structure.

### 5.2.3 Coiled-coil peptides based on the RLIP76 RBD

The stapled peptides discussed in Chapter 2 were based on the α2 helix of the RLIP76 RBD. As discussed in Chapter 2, the α1 helix of the RBD also contains key residues for binding to Ral proteins, therefore a peptide including these residues may have a much greater affinity for the Ral proteins. All of the key contacts made by the RLIP76 RBD are contained within residues 409-440, spanning both helices of the coiled-coil. Arora and colleagues have made good progress in stabilizing miniature coiled-coils with as few as nine residues per helix (215, 216): this approach could be used to produce coiled-coil peptides spanning residues 409-440 to establish a minimal, higher affinity binding sequence.

### 5.2.4 Identification Ral-binding peptides from a naïve selection

As discussed in the previous section, it became apparent throughout this work that the α1 helix of the RLIP76 RBD plays a very important role in binding to the Ral proteins. In order to include the critical residues of this helix, the resulting peptides may need to be much larger:

this would be unfavourable for a therapeutic peptide, as longer sequences are more prone to degradation and are less likely to be made cell-penetrant.

An alternative approach would be to carry out a peptide selection using a naïve library. Selection libraries encoding cyclic peptides have been very successful in producing high affinity ligands for a range of protein targets, including the small GTPases K-Ras, Cdc42 and Rac1 (42, 198, 217), suggesting that this approach could also be used to generate a high-affinity peptide targeting the Ral GTPases.

### 5.3 Implications for therapeutic targeting of small GTPases

Intense efforts to inhibit Ras signalling over the last three decades have shown that these proteins are incredibly challenging to target therapeutically. The Ras proteins are by far the most targeted GTPases to date, yet these archetypal G proteins share many common features with the entire Ras superfamily. Hence, any insights into targeting Ras could be translated to generate inhibitors for a wide range of small GTPases, many of which constitute key targets in a plethora of diseases.

Many attempts have been made to generate small molecules to target K-Ras (reviewed in (218)), however the features of Ras proteins described in Chapter 1 including their smooth surfaces and picomolar affinities for their nucleotide have eluded the identification of effective small molecule inhibitors. There are also concerns regarding toxicity when targeting K-Ras directly, as K-Ras has been shown to be an essential gene in mice (219) and is a master regulator of numerous signalling pathways. As such, it is desirable that any inhibitor should target only the mutated form of K-Ras.

The development of K-RasG12C-specific covalent inhibitors represents a huge leap forward in the direct targeting of Ras proteins. These inhibitors occupy a novel binding pocket close to the switches that is only present in the GDP-bound form of the protein (50). However, the approach is not likely to be translatable for other Ras mutant forms or other small GTPases. The G12C mutant is unusual in that it is able to cycle between GDP and GTP: most commonly-occurring Ras mutations result in impaired intrinsic and GAP-mediated nucleotide hydrolysis, leaving the proteins in a constitutively-activated GTP-bound state where the pocket identified

by Shokat and colleagues would not be accessible. In contrast, the G12D mutant has shown to have an elevated nucleotide exchange rate compared to wild-type Ras (220), meaning that the GDP-bound state is short-lived and is therefore also not expected to be targetable via this pocket. Additionally, this approach requires a reactive cysteine residue to be present close to the desired site of inhibition, which is not the case for any other Ras mutants, or most other small GTPases.

A group at Takeda have successfully used a phage display library of peptides to identify peptide inhibitors with selectivity for the K-RasG12D mutant (42). This mutation accounts for a third of all K-Ras mutations (COSMIC) and is therefore a highly desirable target. Their lead cyclic peptide, KRpep-2d displayed around 25-fold selectivity for the G12D mutant over wild-type K-Ras. The large surface area occupied by peptides compared to small molecules enables exquisite target selectivity, allowing for mutant-specific inhibition. It is interesting to note that from the random library used for phage display, the three main consensus sequences of the peptides identified all contained two cysteine residues, resulting in cyclization of the peptide products. Indeed, addition of DTT to reduce the disulphide bond resulted in a loss of the peptide activity. Macrocycles can have superior binding affinities over linear peptides due to a reduced entropic cost on binding, therefore it is often beneficial to design a peptide library to include cyclization of all sequences (127); this approach has been used successfully to generate cyclic peptides with nanomolar affinities for Cdc42 (198), another small GTPase. Their rigid structures can also result in improved proteolytic stability and several cell-permeable macrocycles exist in nature, albeit with additional modifications including N-methylation required for cell permeability (221).

The RalGEF-Ral effector pathway downstream of Ras offers a promising avenue for targeting Ras-driven cancers, as inhibition of this pathway circumvents the need for a mutant-specific inhibitor. It has been shown that certain cancers become reliant on the Ral pathway for survival, while non-transformed cells are not (115). Despite growing evidence of a reliance on Ral signalling for tumour cell survival and metastasis, this pathway has been understudied to date (77). Early studies in murine cells demonstrated the importance of the MAPK and PI3K pathways downstream of Ras for cancer progression and survival, while it was not until Counter *et al.* performed similar studies in human cells that the importance of the Ral pathway became apparent (112). However the prevalence of mutations in BRaf (18%,

COSMIC) and PI3K (12%, COSMIC) in human cancers also clearly demonstrates that these proteins and their pathways are important cancer targets in their own right, while mutations in the RalGEF-Ral pathway are relatively rare.

As the importance of the Ral pathway comes into focus, more attempts should be made to generate inhibitors for this pathway. Several of the approaches that have been attempted for Ras proteins could prove to be valuable for the inhibition of Ral proteins. For example, early attempts to inhibit Ras membrane-association with farnesyl transferase inhibitors (FTIs) failed due to a compensatory prenylation by GGTase I (33). Ral proteins are normally modified by GGTase I and cannot undergo alternative prenylation in the presence of GGTIs, leading to their mislocalization (117). The first GGTI to enter clinical trials had no toxicity issues in Phase I, however the drug was shown to be rapidly eliminated and was not progressed to Phase II (124). Further progress with GGTase I inhibitors could prove efficacious in Ral inhibition.

As discussed in Chapter 1, peptides based on a helical portion of SOS1 have been developed to inhibit SOS1-mediated nucleotide exchange of Ras proteins. Patgiri *et al.* used a hydrogen bond surrogate approach to stabilize a helical conformation of residues 929-944 of SOS1 (222): their peptide bound weakly to Ras·GDP with a $K_d$ of 160 µM. SOS1 makes significant contacts with Ras proteins other than those contained within residues 929-944 (Figure 5.1A), therefore a peptide based solely on this region is unlikely to achieve an affinity comparable to SOS1. The same is likely true for a peptide based on a RalGEF, as the RalA/Rgl2 structure revealed a very similar mode of interaction to the Ras/SOS1 structure (Figure 5.1B) (223). In Chapters 2 and 3 it was shown that both helices of the RLIP76 RBD were important for Ral-binding and that a sequence based solely on one helix exhibited a great reduction in affinity compared to the coiled-coil domain (~200-fold). In instances where the interaction interface extends much further than a single helix, a selection using naïve cyclic peptide libraries may be more appropriate to identify high affinity binders, rather than attempting to make improvements to a low-affinity template.

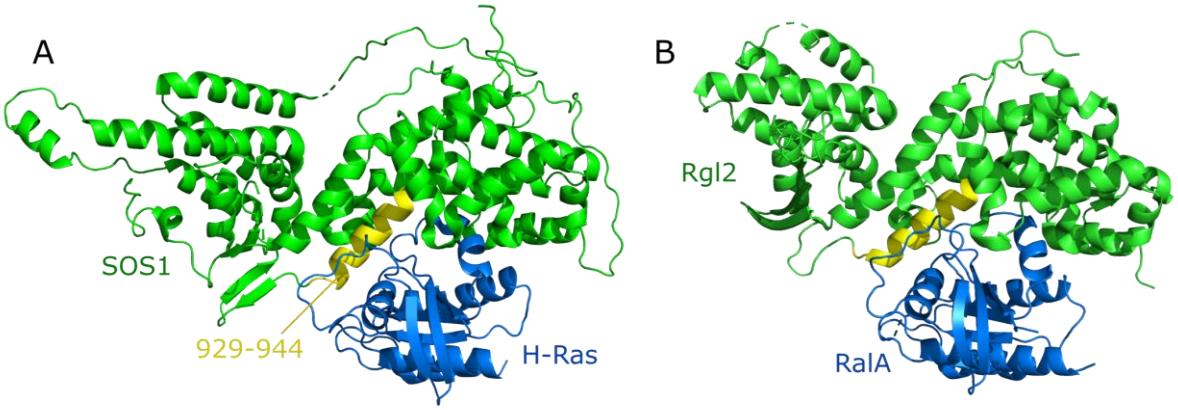


**Figure 5.1. Peptides to inhibit GTPase/GEF interactions.** The H-Ras/SOS1 (**A**, PDB ID: 1NVW) and RalA/Rgl2 (**B**, PDB ID: 5CM8) complex structures are shown. The GTPases are shown in blue and the GEFs are shown in green. Residues 929-944 of SOS1 that have formed the basis for inhibitory peptides are shown in yellow. The equivalent helix in Rgl2 (residues 431-447) is also shown in yellow.

In contrast, helical peptides based on p53 that mimic the Mdm2/Mdmx-binding helix have been very successful (section 1.9.2.1) (147–151). The p53 helix sequence binds Mdm2 with a $K_d$ of 410 nM (149) and addition of a hydrocarbon staple further improved this affinity. This demonstrates that interactions that are primarily made through a single helix can be an excellent starting point for stapled peptide inhibitors. Structural information on the complexes is an invaluable tool for the design of such peptides and information on the energetic contributions made by individual residues would also be very beneficial to assist the design of peptides based on native binding partners. This approach has also been used successfully to target a small GTPase, Rab25, using stapled peptides encompassing all interacting residues of the binding partners FIP1 and FIP3, which exhibited nanomolar affinities for Rab25 (224).

Peptide selections involving vast libraries of sequences (up to $10^{14}$) can now be used to generate high affinity ligands for almost any protein of interest. However, target affinity is not the only requirement for a therapeutic molecule: peptides must be resistant to proteases, be selective for the target and be able to cross the cell membrane if they are to be used for intracellular targets. While the rule of five has long been used as a tool for the design of orally bioavailable small molecules, no such rule book currently exists for peptides. As such, blunt tools including CPPs have been relied upon for the transport of peptides into cells. While there is not one strategy that can be applied to deliver all peptides into cells, there has been

remarkable success with individual peptides including the hydrocarbon-stapled p53 helices. ALRN-6924 is intrinsically cell-penetrant, a feature which has been attributed to the stapling method used in its production and is currently in Phase II trials (153, 154). The Pei group have designed cell-permeable cyclic scaffolds which form the basis for synthetic selection libraries (49). As discussed in Chapter 1, our understanding of the cell-penetrating properties of peptides continues to improve and with it so does the utility of peptides as therapeutic molecules. The growing number of peptides entering clinical trials suggests that effective inhibition of Ras and other small GTPases is soon to be realised.

## 5.4 Final remarks

As discussed in Chapter 1, the Ral GTPases are challenging drug targets and there are currently no well-validated Ral inhibitors that can be used to study Ral activity or to be used as a treatment for Ras-mutant cancers. Given the prevalence of Ras mutations in human cancer, blockades of Ras signalling are desperately needed and inhibition of the Ral proteins offers a promising avenue that has not yet been sufficiently investigated. Through this work, progress has been made towards establishing a tool for the inhibition of Ral proteins. The insights gained here for the design of peptides based on a native binding partner can also be applied to the inhibition of other small GTPases, many of which interact with helical effectors (13), representing key targets in a wide range of diseases.

# 6 Materials and methods

## 6.1 Materials

### 6.1.1 Chemicals

General chemicals were obtained from Sigma-Aldrich, Melford laboratories, ThermoFisher, VWR, Formedium, New England Biolabs, Agilent and Cytiva. $^{15}$N-Ammonium Chloride (98%) was obtained from Sigma-Aldrich.

### 6.1.2 Commercial enzymes

Restriction enzymes were obtained from New England BioLabs, restriction grade Thrombin from Merck and T4 DNA Ligase and Calf intestinal Alkaline Phosphatase from Sigma-Aldrich.

### 6.1.3 Expression vectors

*Table 6.1. Vectors used for recombinant protein expression.*

| Vector | Fusion tag | Protease cleavage site | Antibiotic resistance | Source |
|---|---|---|---|---|
| pGEX-HisP | GST (N)<br>$His_6$ (C) | HRV-3C | Amp | D. Owen *et al.* (225) |
| pGEX2T | GST (N) | Thrombin | Amp | Cytiva |
| pMAT10 | $His_6$-MBP (N) | Thrombin | Amp | M. Hyvönen *et al.* (226) |
| pET16b | $His_{10}$ (N) | Factor Xa | Amp | Novagen |
| pET31b | KSI (N)<br>$His_6$ (C) | N/A - Asp-Pro for acid hydrolysis | Amp | Novagen |
| pOP5BP | $His_8$-GB1 (N)<br>AviTag (C) | HRV-3C | Amp | M. Hyvönen, unpublished |

*Table 6.2. Vectors for expression in mammalian cells.*

| Vector | Fusion tag | Antibiotic resistance | Source |
|---|---|---|---|
| pDEST 12.2 | Flag (N) | Amp | ThermoFisher |
| pcDNA3.1/nV5-DEST | V5 (N) | Amp | ThermoFisher |
| pXJ-GFP | - | Amp | E. Manser, unpublished |

### 6.1.4 Expression constructs

*Table 6.3. Constructs for expression in mammalian cells.*

| Protein | Gene source | Residues | Mutations | Vector |
|---|---|---|---|---|
| RLIP76 | Human | 1-655 | - | pDEST 12.1 |
| RalB | Human | 1-206 | Q72L | pcDNA3.1/nV5-DEST |

*Table 6.4. Expression constructs for recombinant protein production.*

| Protein | Gene source | Residues | Mutations | Vector |
|---|---|---|---|---|
| RalA | Simian | 1-184 | - | pMAT10 |
| | | | Q72L | |
| RalB | Human | 1-185 | Q72L | pMAT10 |
| | | | | pET16b |
| RhoA | Human | 1-186 | F25N, Q63L | pGEX2T |
| Cdc42 | Human | 1-184 | Q61L | pGEX2T |
| RLIP76 | Human | RBD: 393-446 | C411S | pGEX-HisP |
| | | | C411S, Q433L | |
| | | | C411S, E427H, Q433L | |
| | | | C411S, E427H, Q433L, K440R | |
| | | | C411S, E427H, K440R | |
| | | | C411S, Q433L, K440R | |
| | | | C411S, E426W, E427D, L429A, Q433S, R434Q, T437S, K440R | |
| | | | C411S, E426L, E427T, Q433T, R434L, T437R | |
| | | | The following constructs contain a stop codon before the C-terminal His-tag: | |
| | | | C411S | |
| | | | C411S, E427H, Q433L, K440R | |
| | | | C411S, E427S, L429M, Q433L, K440R | |
| | | | C411S, E427D, L429V, Q433L, K440R | |
| | | | C411S, E426N, Q433T, K440R | |
| | | | C411S, E426S, E427D, Q433T | |
| | | | C411S, E426L, E427T, L429H, Q433T, R434L, T437K, K440P | |
| | | | C411S, E426W, E427D, L429A, Q433S, R434Q, T437S, K440R | |
| | | | C411S, E426W, E427D, L429A, Q433S, R434T, T437A, K440Y | |
| | | | C411S, E426W, E427N, L429A, Q433S, R434E, T437L, K440R | |
| | | | C411S, L409A, H413A | |
| | | | C411S, L409A, H413A, E427H, Q433L, K440R | |

### 6.1.5 Bacterial strains

*Table 6.5. Bacterial strains used in this work.*

| Strain | Genotype | Phenotype | Resistance |
|---|---|---|---|
| BL21 (Invitrogen) | F⁻ *ompT hsd*$S_B$ ($r_B^-$, $m_B^-$) | Deficient in Lon and OmpT proteases | None |
| BL21(DE3) (Invitrogen) | F⁻ *ompT hsd*$S_B$ ($r_B^-$, $m_B^-$) *gal dcm* (DE3) | Derived from BL21. Contain a λ prophage carrying the T7 RNA polymerase gene and $lacI^q$ | None |
| BL21(DE3) pBirA (Amid Biosciences) | F⁻ *ompT hsd*$S_B$ ($r_B^-$, $m_B^-$) *gal dcm* (DE3) ΔhsdS pBirA($Str^R$) | As BL21(DE3). Contains an IPTG-inducible BirA expression plasmid for biotinylation of Avi-tagged proteins. | Cam |
| XL1-Blue (Agilent) | *recA1 endA1 gyrA96 thi-1 hsdR17 supE44 relA1 lac* [F´ *proAB* $lacI^q$ *ZΔM15* Tn*10* ($Tet^r$)] | The $lacI^q$ *ZΔM15* gene on the F´ episome allows blue-white screening for recombinant plasmids. | Tet |
| XL10 Gold (Agilent) | *TetrD(mcrA)183 D(mcrCB-hsdSMR-mrr)173 endA1 supE44 thi-1 recA1 gyrA96 relA1 lac Hte* [F´ *proAB* $lacI^q$ *ZΔM15* Tn*10* ($Tet^r$) Amy $Cam^r$]. | The $lacI^q$ *ZΔM15* gene on the F´ episome allows blue-white screening for recombinant plasmids. The strain is deficient in endonuclease A and recombination and all known restriction systems. | Tet, Cam |

### 6.1.6 Antibodies

*Table 6.6. Antibodies used in this work.*

| **Western blotting** | |
|---|---|
| **Antibody (dilution)** | **Product no.** |
| V5-HRP (1:5000) | R961-25 (Invitrogen) |
| Flag-HRP (1:5000) | A8592 (Sigma) |
| His-HRP (1:5000) | sc-8036 HRP (Santa Cruz) |
| Sec5 (1:5000) | ab140620 (Abcam) |
| Goat anti-mouse HRP (1:5000) | GTXMU-DHRPX (Newmarket Scientific) |
| Goat anti-rabbit HRP (1:5000) | GTXRB-DHRPX (Newmarket Scientific) |
| **Co-immunoprecipitation** | |
| **Antibody** | **Product no.** |
| V5 | R960-25 (Invitrogen) |
| **SPAs** | |
| **Antibody** | **Product no.** |
| anti-polyhistidine | H1029 (Sigma) |
| anti-GST | G7781 (Sigma) |

### 6.1.7 Synthetic peptides

The peptides described in section 3.2 were purchased from Eurogentec. The remaining peptides used in this work were produced as described in section 6.2.7.

### 6.1.8 Antibiotic working concentrations

Antibiotics used in this work were prepared at the following concentrations (*Table 6.7*).

*Table 6.7. Preparation of antibiotic solutions.*

| **Antibiotic** | **Working concentration** |
|---|---|
| Ampicillin (Amp) | 100 µg/mL |
| Chloramphenicol (Cam) | 20 µg/mL |
| Tetracycline (Tet) | 10 µg/mL |
| Kanamycin (Kan) | 25 µg/mL |

## 6.2 Methods

### 6.2.1 General methods

#### 6.2.1.1 SDS-PAGE

*Table 6.8. Buffers for SDS-PAGE electrophoresis.*

| Name | Composition |
|---|---|
| Buffer I | 1.5 M Tris-HCl pH 8.8 |
| Buffer II | 0.5 M Tris-HCl pH 6.8 |
| 2x SDS sample buffer | 6.7% SDS, 6 M Urea, 33 mM Tris-HCl pH 7.4, 0.066 M β-mercaptoethanol, bromophenol blue |
| 5x Tris-glycine running buffer | 0.125 M Tris-HCl, 0.96 M glycine, 0.05% SDS |
| 10x Tricine running buffer | 1 M Trizma base, 1 M tricine, SDS (1%) |

*Table 6.9. Laemmli gels.*

| Reagent | 10% separating gel (µL) | 12% separating gel (µL) | 15% separating gel (µL) | 18% Separating gel (µL) | Stacking gel (µL) |
|---|---|---|---|---|---|
| Buffer I | 1500 | 1500 | 1500 | 1500 | - |
| Buffer II | - | - | - | - | 500 |
| 30% acrylamide:bisacrylamide (29:1) | 2000 | 2400 | 3000 | 3600 | 250 |
| MQ $H_2O$ | 2400 | 2000 | 1400 | 800 | 1200 |
| 10% SDS | 60 | 60 | 60 | 60 | 20 |
| 10% ammonium persulphate | 48 | 48 | 48 | 48 | 40 |
| TEMED | 6 | 6 | 6 | 6 | 2 |

SDS-PAGE gels were prepared using the reagent quantities listed in Table 6.9. Samples were mixed with an equivalent volume of 2x SDS sample buffer (Table 6.8), heated at 95 °C for 3 min and centrifuged before loading onto the gel. Gels were run in 1x Tris-glycine running buffer (Table 6.8) at 200 V for 55 min and stained using InstantBlue (Expedeon).

#### 6.2.1.2 Tricine gel electrophoresis

*Table 6.10. 14% Tris-tricine gels.*

| Reagent | 14% separating gel (µL) | Stacking gel (µL) |
|---|---|---|
| 3M Tris-HCl pH 8.45, 0.3% SDS | 2000 | 1330 |
| 50% glycerol | 1200 | - |
| 30% acrylamide:bisacrylamide (29:1) | 2800 | 530 |
| MQ | - | 2100 |
| 10% ammonium persulphate | 48 | 80 |
| TEMED | 6 | 4 |

14% Tricine gels were prepared using the reagent quantities listed in Table 6.10. Samples were prepared as in section 6.2.1.1. Gels were run in 1x tricine running buffer (Table 6.8) at 125 V for 90 min and stained with InstantBlue (Expedeon).

#### 6.2.1.3 Agarose gel electrophoresis

*Table 6.11. Reagents for agarose gel electrophoresis.*

| Name | Composition |
|---|---|
| 50x TAE Buffer | 2 M Tris-base, 5% Acetic acid, 50 mM EDTA, pH 8.0 |
| 5x STOP Buffer | 50% sucrose, 50 mM EDTA pH 7.5, 0.1% Bromophenol blue |

Agarose gels were prepared using TAE buffer (Table 6.11) with ethidium bromide (0.5 µg/mL) at the desired percentage (1-2%). DNA samples were prepared in 5x STOP buffer (Table 6.11). Gels were run in TAE buffer with ethidium bromide (0.5 µg/mL) at 80 V until the desired separation was achieved.

#### 6.2.1.4 Preparation of *E. coli* chemically competent cells

*Table 6.12. Reagents for bacterial cell growth.*

| Name | Composition |
|---|---|
| 2TY | 16 g tryptone, 10 g yeast extract, 5 g NaCl ($L^{-1}$) |
| Agar plates | 16 g tryptone, 10 g yeast extract, 5 g NaCl, 16 g Agar ($L^{-1}$) |
| M9 minimal media | 47 mM $Na_2HPO_4$, 22 mM $KH_2PO_4$, 8.6 mM NaCl, 4 µM $ZnSO_4$,1 pM $MnSO_4$, 0.7 µM $H_3BO_4$,0.7 µM $CuSO_4$, 0.4% (w/v) glucose, 2 nM $FeCl_3$, 2 µM $MgSO_4$, 20 mM $NH_4Cl$, 0.1 µM $CaCl_2$ |

Cultures of *E. coli* were grown at 37 °C with shaking overnight. To 100 mL 2TY (Table 6.12), 0.5 – 1.0 mL overnight culture was added and incubated at 37 °C with shaking until $A_{600}$ of 0.4 was reached. Cultures were incubated on ice for 5 min and pelleted by centrifugation at 2,000 x g for 5 min at 4 °C prior to resuspension in 25 mL cold $MgCl_2$ (100 mM). Samples were centrifuged as before, resuspended in 5 mL cold $CaCl_2$ (100 mM) and incubated on ice for 90 min. Cells were pelleted once more and resuspended in 1 mL cold 85 mM $CaCl_2$ with 17% glycerol. Competent cells were flash frozen on dry ice in 100 µL aliquots and stored at -80 °C.

#### 6.2.1.5 DNA purification

Plasmid purifications from *E.coli* were performed using a GenElute Plasmid Miniprep Kit (Sigma-Aldrich) following the manufacturer's instructions.

#### 6.2.1.6 Transformations into chemically competent *E. coli*

100-200 ng plasmid DNA was added to 50 µL thawed competent cells and incubated on ice for 5 min. The cells were heat shocked in a pre-warmed waterbath at 42 °C for 45 s, followed by incubation on ice for 2 min. 2TY (350 µL) was added to the cells before incubation at 37 °C for 1 h. Cells were plated on 2TY agar plates containing the appropriate antibiotic(s) and incubated at 37 °C for at least 16 h.

### 6.2.2 Cloning of peptide sequences

#### 6.2.2.1 Peptide insert construction

Overlapping oligonucleotides (Sigma) were prepared at 100 ng $\mu L^{-1}$ in sterile analytical water (SAW). 10 µL of each oligonucleotide was added to an Eppendorf and heated to 100 °C for 5 min before being cooled slowly by turning off the heat block. This mixture was diluted to 1 ng/µL in SAW. The inserts listed in Table 6.13 were constructed using this method.

*Table 6.13. Peptide inserts constructed using complementary oligos.*

| Construct name | Vector | Restriction sites | Insert sequence | Oligonucleotides[a] |
|---|---|---|---|---|
| pOP5BP-peptide | pOP5BP | *Bam*HI *Xho*I | LCKEHCLWEVLRILTALRRKLREA | Forward- pGATCCCTGTGCAAAGAACACTGCCTGTGGGAAGTTCTGCGTATCCTGACCGCGCTGCGTCGTAAACTGCGTGAAGCC Reverse - pTCGAGGCTTCACGCAGTTTACGACGCAGCGCGGTCAGGATACGCAGAACTTCCCACAGGCAGTGTTCTTTGCACAGG |
| pET31b-peptide | pET31b | *Alw*NI | DPLCKEHCLWEVLRILTALRRKLREA | Forward- pCTGGATCCGCTGTGCAAAGAACACTGCCTGTGGGAAGTTCTGCGTATCCTGACCGCGCTGCGTCGTAAACTGCGTGAAGCGCAGATG Reverse- pCTGCGCTTCACGCAGTTTACGACGCAGCGCGGTCAGGATACGCAGAACTTCCCACAGGCAGTGTTCTTTGCACAGCGGATCCAGCAT |
| pET31b-double peptide | pET31b | *Alw*NI | DPLCKEHCLWEVLRILTALRRKLREADPLCKEHCLWEVLRILTALRRKLRE | F1 - pGATCCGCTCTGCAAAGAGCAC F2 - TGCCTGTGGGAGGTTCTCCGCATCCTCACCGCGCTCCGTCGTAAA F3 - CTGCGCGAAGCGGACCCGCTGTGCAAGGAACATTGCCTCTGGGAA F4 - GTTCTGCGTATCCTGACGGCGCTGCGCCGTAAGCTGCGTGAGATG R1 - pCTCACGCAGCTTACGGCGCAG R2 - CGCCGTCAGGATACGCAGAACTTCCCAGAGGCAATGTTCCTTGCA R3 - CAGCGGGTCCGCTTCGCGCAGTTTACGACGGAGCGCGGTGAGGAT R4 - GCGGAGAACCTCCCACAGGCAGTGCTCTTTGCAGAGCGGATCCAT |

[a] Sequences complementary to the overhangs generated by digestion of the vector are shown in red. The Asp-Pro motif added for cleavage with acid is underlined.

#### 6.2.2.2 Vector preparation

The vector (5 µg) was digested with *AIw*NI (50 units, pET31b) or *Bam*HI and *Xho*I (100 units each, pOP5BP) in CutSmart buffer in a total reaction volume of 100 µL made up with SAW. The digest was incubated at 37 °C for 4 h. 10 µL of the digest was resolved using agarose gel electrophoresis (section 6.2.1.3) to confirm that the digestion was successful.

Tris-HCl pH 8.0 (100 mM), $MgCl_2$ (10 mM), alkaline phosphatase (5 units) and SAW to give a final volume of 150 µL were added to the digestion mixture and incubated at 37 °C for 45 min, then at 65 °C for 20 min.

#### 6.2.2.3 Ligation

The alkaline phosphatase-treated vector (60 ng) was combined with the peptide insert in 1:2 and 1:5 molar ratios, with 10x ligase buffer (2 µL) and T4 ligase (1 unit) in a total reaction volume of 20 µL. The ligation mixture was centrifuged briefly and incubated at 16 °C overnight. The entire ligation reaction was transformed into competent *E.coli* XL1 cells and plated on 2TY Agar plates containing the appropriate selective antibiotics.

#### 6.2.2.4 Analysis of colonies

Colonies obtained from transforming the ligation mixture were grown overnight and the DNA extracted. Test digests were carried out with *Bam*HI/*Xho*I (pOP5BP) or *Nde*I/*Xho*I (pET31b) in the following quantities: 16 µL miniprep DNA, 2 µL CutSmart buffer (10X), 20 units each restriction enzyme. Digestion mixtures were incubated at 37 °C for 1-3 h and the analysed using agarose gel electrophoresis (section 6.2.1.3) to check for an insert of the appropriate size. Positive colonies were confirmed by sequencing (Department of Biochemistry, DNA sequencing facility).

### 6.2.3 Site-directed mutagenesis

Site-directed mutagenesis was performed using a QuikChange Lightning Multi site-directed mutagenesis kit (Agilent). Reaction mixtures were set up following manufacturer's instructions. The cycling parameters used are listed in Table 6.14.

*Table 6.14. Mutagenesis cycling parameters.*

| Stage | Temperature (°C) | Time (min) |
|---|---|---|
| Denaturation | 95 | 2:00 |
| Annealing and extension (repeat x 30) | 95 | 0:20 |
| | 55 | 0:30 |
| | 65 | 0:30 per kb of template |
| Final extension | 65 | 5:00 |
| Final hold | 4 | hold |

*Dpn*1 (20 units) was added to PCR reaction mixtures and incubated at 37 °C for 1 h. 1.5 µL of digested DNA was transformed into an aliquot of chemically competent XL10 GOLD cells following manufacturer's instructions. Plasmids were sequenced (Department of Biochemistry, DNA sequencing facility) to check for successful mutagenesis.

The constructs listed in Table 6.15 were available in the lab and acted as templates for site-directed mutagenesis, and the constructs listed in Table 6.16 were prepared by site-directed mutagenesis.

*Table 6.15. RLIP76 RBD expression constructs available in the lab.*

| Protein | Cloning sites | Construct name | Mutations |
|---|---|---|---|
| RLIP76 RBD 393-446 in pGEX-HisP | *Bam*HI, *Xho*I | Wild-type -His | C411S |
| | | LTTLRP -His | C411S, E426L, E427T, Q433T, R434L, T437R, K440P |
| | | LR -His | C411S, Q433L, K440R |
| | | WDASR -His | C411S, E426W, E427D, L429A, Q433S, K440R |

*Table 6.16. Constructs prepared by site-directed mutagenesis.*

| **RLIP76 RBD His-tagged constructs** | | | |
|---|---|---|---|
| **Construct name** | **Mutations** | **Template** | **Primer[a]** |
| L -His | C411S, Q433L | LR -His | CTGAGAATTTTGACAGCCCTCAAAAGAAAACTGAGAGAAGC |
| HL -His | C411S, E427H, Q433L | HLR -His | |
| HLR -His | C411S, E427H, Q433L, K440R | LR -His | GGATTTGTCTAAAGAACATAGATTATGGGAAGTACTGAG |
| HR -His | C411S, E427H, K440R | HLR -His | CATAGATTATGGGAAGTACAAAGAATTTTGACAGCCCTC |
| WDASQSR -His | C411S, E426W, E427D, L429A, Q433S, R434Q, T437S, K440R | WDASR -His | GGGACAGAGCATGGGAAGTATCACAAATTTTGTCAGCCCTCCGC |
| LTTLRK -His | C411S, E426L, E427T, Q433T, R434L, T437R | LTTLRP -His | GATTTTGCGCGCCCTCAAAAGAAAACTGAGAGAAGC |
| **RLIP76 RBDs with a STOP codon after Ala446 to remove the C-terminal His-tag** | | | |
| **Construct name** | **Mutations** | **Template** | **Primer** |
| Wild-type | C411S, STOP | Wild-type -His | CTGAGAGAAGCTTAGTCGAGCGGCCGCC |
| HLR | C411S, E427H, Q433L, K440R, STOP | HLR -His | |
| WDASR | C411S, E426W, E427D, L429A, Q433S, K440R, STOP | WDASR -His | |
| LTTLRP | C411S, E426L, E427T, Q433T, R434L, T437R, K440P, STOP | LTTLRP -His | |
| **Constructs lacking a C-terminal His-tag** | | | |
| **Construct name** | **Mutations** | **Template** | **Primer** |
| WDASQSR | C411S, E426W, E427D, L429A, Q433S, R434Q, T437S, K440R, STOP | WDASR | GGGACAGAGCATGGGAAGTATCACAAATTTTGTCAGCCCTCCGC |
| WDASTAY | C411S, E426W, E427D, L429A, Q433S, R434T, T437A, K440Y, STOP | WDASR | GGGAAGTATCAACAATTTTGGCAGCCCTCTACAGAAAACTGAGAGAAGC |
| WNASELR | C411S, E426W, E427N, L429A, Q433S, R434E, T437L, K440R, STOP | WDASR | GTCTAAATGGAACAGAGCATGGGAAGTATCAGAAATTTTGTTAGCCCTCCGC |
| SMLR | C411S, E427S, L429M Q433L, K440R, STOP | HLR | GGGATAAAGGATTTGTCTAAAGAATCTAGAATGTGGGAAGTACTGAG |

| | | | |
|---|---|---|---|
| DVLR | C411S, E427D, L429V, Q433L, K440R, STOP | HLR | GGATTTGTCTAAAGAAGATAGAGTATGGGAAGTACTGAG |
| SST | C411S, E426S, E427S, Q433T, STOP | Wild-type | GGATTTGTCTAAATCATCAAGATTATGGGAAGTAACAAGAATTTTGACAGCCC |
| SDT | C411S, E426S, E427D, Q433T, STOP | SST | GGGATAAAGGATTTGTCTAAATCAGATAGATTATGGGAAG |
| NTR | C411S, E426N, Q433T, K440R, STOP | HLR | GGGATAAAGGATTTGTCTAAAAACGAAAGATTATGGGAAGTAACGAGAATTTTGACAGCC |
| LTHTLKP | C411S, E426L, E427T, L429H, Q433T, R434L, T437K, K440P | LTTLRP | CTAAACTGACAAGACATTGGGAAGTAACACTGATTTTGAAAGCCCTCCCAAG |
| Wild-type L409A/H413A | C411S, L409A, H413A, STOP | Wild-type | GGAGACAGGAGTTTCTTGCGAATAGTTTAGCTCGAGATCTGCAGGG |
| HLR L409A/H413A | C411S, L409A, H413A, E427H, Q433L, K440R, STOP | HLR | |
| **KSI (pET31b) DP → EP** | | | |
| **Construct name** | **Mutations** | **Template** | **Primer** |
| KSI (pET31b) DP → EP | KSI:D38E | pET31b | CCACGGTGGAAGAACCCGTGGGTTCC |
| **Peptides in pET31b** | | | |
| **Construct name** | **Mutations** | **Template** | **Primer** |
| Peptide linker mutagenesis | (vector)MLLE → AGSG | pET31b-double peptide | CGCCGTAAGCTGCGTGAGGCGGGGAGCGGGCACCACCACCACCACC |
| Peptide salt bridges | V432E, L436K, L439E, L443K x2 peptide sequences | Peptide linker mutagenesis | Primer 1 - GCCTGTGGGAGGAACTCCGCATCAAGACCGCGGAGCGTCGTAAAAAGCGCGAAGCGG<br>Primer 2 - CCTCTGGGAAGAACTGCGTATCAAGACGGCGGAGCGCCGTAAGAAGCGTGAGGCG |

[a] Nucleotides that differ from the template are underlined.

### *6.2.4* Preparation of recombinant proteins from *E. coli*

*Table 6.17. Buffers for protein purification.*

| **Lysis buffers** | |
|---|---|
| **Name** | **Composition** |
| RLIP76 RBD | 50 mM Tris-HCl pH 7.5, 250 mM NaCl, 1 mM $MgCl_2$ |
| RhoA<br>Cdc42 | 50 mM Tris-HCl pH 7.5, 250 mM NaCl, 5 mM $MgCl_2$ |
| $Ni^{2+}$ affinity | 50 mM Tris-HCl pH 7.9, 500 mM NaCl, 1 mM $MgCl_2$ |
| **Purification buffers** | |
| **Name** | **Composition** |
| RLIP76 RBD | 50 mM Tris-HCl pH 7.5, 250 mM NaCl, 1 mM $MgCl_2$, 0.05% $NaN_3$ |
| RalB | 50 mM Tris-HCl pH 7.5, 150 mM NaCl, 1 mM $MgCl_2$, 0.05% $NaN_3$ |
| RalA | 20 mM Tris-HCl pH 7.5, 150 mM NaCl, 1 mM $MgCl_2$, 5 mM DTT, 0.05% $NaN_3$ |
| RhoA<br>Cdc42 | 50 mM Tris-HCl pH 7.5, 150 mM NaCl, 5 mM $MgCl_2$, 5 mM DTT, 0.05% $NaN_3$ |
| **Cleavage buffers** | |
| **Name** | **Composition** |
| HRV-3C | 50 mM Tris-HCl pH 7.5, 150 mM NaCl, 1 mM $MgCl_2$, 1 mM DTT |
| Thrombin | 50 mM Tris-HCl pH 8.4, 150 mM NaCl, 2.5 mM $CaCl_2$, 5 mM $MgCl_2$ |
| **$Ni^{2+}$ Affinity purification buffers** | |
| **Name** | **Composition** |
| Buffer A | 20 mM Tris-HCl pH 7.9, 100 mM NaCl, 0.05% $NaN_3$ |
| Buffer B | 20 mM Tris-HCl pH 7.9, 100 mM NaCl, 1 M imidazole pH 7.9, 0.05% $NaN_3$ |

#### 6.2.4.1 Small-scale expression trials

Cultures of *E.coli* transformed with the desired construct were grown in 2TY for at least 16 h. 1 mL of the overnight culture was added to 3 x 10 mL 2TY and incubated at 37 °C until an $A_{600}$ ≈ 0.8 was reached. 2 out of the 3 samples were induced with 0.1 mM IPTG (BL21) or 1 mM IPTG (BL21(DE3)), while the final sample was not induced. One induced sample and the uninduced sample were incubated at 37 °C with shaking for 5 h, and the other induced sample was incubated at 20 °C overnight. The $A_{600}$ of each sample was measured and 1-2 mL each was centrifuged at 13,000 x g for 1 min. The samples were resuspended in a volume of water related to the $A_{600}$ of the sample by the following equation;

$$(\text{volume} = \frac{1000}{12} \times A_{600} \times \text{mL culture})$$

to give a minimum volume of 200 µL for sonication, and a small volume of each was mixed with 2x SDS sample buffer. Lysozyme (2 µL, 20 mg/mL) was added to the induced samples, which were sonicated for 3 x 10 s at 70% intensity (Fisher Scientific™ Model 120 Sonic Dismembrator). The lysed samples were pelleted at 13,000 x g for 1 min and the supernatant was then mixed with an equal volume of 2x SDS sample buffer. The pellets were resuspended in the calculated volume of SAW and an equivalent volume of 2x SDS sample buffer was added. The samples were analysed by SDS-PAGE and the best expression conditions were taken forward into larger-scale preparations.

#### 6.2.4.2 Large-scale protein expression

50 mL overnight cultures of *E.coli* (strains listed in Table 6.18) were diluted into 500 mL fresh 2TY (3 L total for GTPases, 1.5 L total for RLIP76 RBDs). Flasks were incubated with shaking at 37°C until an $A_{600} \approx 0.8$ was reached. Flasks were induced with 0.1 or 1 mM IPTG and incubated at 20 °C overnight or at 37°C for 5 h as indicated (Table 6.18).

*Table 6.18. Protein expression constructs.*

| **GST-, -$His_6$ fusion proteins from pGEX-HisP** | | | | | |
|---|---|---|---|---|---|
| **Protein** | **Strain** | **[IPTG] (mM)** | **Temperature (°C)** | **Time (h)** | **Antibiotic** |
| RLIP76 RBD (all) | BL21 | 0.1 | 20 | 20 | Amp |
| **$His_6$-MBP- fusion proteins from pMAT10** | | | | | |
| **Protein** | **Strain** | **[IPTG] (mM)** | **Temperature (°C)** | **Time (h)** | **Antibiotic** |
| RalA (all) RalB | BL21(DE3) | 1 | 20 | 20 | Amp |
| **$His_{10}$- fusion proteins from pET16b** | | | | | |
| **Protein** | **Strain** | **[IPTG] (mM)** | **Temperature (°C)** | **Time (h)** | **Antibiotic** |
| RalB | BL21(DE3) | 1 | 20 | 20 | Amp |
| **GST- fusion proteins from pGEX2T** | | | | | |
| **Protein** | **Strain** | **[IPTG] (mM)** | **Temperature (°C)** | **Time (h)** | **Antibiotic** |
| Cdc42 | BL21 | 0.1 | 37 | 5 | Amp |
| RhoA | BL21 | 0.1 | 20 | 20 | Amp |

#### 6.2.4.3 Expression of $^{15}$N-labelled RalB for NMR studies

Small-scale expression trials for RalB in pET16b in M9 minimal media (Table 6.12) were carried out as follows. Overnight cultures in 2TY (10 mL) were pelleted by centrifugation at 3,000 x g for 20 min and resuspended in 1 mL 1 x M9 salts prior to inoculation of 3 x 9 mL M9 minimal media. Growth and analysis of small-scale expression cultures was carried out as described previously.

Overnight cultures for the large-scale preparation were set up in 6 x 50 mL 2TY. Cultures were pelleted at 3,000 x g for 20 min and resuspended in 1 mL 1 x M9 salts each prior to inoculation into 6 x 500 mL flasks M9 minimal media supplemented with 0.5g $^{15}NH_4Cl$. Cultures were grown until an $A_{600} \approx 0.8$ was reached and then cooled prior to induction with 1 mM IPTG and overnight incubation at 20 °C with shaking.

#### 6.2.4.4 Preparation of cell lysates for subsequent purification

Large scale cultures were pelleted at 8,000 x g for 15 min and the cell pellet then resuspended in 30 mL lysis buffer or $Ni^{2+}$ lysis buffer (pMAT10 and pET16b) with 1 mM phenylmethylsulfonyl fluoride (PMSF) and a SIGMAFAST™ protease inhibitor cocktail tablet (EDTA-Free) added. Cells were lysed by passing through an Emulsiflex 3 times under pressure and an additional 1 mM PMSF and 0.1% triton was added to the lysate. Insoluble material was pelleted by centrifugation at 45,000 x g for 30 min.

#### 6.2.4.5 GST affinity purification

Lysates containing GST-fusion proteins (pGEX2T and pGEX-HisP) were added to glutathione agarose beads (Sigma) pre-equilibrated in purification buffer (Table 6.17) and incubated at 4 °C with rotation for 2 h. Beads were washed with 3 x 40 mL ice cold purification buffer with 0.1% Triton, and 10 mL HRV-3C cleavage buffer (pGEX-HisP) or 3 x 20 mL thrombin cleavage buffer (pGEX2T) (Table 6.17). HRV-3C (50 µL, 4.8 mg/mL) or thrombin (Novagen, 25 units) protease was added to each set of beads and incubated at 4 °C overnight with rotation to cleave the fusion protein from the GST tag. The beads were pelleted at 1000 x g for 10 min and the supernatant retained. Remaining protein was eluted from the beads with 3 x 10 mL cold purification buffer and all elutions were retained on ice. The presence of the cleaved protein in the eluted fractions was confirmed by SDS-PAGE analysis.

#### 6.2.4.6 $Ni^{2+}$-NTA affinity purification (bead slurry)

Lysates containing His-tagged Ral proteins from pMAT10 were added to charged Ni-NTA agarose beads (2 x 5 mL, Qiagen) equilibrated with Buffer A (Table 6.17) and incubated at 4 °C for 2 h with rotation. The beads were washed with 3 x 45 mL cold Buffer A + 0.1% Triton, followed by 3 x 20 mL thrombin cleavage buffer. Thrombin (Novagen, 25 units) was added to each bead set and incubated at 4 °C for at least 16 h. The thrombin cleavage step was omitted to produce MBP-RalA. For cleaved Ral proteins, beads were pelleted at 1,000 x g and the supernatant was retained. Remaining cleaved Ral protein was eluted by washing the beads

with 3 x 10 mL cold Buffer A. MBP-RalA was eluted with 4 x 10 mL cold Buffer A + 300 mM imidazole. SDS-PAGE analysis confirmed the presence of Ral proteins in the eluted fractions.

#### 6.2.4.7 $Ni^{2+}$-NTA affinity purification (column)

Cleared lysate containing His-tagged RalB was loaded onto a charged Ni-NTA column. Unbound proteins were removed from the column by washing with Buffer A and loosely bound proteins were then eluted with 6% Buffer B (60 mM imidazole) (Table 6.17). The His-tagged RalB was eluted using an increasing gradient of imidazole (60-500 mM). SDS-PAGE analysis was used to identify the fractions containing RalB.

#### 6.2.4.8 Concentration of purified proteins

Following affinity purification, protein solutions were concentrated in a 4 or 15 mL Amicon® centrifugal filter unit (Merck-Millipore) with a 10,000 (GTPases) or 3,000 (RLIP76 RBDs) molecular weight cut off. Proteins were concentrated again after size exclusion chromatography.

#### 6.2.4.9 Size exclusion purification

Superdex S30 (RLIP76 RBDs), S75 (cleaved GTPases) and S200 (MBP-RalA) columns (Cytiva, 120 mL bed volume) were used for size exclusion purification. Columns were equilibrated in 1.5 column volumes purification buffer prior to loading up to 2 mL sample. Columns were eluted with 1.5 column volumes purification buffer at 1 mL/min and collected in 2 mL fractions. Fractions were analysed using SDS-PAGE and those containing the desired protein were pooled and concentrated as described in the previous section.

#### 6.2.4.10 Measuring protein concentration

The $A_{280}$ values of the purified proteins were measured using a NanoDrop™ One using the eluate from the concentration unit as a blank. The protein concentrations were estimated according to the Beer-Lambert law ($A = \varepsilon cl$), where A = absorbance at 280 nm, ε = extinction

coefficient, c = molar concentration, and l = path length in cm. Extinction coefficients for proteins were estimated using EMBOSS Pepstats and the extinction coefficient for a guanine nucleotide (ε = 7950) was included for the GTPase measurements.

### 6.2.5 Nucleotide exchange

*Table 6.19. Nucleotide exchange and HPLC analysis buffers.*

| Name | Composition |
|---|---|
| Exchange buffer 1 | 10 mM Tris-HCl pH 7.5, 0.1 mM $ZnCl_2$ |
| Exchange buffer 2 | 3M $(NH_4)_2SO_4$, 10 mM Tris-HCl pH 7.5 |
| Exchange buffer 3 | 50 mM Tris-HCl pH 7.4, 150 mM NaCl |
| HPLC buffer | 0.6 M monobasic ammonium phosphate pH 4.0 |

#### 6.2.5.1 Exchange of bound nucleotides for GMPPNP

Purified GTPase (500 µL, up to 1 mM), 333 µL 20 mM GMPPNP and 91 µL Exchange buffer 2 (Table 6.19) were added to 80 units alkaline phosphatase beads (Sigma) equilibrated in Exchange buffer 1 (Table 6.19). The mixture was incubated at 37 °C for 4.5 h with rotation and then separated on G25 Sephadex (Sigma) spin columns. Approximately 50 µg exchanged protein was mixed with 3 µL 0.9 M perchloric acid to precipitate the protein and release the nucleotide. Samples were made up to 100 µL in 0.6 M ammonium phosphate pH 4 and centrifuged at 13,000 x g for 1 min. The supernatant was analysed by HPLC to check the exchange efficiency (section 6.2.5.3).

#### 6.2.5.2 Preparation of GDP-RalA

Following purification, the bound nucleotide of wild-type RalA was analysed by HPLC and was found to contain some GTP. The protein was incubated at room temperature for at least 16 h, after which time all of the bound nucleotide had been hydrolysed to GDP as confirmed by HPLC (section 6.2.5.3).

#### 6.2.5.3 Analysis of bound nucleotides

Approximately 50 µg GTPase was precipitated with 3 µL 0.9 M perchloric acid to release the bound nucleotide, and HPLC buffer (Table 6.19) was added up to 100 µL. Samples were centrifuged at 13,000 x g for 5 min prior to loading onto a 1.5 mL Partisphere SAX column (Whatman) equilibrated in HPLC buffer. Nucleotides were eluted in the same buffer at 1.5 mL/min. Standards of nucleotides prepared at 0.1 mM in SAW were also run for comparison of retention times.

#### 6.2.5.4 Radiolabelling proteins for scintillation proximity assays

GTPases were loaded with [8,5′-$^{3}$H]GTP (0.15 mCi, Cytiva) as described previously (227). Excess nucleotide was removed using a 1 mL G25 Sephadex (Superfine, Sigma) column, pre-equilibrated with Exchange buffer 3 (Table 6.19).

### *6.2.6* Production of cysteine-crosslinked peptides from *E.coli*

*Table 6.20. Buffers for purification of recombinant peptides.*

| Name | Composition |
|---|---|
| Peptide lysis | 50 mM Tris-HCl pH 7.9, 500 mM NaCl |
| Buffer A | 20 mM Tris-HCl pH 7.9, 500 mM NaCl, 0.05% $NaN_3$ |
| Buffer B | 20 mM Tris-HCl pH 7.9, 500 mM NaCl, 1 M imidazole pH 7.9, 0.05% $NaN_3$ |
| Peptide buffer | 50 mM Tris-HCl pH 7.5, 150 mM NaCl |
| Inclusion body | 6M Gdn-HCl, 50 mM Tris-HCl pH 7.9, 500 mM NaCl |

*Table 6.21. Growth and induction conditions for peptide expression.*

| **Peptides from pOP5BP** | | | | | |
|---|---|---|---|---|---|
| **Peptide fusion** | **Strain** | **[IPTG] (mM)** | **Temperature (°C)** | **Time (h)** | **Antibiotic** |
| $His_8$GB1-peptide-Avi tag | BL21(DE3) BirA | 0.4 | 20 | 20 | Amp, Cam |
| **Peptides from pET31b** | | | | | |
| **Peptide fusion** | **Strain** | **[IPTG] (mM)** | **Temperature (°C)** | **Time (h)** | **Antibiotic** |
| KSI-peptide (all) | BL21(DE3) | 1 | 37 | 5 | Amp |

#### 6.2.6.1 Large scale peptide expression

50 mL cultures of *E. coli* (strains listed in Table 6.21) were diluted into 500 mL 2TY. Flasks were incubated with shaking at 37 °C until an $A_{600} \approx 0.8$ was reached. Flasks were induced with 0.4 or 1 mM IPTG and incubated at 20 °C for at least 16 h or at 37 °C for 5 h as indicated in Table 6.21.

#### 6.2.6.2 Preparation of soluble peptides from pOP5BP

Cultures were pelleted at 8,000 x g for 15 min and resuspended in Peptide lysis buffer supplemented with 1 mM PMSF and an EDTA-free protease inhibitor cocktail tablet and lysed by passing the culture through an Emulsiflex under pressure (x3). The lysate was centrifuged at 45,000 x g for 30 min to remove insoluble debris and the supernatant was loaded onto a pre-charged 20 mL Ni-NTA column equilibrated in Buffer A (Table 6.20). The column was washed with Buffer A and then again with 3% Buffer B (30 mM imidazole). The protein was eluted with an imidazole gradient (30 – 500 mM) over 10 column volumes. Following concentration to <2.5 mL, A PD10 desalting column (Cytiva) was used to buffer exchange the GB1-peptide fusion into Buffer A. For cleavage of the peptide from the GB1 fusion protein, 1 mM EDTA, 1 mM DTT and HRV-3C protease (100 µL, 4.8 m/mL) were added to the solution and incubated at 4 °C for a minimum of 16 h with rotation.

#### 6.2.6.3 Inclusion body preparation of KSI-peptide fusions

Cultures were centrifuged at 12,000 x g for 10 min and resuspended in Peptide lysis buffer (Table 6.20) supplemented with 1 mM PMSF and an EDTA-free protease inhibitor cocktail tablet and lysed by passing the culture through an Emulsiflex under pressure (x3). The lysate was centrifuged at 12,000 x g for 10 min. The supernatant was removed and the pellet containing the KSI-peptide fusion was resuspended in 20 mL Peptide lysis buffer, using sonication to aid resuspension. The centrifugation and washing steps were repeated to remove soluble proteins from the inclusion body pellet. Finally, the inclusion bodies were resuspended in a small volume of Inclusion body buffer (Table 6.20).

Solubilized inclusion bodies centrifuged at 45,000 x g to remove debris. The supernatant was loaded onto a Ni-NTA column and washed with Inclusion body buffer until a stable baseline was observed. This was followed by washing with Inclusion body buffer + 20 mM imidazole to remove weakly bound proteins. The purified KSI-peptide fusion was eluted from the column using Inclusion body buffer + 300 mM imidazole.

#### 6.2.6.4 Cysteine cross-linking with dibromo-*m*-xylene

The KSI-peptide fusion was concentrated to approximately 1 mM. TCEP (4mM) and 10 equivalents of dibromo-*m*-xylene (10 mM, from 1 M stock in DMF) were added to the KSI-peptide fusion and the reaction was sealed and stirred at room temperature overnight. The reaction was stopped by adding 1 M HCl dropwise until pH <1.0 was reached. The extent of cross-linking was assessed using MALDI-ToF mass spectrometry (Cambridge Centre for Proteomics, University of Cambridge) and samples were typically found to contain 100% cross-linked product with no side products visible.

#### 6.2.6.5 Cleavage and purification of cross-linked peptides

The acidified peptide mixture was heated to 85 °C for 5 h to release the free peptide and His-tagged peptide products. This hydrolysed mixture was dialysed overnight into Peptide buffer using benzoylated tubing (D7884, Sigma). The peptide mixture was loaded onto a 5 mL Ni-NTA column, and the His-tagged peptide was separated from the non-tagged peptide by

elution with an imidazole gradient (20 - 300 mM). Finally, the peptides were purified by size exclusion chromatography using a 24 mL Superdex peptide column equilibrated with Peptide buffer. Peptide concentrations were quantified using the absorbance at 280 nm and then stored at -80 °C.

### 6.2.7 Peptide synthesis

*Table 6.22. Peptide synthesis reagent preparations.*

| Reagent | Preparation |
|---|---|
| HCTU | 32 g in 200 mL DMF |
| DIPEA | 70 mL in 130 mL NMP |
| Capping | 40 mL acetic anhydride, 390 mL DMF, 70 mL pyridine |
| 20% piperidine | 100 mL piperidine, 400 mL DMF |
| King's reagent | 89% TFA, 5% TIPS, 1.5% EDT, 1.5% $H_2O$, 1.5% thioanisole, 1.5% phenol |

#### 6.2.7.1 Automated peptide synthesis

Rink amide MBHA resin (0.15 mmol) was swollen in DCM in a synthesis vessel and washed with DMF. Fmoc-protected natural amino acids and Fmoc-AEEP were coupled using a Prelude automated peptide synthesizer (Gyros) using an HCTU activator, 0.3 M amino acid solutions and DIPEA solutions, followed addition of capping solution (Table 6.22). Resin was washed thoroughly between amino acid coupling and deprotections. Deprotections were carried out using 20% piperidine (Table 6.22, 2 x 10 min). Amino acids were single or double-coupled, except for residues immediately following (*S*)-pentenylalanine, which were triple-coupled.

#### 6.2.7.2 Manual coupling of (*S*)-pentenylalanine

Resin was deprotected using 20% piperidine (2 x 10 min) with shaking and washed extensively with DCM and DMF. Fmoc-(*S*)-pentenylalanine (4 eq), HATU (4 eq) and DIPEA (8 eq) in DMF were added to the deprotected resin and incubated at room temperature for 1 h with horizontal shaking.

#### 6.2.7.3 Peptide stapling with Grubbs metathesis

The resin containing the linear peptide was dried using ether under vacuum and transferred to a reaction vessel. The resin was washed with DCE (2 x 10 mL). Grubbs first generation catalyst (6 mM, 5 mL) in DCE was added and the mixture was sparged with nitrogen for 2 h. The vessel was drained, replaced with fresh catalyst (6 mM, 5 mL) and sparged with nitrogen for 2 h. The resin was washed extensively with DCM and DMF. Finally, the resin was dried with ether under vacuum, and transferred into Prelude reaction vessels for further couplings. Small-scale test cleavages (section 6.2.7.5) were carried out to ensure the stapling reaction had achieved completion.

#### 6.2.7.4 Fluorescent labelling of peptides

The resin was deprotected using 20% piperidine (2 x 10 min) with shaking and washed extensively with DCM and DMF (DMF final washes). 5-carboxyfluorescein (5 eq), HOBt (10 eq) and DIC (10 eq) in DMF were added to the resin. Reaction vessels were covered with foil and incubated at room temperature with horizontal shaking for a minimum of 40 h. Following extensive washes with DCM and DMF, resin colour was used to confirm that the reaction had been successful.

#### 6.2.7.5 Cleavage from resin

***Small-scale test cleavage:*** Approximately 10 mg resin was added to a small syringe with 1 mL King's reagent (Table 6.22) was added to the syringe and incubated at room temperature for 4 h with shaking. TFA was evaporated under a flow of air and the peptide was precipitated with ether (10 mL). The pellet was washed with ether (2 x 10 mL), with centrifugation after addition of ether to re-form the pellet. The pellet was air-dried in a fumehood.

***Cleavage of peptides from resin following complete synthesis:*** King's reagent (12 mL) was added to each resin in a foil-covered syringe and incubated for 4-6 h at room temperature with shaking. TFA was removed by rotary evaporation and the peptide was precipitated with ether (25 mL). The pellet was washed with ether (2 x 25 mL), with centrifugation after addition of ether to re-form the pellet. The pellet was air-dried in a fumehood.

#### 6.2.7.6 Purification by RP-HPLC

Peptides were purified by reversed-phase preparative HPLC (Waters X-Bridge, 19 x 250 mm, C18 OBD) and analyzed by LC/MS (Agilent Polaris C8A, 2.1 x 50 mm); both systems eluting gradients of acetonitrile (0.1% v/v TFA) against water (0.1% v/v TFA).

### 6.2.8 *In vitro* binding assays

*Table 6.23. Buffers for biophysical assays.*

| Name | Composition |
|---|---|
| FP buffer | 50 mM Tris-HCl pH 7.5, 150 mM NaCl, 1 mM $MgCl_2$ |
| SPA reaction mix | 50 mM Tris-HCl pH 7.5, 0.2 mg/mL BSA, 2 mM DTT, 1 mM $MgCl_2$, 0.6% anti-His or 0.7% µL anti-GST, 29% SPA polyvinyltoluene protein A binding beads (Perkin Elmer) in 50 mM Tris-HCl pH 7.5 |
| SPA dilution buffer | 50 mM Tris-HCl pH 7.5, 0.2 mg/mL BSA, 2 mM DTT, 1 mM $MgCl_2$ |
| CD buffer | 20mM $Na_2HPO_4/NaH_2PO_4$ pH 7.4, 150 mM NaF |
| ITC buffer | 50 mM Tris-HCl pH 7.5, 150 mM NaCl, 1 mM $MgCl_2$ |

#### 6.2.8.1 Fluorescence polarization measurements

All experiments were recorded using a BMG Labtech PHERAstar plate reader, with an excitation wavelength of 485 nm and emission wavelength of 520 nm at 298K. Fluorescent peptides (20 nM) and GTPase (at concentrations indicated in the results) were mixed in a 384-well black flat-bottomed plate with a 30 µL well volume in FP buffer (Table 6.23). Plates were spun at 2,000 x g for 1 min and read after 30 min incubation at room temperature. Data were fitted to a single-site binding model using GraphPad Prism 7 to calculate the $K_d$ values and errors.

#### 6.2.8.2 Scintillation proximity assays (SPAs)

***Direct measurements*:** RLIP76 RBD-His (80 nM) was added to SPA reaction mix (Table 6.23). RalA·[$^3$H]GTP or RalB·[$^3$H]GTP was serially diluted in SPA dilution buffer (doubling dilutions

from 16 µM, Table 6.23) in low protein-binding eppendorfs. 175 µL reaction mix and 25 µL [$^3$H]GTP-labelled Ral protein at each concentration were mixed in a 96-well plate and incubated at 18 °C with shaking for 30 min. Plates were centrifuged at 1,000 x g for 2 min before reading. Each well was counted for 5 min in a MicroBeta Scintillation counter (PerkinElmer). Control experiments lacking the effector protein were measured and subtracted from the experimental data. Binding curves were fitted to obtain $K_d$ values and standard errors using GraFit5 as described previously (228).

***Competitions*:** RLIP76 RBD-His (80 nM), GST-Sec5 RBD (20 nM) or GST-Raf RBD (30 nM) were added to SPA reaction mix with [$^3$H]GTP-labelled GTPase at a concentration equivalent to the measured $K_d$ value for the immobilised effector. Protein competitors were diluted in SPA dilution buffer to give final concentrations as indicated in the results. Peptide competitors were diluted in SAW or 2% Tween20 to aid solubility as indicated in the results. Plates were prepared and counted as in the direct binding assays, with 175 µL reaction mix and 25 µL competitor in each well. Competitive binding isotherms were fitted using GraFit5 as described previously (182).

#### 6.2.8.3 Isothermal titration calorimetry (ITC)

ITC data were collected using a MicroCal iTC200 calorimeter at 298 K in ITC buffer (Table 6.23). RalB (40 - 200 µM, 8-10x cell concentration) was titrated into RLIP76 RBD variants (5-20 µM) in 19 x 2 µL additions with 120 s between injections. Control experiments were performed by titrating RalB (200 µM) into buffer. Data were fitted using MicroCal Origin 7.0 software using a single-site binding model.

### 6.2.9 Circular dichroism measurements

#### 6.2.9.1 Sample preparation

Proteins were buffer exchanged into CD buffer (Table 6.23) using 3.5 mL PD10 desalting columns (Cytiva) and prepared at 0.2 mg/mL. Peptide samples were prepared in SAW at 0.2 mg/mL.

#### 6.2.9.2 Secondary structure analyses

Measurements were recorded on an AVIV Biomedical circular dichroism spectrometer model 430 with a quartz cuvette (path length 0.1 cm). Wavelength scans were recorded at 1 nm intervals with a 5 s averaging time from 260 nm to as low a wavelength as possible before the signal quality decreased too far (typically 185 nm). Three scans were recorded for each sample and blank background measurements were subtracted. The machine units (in millidegrees, θ) were converted to mean residue ellipticity using the equation $[\theta] = \frac{\theta \times 100 \times M_r}{c \times l \times n}$ where θ is the ellipticity in degrees, $M_r$ is the molecular weight of the sample, c is concentration in mg/mL, l is the path length (cm) and n is the number of residues in the sample. The percentage of alpha helicity was estimated by the CDSSTR method and reference set 3 using Dichroweb (183–185). For the stapled peptides, the fluorescein label and PEG linker were included in the residue counts.

### 6.2.10 X-ray crystallography

#### 6.2.10.1 Preparation of RalB/RLIP76 RBD mutant complexes for crystallisation

RalB was added to an excess of RLIP76 RBD (HLR or SMLR) and incubated at room temperature with rotation. The complex mixture was purified by gel filtration on a Superdex S75 column in RalB purification buffer (Table 6.17). SDS-PAGE analysis was used to identify fractions containing the complex and these fractions were pooled and concentrated.

#### 6.2.10.2 Crystallization trials

Samples containing 10 and 5 mg/mL complex were prepared in RalB purification buffer (Table 6.17). Crystallization trials were set up using the Mosquito robotics system (SPT Labtech). Drops were set up with 0.2 µL protein solution and 0.2 µL screen solution using the sitting drop vapour-diffusion method with pHClear Suite I (Qiagen), ProPlex and JCSG+ HTS commercial plates. Plates were stored at 20 °C in a Rock Imager 1000 (Formulatrix) with regular images automatically taken to monitor crystal formation.

High quality crystals formed in the pHClear Suite I condition containing 0.1 M Bicine, pH 9.0 and 30% w/v polyethylene glycol 6000 at 20 °C. The crystals were frozen in liquid nitrogen prior to data collection.

#### 6.2.10.3 X-ray crystallography measurements

X-ray diffraction data was collected at the Diamond Light Source on beamlines IO3 and IO4 and processed using the pipedream package (Global Phasing Ltd). The structures were determined by molecular replacement using Phaser (229) from the CCP4 package (230) and were iteratively built and refined using Coot (231) and PHENIX (232). Co-ordinates have been deposited to the protein data bank under the accession codes 6ZQT (HLR mutant) and 6ZRN (SMLR mutant).

### 6.2.11 $^{1}H,^{15}N$ HSQC NMR Spectroscopy

Experiments were recorded on a Bruker AV800 at 298 K using 100 µM $^{15}N$-labeled RalB·GMPPNP in 50mM Tris-HCl pH 7.5, 100 mM NaCl, 1 mM $MgCl_2$, 10% $D_2O$. For the titration experiments, 0.25, 0.5, 1.0, 1.25 and 2.0 equivalents of HLR-sol were added to the protein solution and spectra recorded after each peptide addition. Chemical shift perturbations (δ) were calculated using the following equation; $\delta = \sqrt{\delta_{1H}^2 + (0.15\delta_{15N})}$, where $\delta^{1}H$ and $\delta^{15}N$ are the chemical shift changes for the $^{1}H$ and $^{15}N$ dimensions, respectively. NMR data were processed using the AZARA package (Wayne Boucher, University of Cambridge) and analyzed using CCPN ANALYSIS (233).

### 6.2.12 Cell culture methods

*Table 6.24. Cell culture reagents.*

| Name | Ingredients |
|---|---|
| Lysis buffer | 50 mM Tris-HCl pH 7.8, 150 mM NaCl, 1% Triton, 1 mM EDTA, 1 mM sodium orthovanadate, 1 mM β-glycerophosphate and protease inhibitor cocktail (Sigma-Aldrich |
| PBS | 150 mM NaCl, 16 mM $Na_2HPO_4$, 4 mM $NaH_2PO_4$ (pH 7.3) |
| PBS-T | PBS + 0.1% Tween20 |
| Dimethyl pimelimidate (DMP) | 200 mM in 0.2 M triethanolamine pH 8.2 |
| 2x LDS sample buffer | 4x LDS sample buffer (ThermoFisher, 50%), $H_2O$ (35%), β-mercaptoethanol (15%) |
| Luminol Solution | 100 mM Tris-HCl pH 8.6, 1.25 mM Sodium Luminol Salt |
| Enhancer Solution | 1.1 mg/mL *p*-Coumaric acid in DMSO |
| Enhanced Chemiluminescence Solution (ECL) | 5 mL Luminol Solution, 1.5 µL 30% $H_2O_2$, 50 µL Enhancer Solution |

#### 6.2.12.1 DNA purification for transfection of mammalian cells

An EndoFree Plasmid Maxi Kit (Qiagen) was used to purify DNA for use in mammalian cell transfections following the manufacturer's instructions.

#### 6.2.12.2 Transfections with PEI

3 x $10^6$ HEK293T cells were seeded in 10 cm dishes 24 h prior to transfection. For each 10 cm dish, 1 mL DMEM with the DNA amounts listed in Table 6.25 and PEI (30 µL, 1 mg/mL) was prepared and incubated at room temperature for 10 min. The mixture was added dropwise onto the dishes. The cells were incubated for 24 h before lysis.

*Table 6.25. DNA amounts for transfections of HEK293T cells.*

| **RalB/RLIP76 transfections** | |
|---|---|
| **Condition** | **µg** |
| GFP | 11 |
| GFP<br>V5-RalB Q72L<br>Flag-RLIP76 | 1<br>5<br>5 |
| **RalB transfections** | |
| **Condition** | **µg** |
| GFP | 6 |
| GFP<br>V5-RalB | 1<br>5 |

#### 6.2.12.3 Preparation of Dynabeads for co-immunoprecipitation experiments

Protein G Dynabeads (30 µL, ThermoFisher) were washed with 500 µL PBS-T and resuspended in 200 µL PBS-T with anti-V5 (1 µg). The antibody was incubated on the beads for 30 min at room temperature with rotation. The beads were washed with 0.2 M triethanolamine pH 8.2 (2 x 500 µL) and incubated with 500 µL DMP (Table 6.24) at room temperature with rotation for 20 min. The beads were resuspended in 50 mM Tris-HCl pH 7.4 and incubated at room temperature with rotation for 15 min. Finally, the beads were washed with PBS-T (3 x 500 µL).

#### 6.2.12.4 Co-immunoprecipitation of Ral-effector complexes

Dishes were lysed in 1 mL lysis buffer (Table 6.24). Lysates (1 mL) were centrifuged at 17,000 x g for 20 min and added to Protein G Dynabeads (30 µL, Invitrogen) that had been cross-linked with anti-V5 (section 6.2.12.3) Peptides, at the concentrations indicated in the results, were added and incubated with rotation for 1 h at 4 °C. Precipitated complexes were washed with lysis buffer (3 x 500 µL), and resuspended in equal volumes of PBS and 2x LDS sample buffer (Table 6.24).

#### 6.2.12.5 Preparation of lysate samples for western blot analysis

Cells were lysed in an appropriate volume of sample buffer (1 mL – 10 cm dish, 160 µL – 6-well plate) and were centrifuged at 17,000 x g for 20 min. Clarified lysates were added to an equal volume of 2 x LDS sample buffer (Table 6.24).

#### 6.2.12.6 Western blotting

Samples in LDS sample buffer were boiled at 100 °C and centrifuged at 17,000 x g for 1 min prior to loading (10 µL each) onto an SDS-PAGE gel. Samples were resolved by SDS-PAGE and transferred to polyvinylidene difluoride membranes (Immobilon-P) using a semi-dry transfer module (Hoefer). Membranes were blocked in 10% milk for 1 h and incubated with the antibodies listed in Table 6.6 for at least 16 h. Membranes were washed with PBS-T (3 x 15 min, 10 mL) and then incubated with an appropriate secondary antibody (Table 6.6) in 10% milk for 2 h if required. Membranes were washed again with PBS-T (3 x 15 min, 10 mL) prior to visualization with ECL (Table 6.6).

### 6.2.13 Confocal microscopy

***Live cells:*** HEK293T cells were seeded in micro-inserts in 35 mm µ-dishes (Ibidi). Prior to imaging, the cells were washed three times with PBS and the media was replaced with FluoroBrite™ DMEM (Gibco) supplemented with 20 mM HEPES (Sigma). Confocal images were acquired on an inverted Ti-E microscope (Nikon) using a 100x 1.40 oil objective lens (Plan Apo VC,Nikon). Images were collected with an EMCCD camera (Evolve Delta, Photometrics) with Metamorph software (version 7.8.2.0). Images were processed with Fiji (234, 235).

***Fixed cells:*** HEK293T cells (150,000) were seeded on 13 mm coverslips in 12-well plates 24 h prior to fixing. The wells were washed with PBS and fixed with 4% paraformaldehyde in PBS-T (1 mL) for 15 min. Wells were aspirated and 1% triton (1 mL) was added to each well for 10 min. Following aspiration, 4% BSA in PBS-T (1 mL) was added for 10 min. The coverslips were transferred to a parafilm-coated block and were incubated with 4% BSA in PBS-T with Alexa647-phalloidin conjugate (1:500, 20 µL) in darkness. The coverslips were finally washed with 3 x PBS-T and mounted onto slides using SouthernBlot DAPI-fluoromount G. Confocal

images were acquired on a Zeiss LSM 700 laser scanning confocal microscope using a 40x oil-immersion objective. Images were processed with Fiji (234, 235).

# 7 References


1. Wennerberg, K. (2005) The Ras superfamily at a glance. *J. Cell Sci.* **118**, 843–846
2. Bos, J., Rehmann, H., and Wittinghofer, A. (2007) GEFs and GAPs : Critical Elements in the Control of Small G Proteins. *Cell*. **129**, 865–877
3. Cherfils, J., and Zeghouf, M. (2013) Regulation of small GTPases by GEFs, GAPs, and GDIs. *Physiol. Rev.* **93**, 269–309
4. Wittinghofer, A., and Vetter, I. R. (2011) Structure-Function Relationships of the G Domain, a Canonical Switch Motif. *Annu. Rev. Biochem.* **80**, 943–971
5. Bourne, H. R., Sanders, D. A., and McCormick, F. (1991) The GTPase superfamily: conserved structure and molecular mechanism. *Nature*. **349**, 117–127
6. Milburn, M. V., Tong, L., DeVos, A. M., Brünger, A., Yamaizumi, Z., Nishimura, S., and Kim, S. H. (1990) Molecular switch for signal transduction: Structural differences between active and inactive forms of protooncogenic ras proteins. *Science*. **247**, 939–945
7. Vetter, I. R., and Wittinghofer, A. (2001) The guanine nucleotide-binding switch in three dimensions. *Science*. **294**, 1299–1304
8. Franco, M., Chardin, P., Chabre, M., and Paris, S. (1996) Myristoylation-facilitated binding of the G protein ARF1GDP to membrane phospholipids is required for its activation by a soluble nucleotide exchange factor. *J. Biol. Chem.* **271**, 1573–1578
9. Carlos Amor, J., Harrison, D. H., Kahn, R. A., and Ringe, D. (1994) Structure of the human ADP-ribosylation factor 1 complexed with GDP. *Nature*. **372**, 704–708
10. Antonny, B., Beraud-Dufour, S., Chardin, P., and Chabre, M. (1997) N-terminal hydrophobic residues of the G-protein ADP-ribosylation factor-1 insert into membrane phospholipids upon GDP to GTP exchange. *Biochemistry*. **36**, 4675–4684
11. Vetter, I. R., Nowak, C., Nishimoto, T., Kuhlmann, J., and Wittinghofer, A. (1999) Structure of a Ran-binding domain complexed with Ran bound to a GTP analogue: Implications for nuclear transport. *Nature*. **398**, 39–46
12. Scheffzek, K., Klebe, C., Fritz-Wolf, K., Kabsch, W., and Wittinghofer, A. (1995) Crystal structure of the nuclear Ras-related protein Ran in its GDP-bound form. *Nature*. **374**, 378–381

13. Mott, H. R., and Owen, D. (2015) Structures of Ras superfamily effector complexes: What have we learnt in two decades? *Crit. Rev. Biochem. Mol. Biol.* **50**, 85–133
14. Cox, A. D., and Der, C. J. (2010) Ras history. *Small GTPases*. **1**, 2–27
15. Barbacid, M. (1987) Ras Genes. *Annu. Rev. Biochem.* **56**, 779–827
16. Karnoub, A. E., and Weinberg, R. A. (2008) Ras oncogenes: Split personalities. *Nat. Rev. Mol. Cell Biol.* **9**, 517–531
17. Hancock, J. F., Paterson, H., and Marshall, C. J. (1990) A polybasic domain or palmitoylation is required in addition to the CAAX motif to localize p21ras to the plasma membrane. *Cell*. **63**, 133–139
18. Hancock, J. F., Cadwallader, K., Paterson, H., and Marshall, C. J. (1991) A CAAX or a CAAL motif and a second signal are sufficient for plasma membrane targeting of ras proteins. *EMBO J.* **10**, 4033–4039
19. Otto, J. C., Kim, E., Young, S. G., and Casey, P. J. (1999) Cloning and characterization of a mammalian prenyl protein-specific protease. *J. Biol. Chem.* **274**, 8379–8382
20. Dai, Q., Choy, E., Chiu, V., Romano, J., Slivka, S. R., Steitz, S. A., Michaelis, S., and Philips, M. R. (1998) Mammalian prenylcysteine carboxyl methyltransferase is in the endoplasmic reticulum. *J. Biol. Chem.* **273**, 15030–15034
21. Clarke, S., Vogel, J. P., Deschenes, R. J., and Stock, J. (1988) Posttranslational modification of the Ha-ras oncogene protein: Evidence for a third class of protein carboxyl methyltransferases. *Proc. Natl. Acad. Sci. U. S. A.* **85**, 4643–4647
22. Buday, L., and Downward, J. (2008) Many faces of Ras activation. *Biochim. Biophys. Acta - Rev. Cancer*. **1786**, 178–187
23. Ullrich, A., and Schlessinger, J. (1990) Signal transduction by receptors with tyrosine kinase activity. *Cell*. **61**, 203–212
24. Schlessinger, J. (1988) Signal transduction by allosteric receptor oligomerization. *Trends Biochem. Sci.* **13**, 443–447
25. Aronheim, A., Engelberg, D., Li, N., Al-Alawi, N., Schlessinger, J., and Karin, M. (1994) Membrane targeting of the nucleotide exchange factor Sos is sufficient for activating the Ras signaling pathway. *Cell*. **78**, 949–961
26. Rajalingam, K., Schreck, R., Rapp, U. R., and Albert, Š. (2007) Ras oncogenes and their downstream targets. *Biochim. Biophys. Acta - Mol. Cell Res.* **1773**, 1177–1195

27. Downward, J. (2003) Targeting Ras Signalling Pathways in Cancer Therapy. *Nature*. **3**, 11–22

28. Castellano, E., and Downward, J. (2011) Ras interaction with PI3K: More than just another effector pathway. *Genes Cancer*. **2**, 261–274

29. Neel, N. F., Martin, T. D., Stratford, J. K., Zand, T. P., Reiner, D. J., and Der, C. J. (2011) The RalGEF-Ral Effector Signaling Network. *Genes Cancer*. **2**, 275–287

30. Prior, I. A., Hood, F. E., and Hartley, J. L. (2020) The frequency of Ras mutations in cancer. *Cancer Res.* **80**, 2969–2974

31. Scheffzek, K., Ahmadian, M. R., Kabsch, W., Wiesmüller, L., Lautwein, A., Schmitz, F., and Wittinghofer, A. (1997) The Ras-RasGAP complex: structural basis for GTPase activation and its loss in oncogenic Ras mutants. *Science*. **277**, 333–338

32. John, J., Sohmen, R., Feuerstein, J., Linke, R., Wittinghofer, A., and Goody, R. S. (1990) Kinetics of Interaction of Nucleotides with Nucleotide-Free H-ras p21. *Biochemistry*. **29**, 6058–6065

33. Whyte, D. B., Kirschmeier, P., Hockenberry, T. N., Nunez-Oliva, I., James, L., Catino, J. J., Bishop, W. R., and Pai, J. K. (1997) K- and N-Ras are geranylgeranylated in cells treated with farnesyl protein transferase inhibitors. *J. Biol. Chem.* **272**, 14459–14464

34. Kato, K., Cox, A. D., Hisaka, M. M., Graham, S. M., Buss, J. E., and Der, C. J. (1992) Isoprenoid addition to Ras protein is the critical modification for its membrane association and transforming activity. *Proc. Natl. Acad. Sci. U. S. A.* **89**, 6403–6407

35. Ho, A., Chau, N., Garcia, I. B., Ferte, C., Even, C., Burrows, F., Kessler, L., Mishra, V., Magnuson, K., Scholz, C., and Gualberto, A. (2018) Preliminary Results From a Phase 2 Trial of Tipifarnib in HRAS-Mutant Head and Neck Squamous Cell Carcinomas. *Int. J. Radiat. Oncol.* **100**, 1367

36. Ho, A. L., Chau, N., Bauman, J., Bible, K., Chintakuntlawar, A., Cabanillas, M. E., Wong, D. J., Braña Garcia, I., Brose, M. S., Boni, V., Even, C., Razaq, M., Mishra, V., Bracken, K., Wages, D., Scholz, C., and Gualberto, A. (2018) Preliminary results from a phase II trial of tipifarnib in squamous cell carcinomas (SCCs) with HRAS mutations. *Ann. Oncol.* **29**, 373

37. Novotny, C. J., Hamilton, G. L., McCormick, F., and Shokat, K. M. (2017) Farnesyltransferase-Mediated Delivery of a Covalent Inhibitor Overcomes Alternative

Prenylation to Mislocalize K-Ras. *ACS Chem. Biol.* **12**, 1956–1962

38. Patgiri, A., Yadav, K. K., Arora, P. S., and Bar-Sagi, D. (2011) An orthosteric inhibitor of the Ras-Sos interaction. *Nat. Chem. Biol.* **7**, 585–587
39. Patgiri, A., Jochim, A. L., and Arora, P. S. (2008) A Hydrogen Bond Surrogate Approach for Stabilization of Short Peptide Sequences in α-Helical Conformation. *Acc. Chem. Res.* **41**, 1289–1300
40. Leshchiner, E. S., Parkhitko, A., Bird, G. H., Luccarelli, J., Bellairs, J. A., Escudero, S., Opoku-Nsiah, K., Godes, M., Perrimon, N., and Walensky, L. D. (2015) Direct inhibition of oncogenic KRAS by hydrocarbon-stapled SOS1 helices. *Proc. Natl. Acad. Sci. U. S. A.* **112**, 1761–1766
41. Ng, S., Juang, Y.-C., Chandramohan, A., Kristal Kaan, H. Y., Sadruddin, A., Yuen, T. Y., Ferrer, F. J., Lee, X. C., Xi, L., Johannes, C. W., Brown, C. J., Kannan, S., Aronica, P. G., Berglund, N., Verma, C. S., Liu, L., Stoeck, A., Sawyer, T. K., Partridge, A. W., and Lane, D. P. (2020) De-risking drug discovery of intracellular targeting peptides: screening strategies to eliminate false-positive hits. *ACS Med. Chem. Lett.* in press
42. Sakamoto, K., Kamada, Y., Sameshima, T., Yaguchi, M., Niida, A., Sasaki, S., Miwa, M., Ohkubo, S., Sakamoto, J., Kamaura, M., Cho, N., and Tani, A. (2017) K-Ras(G12D)-selective inhibitory peptides generated by random peptide T7 phage display technology. *Biochem. Biophys. Res. Commun.* **484**, 605–611
43. Sogabe, S., Kamada, Y., Miwa, M., Niida, A., Sameshima, T., Kamaura, M., Yonemori, K., Sasaki, S., Sakamoto, J., and Sakamoto, K. (2017) Crystal Structure of a Human K-Ras G12D Mutant in Complex with GDP and the Cyclic Inhibitory Peptide KRpep-2d. *ACS Med. Chem. Lett.* **8**, 732–736
44. Wu, X., Wang, L., Han, Y., Regan, N., Li, P. K., Villalona, M. A., Hu, X., Briesewitz, R., and Pei, D. (2011) Creating diverse target-binding surfaces on FKBP12: Synthesis and evaluation of a rapamycin analogue library. *ACS Comb. Sci.* **13**, 486–495
45. Wu, X., Upadhyaya, P., Villalona-Calero, M. A., Briesewitz, R., and Pei, D. (2013) Inhibition of Ras-effector interactions by cyclic peptides. *Medchemcomm*. **4**, 378–382
46. Qian, Z., Liu, T., Liu, Y. Y., Briesewitz, R., Barrios, A. M., Jhiang, S. M., and Pei, D. (2013) Efficient delivery of cyclic peptides into mammalian cells with short sequence motifs. *ACS Chem. Biol.* **8**, 423–431

47. Upadhyaya, P., Qian, Z., Selner, N. G., Clippinger, S. R., Wu, Z., Briesewitz, R., and Pei, D. (2015) Inhibition of Ras Signaling by Blocking Ras-Effector Interactions with Cyclic Peptides. *Angew. Chemie - Int. Ed.* **54**, 7602–7606

48. Upadhyaya, P., Qian, Z., Habir, N., and Pei, D. (2014) Direct Ras Inhibitors Identified from a Structurally Rigidified Bicyclic Peptide Library. *Tetrahedron*. **70**, 7714–7720

49. Trinh, T. B., Upadhyaya, P., Qian, Z., and Pei, D. (2016) Discovery of a Direct Ras Inhibitor by Screening a Combinatorial Library of Cell-Permeable Bicyclic Peptides. *ACS Comb. Sci.* **18**, 75–85

50. Ostrem, J. M., Peters, U., Sos, M. L., Wells, J. A., and Shokat, K. M. (2013) K-Ras(G12C) inhibitors allosterically control GTP affinity and effector interactions. *Nature*. **503**, 548–551

51. Patricelli, M. P., Janes, M. R., Li, L. S., Hansen, R., Peters, U., Kessler, L. V., Chen, Y., Kucharski, J. M., Feng, J., Ely, T., Chen, J. H., Firdaus, S. J., Babbar, A., Ren, P., and Liu, Y. (2016) Selective inhibition of oncogenic KRAS output with small molecules targeting the inactive state. *Cancer Discov.* **6**, 316–329

52. Janes, M. R., Zhang, J., Li, L. S., Hansen, R., Peters, U., Guo, X., Chen, Y., Babbar, A., Firdaus, S. J., Darjania, L., Feng, J., Chen, J. H., Li, S., Li, S., Long, Y. O., Thach, C., Liu, Y., Zarieh, A., Ely, T., Kucharski, J. M., Kessler, L. V., Wu, T., Yu, K., Wang, Y., Yao, Y., Deng, X., Zarrinkar, P. P., Brehmer, D., Dhanak, D., Lorenzi, M. V., Hu-Lowe, D., Patricelli, M. P., Ren, P., and Liu, Y. (2018) Targeting KRAS Mutant Cancers with a Covalent G12C-Specific Inhibitor. *Cell*. **172**, 578–589

53. Lanman, B. A., Allen, J. R., Allen, J. G., Amegadzie, A. K., Ashton, K. S., Booker, S. K., Chen, J. J., Chen, N., Frohn, M. J., Goodman, G., Kopecky, D. J., Liu, L., Lopez, P., Low, J. D., Ma, V., Minatti, A. E., Nguyen, T. T., Nishimura, N., Pickrell, A. J., Reed, A. B., Shin, Y., Siegmund, A. C., Tamayo, N. A., Tegley, C. M., Walton, M. C., Wang, H. L., Wurz, R. P., Xue, M., Yang, K. C., Achanta, P., Bartberger, M. D., Canon, J., Hollis, L. S., McCarter, J. D., Mohr, C., Rex, K., Saiki, A. Y., San Miguel, T., Volak, L. P., Wang, K. H., Whittington, D. A., Zech, S. G., Lipford, J. R., and Cee, V. J. (2020) Discovery of a Covalent Inhibitor of KRASG12C (AMG 510) for the Treatment of Solid Tumors. *J. Med. Chem.* **63**, 52–65

54. Canon, J., Rex, K., Saiki, A. Y., Mohr, C., Cooke, K., Bagal, D., Gaida, K., Holt, T., Knutson, C. G., Koppada, N., Lanman, B. A., Werner, J., Rapaport, A. S., San Miguel, T., Ortiz, R.,

Osgood, T., Sun, J. R., Zhu, X., McCarter, J. D., Volak, L. P., Houk, B. E., Fakih, M. G., O'Neil, B. H., Price, T. J., Falchook, G. S., Desai, J., Kuo, J., Govindan, R., Hong, D. S., Ouyang, W., Henary, H., Arvedson, T., Cee, V. J., and Lipford, J. R. (2019) The clinical KRAS(G12C) inhibitor AMG 510 drives anti-tumour immunity. *Nature*. **575**, 217–223

55. Gehringer, M., and Laufer, S. A. (2019) Emerging and Re-Emerging Warheads for Targeted Covalent Inhibitors: Applications in Medicinal Chemistry and Chemical Biology. *J. Med. Chem.* **62**, 5673–5724

56. Prior, I. A., Lewis, P. D., and Mattos, C. (2012) A comprehensive survey of ras mutations in cancer. *Cancer Res.* **72**, 2457–2467

57. Seo, K. Y., Jelinsky, S. A., and Loechler, E. L. (2000) Factors that influence the mutagenic patterns of DNA adducts from chemical carcinogens. *Mutat. Res.* **463**, 215–246

58. Chen, M., Peters, A., Huang, T., and Nan, X. (2016) Ras Dimer Formation as a New Signaling Mechanism and Potential Cancer Therapeutic Target. *Rev. Med. Chem.* **16**, 391–403

59. Spencer-Smith, R., Koide, A., Zhou, Y., Eguchi, R. R., Sha, F., Gajwani, P., Santana, D., Gupta, A., Jacobs, M., Herrero-Garcia, E., Cobbert, J., Lavoie, H., Smith, M., Rajakulendran, T., Dowdell, E., Okur, M. N., Dementieva, I., Sicheri, F., Therrien, M., Hancock, J. F., Ikura, M., Koide, S., and O'Bryan, J. P. (2017) Inhibition of RAS function through targeting an allosteric regulatory site. *Nat. Chem. Biol.* **13**, 62–68

60. Khan, I., Spencer-Smith, R., and O'Bryan, J. P. (2019) Targeting the α4–α5 dimerization interface of K-RAS inhibits tumor formation in vivo. *Oncogene*. **38**, 2984–2993

61. Sarkar-Banerjee, S., Sayyed-Ahmad, A., Prakash, P., Cho, K. J., Waxham, M. N., Hancock, J. F., and Gorfe, A. A. (2017) Spatiotemporal Analysis of K-Ras Plasma Membrane Interactions Reveals Multiple High Order Homo-oligomeric Complexes. *J. Am. Chem. Soc.* **139**, 13466–13475

62. Prakash, P., Sayyed-Ahmad, A., Cho, K. J., Dolino, D. M., Chen, W., Li, H., Grant, B. J., Hancock, J. F., and Gorfe, A. A. (2017) Computational and biochemical characterization of two partially overlapping interfaces and multiple weak-affinity K-Ras dimers. *Sci. Rep.* **7**, 1–11

63. Bery, N., Legg, S., Debreczeni, J., Breed, J., Embrey, K., Stubbs, C., Kolasinska-Zwierz, P., Barrett, N., Marwood, R., Watson, J., Tart, J., Overman, R., Miller, A., Phillips, C., Minter,

R., and Rabbitts, T. H. (2019) KRAS-specific inhibition using a DARPin binding to a site in the allosteric lobe. *Nat. Commun.* **10**, 1–10

64. Poulikakos, P. I., and Rosen, N. (2011) Mutant BRAF melanomas-dependence and resistance. *Cancer Cell*. **19**, 11–15
65. Poulikakos, P. I., Zhang, C., Bollag, G., Shokat, K. M., and Rosen, N. (2010) RAF inhibitors transactivate RAF dimers and ERK signalling in cells with wild-type BRAF. *Nature*. **464**, 427–430
66. Hatzivassiliou, G., Song, K., Yen, I., Brandhuber, B. J., Anderson, D. J., Alvarado, R., Ludlam, M. J. C., Stokoe, D., Gloor, S. L., Vigers, G., Morales, T., Aliagas, I., Liu, B., Sideris, S., Hoeflich, K. P., Jaiswal, B. S., Seshagiri, S., Koeppen, H., Belvin, M., Friedman, L. S., and Malek, S. (2010) RAF inhibitors prime wild-type RAF to activate the MAPK pathway and enhance growth. *Nature*. **464**, 431–435
67. Cheng, Y., and Tian, H. (2017) Current development status of MEK inhibitors. *Molecules*. **22**, 1–20
68. Wee, S., Jagani, Z., Kay, X. X., Loo, A., Dorsch, M., Yao, Y. M., Sellers, W. R., Lengauer, C., and Stegmeier, F. (2009) PI3K pathway activation mediates resistance to MEK inhibitors in KRAS mutant cancers. *Cancer Res.* **69**, 4286–4293
69. Johnson, G. L., Stuhlmiller, T. J., Angus, S. P., Zawistowski, J. S., and Graves, L. M. (2014) Molecular pathways: Adaptive Kinome reprogramming in response to targeted inhibition of the BRAF-MEK-ERK pathway in cancer. *Clin. Cancer Res.* **20**, 2516–2522
70. Yang, J., Nie, J., Ma, X., Wei, Y., Peng, Y., and Wei, X. (2019) Targeting PI3K in cancer: Mechanisms and advances in clinical trials. *Mol. Cancer*. **18**, 1–28
71. Arend, R. C., Davis, A. M., Chimiczewski, P., O'Malley, D. M., Provencher, D., Vergote, I., Ghamande, S., and Birrer, M. J. (2020) EMR 20006-012: A phase II randomized double-blind placebo controlled trial comparing the combination of pimasertib (MEK inhibitor) with SAR245409 (PI3K inhibitor) to pimasertib alone in patients with previously treated unresectable borderline or low grade. *Gynecol. Oncol.* **156**, 301–307
72. Bardia, A., Gounder, M., Rodon, J., Janku, F., Lolkema, M. P., Stephenson, J. J., Bedard, P. L., Schuler, M., Sessa, C., LoRusso, P., Thomas, M., Maacke, H., Evans, H., Sun, Y., and Tan, D. S. W. (2020) Phase Ib Study of Combination Therapy with MEK Inhibitor Binimetinib and Phosphatidylinositol 3-Kinase Inhibitor Buparlisib in Patients with

Advanced Solid Tumors with RAS/RAF Alterations. *Oncologist*. **25**, 160–169

73. Shapiro, G. I., LoRusso, P., Kwak, E., Pandya, S., Rudin, C. M., Kurkjian, C., Cleary, J. M., Pilat, M. J., Jones, S., de Crespigny, A., Fredrickson, J., Musib, L., Yan, Y., Wongchenko, M., Hsieh, H. J., Gates, M. R., Chan, I. T., and Bendell, J. (2020) Phase Ib study of the MEK inhibitor cobimetinib (GDC-0973) in combination with the PI3K inhibitor pictilisib (GDC-0941) in patients with advanced solid tumors. *Invest. New Drugs*. **38**, 419–432
74. Ramanathan, R. K., Von Hoff, D. D., Eskens, F., Blumenschein, G., Richards, D., Genvresse, I., Reschke, S., Granvil, C., Skubala, A., Peña, C., and Mross, K. (2020) Phase Ib Trial of the PI3K Inhibitor Copanlisib Combined with the Allosteric MEK Inhibitor Refametinib in Patients with Advanced Cancer. *Target. Oncol.* **15**, 163–174
75. Bedard, P. L., Tabernero, J., Janku, F., A.wainberg, Z., Paz-Ares, L., Vansteenkiste, J., Cutsem, E. Van, Pérez-García, J., Stathis, A., Britten, C. D., Le, N., Carter, K., Demanse, D., Csonka, D., Peters, M., Zubel, A., Nauwelaerts, H., and Sessa, C. (2015) A Phase Ib dose-escalation study of the oral pan-PI3K inhibitor buparlisib (BKM120) in combination with the oral MEK1/2 inhibitor trametinib (GSK1120212) in patients with selected advanced solid tumors. *Clin. Cancer Res.* **21**, 730–738
76. Grilley-Olson, J. E., Bedard, P. L., Fasolo, A., Cornfeld, M., Cartee, L., Razak, A. R. A., Stayner, L. A., Wu, Y., Greenwood, R., Singh, R., Lee, C. B., Bendell, J., Burris, H. A., Del Conte, G., Sessa, C., and Infante, J. R. (2016) A phase Ib dose-escalation study of the MEK inhibitor trametinib in combination with the PI3K/mTOR inhibitor GSK2126458 in patients with advanced solid tumors. *Invest. New Drugs*. **34**, 740–749
77. Yan, C., and Theodorescu, D. (2018) RAL GTPases: Biology and Potential as Therapeutic Targets in Cancer. *Pharmacol. Rev.* **70**, 1–11
78. Feig, L. A., Urano, T., and Cantor, S. (1996) Evidence for a Ras/Ral signaling cascade. *Trends Biochem. Sci.* **21**, 438–441
79. Chardin, P., and Tavitian, A. (1986) The ral gene: a new ras related gene isolated by the use of a synthetic probe. *EMBO J.* **5**, 2203–2208
80. Gentry, L. R., Nishimura, A., Cox, A. D., Martin, T. D., Tsygankov, D., Nishida, M., Elston, T. C., and Der, C. J. (2015) Divergent roles of CAAX motif-signaled posttranslational modifications in the regulation and subcellular localization of Ral GTPases. *J. Biol. Chem.* **290**, 22851–22861

81. Gentry, L. R., Martin, T. D., Reiner, D. J., and Der, C. J. (2014) Ral small GTPase signaling and oncogenesis: More than just 15 minutes of fame. *Biochim. Biophys. Acta - Mol. Cell Res.* **1843**, 2976–2988

82. Shirakawa, R., Fukai, S., Kawato, M., Higashi, T., Kondo, H., Ikeda, T., Nakayama, E., Okawa, K., Nureki, O., Kimura, T., Kita, T., and Horiuchi, H. (2009) Tuberous sclerosis tumor suppressor complex-like complexes act as GTPase-activating proteins for Ral GTPases. *J. Biol. Chem.* **284**, 21580–21588

83. Casey, P. J., and Seabra, M. C. (1996) Protein prenyltransferases. *J. Biol. Chem.* **271**, 5289–5292

84. Lim, K.-H., Brady, D. C., Kashatus, D. F., Ancrile, B. B., Der, C. J., Cox, A. D., and Counter, C. M. (2010) Aurora-A Phosphorylates, Activates, and Relocalizes the Small GTPase RalA. *Mol. Cell. Biol.* **30**, 508–523

85. Wu, J. C., Chen, T. Y., Yu, C. T. R., Tsai, S. J., Hsu, J. M., Tang, M. J., Chou, C. K., Lin, W. J., Yuan, C. J., and Huang, C. Y. F. (2005) Identification of V23RalA-Ser194 as a critical mediator for Aurora-A-induced cellular motility and transformation by small pool expression screening. *J. Biol. Chem.* **280**, 9013–9022

86. Wang, H., Owens, C., Chandra, N., Conaway, M. R., Brautigan, D. L., and Theodorescu, D. (2010) Phosphorylation of RalB is important for bladder cancer cell growth and metastasis. *Cancer Res.* **70**, 8760–8769

87. Martin, T. D., Mitin, N., Cox, A. D., Yeh, J. J., and Der, C. J. (2012) Phosphorylation by protein kinase Cα regulates RalB small GTPase protein activation, subcellular localization, and effector utilization. *J. Biol. Chem.* **287**, 14827–14836

88. Park, S. H., and Weinberg, R. A. (1995) A putative effector of Ral has homology to Rho/Rac GTPase activating proteins. *Oncogene*. **11**, 2349–2355

89. Jullien-Flores, V., Dorseuil, O., Romero, F., Letourneur, F., Saragosti, S., Berger, R., Tavitian, A., Gacon, G., and Camonis, J. H. (1995) Bridging Ral GTPase to Rho Pathways. *J. Biol. Chem.* **270**, 22473–22477

90. Cantor, S. B., Urano, T., and Feig, L. a (1995) Identification and characterization of Ral-binding protein 1, a potential downstream target of Ral GTPases. *Mol. Cell. Biol.* **15**, 4578–4584

91. Fenwick, R. B., Campbell, L. J., Rajasekar, K., Prasannan, S., Nietlispach, D., Camonis, J.,

Owen, D., and Mott, H. R. (2010) The RalB-RLIP76 complex reveals a novel mode of ral-effector interaction. *Structure*. **18**, 985–995

92. Matsubara, K., Hinoi, T., Koyama, S., and Kikuchi, A. (1997) The post-translational modifications of Ral and Rac1 are important for the action of Ral-binding protein 1, a putative effector protein of Ral. *FEBS Lett.* **410**, 169–174
93. Mott, H. R., and Owen, D. (2010) RLIP76 (RalBP1): The first piece of the structural puzzle. *Small GTPases*. **1**, 157–160
94. Mott, H. R., and Owen, D. (2014) Structure and function of RLIP76 (RalBP1): An intersection point between Ras and Rho signalling. *Biochem. Soc. Trans.* **42**, 52–58
95. Jullien-Flores, V., Mahé, Y., Mirey, G., Leprince, C., Meunier-Bisceuil, B., Sorkin, A., and Camonis, J. H. (2000) RLIP76, an effector of the GTPase Ral, interacts with the AP2 complex: involvement of the Ral pathway in receptor endocytosis. *J. Cell Sci.* **113**, 2837–2844
96. Yamaguchi, A., Urano, T., Goi, T., and Feig, L. A. (1997) An Eps homology (EH) domain protein that binds to the Ral-GTPase target, RalBP1. *J. Biol. Chem.* **272**, 31230–31234
97. Ikeda, M., Ishida, O., Hinoi, T., Kishida, S., and Kikuchi, A. (1998) Identification and characterization of a novel protein interacting with Ral-binding protein 1, a putative effector protein of Ral. *J. Biol. Chem.* **273**, 814–821
98. Coon, B. G., Burgner, J., Camonis, J. H., and Aguilar, R. C. (2010) The Epsin family of endocytic adaptors promotes fibrosarcoma migration and invasion. *J. Biol. Chem.* **285**, 33073–33081
99. Smith, S. C., Oxford, G., Baras, A. S., Owens, C., Havaleshko, D., Brautigan, D. L., Safo, M. K., and Theodorescu, D. (2007) Expression of Ral GTPases, their effectors, and activators in human bladder cancer. *Clin. Cancer Res.* **13**, 3803–3813
100. Hudson, M. E., Pozdnyakova, I., Haines, K., Mor, G., and Snyder, M. (2007) Identification of differentially expressed proteins in ovarian cancer using high-density protein microarrays. *Proc. Natl. Acad. Sci. U. S. A.* **104**, 17494–17499
101. Vatsyayan, R., Lelsani, P. C. R., Awasthi, S., and Singhal, S. S. (2010) RLIP76: A versatile transporter and an emerging target for cancer therapy. *Biochem. Pharmacol.* **79**, 1699–1705
102. Moskalenko, S., Henry, D. O., Rosse, C., Mirey, G., Camonis, J. H., and White, M. A.

(2002) The exocyst is a Ral effector complex. *Nat. Cell Biol.* **4**, 66–72

103. Jin, R., Junutula, J. R., Matern, H. T., Ervin, K. E., Scheller, R. H., and Brunger, A. T. (2005) Exo84 and Sec5 are competitive regulatory Sec6/8 effectors to the RalA GTPase. *EMBO J.* **24**, 2064–2074
104. Sugihara, K., Asano, S., Tanaka, K., Iwamatsu, A., Okawa, K., and Ohta, Y. (2002) The exocyst complex binds the small GTPase RalA to mediate filopodia formation. *Nat. Cell Biol.* **4**, 73–78
105. Moskalenko, S., Tong, C., Rosse, C., Mirey, G., Formstecher, E., Daviet, L., Camonis, J., and White, M. A. (2003) Ral GTPases Regulate Exocyst Assembly through Dual Subunit Interactions. *J. Biol. Chem.* **278**, 51743–51748
106. Bodemann, B. O., Orvedahl, A., Cheng, T., Ram, R. R., Ou, Y. H., Formstecher, E., Maiti, M., Hazelett, C. C., Wauson, E. M., Balakireva, M., Camonis, J. H., Yeaman, C., Levine, B., and White, M. A. (2011) RalB and the exocyst mediate the cellular starvation response by direct activation of autophagosome assembly. *Cell*. **144**, 253–267
107. Chien, Y., Kim, S., Bumeister, R., Loo, Y. M., Kwon, S. W., Johnson, C. L., Balakireva, M. G., Romeo, Y., Kopelovich, L., Gale, M., Yeaman, C., Camonis, J. H., Zhao, Y., and White, M. A. (2006) RalB GTPase-Mediated Activation of the IκB Family Kinase TBK1 Couples Innate Immune Signaling to Tumor Cell Survival. *Cell*. **127**, 157–170
108. Frankel, P., Aronheim, A., Kavanagh, E., Balda, M. S., Matter, K., Bunney, T. D., and Marshall, C. J. (2005) Ra1A interacts with ZONAB in a cell density-dependent manner and regulates its transcriptional activity. *EMBO J.* **24**, 54–62
109. Ohta, Y., Suzuki, N., Nakamura, S., Hartwig, J. H., and Stossel, T. P. (1999) The small GTPase RaIA targets filamin to induce filopodia. *Proc. Natl. Acad. Sci. U. S. A.* **96**, 2122–2128
110. Sidhu, R. S., Clough, R. R., and Bhullar, R. P. (2005) Regulation of phospholipase C-δ1 through direct interactions with the small GTPase Ral and calmodulin. *J. Biol. Chem.* **280**, 21933–21941
111. Luo, J. Q., Liu, X., Frankel, P., Rotunda, T., Ramos, M., Flom, J., Jiang, H., Feig, L. A., Morris, A. J., Kahn, R. A., and Foster, D. A. (1998) Functional association between ArF and RalA in active phospholipase D complex. *Proc. Natl. Acad. Sci. U. S. A.* **95**, 3632–3637

112. Hamad, N. M., Elconin, J. H., Karnoub, A. E., Bai, W., Rich, J. N., Abraham, R. T., Der, C. J., and Counter, C. M. (2002) Distinct requirements for Ras oncogenesis in human versus mouse cells. *Genes Dev.* **16**, 2045–2057

113. Lim, K., Hayer, K. O., Adam, S. J., Kendall, S. D., Campbell, P. M., Der, C. J., Counter, C. M., Carolina, N., Hill, C., and Carolina, N. (2006) Divergent Roles for RalA and RalB in Malignant Growth of Human Pancreatic Carcinoma Cells. *Curr. Biol.* **16**, 2385–2394

114. Lim, K., Baines, A. T., Fiordalisi, J. J., Shipitsin, M., Feig, L. A., Cox, A. D., Der, C. J., and Counter, C. M. (2005) Activation of RalA is critical for Ras-induced tumorigenesis of human cells. *Cancer Cell*. **7**, 533–545

115. Chien, Y., and White, M. A. (2003) RAL GTPases are linchpin modulators of human tumour-cell proliferation and survival. *EMBO Rep.* **4**, 800–806

116. Neel, N. F., Rossman, K. L., Martin, T. D., Hayes, T. K., Yeh, J. J., and Der, C. J. (2012) The RalB Small GTPase Mediates Formation of Invadopodia through a GTPase-Activating Protein-Independent Function of the RalBP1 / RLIP76 Effector. *Mol. Cell. Biol.* **32**, 1374–1386

117. Falsetti, S. C., Wang, D., Peng, H., Carrico, D., Cox, A. D., Der, C. J., Hamilton, A. D., and Sebti, S. M. (2007) Geranylgeranyltransferase I inhibitors target RalB to inhibit anchorage-dependent growth and induce apoptosis and RalA to inhibit anchorage-independent growth. *Mol. Cell. Biol.* **27**, 8003–8014

118. Yan, C., Liu, D., Li, L., Wempe, M. F., Guin, S., Khanna, M., Meier, J., Hoffman, B., Owens, C., Wysoczynski, C. L., Nitz, M. D., Knabe, W. E., Ahmed, M., Brautigan, D. L., Paschal, B. M., Schwartz, M. A., Jones, D. N. M., Ross, D., Meroueh, S. O., and Theodorescu, D. (2014) Discovery and characterization of small molecules that target the GTPase Ral. *Nature*. **515**, 443–447

119. Walsh, T. G., Wersäll, A., and Poole, A. W. (2019) Characterisation of the Ral GTPase inhibitor RBC8 in human and mouse platelets. *Cell. Signal.* **59**, 34–40

120. Cuesta, A., and Taunton, J. (2019) Lysine-targeted inhibitors and chemoproteomic probes. *Annu. Rev. Biochem.* **88**, 365–381

121. Gambini, L., Baggio, C., Udompholkul, P., Jossart, J., Salem, A. F., Perry, J. J. P., and Pellecchia, M. (2019) Covalent Inhibitors of Protein-Protein Interactions Targeting Lysine, Tyrosine, or Histidine Residues. *J. Med. Chem.* **62**, 5616–5627

122. Bum-Erdene, K., Liu, D., Gonzalez-Gutierrez, G., Ghozayel, M. K., Xu, D., and Meroueh, S. O. (2020) Small-molecule covalent bond formation at tyrosine creates a binding site and inhibits activation of Ral GTPases. *Proc. Natl. Acad. Sci.* **117**, 7131–7139

123. Cox, A. D., and Der, C. J. (1992) Protein prenylation: more than just glue? *Curr. Opin. Cell Biol.* **4**, 1008–1016

124. Karasic, T. B., Chiorean, E. G., Sebti, S. M., and O'Dwyer, P. J. (2019) A Phase I Study of GGTI-2418 (Geranylgeranyl Transferase I Inhibitor) in Patients with Advanced Solid Tumors. *Target. Oncol.* **14**, 613–618

125. Thomas, J. C., Cooper, J. M., Clayton, N. S., Wang, C., White, M. A., Abell, C., Owen, D., and Mott, H. R. (2016) Inhibition of Ral GTPases using a stapled peptide approach. *J. Biol. Chem.* **291**, 18310–18325

126. Hurd, C. A., Mott, H. R., and Owen, D. (2020) Therapeutic Peptides Targeting the Ras Superfamily. *Pept. Sci.* in press

127. Vinogradov, A. A., Yin, Y., and Suga, H. (2019) Macrocyclic Peptides as Drug Candidates: Recent Progress and Remaining Challenges. *J. Am. Chem. Soc.* **141**, 4167–4181

128. Deyle, K., Kong, X. D., and Heinis, C. (2017) Phage Selection of Cyclic Peptides for Application in Research and Drug Development. *Acc. Chem. Res.* **50**, 1866–1874

129. Passioura, T., and Suga, H. (2017) A RaPID way to discover nonstandard macrocyclic peptide modulators of drug targets. *Chem. Commun.* **53**, 1931–1940

130. Tavassoli, A. (2017) SICLOPPS cyclic peptide libraries in drug discovery. *Curr. Opin. Chem. Biol.* **38**, 30–35

131. Bullock, B. N., Jochim, A. L., and Arora, P. S. (2011) Assessing helical protein interfaces for inhibitor design. *J. Am. Chem. Soc.* **133**, 14220–14223

132. Kim, Y.-W., Grossmann, T. N., and Verdine, G. L. (2011) Synthesis of all-hydrocarbon stapled α-helical peptides by ring-closing olefin metathesis. *Nat. Protoc.* **6**, 761–771

133. Schafmeister, C. E., Po, J., and Verdine, G. L. (2000) An All-Hydrocarbon Cross-Linking System for Enhancing the Helicity and Metabolic Stability of Peptides. *J. Am. Chem. Soc.* **122**, 5891–5892

134. Lau, Y. H., De Andrade, P., Wu, Y., and Spring, D. R. (2015) Peptide stapling techniques based on different macrocyclisation chemistries. *Chem. Soc. Rev.* **44**, 91–102

135. Fairlie, D. P., and Dantas de Araujo, A. (2016) Stapling peptides using cysteine

crosslinking. *Biopolymers*. **106**, 843–852

136. Baek, S., Kutchukian, P. S., Verdine, G. L., Huber, R., Holak, T. A., Lee, K. W., and Popowicz, G. M. (2012) Structure of the stapled p53 peptide bound to Mdm2. *J. Am. Chem. Soc.* **134**, 103–6
137. Walensky, L. D., and Bird, G. H. (2014) Hydrocarbon-stapled peptides: principles, practice, and progress. *J. Med. Chem.* **57**, 6275–6288
138. Bird, G. H., Mazzola, E., Opoku-Nsiah, K., Lammert, M. A., Godes, M., Neuberg, D. S., and Walensky, L. D. (2016) Biophysical determinants for cellular uptake of hydrocarbon-stapled peptide helices. *Nat. Chem. Biol.* **12**, 845–852
139. Jo, H., Meinhardt, N., Wu, Y., Kulkarni, S., Hu, X., Low, K. E., Davies, P. L., Degrado, W. F., and Greenbaum, D. C. (2012) Development of α - Helical Calpain Probes by Mimicking a Natural Protein − Protein Interaction. *J. Am. Chem. Soc.* **134**, 17704–17713
140. Shepherd, N. E., Hoang, H. N., Abbenante, G., and Fairlie, D. P. (2005) Single turn peptide alpha helices with exceptional stability in water. *J. Am. Chem. Soc.* **127**, 2974–2983
141. Spokoyny, A. M., Zou, Y., Ling, J. J., Yu, H., Lin, Y. S., and Pentelute, B. L. (2013) A perfluoroaryl-cysteine SNAr chemistry approach to unprotected peptide stapling. *J. Am. Chem. Soc.* **135**, 5946–5949
142. Wang, Y., and Chou, D. H. C. (2015) A Thiol-Ene Coupling Approach to Native Peptide Stapling and Macrocyclization. *Angew. Chemie - Int. Ed.* **54**, 10931–10934
143. Kawamoto, S. A., Coleska, A., Ran, X., Yi, H., Yang, C. Y., and Wang, S. (2012) Design of triazole-stapled BCL9 α-helical peptides to target the β-catenin/B-cell CLL/lymphoma 9 (BCL9) protein-protein interaction. *J. Med. Chem.* **55**, 1137–1146
144. Blackwell, H. E., and Grubbs, R. H. (1998) Highly efficient synthesis of covalently cross-linked peptide helices by ring-closing metathesis. *Angew. Chemie - Int. Ed.* **37**, 3281–3284
145. Walensky, L. D., Kung, A. L., Escher, I., Malia, T. J., Barbuto, S., Wright, R. D., Wagner, G., Verdine, G. L., and Korsmeyer, S. J. (2004) Activation of apoptosis in vivo by a hydrocarbon-stapled BH3 helix. *Science*. **305**, 1466–1470
146. Sawyer, T. K., Partridge, A. W., Kaan, H. Y. K., Juang, Y. C., Lim, S., Johannes, C., Yuen, T. Y., Verma, C., Kannan, S., Aronica, P., Tan, Y. S., Sherborne, B., Ha, S., Hochman, J.,

Chen, S., Surdi, L., Peier, A., Sauvagnat, B., Dandliker, P. J., Brown, C. J., Ng, S., Ferrer, F., and Lane, D. P. (2018) Macrocyclic α helical peptide therapeutic modality: A perspective of learnings and challenges. *Bioorganic Med. Chem.* **26**, 2807–2815

147. Chang, Y. S., Graves, B., Guerlavais, V., Tovar, C., Packman, K., To, K.-H., Olson, K. A., Kesavan, K., Gangurde, P., Mukherjee, A., Baker, T., Darlak, K., Elkin, C., Filipovic, Z., Qureshi, F. Z., Cai, H., Berry, P., Feyfant, E., Shi, X. E., Horstick, J., Annis, D. A., Manning, A. M., Fotouhi, N., Nash, H., Vassilev, L. T., and Sawyer, T. K. (2013) Stapled α−helical peptide drug development: A potent dual inhibitor of MDM2 and MDMX for p53-dependent cancer therapy. *Proc. Natl. Acad. Sci. U. S. A.* **110**, 3445–3454

148. Brown, C. J., Quah, S. T., Jong, J., Goh, A. M., Chiam, P. C., Khoo, K. H., Choong, M. L., Lee, M. A., Yurlova, L., Zolghadr, K., Joseph, T. L., Verma, C. S., and Lane, D. P. (2013) Stapled peptides with improved potency and specificity that activate p53. *ACS Chem. Biol.* **8**, 506–512

149. Bernal, F., Wade, M., Godes, M., Davis, T. N., Whitehead, D. G., Kung, A. L., Wahl, G. M., and Walensky, L. D. (2010) A Stapled p53 Helix Overcomes HDMX-Mediated Suppression of p53. *Cancer Cell*. **18**, 411–422

150. Wachter, F., Morgan, A. M., Godes, M., Mourtada, R., Bird, G. H., and Walensky, L. D. (2017) Mechanistic validation of a clinical lead stapled peptide that reactivates p53 by dual HDM2 and HDMX targeting. *Oncogene*. **36**, 2184–2190

151. Bernal, F., Tyler, A. F., Korsmeyer, S. J., Walensky, L. D., and Verdine, G. L. (2007) Reactivation of the p53 tumor suppressor pathway by a stapled p53 peptide. *J. Am. Chem. Soc.* **129**, 2456–2457

152. Kussie, P. H., Gorina, S., Marechal, V., Elenbaas, B., Moreau, J., Levine, A. J., and Pavletich, N. P. (1996) Structure of the MDM2 oncoprotein bound to the p53 tumor suppressor transactivation domain. *Science*. **274**, 948–953

153. Meric-Bernstam, F., Saleh, M. N., Infante, J. R., Goel, S., Falchook, G. S., Shapiro, G., Chung, K. Y., Conry, R. M., Hong, D. S., Wang, J. S.-Z., Steidl, U., Walensky, L. D., Guerlavais, V., Payton, M., Annis, D. A., Aivado, M., and Patel, M. R. (2017) Phase I trial of a novel stapled peptide ALRN-6924 disrupting MDMX- and MDM2-mediated inhibition of WT p53 in patients with solid tumors and lymphomas. *J. Clin. Oncol.* **35**, 2505–2505

154. Shustov, A. R., Horwitz, S. M., Zain, J., Patel, M. R., Goel, S., Sokol, L., Meric-Bernstam, F., Shapiro, G., Dwivedy Nasta, S., Janakiram, M., Weinstock, D. M., Korn, R., Payton, M., Annis, D. A., Pinchasik, D., Aivado, M., and Mehta, A. (2018) Preliminary Results of the Stapled Peptide ALRN-6924, a Dual Inhibitor of MDMX and MDM2, in Two Phase IIa Dose Expansion Cohorts in Relapsed/Refractory TP53 Wild-Type Peripheral T-Cell Lymphoma. *Blood*. **132**, 1623–1623

155. Matsson, P., Doak, B. C., Over, B., and Kihlberg, J. (2016) Cell permeability beyond the rule of 5. *Adv. Drug Deliv. Rev.* **101**, 42–61

156. Chatterjee, J., Gilon, C., Hoffman, A., and Kessler, H. (2008) N-methylation of peptides: A new perspective in medicinal chemistry. *Acc. Chem. Res.* **41**, 1331–1342

157. Chatterjee, J., Rechenmacher, F., and Kessler, H. (2013) N-Methylation of peptides and proteins: An important element for modulating biological functions. *Angew. Chemie - Int. Ed.* **52**, 254–269

158. Gräslund, A., Madani, F., Lindberg, S., Langel, Ü., and Futaki, S. (2011) Mechanisms of cellular uptake of cell-penetrating peptides. *J. Biophys.* 10.1155/2011/414729

159. Guidotti, G., Brambilla, L., and Rossi, D. (2017) Cell-Penetrating Peptides: From Basic Research to Clinics. *Trends Pharmacol. Sci.* **38**, 406–424

160. Hewitt, W. M., Leung, S. S. F., Pye, C. R., Ponkey, A. R., Bednarek, M., Jacobson, M. P., and Lokey, R. S. (2015) Cell-permeable cyclic peptides from synthetic libraries inspired by natural products. *J. Am. Chem. Soc.* **137**, 715–721

161. White, T. R., Renzelman, C. M., Rand, A. C., Rezai, T., McEwen, C. M., Gelev, V. M., Turner, R. A., Linington, R. G., Leung, S. S. F., Kalgutkar, A. S., Bauman, J. N., Zhang, Y., Liras, S., Price, D. A., Mathiowetz, A. M., Jacobson, M. P., and Lokey, R. S. (2011) On-resin N-methylation of cyclic peptides for discovery of orally bioavailable scaffolds. *Nat. Chem. Biol.* **7**, 810–817

162. Rezai, T., Yu, B., Millhauser, G. L., Jacobson, M. P., and Lokey, R. S. (2006) Testing the conformational hypothesis of passive membrane permeability using synthetic cyclic peptide diastereomers. *J. Am. Chem. Soc.* **128**, 2510–2511

163. Chu, Q., Moellering, R. E., Hilinski, G. J., Kim, Y., Grossmann, T. N., Yeh, T., and Verdine, G. L. (2014) Towards understanding cell penetration by stapled peptides. *Medchemcomm*. **6**, 111–119

164. Sakagami, K., Masuda, T., Kawano, K., and Futaki, S. (2018) Importance of Net Hydrophobicity in the Cellular Uptake of All-Hydrocarbon Stapled Peptides. *Mol. Pharm.* **15**, 1332–1340

165. Green, M., and Loewenstein, P. M. (1988) Autonomous functional domains of chemically synthesized human immunodeficiency virus tat trans-activator protein. *Cell*. **55**, 1179–1188

166. Derossi, D., Joliot, A. H., Chassaing, G., and Prochiantz, A. (1994) The third helix of the Antennapedia homeodomain translocates through biological membranes. *J. Biol. Chem.* **269**, 10444–10450

167. Hinshaw, J. C., and Prestwich, G. D. (2001) The design, synthesis, and evaluation of molecules that enable or enhance cellular uptake: Peptoid molecular transporters. *Chemtracts*. **14**, 391–394

168. Elmquist, A., Lindgren, M., Bartfai, T., and Langel, Ü. (2001) Ve-cadherin-derived cell-penetrating peptide, pVEC with carrier functions. *Exp. Cell Res.* **269**, 237–244

169. Oehlke, J., Scheller, A., Wiesner, B., Krause, E., Beyermann, M., Klauschenz, E., Melzig, M., and Bienert, M. (1998) Cellular uptake of an α-helical amphipathic model peptide with the potential to deliver polar compounds into the cell interior non-endocytically. *Biochim. Biophys. Acta - Biomembr.* **1414**, 127–139

170. Pooga, M., Soomets, U., Hallbrink, M., Valkna, A., Saar, K., Rezaei, K., Kahl, U., Hao, J. X., Xu, X. J., Wiesenfeld-Hallin, Z., Hokfelt, T., Bartfai, T., and Langel, U. (1998) Cell penetrating PNA constructs regulate galanin receptor levels and modify pain transmission in vivo. *Nat. Biotechnol.* **16**, 857–861

171. Bruno, B. J., Miller, G. D., and Lim, C. S. (2013) Basics and recent advances in peptide and protein drug delivery. *Ther. Deliv.* **4**, 1443–1467

172. Smith, G. P. (1985) Filamentous fusion phage: Novel expression vectors that display cloned antigens on the virion surface. *Science*. **228**, 1315–1317

173. Hoogenboom, H. R., Griffiths, A. D., Johnson, K. S., Chiswell, D. J., Hudson, P., and Winter, G. (1991) Multi-subunit proteins on the surface of filamentous phage: Methodologies for displaying antibody (Fab) heavy and light chains. *Nucleic Acids Res.* **19**, 4133–4137

174. Clackson, T., Hoogenboom, H. R., Griffiths, A. D., and Winter, G. (1991) Making

antibody fragments using phage display libraries. *Nature*. **352**, 624–628

175. Pelletier, J. N., Arndt, K. M., Pluckthun, A., and Michnick, S. W. (1999) An in vivo library-versus-library selection of optimized protein-protein interactions. *Nat. Biotechnol.* **17**, 683–690
176. Tavassoli, A., and Benkovic, S. J. (2007) Split-intein mediated circular ligation used in the synthesis of cyclic peptide libraries in E. coli. *Nat. Protoc.* **2**, 1126–1133
177. Scott, C. P., Abel-Santos, E., Wall, M., Wahnon, D. C., and Benkovic, S. J. (1999) Production of cyclic peptides and proteins in vivo. *Proc. Natl. Acad. Sci. U. S. A.* **96**, 13638–13643
178. Odegrip, R., Coomber, D., Eldridge, B., Hederer, R., Kuhlman, P. A., Ullman, C., FitzGerald, K., and McGregor, D. (2004) CIS display: In vitro selection of peptides from libraries of protein-DNA complexes. *Proc. Natl. Acad. Sci.* **101**, 2806–2810
179. Roberts, R. W., and Szostak, J. W. (1997) RNA-peptide fusions for the in vitro selection of peptides and proteins. *Proc. Natl. Acad. Sci.* **94**, 12297–12302
180. Galá, A., Comor, L., Horvatic´, A., Horvatic´, H., Kuleš, J., Guillemin, N., Mrljak, V., and Bhide, M. (2016) Library-based display technologies: where do we stand? *Mol. BioSyst*. **12**, 2342
181. Campbell, L. J., Peppa, M., Crabtree, M. D., Shafiq, A., McGough, N. F., Mott, H. R., and Owen, D. (2015) Thermodynamic mapping of effector protein interfaces with RalA and RalB. *Biochemistry*. **54**, 1380–1389
182. Owen, D., Campbell, L. J., Littlefield, K., Evetts, K. A., Li, Z., Sacks, D. B., Lowe, P. N., and Mott, H. R. (2008) The IQGAP1-Rac1 and IQGAP1-Cdc42 interactions: Interfaces differ between the complexes. *J. Biol. Chem.* **283**, 1692–1704
183. Whitmore, L., and Wallace, B. A. (2004) DICHROWEB, an online server for protein secondary structure analyses from circular dichroism spectroscopic data. *Nucleic Acids Res.* **32**, 668–673
184. Sreerama, N., and Woody, R. W. (2000) Estimation of protein secondary structure from circular dichroism spectra: comparison of CONTIN, SELCON, and CDSSTR methods with an expanded reference set. *Anal. Biochem.* **287**, 252–260
185. Manavalan, P., and Johnson, W. C. (1987) Variable selection method improves the prediction of protein secondary structure from circular dichroism spectra. *Anal.*

*Biochem.* **167**, 76–85

186. Lau, S. Y., Taneja, a K., and Hodges, R. S. (1984) Synthesis of a model protein of defined secondary and quaternary structure. Effect of chain length on the stabilization and formation of two-stranded alpha-helical coiled-coils. *J. Biol. Chem.* **259**, 13253–13261
187. Zhou, N. E., Kay, C. M., and Hodges, R. S. (1992) Synthetic model proteins. *J. Biol. Chem.* **267**, 2664–2670
188. Gorman, C., Skinner, R. H., Skelly, J. V., Neidle, S., and Lowe, P. N. (1996) Equilibrium and kinetic measurements reveal rapidly reversible binding of Ras to Raf. *J. Biol. Chem.* **271**, 6713–6719
189. Chee, S. M. Q., Wongsantichon, J., Siau, J., Thean, D., Ferrer, F., Robinson, R. C., Lane, D. P., Brown, C. J., and Ghadessy, F. J. (2017) Structure-activity studies of Mdm2/Mdm4-binding stapled peptides comprising non-natural amino acids. *PLoS One*. **12**, 1–15
190. Moerke, N. J. (2009) Fluorescence Polarization (FP) Assays for Monitoring Peptide-Protein or Nucleic Acid-Protein Binding. *Curr. Protoc. Chem. Biol.* **1**, 1–15
191. Marqusee, S., and Baldwin, R. L. (1987) Helix stabilization by Glu-...Lys+ salt bridges in short peptides of de novo design. *Proc. Natl. Acad. Sci. U. S. A.* **84**, 8898–8902
192. Verdine, G. L., and Hilinski, G. J. (2012) Stapled peptides for intracellular drug targets. *Methods Enzymol.* **503**, 3–33
193. Creamer, T. P., and Rose, G. D. (1995) Interactions between hydrophobic side chains within α-helices. *Protein Sci.* **4**, 1305–1314
194. Williamson, M. P. (2013) Using chemical shift perturbation to characterise ligand binding. *Prog. Nucl. Magn. Reson. Spectrosc.* **73**, 1–16
195. Prasannan, S., Fenwick, R. B., Campbell, L. J., Evetts, K. A., Nietlispach, D., Owen, D., and Mott, H. R. (2007) 1H, 13C, and 15N resonance assignments for the small G protein RalB in its active conformation. *Biomol. NMR Assign.* **1**, 147–149
196. Fenwick, R. B., Prasannan, S., Campbell, L. J., Evetts, K. A., Nietlispach, D., Owen, D., and Mott, H. R. (2008) 1H, 13C and 15N resonance assignments for the active conformation of the small G protein RalB in complex with its effector RLIP76. *Biomol. NMR Assign.* **2**, 179–182
197. Plank, C., Oberhauser, B., Mechtler, K., Koch, C., and Wagner, E. (1994) The influence

of endosome-disruptive peptides on gene transfer using synthetic virus-like gene transfer systems. *J. Biol. Chem.* **269**, 12918–12924

198. Tetley, G. J. N., Murphy, N. P., Bonetto, S., Ivanova-Berndt, G., Revell, J., Mott, H. R., Cooley, R. N., and Owen, D. (2020) The discovery and maturation of peptide biologics targeting the small G protein Cdc42: a bioblockade for Ras-driven signalling. *J. Biol. Chem.* **295**, 2866–2884
199. Adachi, Y., Sakamoto, K., Umemoto, T., Fukuda, Y., Tani, A., and Asami, T. (2017) Investigation on cellular uptake and pharmacodynamics of DOCK2-inhibitory peptides conjugated with cell-penetrating peptides. *Bioorganic Med. Chem.* **25**, 2148–2155
200. Nakase, I., Niwa, M., Takeuchi, T., Sonomura, K., Kawabata, N., Koike, Y., Takehashi, M., Tanaka, S., Ueda, K., Simpson, J. C., Jones, A. T., Sugiura, Y., and Futaki, S. (2004) Cellular uptake of arginine-rich peptides: Roles for macropinocytosis and actin rearrangement. *Mol. Ther.* **10**, 1011–1022
201. Thorén, P. E. G., Persson, D., Isakson, P., Goksör, M., Önfelt, A., and Nordén, B. (2003) Uptake of analogs of penetratin, Tat(48-60) and oligoarginine in live cells. *Biochem. Biophys. Res. Commun.* **307**, 100–107
202. Qian, Z., Martyna, A., Hard, R. L., Wang, J., Appiah-Kubi, G., Coss, C., Phelps, M. A., Rossman, J. S., and Pei, D. (2016) Discovery and Mechanism of Highly Efficient Cyclic Cell-Penetrating Peptides. *Biochemistry*. **55**, 2601–2612
203. Song, J., Qian, Z., Sahni, A., Chen, K., and Pei, D. (2019) Cyclic Cell-Penetrating Peptides with Single Hydrophobic Groups. *ChemBioChem*. **20**, 2085–2088
204. Paiva, S. L., and Crews, C. M. (2019) Targeted protein degradation: elements of PROTAC design. *Curr. Opin. Chem. Biol.* **50**, 111–119
205. Lau, Y. H., De Andrade, P., Wu, Y., and Spring, D. R. (2015) Peptide stapling techniques based on different macrocyclisation chemistries. *Chem. Soc. Rev.* **44**, 91–102
206. Peraro, L., Siegert, T. R., and Kritzer, J. A. (2016) Conformational Restriction of Peptides Using Dithiol Bis-Alkylation. *Methods Enzymol.* **580**, 303–332
207. Timmerman, P., Beld, J., Puijk, W. C., and Meloen, R. H. (2005) Rapid and quantitative cyclization of multiple peptide loops onto synthetic scaffolds for structural mimicry of protein surfaces. *ChemBioChem*. **6**, 821–824
208. Cheng, Y., and Patel, D. J. (2004) An efficient system for small protein expression and

refolding. *Biochem. Biophys. Res. Commun.* **317**, 401–405

209. Cheng, Y., Liu, D., Feng, Y., and Jing, G. (2005) An Efficient Fusion Expression System For Protein And Peptide Overexpression In Escherichia Coli And Nmr Sample Preparation. *Protein Pept. Lett.* **10**, 175–181
210. Marcus, F. (1985) Preferential cleavage at aspartyl-prolyl peptide bonds in dilute acid. *Int. J. Pept. Protein Res.* **25**, 542–546
211. Gram, H., Ramage, P., Memmert, K., Gamse, R., and Kocher, H. P. (1994) A novel approach for high level production of a recombinant human parathyroid hormone fragment in Escherichia coli. *Biotechnology. (N. Y).* **12**, 1017–1023
212. Gavit, P., and Better, M. (2000) Production of antifungal recombinant peptides in Escherichia coli. *J. Biotechnol.* **79**, 127–136
213. Marshall, G. R., Hodgkin, E. E., Langs, D. A., Smith, G. D., Zabrocki, J., and Leplawy, M. T. (1990) Factors governing helical preference of peptides containing multiple α,α-dialkyl amino acids. *Proc. Natl. Acad. Sci. U. S. A.* **87**, 487–491
214. Bondeson, D. P., Smith, B. E., Burslem, G. M., Buhimschi, A. D., Hines, J., Jaime-Figueroa, S., Wang, J., Hamman, B. D., Ishchenko, A., and Crews, C. M. (2018) Lessons in PROTAC Design from Selective Degradation with a Promiscuous Warhead. *Cell Chem. Biol.* **25**, 78-87.e5
215. Wuo, M. G., Hong, S. H., Singh, A., and Arora, P. S. (2018) Synthetic Control of Tertiary Helical Structures in Short Peptides. *J. Am. Chem. Soc.* **140**, 16284–16290
216. Wuo, M. G., Mahon, A. B., and Arora, P. S. (2015) An Effective Strategy for Stabilizing Minimal Coiled Coil Mimetics. *J. Am. Chem. Soc*. **137**, 11618–11621
217. Sakamoto, K., Adachi, Y., Komoike, Y., Kamada, Y., Koyama, R., Fukuda, Y., Kadotani, A., Asami, T., and Sakamoto, J. ichi (2017) Novel DOCK2-selective inhibitory peptide that suppresses B-cell line migration. *Biochem. Biophys. Res. Commun.* **483**, 183–190
218. Ostrem, J. M. L., and Shokat, K. M. (2016) Direct small-molecule inhibitors of KRAS: From structural insights to mechanism-based design. *Nat. Rev. Drug Discov.* **15**, 771–785
219. Johnson, L., Greenbaum, D., Cichowski, K., Mercer, K., Murphy, E., Schmitt, E., Bronson, R. T., Umanoff, H., Edelmann, W., Kucherlapati, R., and Jacks, T. (1997) K-ras is an essential gene in the mouse with partial functional overlap with N-ras. *Genes Dev.* **11**,

2468–2481

220. Hunter, J. C., Manandhar, A., Carrasco, M. A., Gurbani, D., Gondi, S., and Westover, K. D. (2015) Biochemical and structural analysis of common cancer-associated KRAS mutations. *Mol. Cancer Res.* **13**, 1325–1335

221. Samson, M., Porter, N., Orekoya, O., Hebert, J. R., Adams, S. A., Bennett, C. L., and Steck, S. E. (2017) Beyond cyclosporine A: conformation-dependent passive membrane permeabilities of cyclic peptide natural products Christopher. *Future Med. Chem.* **155**, 3–12

222. Patgiri, A., Yadav, K. K., Arora, P. S., and Bar-Sagi, D. (2011) An orthosteric inhibitor of the Ras-Sos interaction. *Nat. Chem. Biol.* **7**, 585–587

223. Popovic, M., Schouten, A., Rensen-de Leeuw, M., and Rehmann, H. (2016) The structure of the Guanine Nucleotide Exchange Factor Rlf in complex with the small G-protein Ral identifies conformational intermediates of the exchange reaction and the basis for the selectivity. *J.Struct.Biol.* **193**, 106–114

224. Mitra, S., Montgomery, J. E., Kolar, M. J., Li, G., Jeong, K. J., Peng, B., Verdine, G. L., Mills, G. B., and Moellering, R. E. (2017) Stapled peptide inhibitors of RAB25 target context-specific phenotypes in cancer. *Nat. Commun.* **8**, 1–11

225. Hutchinson, C. L., Lowe, P. N., McLaughlin, S. H., Mott, H. R., and Owen, D. (2011) Mutational analysis reveals a single binding interface between RhoA and its effector, PRK1. *Biochemistry*. **50**, 2860–2869

226. Peränen, J., Rikkonen, M., Hyvönen, M., and Kääriäinen, L. (1996) T7 Vectors with a Modified T7/ac Promoter for Expression of Proteins in Escherichia coli. *Anal. Biochem.* **236**, 371–373

227. Fenwick, R. B., Prasannan, S., Campbell, L. J., Nietlispach, D., Evetts, K. A., Camonis, J., Mott, H. R., and Owen, D. (2009) Solution structure and dynamics of the small GTPase RalB in its active conformation: Significance for effector protein binding. *Biochemistry*. **48**, 2192–2206

228. Thompson, G., Owen, D., Chalk, P. a, and Lowe, P. N. (1998) Delineation of the Cdc42 / Rac-Binding Domain of p21-Activated Kinase Delineation of the Cdc42 / Rac-Binding Domain of p21-Activated Kinase. *Biochemistry*. **37**, 7885–7891

229. McCoy, A. J., Grosse-Kunstleve, R. W., Adams, P. D., Winn, M. D., Storoni, L. C., and

Read, R. J. (2007) Phaser crystallographic software. *J. Appl. Crystallogr.* **40**, 658–674

230. 4, C. C. P. N. (1994) The CCP4 suite: Programs for protein crystallography. *Acta Crystallogr. Sect. D Biol. Crystallogr.* **50**, 760–763
231. Emsley, P., and Cowtan, K. (2004) Coot: Model-building tools for molecular graphics. *Acta Crystallogr. Sect. D Biol. Crystallogr.* **60**, 2126–2132
232. Adams, P. D., Grosse-Kunstleve, R. W., Hung, L. W., Ioerger, T. R., McCoy, A. J., Moriarty, N. W., Read, R. J., Sacchettini, J. C., Sauter, N. K., and Terwilliger, T. C. (2002) PHENIX: Building new software for automated crystallographic structure determination. *Acta Crystallogr. Sect. D Biol. Crystallogr.* **58**, 1948–1954
233. Vranken, W. F., Boucher, W., Stevens, T. J., Fogh, R. H., Pajon, A., Llinas, M., Ulrich, E. L., Markley, J. L., Ionides, J., and Laue, E. D. (2005) The CCPN data model for NMR spectroscopy: Development of a software pipeline. *Proteins Struct. Funct. Genet.* **59**, 687–696
234. Schindelin, J., Arganda-Carreras, I., Frise, E., Kaynig, V., Longair, M., Pietzsch, T., Preibisch, S., Rueden, C., Saalfeld, S., Schmid, B., Tinevez, J. Y., White, D. J., Hartenstein, V., Eliceiri, K., Tomancak, P., and Cardona, A. (2012) Fiji: An open-source platform for biological-image analysis. *Nat. Methods*. **9**, 676–682
235. Rueden, C. T., Schindelin, J., Hiner, M. C., DeZonia, B. E., Walter, A. E., Arena, E. T., and Eliceiri, K. W. (2017) ImageJ2: ImageJ for the next generation of scientific image data. *BMC Bioinformatics*. **18**, 529